Technische Universität München

TUM Campus Straubing für Biotechnologie und Nachhaltigkeit

Optimization of biomass heating networks through integration of heat pumps

Yusheng Chen

Vollständiger Abdruck der von dem TUM Campus Straubing für Biotechnologie und Nachhaltigkeit der Technischen Universität München zur Erlangung des akademischen Grades eines

Doktors der Ingenieurwissenschaften (Dr.-Ing.)

genehmigten Dissertation.

Vorsitz: Prof. Dr. Magnus Fröhling

Prüfende der Dissertation:

1. Prof. Dr.-Ing. Matthias Gaderer
2. Prof. Dr.-Ing. Jakob Burger

Die Dissertation wurde am 19.03.2024 bei der Technischen Universität München eingereicht und durch den TUM Campus Straubing für Biotechnologie und Nachhaltigkeit am 16.08.2024 angenommen.

Acknowledgment

This thesis was completed during my work as a research assistant at the Professorship of Regenerative Energy Systems (RES) at the Technical University of Munich. I would like to express my deepest gratitude and appreciation to everyone who has supported me throughout the journey of completing this PhD thesis. Your encouragement, guidance, and assistance have been invaluable in helping me achieve this milestone.

First and foremost, I extend my heartfelt gratitude to my supervisor, Prof. Dr.–Ing. Matthias Gaderer, for providing me with the opportunity to work at the professorship. His unwavering support, extensive knowledge, and constructive feedback have been crucial in shaping my research and writing. I am incredibly thankful for his mentorship and the professional growth I have experienced under his guidance.

I am also immensely grateful to my mentor, Prof. Dr. Josef Kainz, who has generously shared his expertise and wisdom. His passion for research and dedication to advancing the field have been truly inspiring, and I have learned a great deal from him.

I would also like to thank my colleague at TUM Campus Straubing, whose camaraderie and collaboration have made the process of working on this thesis more enjoyable and productive. Your insights and encouragement have been essential in helping me overcome challenges and maintain motivation.

On a personal note, I would like to express my deepest appreciation to my family for their unwavering love, understanding, and support throughout this journey. Their love and support have been instrumental in my academic and personal achievements. Lastly, I would like to extend my thanks to my friends who have stood by me and offered encouragement during this journey. Their encouragement and faith in me have been a constant source of strength, and I could not have done this without them.

Straubing, 04.03.2024

Yusheng Chen

Abstract

In recent years, studies have shown that enhancing the efficiency of biomass heating has become increasingly important for improving their competitiveness. A promising solution is the integration of heat pumps into these systems to recover heat from exhaust gases. There are different variants to integrating heat pumps into biomass heating, either into the flue gas condenser or into the network return flow. However, this integration necessitates additional electricity consumption, which in many countries comes with a high emission factor or high price. Small-scale cogeneration is considered a superior technology for providing the necessary power for heat pumps. Nonetheless, the multiple possibilities of integrating these components imply a high degree of system complexity and, therefore, higher design requirements.

This thesis aims to develop a transferable method to optimize biomass heating networks from technical, economic, and environmental perspectives, through the innovative integration of heat pumps and, if necessary, cogeneration units for onsite-power supply. To this end, a detailed simulation model was developed and validated against measured data from real cases. Additionally, a multi-objective simulation optimization framework was implemented by coupling this model with a genetic algorithm.

For the evaluation of the integration concepts and a feasibility study in Germany, three biomass heating networks with different hydraulic configurations were investigated. It turned out that both integration variants of heat pump improved the system overall efficiency by more than 17 % in practice. In general, this thesis demonstrates the feasibility of effectively utilizing biomass resources while simultaneously achieving the economic and environmental viability of the system through appropriate design. The success of this integration depends on careful selection of design parameters. The prices of biomass fuel and electricity are crucial factors affecting the economic viability of the integration concepts. The proposed method allows decision-makers to achieve an optimal system design under the given conditions.

Kurzfassung

In den letzten Jahren haben Studien gezeigt, dass die Steigerung der Effizienz der Biomasseheizung zunehmend wichtiger geworden ist, um ihre Wettbewerbsfähigkeit zu verbessern. Eine vielversprechende Lösung ist die Integration von Wärmepumpen, um Wärme aus Abgasen zurückzugewinnen. Es gibt verschiedene Ansätze zur Integration von Wärmepumpen in Biomasseheizungen, entweder in den Abgaskondensator oder in den Netzrücklauf. Dabei ist zusätzlicher Stromverbrauch für Wärmepumpe erforderlich, der in vielen Ländern mit einem hohen Emissionsfaktor oder hohen Kosten verbunden ist. Die Integration einer kleinen Kraft-Wärme-Kopplung gilt als mögliche Technologie zur Bereitstellung der erforderlichen elektrischen Leistung für Wärmepumpen. Die vielfältigen Möglichkeiten zur Integration dieser Komponenten bedeuten jedoch einen höheren Grad an Systemkomplexität und daher höhere Anforderungen an die Auslegung.

Ziel dieser Arbeit ist es, eine übertragbare Methode zu entwickeln, um Biomasseheizungsnetzen aus technischer, wirtschaftlicher und ökologischer Perspektive zu optimieren, durch die innovative Integration von Wärmepumpen und, falls notwendig, einer Kraft-Wärme-Kopplung für ihre Eigenstromversorgung. Zu diesem Zweck wurde ein detailliertes Simulationsmodell entwickelt und anhand von Messdaten aus realen Heizwerken soweit möglich validiert. Darüber hinaus wurde ein mehrdimensionaler Simulationsoptimierungsrahmen durch die Kopplung dieses Modells mit einem genetischen Algorithmus implementiert. Für die Bewertung der Integrationskonzepte und der Machbarkeitsstudie in Deutschland wurden drei Biomasse-Wärmenetze mit unterschiedlichen Hydrauliken untersucht. Es stellte sich heraus, dass beide Integrationsvarianten der Wärmepumpen die Gesamteffizienz des Systems in der Praxis um mehr als 17 % verbessern können. Die Ergebnisse zeigen, dass es möglich ist, die effektive Nutzung von Biomasse-Ressourcen sicherzustellen und gleichzeitig die wirtschaftliche und ökologische Tragfähigkeit des Systems durch ein geeignetes Optimierungsdesign zu erreichen. Der Erfolg dieser Integration hängt von einer sorgfältigen Auswahl der Designparameter ab. Die Preise für Biomassebrennstoff und Strom sind entscheidende Faktoren, die die wirtschaftliche Tragfähigkeit der Integrationskonzepte beeinflussen.

Table of contents

1. Introduction

1.1 Background

In the nineteenth century, the combustion of fossil fuels lit the fire of the industrial revolution and illuminated the way forward for human civilization. With the continuous development of human society, the use of fossil energy resources also caused a dramatic rise in carbon dioxide emissions [1]. By 2020 it had reached 34.81 billion metric tons [2], and the global average surface temperature had increased by 1.0 °C [3] and will continue to rise by 2 °C by the middle of this century, according to the present trend [4]. According to the Paris Agreement[1] [5], the global average temperature increase is targeted not to exceed 2 °C by the end of this century, and to stay below 1.5 °C compared to pre-industrial levels preferably.

Under the former climate change legislation, the EU (European Union) has targeted a minimum of a 40 % reduction in greenhouse gas emissions by 2030 compared to 1990 [6]. As part of the EU Climate Change Act negotiations, this target has been raised to 55 % under the European Green Deal [7]. In addition, the share of renewable energies in the EU's final energy consumption is to be increased to 32 %, and the EU's primary energy consumption is to be reduced by 32.5 % compared to an underlying reference development [8]. By 2050, greenhouse gas emissions in the EU are to be reduced by 80 to 95 % compared to 1990 levels [9].

A sustainable energy supply plays a critical role in addressing environmental problems and achieving climate targets. According to the BMUB[2], the entire building sector is responsible for 40 % of total energy consumption for heating, hot water, and lighting and almost 30 % of total CO_2 emissions [10]. Therefore, improving energy efficiency in this sector offers considerable potential for reducing greenhouse gas emissions and primary energy demand [11]. In many cases, synergies can be exploited to improve the energy

[1] Adopted Dec. 12, 2015; entered into force Nov. 4, 2016

[2] German Federal Ministry for the Environment, Nature Conservation, Nuclear Safety and Consumer Protection

efficiency of communities by constructing or refurbishing district energy systems [12,13]. Because of its lower environmental impact and flexibility, biomass is well suited to replace traditional fossil energy as an alternative fuel for sustainable heating plants [14,15].

1.2 Problem

By the end of the last century, intensive construction of biomass heating networks began across Europe to reduce carbon emissions from the energy supply [16]. However, since biomass fuel costs were relatively favorable at that time, little emphasis was placed on the efficiency of the fuel energy conversion to heating energy in the plant designs. As a result, many older biomass heating networks are currently operated at low efficiency rates. The average annual conversion efficiency rate in biomass heating networks from the initial heating value of the fuel to the final energy supplied to the consumer ranges currently from 55 % to 80 % [17]. Due to the limited resource potential and the rising price of bioenergy [18], it has become increasingly critical to improve biomass energy's efficiency to enhance its profitability and competitiveness [19]. To compensate for the relatively low efficiency of these heating networks, heat recovery from flue gas is highly recommended [20]. Since biomass fuel has a high moisture content, district heating with biomass fuel offers a high potential for heat recovery especially from latent heat [21].

The installation of flue gas condensation systems is one of the most effective measures to increase the efficiency of biomass heating plants, with a potential increase in efficiency of up to 30 % [22]. Many studies have already investigated latent heat recovery from flue gases using this technique. For example, Shang et al. [23] proposed a non-contact total heat recovery system to enhance gas boiler efficiency from flue gas, demonstrating an annual energy saving potential of 12.97 % compared to a traditional boiler. Terhan and Caomakli [24] studied a real case of flue gas condensation in the natural gas district heating systems of a university. The economic analysis of this study demonstrated that this technology could benefit the studied system by 0.4 Mio $ per year. Additionally, Ziembicki et al. [25] introduced a condensing system dedicated to flue gas cleaning and heat recovery for liquid fuel combustion. Since conventional metal heat exchangers are usually susceptible to corrosion, Xiong and Tan et al. [26] investigated a condensing system experimentally. They used a two-stage fluoroplastic heat exchanger to study the recovery potential of water and latent heat from flue gases while overcoming the drawbacks of metal heat exchangers in wet

flue gases. For many older heating networks, however, the implementation of flue gas condensing systems is facing significant challenges due to high return temperatures that are often above the dew point of the flue gas [17].

An innovative concept is the integration of heat pumps in the biomass heating networks. In recent years, a few biomass heating networks have accomplished the integration of flue gas condensation and heat pumps, mostly in northern Europe [27] and Austria [28,29]. However, these integrated solutions cannot yet be described as mature and as technology that can be purchased "off the shelf", as specific challenges and problems arising during the operation. Furthermore, the integration of heat pumps in existing heating networks has encountered setbacks in Germany [30], especially due to high return temperatures, high investments and high electricity prices [31].

After conducting a thorough literature review, it has been found that there is currently no established method for integrating compression heat pumps into biomass heating networks that accounts for both the characteristics of biomass fuels and the thermodynamic cycle of the heat pumps. Additionally, significant research gaps exist in providing comprehensive analyses of the impact of heat pump cycle design on entire heating systems, considering the techno-economic and environmental aspects. It is important to note that the operating temperature of the heat pump plays a crucial role in determining the electricity consumption and equipment sizes, which ultimately affect the economic profitability of the system. Furthermore, the refrigerant market is currently undergoing significant changes due to stricter emission control regulations. As a result, refrigerants such as R134a, which were previously considered state-of-the-art, can no longer be viewed as viable options for the future. This also applies to other established refrigerant alternatives if they contribute to the greenhouse effect. To address these challenges, alternative refrigerants must be identified and evaluated for their suitability in different application scenarios. By developing an optimized method for integrating compression heat pumps into biomass heating networks, which considers the unique characteristics of biomass fuels and the thermodynamic cycle of the heat pump, the economic profitability and environmental impact of these systems can be improved.

In addition, there are different variants of integrating heat pumps into heating networks with a flue gas condensation system. There are only few studies found that provide a techno-economic comparison of the various integration methods of compression heat pumps for

heat recovery. A comprehensive analysis of the costs and system efficiencies of different integration concepts is crucial, as it provides valuable insights for biomass heat network operators in the planning and operation of their plants.

Moreover, electrical power is needed to operate the integrated heat pump. This significantly increases the electricity demand of the heating networks, the cost of which can be prohibitive in many European countries. Vannoni et al. [32] demonstrated that the integration of heat pumps for heat recovery would be advantageous only for low electricity price conditions. Furthermore, Averfalk et al. [33] investigated the operating situation of heat pumps in Swedish district heating systems and indicated that the increasing electricity prices have caused heat pumps to lose competitiveness in some areas. In some countries, such as Germany, the integration of low carbon captive power generators may be critical to drive such heat recovery heat pumps from an economic point of view due to high CO_2 factors and electricity prices.

In this context, the employment of a small cogeneration unit could be an ideal way to reduce the amount of electricity purchased from the grid as much as possible. There are various technologies that can be employed for decentralized small scale power cogeneration [34]. The ideal cogeneration technology is one that reliably delivers the required electrical output with a high level of electrical efficiency and at the lowest possible complexity and cost. Within this work, the most promising technologies for the cogeneration of electricity in a biomass heating network should be investigated and evaluated for techno- economic and environmental points of view.

Another important point that deserves to be discussed is that the additional integration of heat pump and cogeneration unit also implies a high degree of complexity of the overall system, resulting in higher design requirements as well as higher initial capital costs. In a standard biomass heating network without heat pump and cogeneration unit, system efficiency is inversely correlated to the exhaust gas temperature. However, if other energy-producing equipment are integrated, system efficiency will be influenced simultaneously by several factors. To maximize the benefits of a system that integrates heat exchangers, heat pumps and cogeneration units, the connections of these system components and their optimal sizing should be adequately planned.

Overall, the planning and construction of such a biomass energy system with the integration of multiple devices is a complex process. For diligent planning of the different possible complex systems, developing an optimization approach at the system level is necessary to account for the technical, economic, and environmental constraints as well as the interactions between the system components. Moreover, the connection variants of the heat pump and its various parameter choices makes the investigation of an optimization approach a feasible and recommended solution to achieve an optimal design of the entire system.

1.3 Objectives and Methods

Based on all points above, the main objective of this thesis is to develop a transferable method to optimize biomass heating networks (BHN) through innovative integration of heat pumps (HP) and, if necessary, a cogeneration (CHP) unit for onsite-power supply.

To this end, a detailed simulation model will be proposed that enables the integration of HP and different types of CHP into biomass heating networks, considering complex thermodynamic processes, such as the impact of biomass fuels composition and the thermodynamic cycle of heat pumps, as well as the interactions between system components such as the different connection variants of the heat pump. To achieve optimization of the integration concepts, the model will be coupled with an independent optimization algorithm to identify the best combination of design parameters.

To validate the proposed simulation model and evaluate the effectiveness of heat pump integration concepts in real-world applications, three biomass heating networks will be studied. The first two of which have already been equipped with compression heat pumps in different integration variants, while the third network represents a standard BHN in Germany without flue gas condensation and heat pump, which had a significantly bad experience with flue gas condenser without integration of heat pumps. Based on the real operation data collected, the actual effects of the heat pump integration concepts will be investigated , combining both real-world observations and simulations. The practical experience of the few real-world cases will be valuable in improving the concepts.

Next, a thermodynamic analysis based on the first BHN will be performed to investigate the effect of the different technical parameters on heat pump integration. This aims to develop an ideal heat pump cycle.

Furthermore, a techno-economic comparison and analysis of different heat pump integration variants will be carried out for the feasibility study in Germany, with a focus on the third biomass heating network. This study will provide an overview of the differences between two heat pump connection variants, assess the suitability of different cogeneration technologies, and examine the impacts of different design parameters on the overall system.

To optimize the proposed biomass heating networks with integrated heat pumps, a simulation-optimization framework will be implemented by combining the proposed simulation model with an independent genetic optimization algorithm. By identifying the optimization objectives and the range of the decision variables to be optimized, multi-objective optimization of the system can be performed to find the most optimal system design. Where the techno-economic and environmental indicators can be considered as the optimization objectives, while the decision variables will include selectable integer and continuous design parameters of the system components, such as the design annual full utilization hours and air ratio of the biomass boiler, heat pump connection variants, heat pump operating temperatures, as well as the refrigerant selection. Utilizing the multi-objective optimization approach, the most efficient system design will be identified based on the selected techno-economic or environmental indicators. This framework will enable a comprehensive and efficient optimization process to achieve the desired objectives.

The main contributions and novelties of this work can be summarized as follows:

- Development of a transferable method for integrating compression heat pumps in biomass heating networks for heat recovery.
- Examination of the practical benefits of different heat pump connection variants based on operational data from the few real-world use cases.
- Identification and evaluation of the techno-economic and environmental performance differences between the two heat pump connection variants under similar conditions.
- Investigation of the impact of various design parameters on the overall techno-economic performance of the biomass district heating system.
- Comparison and evaluation of the most promising cogeneration technologies for for onsite-power supply.

- Development of a multi-objective simulation-optimization framework using the heuristic algorithm to maximize the benefits of the proposed integrated system.

The proposed method in this work can serve as a supportive decision-making tool for evaluating the techno-economic and environmental potentials of heat pump integration into biomass heating networks, and for optimizing the parameter design of different system components.

1.4 Structure of thesis

The overall structure of this thesis is depicted in Figure 1 and can be summarized as follows:

Chapter 1 introduces the background and outlines the problems that are currently faced, from which the main objectives and potential contributions of this research are derived.

Chapter 2 describes the technologies of the system components involved in this thesis, including their basic principles and the current state of the art. In addition, the technical focus of this work is identified, i.e., the recovery of waste heat by compression heat pumps (Section 2.3.4). Section 2.4.2 provides a preliminary selection of potentially suitable cogeneration technologies for self-power generation.

Chapter 3 focuses on the introduction of the different integration concepts. Section 3.1 outlines how different system components can be integrated into the system and the functions they achieve. The second part, Section 3.2, defines the systems with different integration concepts and analyzes the complexity of the different systems based on their mass and energy flows.

Chapter 4 provides a comprehensive description of the proposed simulation model, where Section 4.1 presents the modeling of the different system components and Section 4.2 illustrates how the different component models are integrated into the system model. Section 4.3 defines the indicators to evaluate the different integration concepts from system level. Chapter 5 elucidates how the simulation model proposed in Chapter 4 can be coupled with an independent genetic optimization algorithm as an optimization framework. Section 5.2.1 presents the mathematical representation of the optimization framework and Section 5.2.2 describes the detailed optimization process.

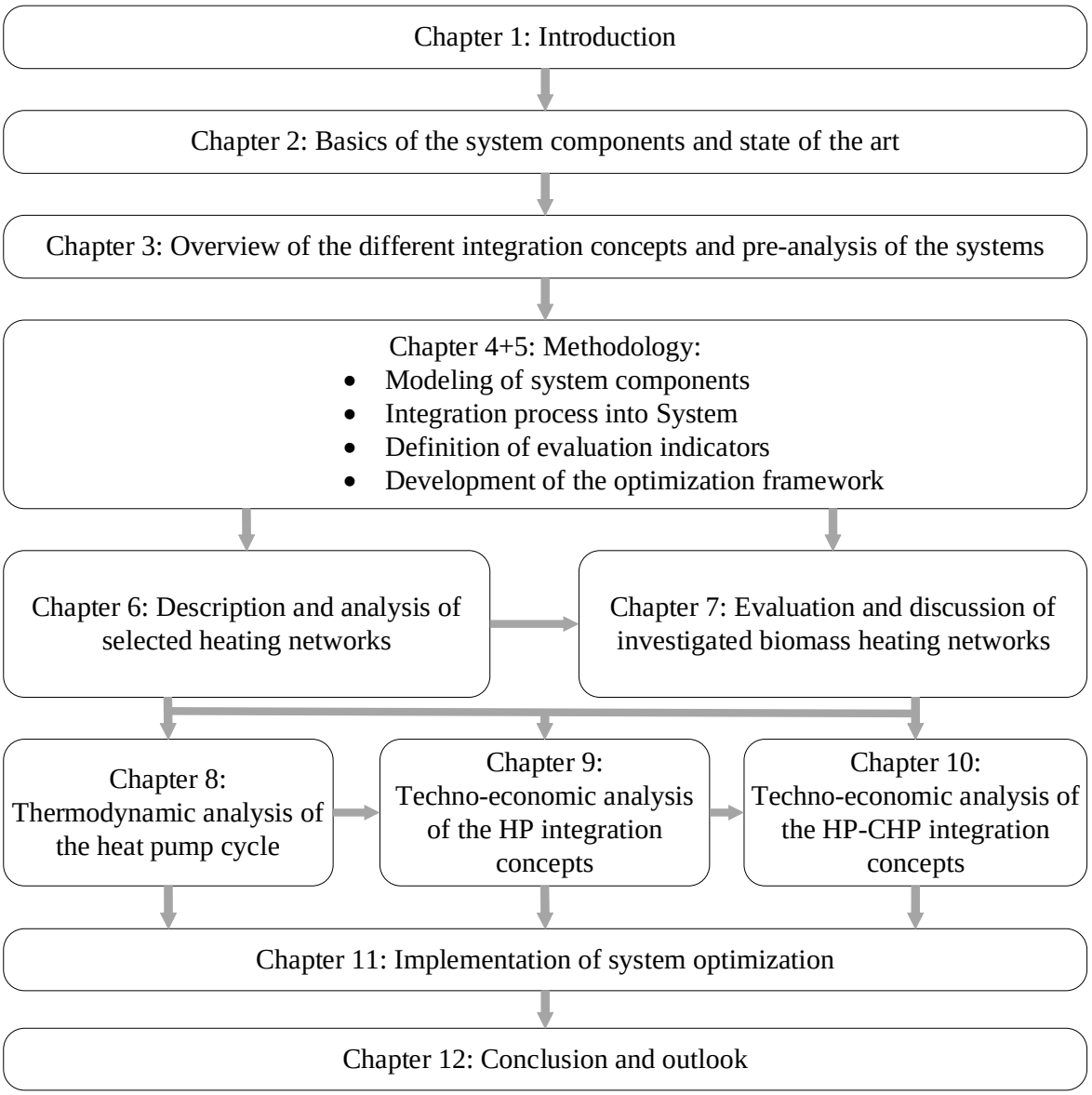

Figure 1: Overview of the thesis structure

Chapter 6 introduces the three real biomass heat networks that are the focus in this thesis, including their system configurations, technical parameters, and operating parameters. In Chapter 7, the reliability of the proposed model is verified by simulating the selected heating networks, and a comprehensive evaluation of the three heat networks is conducted.

Chapter 8 conducts an analysis of the impact of heat pump cycles on system efficiency. Chapter 9 presents a technical and economic comparison and analysis of different heat pump integration variants, i.e., flue gas side integration and network side integration. The analysis also includes the impact of different techno-economic parameters on the results. Chapter 10 provides a techno-economic analysis of the integration of different cogeneration

technologies, using flue gas side integration concept as an example, and analyzes the impact of different parameters.

Chapter 11 performs a multi-objective optimization of the system based on the proposed optimization framework and provides a thorough analysis and discussion of the results obtained through the optimization process.

Lastly, Chapter 12 provides a comprehensive summary of the thesis, including its major findings, and outlines outlook of this research. The effectiveness of the proposed method in achieving the desired outcomes is evaluated and its potential for future applications is also discussed.

2. Basics of the system components and state of the art

This chapter provides an overview of the theoretical background and the state of the art for the thermal utilization of solid biomass and technologies for recovery of waste heat from its flue gas through heat pumps. Firstly, the technical fundamentals of biomass utilization and its combustion, as well as the status of biomass heating are introduced in Section 2.1. Section 2.2 presents the working principle, the influencing parameters, and the status of the application of flue gas condensation technology and points out the current problems of the application. Section 2.3 describes the technical background of heat pumps and their current status of research and applications for heat recovery, and compares the applicability of absorption heat pumps and compression heat pumps to the addressed research topic. Finally, Section 2.4 discusses various small scale cogeneration technologies that could be used for the onsite-power supply for heat pumps and offers a comparison of the advantages and disadvantages for the integration into a biomass heating network.

2.1 Biomass heating plants

2.1.1 Biomass as fuel

Biomass comprises all organic matter of plant or animal origin that has not yet been classified as fossil raw materials [35]. In practice, the use of biomass as a fuel is widespread, however, its application is highly geographically limited due to transportation costs. Specifically, most wood chips used as biomass originate from nearby areas [36,37]. The use of residual and waste materials, as well as special crops such as miscanthus, also occurs sporadically in practice.

Biomass fuels typically have a water content ranging from 8 % and 60 % relative to the fresh substance. During combustion, the moisture of the biomass is evaporated and the hydrogen atoms react with oxygen to form water vapor.

When burning dry fuels at a low air ratio, the efficiency of the boiler is higher compared to burning wet fuels. The reason for this is that, during the combustion of dry fuels, a smaller proportion of the fuel's available energy (calorific value) is consumed to heat and evaporate the fuel's water content, thereby increasing the combustion temperature in the chamber. As

shown in Figure 2, the higher starting point of combustion temperature also enables more effective cooling of the flue gases at the same exhaust gas temperature.

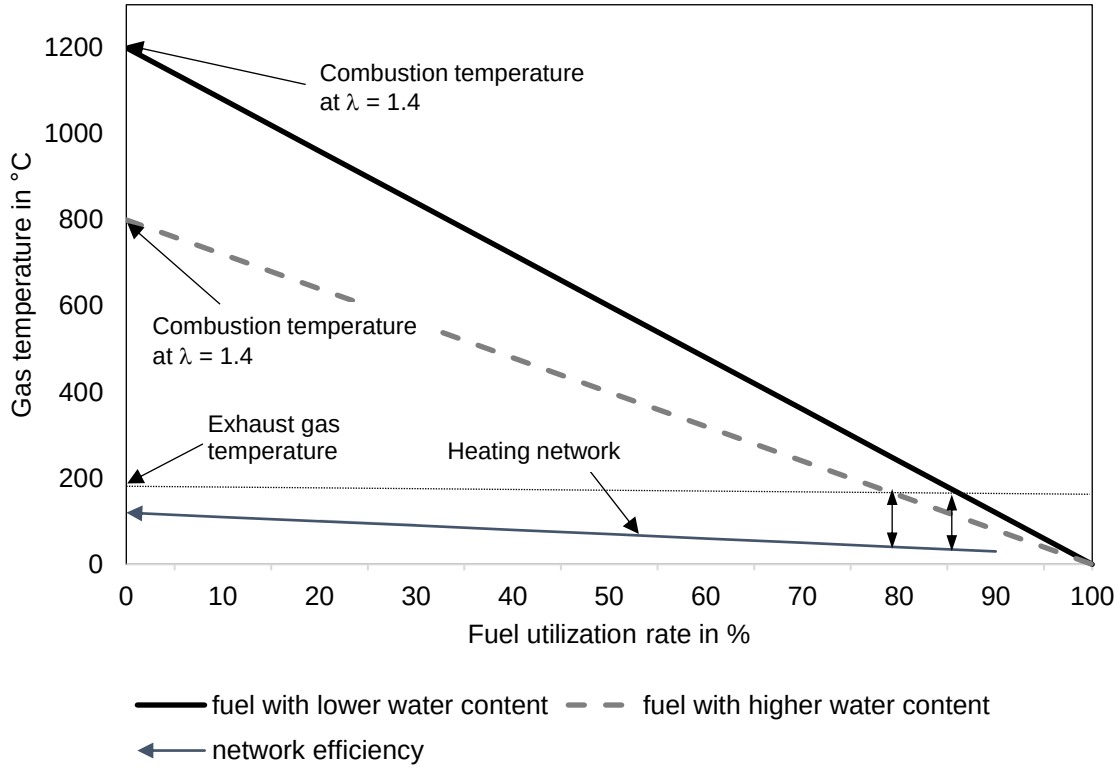

Figure 2: Fuel utilization efficiency of a boiler with different water contents at different gas temperatures (own representation, adapted from [17]).

However, at low fuel water contents, combustion temperatures often rise to an unacceptable range, leading to the sintering and softening of fuel ash on the grate [38]. Common countermeasures to lower the combustion temperature include increasing the combustion air flow or recirculating flue gas. For this reason, many heating plants prefer using biomass fuels with relatively higher water content. These are less expensive but cannot be stored for long periods due to the high moisture, as substance degradation by microorganisms and mold growth occurs. However, this is not a significant problem in many regions, as the logistics of most heating plants are designed for a short storage period of only a few weeks at most. The use of moist fuels is therefore feasible in principle and is also carried out in practice. Yet, higher water contents also lead to low boiler efficiency, as also seen in Figure 2. To compensate for the disadvantage in boiler efficiency, the use of flue gas condensation is recommended.

Moreover, due to the different physical properties, such as water content and ash sintering temperature, heating plant design needs to be adapted to the fuel. Hartmann et al. [39] pointed out that the chosen fuel is an essential basis for the design and layout of the plant and can therefore not be easily changed during operation. Possible exceptions to this are, for example, to replace the design fuel with a higher quality alternative, e.g., wood pellets in place of straw or wood chips. In addition, a trouble-free operation can often be ensured for fuels within a tolerance range around the design point, which may allow for the mixing of different materials. Moreover, for some boilers, adding a second burner for alternate fuels, such as pellets, oil or gas, is also possible.

2.1.2 Biomass combustion furnace

The most important equipment in a biomass heating plant is the combustion furnace, where the energy contained in the fuel is converted into thermal energy. The engineering of plant components and the associated planning and operational know-how have significantly improved since the 1980s. Extensive studies for these have been conducted in this field, notably at the Technical University of Graz [40–43] and the ETH Zurich [44,45] during the 1990s. Well-planned heating plants still have an excellent economical basis today. However, there are also many plants whose planning and operation is insufficient for various reasons, leading to poorer economic performance.

Figure 3 illustrates an example of the schematic structure of a standard biomass heating plant, showcasing typical combustion technology equipped with flue gas recirculation and cleaning. Starting from the bottom, the diagram shows a boiler with fixed-bed firing. A typical feature of biomass combustion, such as with wood chips, is the staged air supply. This means dividing the combustion air into primary air, supplied to the fixed bed, and secondary air, supplied above the bed to the upper combustion chamber. This allows the complete combustion without exceeding the ash softening temperature of biomass on the grate [17]. Additionally, flue gas recirculation helps to prevent excessive temperatures in the boiler and reduce NO_x emissions. Additional preheating of the combustion air is also possible, but not shown in this example.

It should also be noted that compressed air is regularly injected into the first and second flue gas passages. This is one way of removing impurities from the heat exchanger surfaces.

Alternatively, this cleaning can also be performed mechanically by scraping, knocking, or water jet [46].

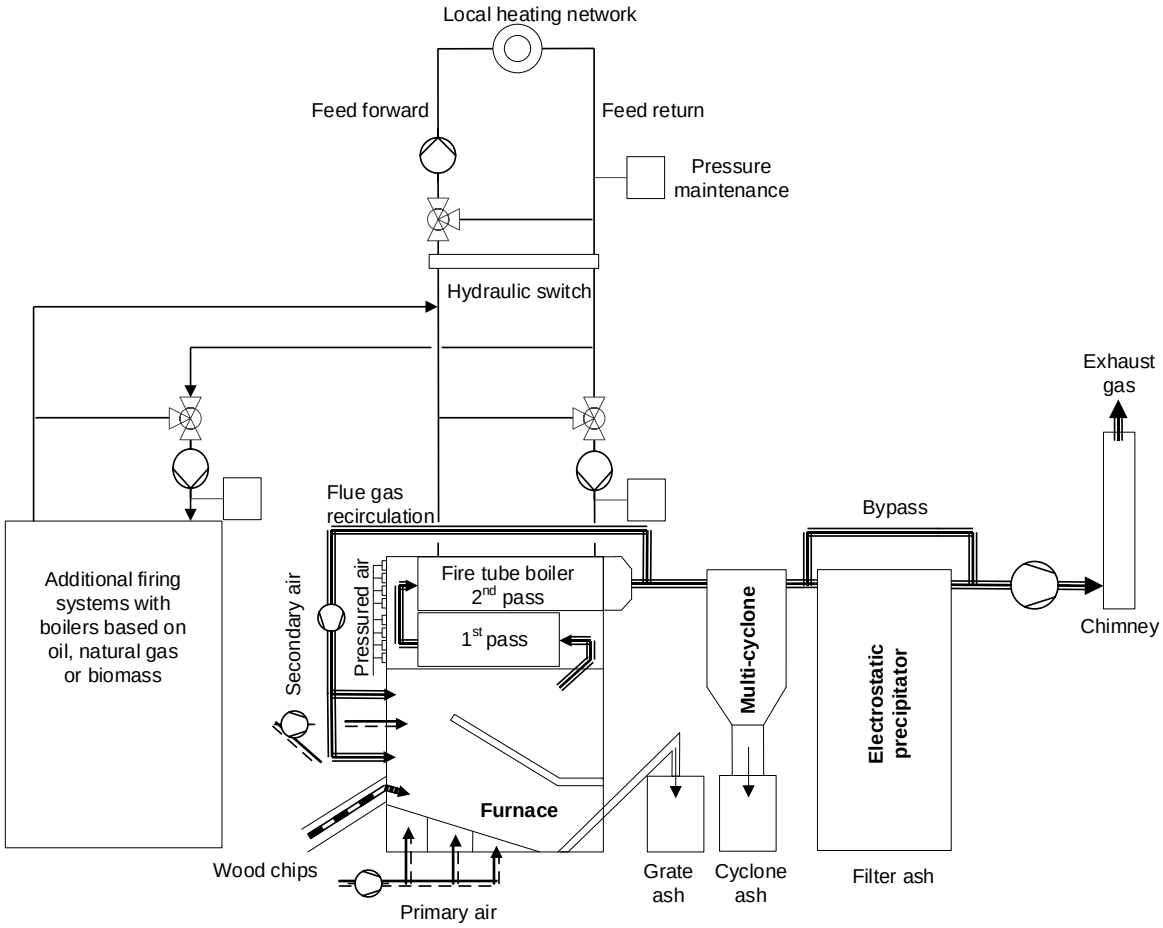

Figure 3: Layout of a standard biomass heating plant with flue gas recirculation (adapted from [17]).

The furnace is followed by flue gas treatment, which starts in the example with a multi-cyclone that removes coarse particles from the flue gas. An improved dust removal can be done with an electrostatic precipitator. Depending on fuel quality, plant size and year of commissioning, the flue gas treatment process can be simpler or more complex. This is usually necessary to comply with applicable emission protection laws. For the proper design of electrostatic precipitator systems, various input parameters must be considered [47].

In practice, the required heat is often provided by several boilers together when the plant reaches a certain size (as also seen in Figure 3). The motivation behind this configuration is to facilitate the utilization of heterogeneous energy sources through disparate boilers. More importantly, it addresses operational constraints that vary significantly with boiler design. A

multiple boiler design can improve the threshold of controllability. For instance, conventional biomass boilers are capable of part-load operation up to 30% of their rated capacity [39]. To compensate for periods of low demand that fall below the operational threshold of the boilers, it is essential either to maintain a buffer storage of significant capacity or to employ additional small-scale heat generators. These generators must also be capable of functioning efficiently with a lower heat consumption. These can be realized through the implementation of a gas boiler or oil boiler, which typically offers improved control dynamics. Another purpose of the multiple boiler design is to maximize the utilization and efficiency of the "main boiler" by distributing peak loads among additional auxiliary boilers.

2.1.3 Status of biomass heating systems

The expansion of biomass heating took off in many European countries in the 1990s with robust policy support and significant financial incentives, especially in Germany. The motivation for this expansion was the independence of energy supply from fossil energy sources. Also, the financial promotion, reduction of heating costs and utilization of locally produced biomasses, are also decisive drivers for this. These heating networks provide a low-emission heat supply for local houses and other facilities. By 2021, there are approximately 1200 biomass heating plants with a thermal output of greater than 500 kW and around 170 bioenergy villages in Germany [48]. These villages meet a substantial portion of their electricity and heat requirements predominantly through locally sourced biomass. For instance, the bioenergy village Büsingen [49] (1,390 inhabitants) combines solar thermal energy and a woodchip plant in its local heating network. Another example of a rural heating network with central bioenergy plants (biogas plant, woodchip plant) is the village of Jühnde [50] (750 inhabitants).

During the initial stages of biomass heating networks' development, the focus was not placed on energy conversion efficiency, largely due to the favorable prices of biomass fuel at the time. Consequently, many biomass heating networks currently operate with efficiencies that are inferior when compared to those of natural gas furnaces. Generally, the average annual energy conversion efficiency - from fuel to final energy for consumers – ranges from 55 and 80% in biomass heating plants that are connected local heating networks [17,51]. However, studies in [19] have shown that, due to the increase in biomass energy

prices and the development of alternative technologies in the last decade, it has become increasingly important to improve the efficiency of biomass heating plants to enhance their competitiveness.

Local district heating networks are often operated for extended periods, sometimes spanning up to five decades. Typically, the repayment period for these heating systems in urban areas ranges from 15 to 30 years. The furnaces, on the other hand, have a shorter expected lifespan, approximately 20 years. Therefore, operators of biomass heating plants established between 1995 and 2005 are now facing the need for new investments in essential system components, including the combustion mechanism, boilers, and pumps. With the new investments, the operators have the opportunity to implement additional efficiency-increasing measures. Beyond enhancing efficiency, another significant consideration is the reduction of emissions from biomass heating plants. This has become a priority as European governments have introduced regulations mandating specific actions for emission reduction. In Germany, for instance, important aspects are the reduction of particulate matter, CO and NOx emissions , in alignment with the Federal Immission Control Act (BImSchV)[3] [52,53].

2.2 Flue gas condensation

To increase the boiler efficiency of a biomass heating plant, the installation of a flue gas condenser (COND) is an effective instrument [21]. A flue gas condenser is essentially a heat exchanger that cools the exhaust gases to below their dew point. Consequently, water vapor condenses into liquid, releasing the heat of condensation. This phase transition liberates a substantial quantity of low-temperature heat, typically around or below 55 °C.

2.2.1 Working principle and structural design

The flue gas condensation is a very effective way to increase the utilization rate of biomass. The fuel utilization rate η_{util} of a biomass heating system is defined as follows [35]:

$$\eta_{ulti} = \frac{Q_{util}}{H_{fuel}} \tag{1}$$

[3] Ordinance on the Implementation of the Federal Immission Control Act (in German: Verordnung zur Durchführung des Bundes-Immissionsschutzgesetzes)

Where Q_{util} stands for the utilized heat by the whole biomass heating plant and H_{fuel} stands for the chemical energy supplied in the form of biomass fuel based on the lower heating value. This rate is particularly relevant for assessments over extended periods, such as a calendar year, which accounts for varying operational conditions and inherent energy losses throughout the entire system [35].

As mentioned above, the annual average biomass utilization rate typically reaches up to approximately 80 %. Implementing a flue gas condenser in the plant can potentially increase the fuel utilization rate by up to 30 % under certain conditions [22]. When the lower heating value (LHV) is used as the benchmark, this improvement can theoretically result in an efficiency exceeding 100 %. By definition, The LHV accounts only for the energy released when the water produced during combustion remains in vapor form [54]. Thus, the latent heat released when the fuel's water is converted from gaseous to liquid is not considered in equation (1). With a flue gas condenser, the heat of condensation can be utilized, making efficiencies greater than 100 % possible. Boilers that incorporate this technology are commonly known as condensing boilers due to their ability to condense the exhaust gas and capture this additional heat.

There are various options for extracting heat from the exhaust gas. This can be achieved by means of a non-contact heat exchanger in the exhaust gas path or by direct contact of the exhaust gas with the cooling medium [22]. A compact overview of both variants is provided by Figure 4.

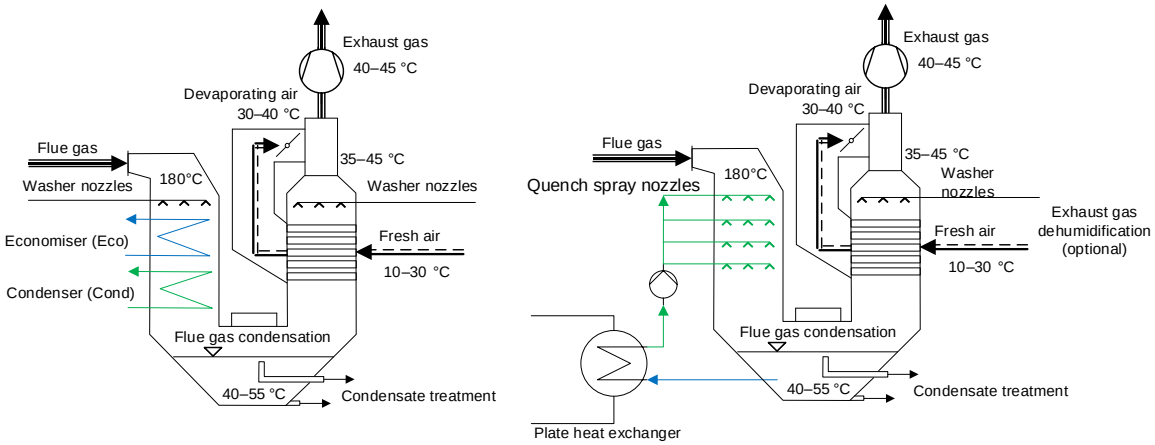

Figure 4: Condensation of water vapor in the flue gas, left: Indirect-contact flue gas condensation using heat exchange bundles, right: Direct-contact flue gas condensation by means of injection of quench water (evaporative cooling and subcooling) (own representation, adapted from [17]).

Indirect-contact flue gas condensation

In indirect-contact flue gas condensation, the cooling medium circulates through the condenser tube bundle within the heat exchanger, facilitating heat transfer between the exhaust gas and the cooling medium without direct contact. This can employ either plate heat exchangers or shell-and-tube heat exchangers. According to [22], shell-and-tube heat exchangers are often preferred due to their lower maintenance and cleaning requirements.

A variety of materials are suitable for use in these heat exchangers, with stainless steels being the most utilized due to their durability and corrosion resistance. Other materials like ceramics, carbon, and glass are less frequently used, due to specific considerations such as cost, availability, or performance characteristics in certain environments.

The heat transferred can be calculated using the general formula:

$$\dot{Q}_{hex} = U * A * \Delta T_m \tag{2}$$

Where $\dot{Q}_{hex}$ represents the heat transfer rate. *A* represents the total heat transfer area. ΔT_m is the logarithmic mean temperature difference between the two fluids in the heat exchanger. And *U* is the total heat transfer coefficient (W/m^2K).

During design of a heat exchanger, determining the correct value of the total heat transfer coefficient *U* is essential but often imprecise [55]. This coefficient is influenced by various factors, including the geometry of the heat exchanger, the material of pipes and the coating layers, as well as the physical properties of the flue gas such as its density, viscosity, thermal capacity, thermal conductivity. Additionally, the properties and flow rate of the cooling medium also affect the *U* value. The determination of *U* requires an experimental approach, the exact calculation method is described in Appendix A.

Direct-contact flue gas condensation

In contrast to the above-mentioned structure, an alternative structural design of flue gas condensation is the use of substantial quantities of water, as depicted in Figure 4 (right). In this configuration, the flue gas comes into direct contact with circulating water, allowing for simultaneous heat and mass transfer. The water vapor in the flue gas condenses upon contact with the cooler circulating water, transferring its latent heat to it. Following this, the heated circulating water will be recooled by the return flow from the local heating network. This

recooling process occurs through an additional heat exchanger, which is situated externally to the condenser.

The working principle of direct-contact flue gas condensation can be expressed by the following mass and energy balance equations:

$$\dot{m}_{fg,dry}^{in} * x_{H20,fg,in} + \dot{m}_{cw}^{in} = \dot{m}_{fg,dry}^{out} * x_{sat\ H20,fg,cond} + \dot{m}_{cw}^{out} \quad (3)$$

Where $\dot{m}_{fg,dry}^{in}$ and $\dot{m}_{fg,dry}^{out}$ are the dry mass flow rates of inlet and outlet flue gas (kg/s), respectively, which should be the same. $x_{H20,fg,in}$ denotes the water vapor content of the flue gas entering the condenser ($kg_{H20}/kg_{fg,\ dry}$), while $x_{sat\ H20,fg,cond}$ denotes the saturated water vapor content at the average temperature of the condensing surface ($kg_{H20}/kg_{fg,\ dry}$). $\dot{m}_{cw}^{in}$ and $\dot{m}_{cw}^{out}$ represent the mass flow rates of the cooling water at the inlet and outlet (kg/s), respectively.

$$\dot{m}_{fg,dry}^{in} * \left(h_{fg,dry}^{in} + x_{H20,fg,in} * h_{H20,fg,in}^{in}\right) + \dot{m}_{cw}^{in} * h_{cw}^{in} = \dot{m}_{fg,dry}^{out} * \left(h_{fg,dry}^{out} + x_{sat\ H20,fg,cond} * h_{sat\ H20,fg,cond}^{out}\right) + \dot{m}_{cw}^{out} * h_{cw}^{out} \quad (4)$$

In this equation, $h_{fg,dry}^{in}$, $h_{H20,fg,in}^{in}$, h_{cw}^{in}, $h_{fg,dry}^{out}$, $h_{sat\ H20,fg,cond}^{out}$, and h_{cw}^{out} indicate enthalpies of the respective flows at their corresponding temperatures (kJ/kgK). The heat transfer rate can be calculated as:

$$\dot{Q}_{hex} = \dot{m}_{cw}^{out} * h_{cw}^{out} - \dot{m}_{cw}^{in} * h_{cw}^{in} \quad (5)$$

The primary drawback of the direct-contact flue gas condensation is the high electrical energy consumption, which is necessary for pumping the substantial volumes of quench water. Additionally, this method is prone to lime deposits forming in the condenser. The advantage is a low susceptibility to corrosion due to the highly diluted and wet operation. The main product suppliers for large-scale plants are the companies Scheuch, Heger and SaveEnergy from Austria and Switzerland.

It is observed from available data that most plants in practice tend to favor the indirect-contact flue gas condenser over the direct-contact method.

Both the indirect-contact and direct-contact flue gas condensation systems, in addition to their cooling effects, contribute to reducing particulate emissions from the exhaust gas. On the one hand, soot and ash particles separate on water droplets and can thus be discharged together as condensate sludge. On the other hand, the lower temperatures achieved also lead

to the condensation of unburned, volatile hydrocarbons, which would otherwise appear as aerosols in the exhaust gas. However, the process of particle separation can present challenges. If the design of the equipment does not adequately account for the removal of the generated condensate sludge, it can lead to increased maintenance demands. To mitigate this, it is recommended that an electrostatic precipitator should be installed upstream of the flue gas condensation system [47]. Additionally, the treatment of the condensate is a critical aspect of the system's design. Typically, at least one settling tank is necessary for the process. Depending on the pH value, it may also be necessary to add (sodium) hydroxide solution for neutralization to reduce the solubility of heavy metals, as the fine particles separated here are heavily contaminated [56].

Possibilities for using the residual heat in the exhaust gas after condensation are described in [17]. Due to its low temperature, this heat is technically viable mainly for air preheating. This heat can be utilized either to preheat the combustion air, enhancing the plant efficiency, or to warm up the de-vaporization air to reduce the energy demand for ventilation, as shown in Figure 4.

Besides, it should be noted that the term “flue gas condensation system” in the figure - as is sometimes the case in practice – may refer not only to the individual component condenser, but also the entire setup encompassing the economizer, condenser and de-vaporization unit.

In the design of a flue gas condensation system, one common issue is the non-optimal design of the heat exchanger's gas flow, including flow rate and temperature. This problem can significantly diminish the performance of the system. A notable challenge arises in heating networks with fluctuating temperatures. The fluctuating network temperatures in heating networks can disrupt continuous operation and full gas condensation, increasing corrosion risks and potentially damaging the heat exchanger. This can lead to the accelerated degradation of the heat exchanger due to the accumulation of corrosive compounds on its surface and subsequent corrosion.

A promising solution to this issue is the integration of heat pumps, which is the key focus of the research discussed in this work and will be further elaborated in the following content.

2.2.2 Influencing variables

The efficiency gain achieved through flue gas condensation is significantly influenced by several key factors, including air ratio of combustion, exhaust gas temperature after the condenser (which depends on the temperature level of the cooling medium, for example, the return flow of the district heating network) and the fuel water content.

Air ratio

The air ratio is specified as a dimensionless number λ, which represents the ratio of the actual volume of air supplied for combustion m_{air} to the minimum amount of air required for complete combustion of the fuel $m_{air,min}$ [57].

$$\lambda = \frac{m_{air}}{m_{air,min}} \tag{6}$$

To achieve complete oxidation of the fuel, sufficient combustion air must be available. The minimum required air volume $m_{air,min}$ describes the stoichiometrically necessary amount of air for the complete chemical combustion of the fuel. Since the mixing of combustion gases and fresh combustion air in the combustion chamber is not always optimal, in practice more fresh air is supplied than is stoichiometrically necessary. This results in an air ratio λ of between 1.2 and 2.7 [39]. Additionally, there is an alternative formula for determining the air ratio, which is based on the measurement of certain gas properties and is detailed in [58].

$$\lambda = \frac{21}{21 - O_{2,dry}} \tag{7}$$

In this process, the excess air ratio λ is determined by the dry volume concentration of oxygen in the dry flue gas. $O_{2,dry}$, which is easy to be measured. This method offers a different approach to calculating λ, often used for its practicality in operational settings.

In the context of flue gas condensation, a low air ratio is beneficial for enhancing efficiency. A lower air ratio leads to more effective flue gas condensation, because it reduces the "dilution" of the flue gas with air, which in turn maintains a higher moisture content in the flue gas. High moisture levels are conducive to condensation, facilitating the release of latent heat from the exhaust gas. Thus, it is crucial to avoid excess mixing of water vapor with combustion air by minimizing the air ratio.

To ensure complete fuel combustion despite a lower air ratio, flue gas recirculation can be implemented in the flue gas path. This process involves recycling cooled-down flue gases back into the furnace. Typically, flue gas is extracted at temperatures between 100-200 °C either downstream of the boiler econmiser, or downstream of the flue gas cleaning units. These flue gases have a low residual oxygen content. By feeding them back into the combustion process, the air ratio λ can be lowered, which reduces the residual oxygen content in the flue gas. In addition to the positive effect on flue gas condensation, The flue gas recirculation can also contribute to reducing NO_x and CO emissions [59]. Additionally, flue gas recirculation can help maintain lower combustion temperatures, ensuring that the temperature remains below the ash softening point. This aspect is crucial for preventing operational issues related to ash handling and deposition [17].

Fuel water content

The efficiency improvement obtained through flue gas condensation is also significantly influenced by the fuel water content. The definition of the fuel water content is the ratio of the mass of water in the fuel m_W to the sum of the mass of the absolutely dry fuel $m_{fuel,dry}$ and the mass of water in the fuel m_W [60]:

$$w = \frac{m_W}{m_{fuel,dry} + m_W} \tag{8}$$

The proportion of water in the fuel is usually specified as fuel water content. Alternatively, it can also be given as fuel moisture u. The conversion from fuel moisture u to fuel water content w is performed according to the following equation [60]:

$$w = \frac{100 * u}{100 + u} \tag{9}$$

Increased fuel moisture, resulting in a higher amount of water vapor in flue gas, is favorable for flue gas condensation. Thus, drying the fuel in conjunction with flue gas condensation should generally be avoided, as it decreases the efficiency of the condensation process. Even though fuel drying can provide some benefits, such as stabilizing the combustion process and reducing storage losses [61].

In addition, as described in section 2.1.1, increased fuel moisture is often advantageous, particularly in keeping the combustion temperature low. This aspect is crucial because if the furnace temperature is above the ash softening temperature, it leads to the formation

of deposits. Such deposits can significantly impair heat transfer within the boiler, affecting its efficiency and potentially leading to operational challenges [58].

Exhaust gas temperature

Another parameter associated with the efficiency increase through flue gas condensation is the exhaust gas temperature after the condenser. This temperature provides an indication of how much heat has been removed from the flue gas by condensation. The exhaust gas temperature after the condenser corresponds to the lowest temperature level of the heat demand, which is typically associated with the return flow of the district heating network. The return flow from the local heating network or from other heat consumers has a system-dependent temperature, which represents the minimum temperature to which the flue gas can be cooled. A lower temperature level of this return flow enables more extensive cooling of the flue gas, thereby enhancing the efficiency of the flue gas condensation process.

This relationship is illustrated in Figure 5. Under the specific conditions on which Figure 5 is based (ambient pressure 1.013 bar, wood chips as fuel), the flue gas condenses from approx. 70 °C onwards. The diagram clearly shows that the slope of the curve changes sharply at a specific temperature point. The further the gas temperature falls below the condensation temperature, the more effective the flue gas condensation. As the exhaust gas temperature falls below the condensation temperature, an increasing amount of latent heat becomes usable, which increases the boiler efficiency to a maximum of 117 %.

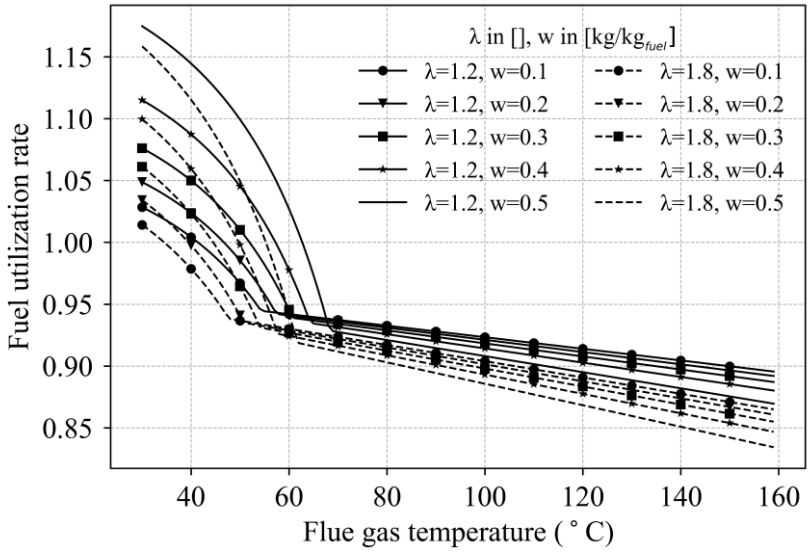

Figure 5: Example of the boiler efficiency of a wood chip biomass boiler related to the lower heating value as a function of the flue gas temperature (own illustration based on a simple simulation).

2.2.3 Current status and challenges

Flue gas condensing technology is now already standard in fossil-fuel firing systems based on natural gas and heating oil, which has been already fully recognized and implemented in household. However, for biomass heating networks, flue gas condensation is not yet broadly applied. Only due to external legal pressure within the framework of the Ecodesign Directive [62] and the tightening of the emission limits [63,64], manufacturers of small boilers are increasingly considering the integration of flue gas condensation technology as a supplementary feature to enhance the functionality of the boiler. In the small capacity range, for example, This concept has been already realized by manufactures, like Ökofen [65] and Fröling [66], as integrated components.

For biomass heating plants with medium capacity, flue gas condensation technology is still rare, despite its advantages. This is mainly attributed to the high return temperatures prevalent in existing heating networks [67]. Most old networks have a return temperature of more than 55 °C, while effective flue gas condensation typically requires temperatures below this threshold [17]. Consequently, water vapor condensation in the flue gas condenser is impeded without additional interventions, preventing the direct utilization of the flue gas's latent heat.

In Germany, heating networks with low return temperatures have been demonstrated mainly in research projects, often in combination with solar thermal systems. One example is the heat supply at the Ackermannbogen in Munich [68]. Achieving such low return temperatures requires meticulous planning and implementation, which is not common in current standard practices. For this reason, only few networks have return temperatures of below 55 °C. Modifying the return temperature in existing networks is challenging and must be assessed on a case-by-case basis, which hinders the straightforward implementation of condensation technologies.

Furthermore, the operation of a flue gas condensation system in the existing plants is seen as critical if the network return temperature fluctuates strongly. Fluctuating temperatures, especially when the temperature is often above 55 °C, can lead to intermittent condensation, causing severe corrosion efffects and rapid deterioration of the condensation system [69].

Heat pump technology offers a solution in such scenarios. By cooling the flue gas in the condenser or by cooling the network return, the heat pump ensures that the flue gas

temperature reliably falls below the dew point temperature. It also elevates the temperature level of the recovered heat to match the local heating network, allowing for the utilization of latent heat. In addition, heat pumps stabilize the temperature in the condenser heat exchanger bundles, thus enabling the reliable use of the flue gas condensation even in existing heating networks with high return temperature levels.

2.3 Heat pump

As mentioned above, the challenge of operating flue gas condensation can be effectively addressed through the integration of a heat pump. The integrated heat pump cools the flue gas, either directly or indirectly, ensuring that its temperature reliably falls below the dew point temperature.

In general, a heat pump refers to a technical device that extracts heat at a low temperature and releases it at a higher temperature level [70]. Numerous options are available to achieve this, based on various physical phenomena. In practice, two main types of heat pump are employed: the compression heat pump and the absorption heat pump. This section first introduces the technical basis of these two types of heat pumps in section 2.3.1 and section 2.3.2, respectively. Then the current status of their research and application in heat recovery is presented in section 2.3.3. Finally, section 2.3.4 compares the pros and cons of the two types of heat pumps and establishes the research focus of this thesis.

2.3.1 Compression heat pumps

The compression heat pump typically operates on the Reversed Clausius-Rankine process (counterclockwise) [71], also known as the vapor-compression refrigeration cycle. Additionally, it is possible to develop a heat pump based on a reversed Joule process [72]. However, as this technology is not yet considered state of the art, this work focuses exclusively on the conventional compression heat pump. This involves a counterclockwise cycle in the wet steam region of the working fluid with 4 steps: compression, condensation, expansion and evaporation.

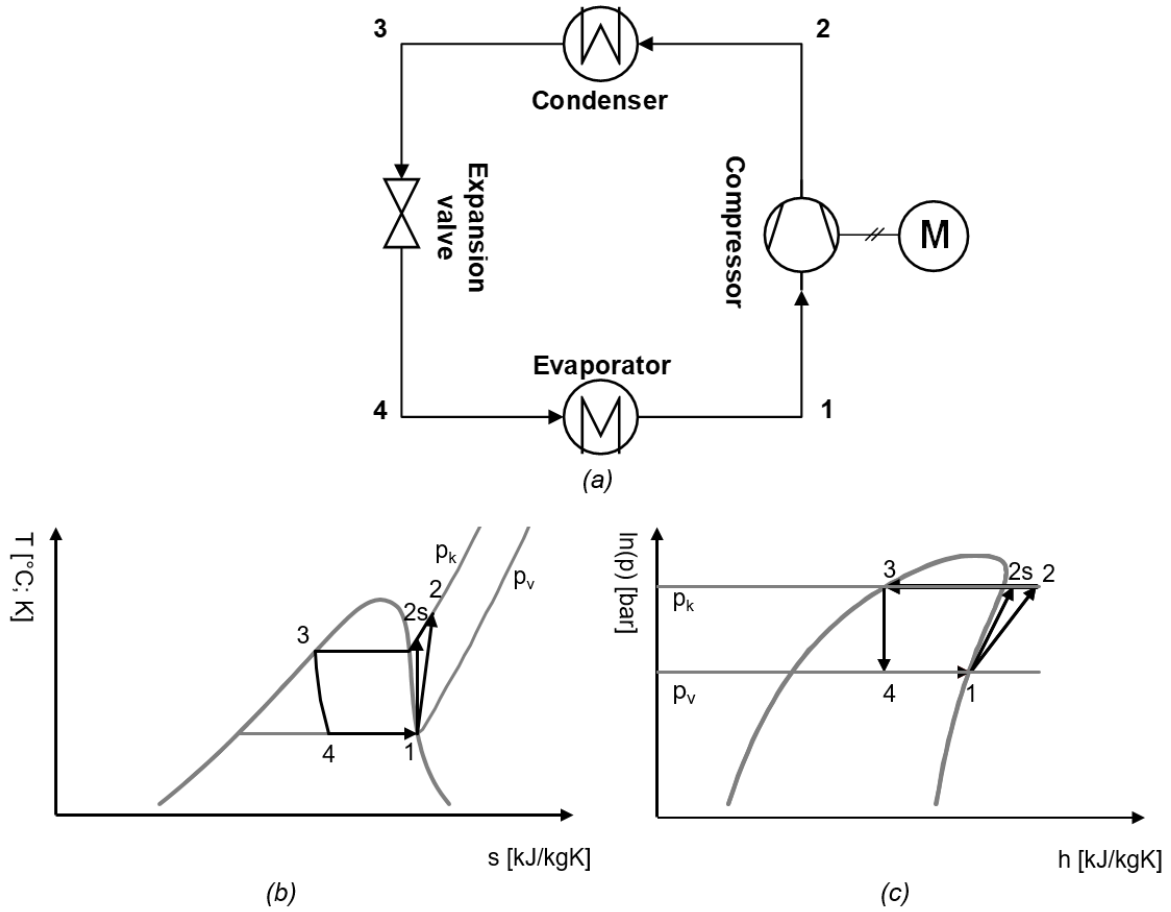

Figure 6: Simplified scheme of a heat pump (a) and the thermodynamic cycle of a heat pump: T-s-diagram (b); ln p-h-diagram (c) (own illustration).

Ideally, the compression and expansion processes are isentropic, while the evaporation (heat gain) and condensation (heat dissipation) processes are isobaric. The expansion process is typically implemented using an adiabatic throttling valve. A schematic representation of the heat pump and the corresponding thermodynamic diagrams are presented in Figure 6. However, in practice, the phase transition process often does not end precisely at the saturation or dew point of the working medium. Instead, it typically involves subcooling of the saturated liquid and superheating of the saturated vapor. Additionally, technical power losses in the compressor cause the 'isentropic' state changes in the T-s diagram to appear inclined. Furthermore, the isobaric state change of the refrigerant cannot be fully realized due to the flow pressure loss [73].

The four steps of the heat pump are implemented by four main components, as depicted in Figure 6. Among these, the most important component is the compressor, which has different construction designs and working principles.

Compressors

The design of a compressor can vary significantly, regardless of the working principles. In [74], compressors are classified into hermetic, semi-hermetic and open design, as illustrated in Figure 7. The hermetic design, characterized by the motor and compressor being enclosed in a sealed housing, is prevalent in low-capacity applications like refrigerators and household heat pumps. This design's primary advantage is the elimination of rotary unions, allowing for simple and reliable sealing. Additionally, the refrigerant cools the motor, enhancing efficiency. However, this design may be problematic, or even unsuitable, for aggressive media such as ammonia [75]. A notable disadvantage of the hermetic design is the difficulty in conducting repairs or maintenance. In cases where maintenance is necessary, such as in heavily used industrial plants, the semi-hermetic design is preferable. This design features a joint, separable housing for the compressor and motor, granting access to the internal components. For higher capacities or when more flexibility is required in the drive mechanism, the open design is chosen. In this design, the compressor is a separate unit from the motor, with power transmitted via a shaft extending out of the compressor housing, which requires radial sealing.

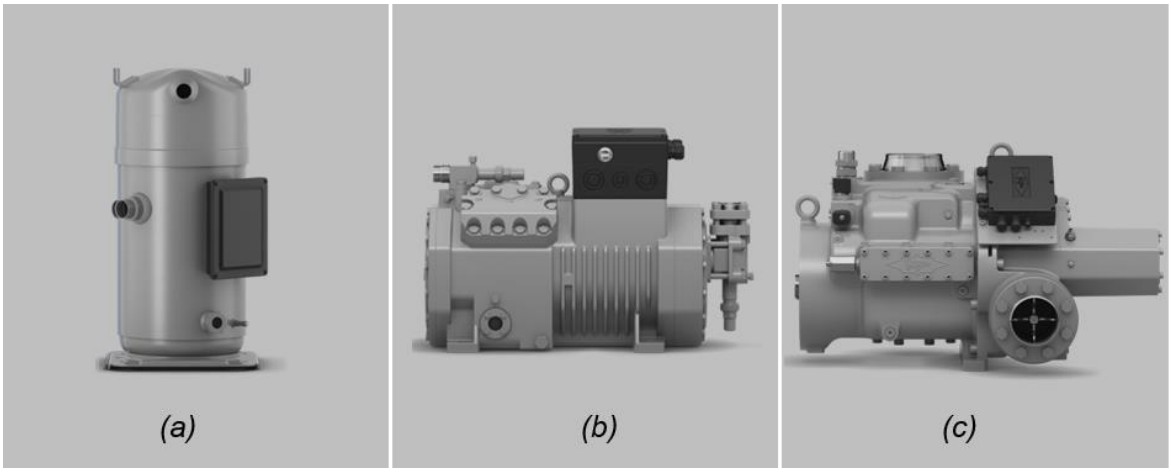

Figure 7: Compressors with different designs: (a) hermetic [76], (b) semi-hermetic [77], (c) open [78].

With regard to the working principles, there are also several possibilities for implementation, such as piston, screw, scroll, or turbo compressors (as seen in Figure 8).

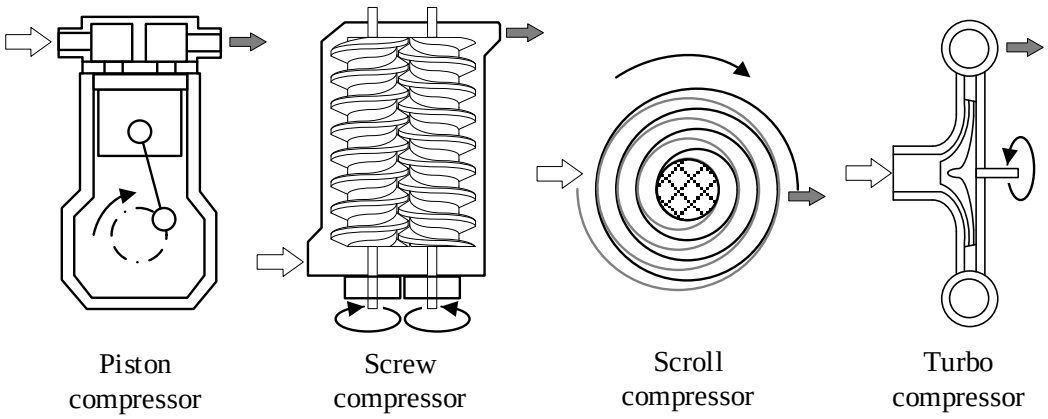

Figure 8: Compressors with different working principles (own illustration, adapted from [79]).

Piston compressors: Also known as reciprocating compressors, piston compressors are the oldest type, being relatively simple to manufacture and seal [80]. Their design is comparable to that of a piston engine, presenting similar challenges in compensating for vibrations. For internal power control, cylinder deactivation is predominantly used, whereby the number of partial load stages depends on the number of cylinders [81]. The achievable pressure ratios may be limited by the polytropic compression, due to the maximum permissible heating of the gas [82].

Screw compressors: Positioned in the medium performance segment, screw compressors are more complex to manufacture but offer maintenance advantages due to low mechanical wear [82]. However, the average efficiencies are worse than those of piston compressors, mainly due to frequent part-load operation. Performance adjustment within the compressor is possible through the use of a control slide valve, which reduces the active rotor length as necessary [81].

Scroll compressors: Often found in the low power range (up to a few kW), scroll compressors are limited in market capacity range to this segment. They are typically hermetically sealed [74] and have a comparatively simple design requiring minimal maintenance. The possibilities for internal capacity control are limited, since these measures are either less efficient (e.g. bypass) or complex to implement [74].

Turbo compressors: Turbo compressors are categorized into centrifugal and axial types [83]. In axial design, the gas flows parallel to the shaft. While in centrifugal design, the gas enters axially into the impeller and is then deflected outward (radially). Therefore, Multi-stage compressors with radial designs require flow diversion after each stage. Generally,

axial compressors deliver higher flow rates, while centrifugal compressors produce higher pressures. The combined design draws a large volume flow through its axial stage group, which is then compressed to a high pressure in the subsequent radial stage group. Diagonal compressors [84] , for example, are a combination of these two principles.

An important metric for evaluating and comparing compressors is the pressure ratio (equation (10)). This ratio indicates the pressure increase between the suction and discharge sides of the compressor. The delivery performance, determined by the pressure difference, varies significantly based on the working principle.

$$\pi = \frac{p_c}{p_e} \tag{10}$$

However, if a desired pressure ratio cannot be achieved with a single compressor or the favored working principle, it is not necessary to switch to another type: Multi-stage compression, i.e. the serial connection of several compressors, offers the possibility to attain higher pressures and is available on the market as a specialized, integrated component.

Furthermore, efficiency in compression is another key figure of a compressor. Losses occur due to non-ideal isentropic compression, additional mechanical losses in the compressor (such as friction on bearings, etc.) and motor efficiency. Motors are usually electrically driven, and modern electric machines, often controlled via power electronics (e.g., frequency converters), may also contribute to losses. These factors influence both the energy consumption and the gas discharge temperature of the compressor. There are significant differences in this regard among various compressor designs. In (semi-)hermetic compressors, the working medium cools all system components, potentially including any power electronics. Therefore, all power loss flows could contribute to the heating of the refrigerant. Conversely, in open-design compressors, standard electric machines typically dissipate waste heat to the ambient air via cooling fins, omitting this heat flow. With regard to the working principles, screw compressors are internally cooled by injected oil, which allows almost isothermal compression [82]. Similarly, the cylinder heads of piston compressors can be cooled by oil or water, dissipating heat or repurposing it for other uses.

Refrigerant

A wide range of working fluids is available for compression heat pumps. Depending on the application scenario, heat pumps have different requirements on refrigerants [85]. The

choice of refrigerant can be considered from three aspects: chemical-physical properties, safety risks, environmental factor.

Chemical-physical properties and their suitability for specific applications are typically evaluated based on parameters such as specific evaporation enthalpy, boiling temperature at ambient pressure, pressure ratio, and the critical point. Thermodynamically, the refrigerant's vapor pressure curve is particularly significant, which influences the specific evaporation enthalpy. A broader wet steam range at evaporating and condensing temperatures allows for greater heat recovery and supply at a constant power input. During the design, it should also be noted that the pressure in the entire system never falls below ambient pressure to prevent the ingress of foreign matter [86]. This necessitates specific requirements for the refrigerant's boiling temperature at ambient pressure. Moreover, to avoid excessively high equipment construction costs, the maximum pressure of the system should be reasonably limited, which is why a low pressure ratio is desirable. Additionally, the minimum evaporation temperature is constrained by the triple point, and depending on the equipment's design, the critical point may set an upper limit for the maximum condensation temperature.

Possible safety risks are also critical for the operation of compression heat pumps. These risks include toxicity, flammability and combustibility of the refrigerants. The potential hazards of refrigerants evaluated according to EN 378-1 [87], with an overview presented in Table 1. Where the letters ‘A’ or ‘B’ stand for the toxicity class, while ‘1’, ‘2L’, ‘2’, or ‘3’ designate the flammability class. The designation of refrigerants is regulated at international level in ISO 817 [88]. Additionally, in Germany, DIN 8960 is applicable, which incorporates the designations from ISO 817 [89]. Depending on factors such as toxicity, flammability and construction of the heat pump, the maximum permissible refrigerant charge of a system may be limited [87]. Moreover, it is essential to consider the potential corrosive effects of the refrigerant, its compatibility with other components such as seals, and the solubility of lubricating oil in the refrigerant [90].

Table 1: Refrigerant safety groups with corresponding examples [29].

	Low toxicity	***Higher toxicity***
Higher flammability	**A3** Hydrocarbons: R170, RE170, R290, R1270, R600, R600a, R601, R601A ***L3***	**B3** no any
Low flammability	**A2** R152a ***L2***	**B2** R30
Low flammability and flame spread< 10 cm/s	**A2L** R32, R143a, R1234yf, R1234ze	**B2L** R717
no flame preparation	**A1** R125, R134a, R236fa, R-C318, R407A bis R407F, R410A, R417A, R417B, R422A bis R422D, R424A, R507A, R513A, R744 ***L1***	**B1** R123, R245fa

Futhermore, the environmental impact of refrigerants also plays a decisive role, governed by the corresponding legislation. The Ozone Depletion Potential (ODP) and Global Warming Potential (GWP) of these substances are highly correlated. For ODP, the Montreal Protocol is decisive [91]. In the Montreal Protocol, the reduction of the production and use of ozone-depleting substances was agreed at the international level in 1987. "Safety refrigerants" such as R11, R12 or R22, which were widely used at the time as working fluids in air-conditioning units [73], belong to the category of chlorofluorocarbons (CFCs), which harm the earth's ozone layer upon atmospheric release. Consequently, a phased ban on the production and sale of CFCs was enforced, leading to their near-complete prohibition by 2000. With the decline of CFCs, attention has shifted from ODP to GWP, which measures the climate impact of a substance over a 100-year period, using CO_2 as a baseline. Where CO_2 has a value of 1 by definition. In this context, emissions are often expressed in terms of CO2 equivalents. For example, R134a, a frequent CFC substitute, has a GWP of 1430 [92], meaning 1 kg of R134a equates to 1430 kg of CO_2 emissions.

In efforts to reduce greenhouse emissions, the EU implemented the F-Gases Regulation. Effective from 01.01.2020, this regulation prohibits the use of refrigerants with a GWP of 2500 or higher in systems with a charge of 40 t CO2 equivalent or more, except in certain cases [93]. As a further measure, companies selling refrigerants are subject to annually decreasing quotas (in tons of CO_2 equivalent), a strategy known as “phasedown” [93,94]. R134a is officiallybanned on new refrigeration equipment since 2022. Manufacturers of refrigeration systems have been interested in alternatives with lower GWPs. It is noteworthy that the climate impact of a refrigerant is significant only when it is released into the atmosphere; therefore, various measures are in place to minimize the releases [94].

Given these considerations, the design of a heat pump must ensure that the chosen working medium is legally available at reasonable prices throughout the system's lifecycle or that it can be replaced by a suitable alternative if necessary.

In addition to single-component refrigerants, compression heat pumps can also utilize mixtures of different media. The motivation behind is to achieve improved properties compared to individual substances. This is particularly relevant when seeking suitable replacements for refrigerants that are phased out (e.g., due to their ozone depletion potential), allowing existing systems to be retrofitted with minimal technical modifications [90].

Key performance indicators of compression heat pumps

A heat pump is distinguished by its high energy efficiency. In the technical field, this value is often quantified as the Coefficient of Performance (COP). According to [95], the COP of a heat pump is defined as:

$$COP = \frac{\dot{Q}_{sink}}{P_{comp}} \tag{11}$$

Here is $\dot{Q}_{sink}$ the usable heat flow for heat sink and P_{comp} the mechanical or electrical power supplied to the compressor. If necessary, additional auxiliary energy for e.g. pumps should also be included. Also of interest is the COP of the ideal Carnot process operating between the same temperature levels, which represents its maximum possible value.

$$COP_{carnot} = \frac{T_c}{T_c - T_e} \tag{12}$$

Where T_e is the evaporation temperature and T_c the condensation temperature. This formula demonstrates that the highest possible COP is primarily achieved through a low temperature lift in the heat pump. To describe how closely a real heat pump process approximates the theoretical ideal, the relative coefficient of performance $\eta_{relative}$ is defined:

$$\eta_{relative} = \frac{COP_{real}}{COP_{carnot}} \tag{13}$$

This metric provides a measure of the quality of the process that is independent of the temperature levels. In principle, this metric can be applied to all types of compression heat pumps to assess the equipment quality.

2.3.2 Absorption heat pumps

Absorption heat pumps differ from compression heat pumps in that they are driven by heat rather than mechanical work. While the refrigerant cycle process in absorption heat pumps is fundamentally similar to that of a compression heat pump (Section 2.3.1), the key difference lies in the way the refrigerant is handled. Instead of being compressed mechanically, the refrigerant in an absorption heat pump is absorbed into and subsequently desorbed from a medium. Consequently, absorption heat pumps do not use a single refrigerant but a working pair, consisting of refrigerant and solven [73]. example of such a pair is ammonia/water, where ammonia serves as the refrigerant and water as the solvent, representing the oldest known working fluid pair.

The schematic structure of a absorption heat pump is shown in Figure 9. The total system can be divided conceptually into two individual circuits: The refrigerant circuit (illustrated on the left) and the solution circuit (shown on the right). Both the solvent and working medium flow through the solution circuit, while only working medium flows in the refrigerant circuit. If a balance envelope around the solution circuit is drawn and considered as a single component, the same structure is obtained as in the diagram for a compression heat pump, as shown in Figure 6. The primary distinction is that in absorption heat pumps, heat is supplied to the 'compressor' instead of mechanical work. Therefore, the description of the refrigerant circuit can be referred to section 2.3.1. Following [73] the solution circuit, which functions as the "thermal compressor", may be described as follows.

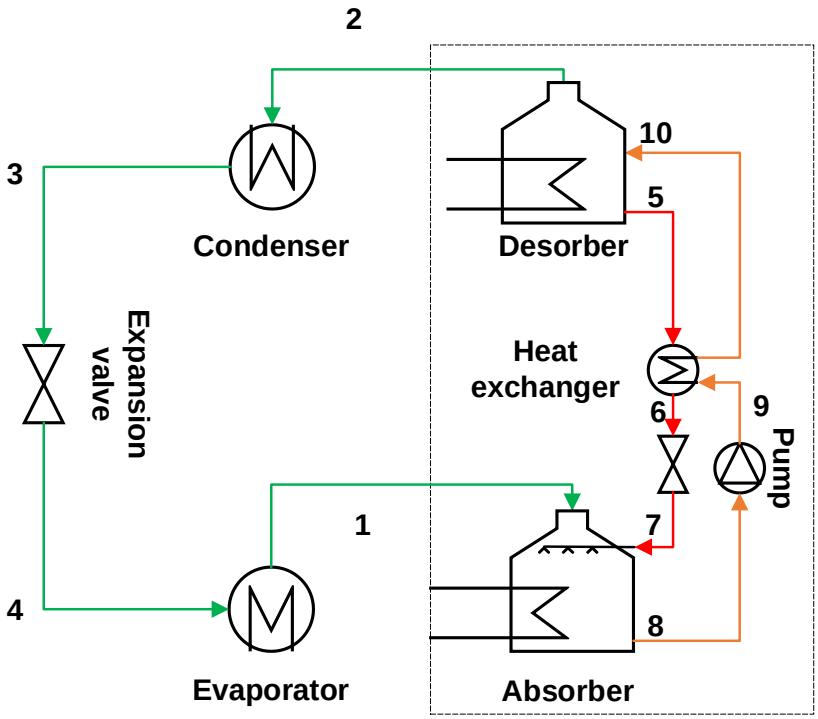

Figure 9: Schematic structure of a sorption heat pump (own illustration).

First, evaporated working medium at state 1, along with a mixture of solvent and working medium at state 7 (termed the “poor solution”), enters the absorber at low pressure. In the absorber, the refrigerant vapor is absorbed by the poor solution, transforming it into a rich solution and releasing heat in the process. The rich solution after absorption is then pumped to a higher pressure level by the solution pump. Subsequently, it passes through a heat exchanger (an optional feature for efficiency enhancement) before entering the desorber. Within this internal heat exchanger, the rich solution is heated while the poor solution is cooled. In the desorber, external heat is supplied, causing the working medium to vaporize at the high pressure level and proceed to the refrigerant circuit. The depleted poor solution then returns to the absorber via the heat exchanger, undergoing expansion through a throttle valve.

This circuit essentially compresses the refrigerant via heat supply rather than mechanical work, introducing two additional heat flows: heat gain in the desorber and heat release in the absorber, alongside the existing heat flows in the evaporator and condenser. However, all four temperature levels are different. The heat input for driving out the refrigerant in the desorber must be at a higher temperature than the useful heat output from the condenser. Additionally, the heat released in the absorber should be at the same or a slightly lower

temperature than the condensing temperature, allowing for its utilization. The maximum achievable temperature of the useful heat thus depends on the temperature of the "drive heat" for the desorber.

Further limitations resulting from the working fluid pair also need to be considered. The maximal pressure in the system must not exceed a technically viable level. This is a key reason for preferring water-lithium bromide over ammonia-water at temperatures above 0 °C. However, this preference imposes a evaporating temperature limit of due to the need to maintain a safe margin above the mixture's crystallization temperature.

Key performance indicators of absorption heat pumps

For absorption heat pumps, performance evaluation differs from that of compression heat pumps. It is assessed using a heat ratio ζ or COPW (equation (14)), which represents the ratio between useful heat dissipated for heat sink $\dot{Q}_{sink}$ and supplied drive heat $\dot{Q}_{des}$ for desorber [17,73].

$$COPW = \frac{\dot{Q}_{sink}}{\dot{Q}_{des}} \tag{14}$$

The drive power of the solvent pump is neglected, as it is significantly smaller compared to the heat flows [73]. To compare the real process with an ideal one, the heat ratio of the ideal process $COPW_{max}$ is used as a benchmark, which is defined as:

$$COPW_{max} = \frac{T_c}{T_c - T_e} * \frac{T_h - T_c}{T_h} \tag{15}$$

Here T_h indicates the temperature of the heat source. The quality of the real process compared to an ideal one can also be accessed using the the relative coefficient of performance $\eta_{relative}$:

$$\eta_{relative} = \frac{COPW}{COPW_{max}} \tag{16}$$

2.3.3 Heat pump for heat recovery

The integration of a heat pump with a flue gas condenser has been emphasized as an effective method for heat recovery in numerous studies, introducing it as a viable solution. This approach, known as active condensation, requires additional energy input. Chua et al.

[96] conducted a review of various innovative applications of heat pump systems, demonstrating their effective integration into energy systems through the utilization of waste heat. Similarly, Wang et al. [97] proposed a guideline for integrating various heat pump solutions into industrial processes to achieve low-value waste heat utilization. Depending on the connection variants, different heat pump integration concepts can also be implemented for district heating. Furthermore, Kahrman and Celebi [98] explored the feasibility of integrating a heat pump for waste heat recovery into district heating. This research supports the suitability of heat pumps as a heat recovery solution in numerous countries.

Heat recovery through absorption heat pumps

Several studies have concentrated on combining flue gas condensation with absorption heat pumps. A primary advantage of absorption heat pumps is that they use thermal energy as the "driver" rather than the more expensive electrical energy. This provides significant economic benefits, when an existing heat source is available [99]. Wang et al. [100] and Zhang et al. [101] studied on absorption heat pump systems for simultaneous recovery of heat and water from flue gas with high humidity for coal-fired plants, demonstrating its ability to effectively improve coal utilization. Qu et al. [102] investigated various configurations of integrating an absorption heat pump coupled with a non-contact flue gas condenser. The results demonstrated a 5-10% increase in boiler efficiency for the experimental unit. In addition, Zhu et al. [103] simulated the combination of an absorption heat pump with an open flue gas condensing system for a gas boiler. And Wei et al. 2015 [104] have proposed an approach to recover waste heat from the flue gas of a gas boiler using an open-loop absorption heat pump. Both results by Zhu et al. and Wang et al. showed an improvement of approx. 12% in boiler efficiencies. To further improve the efficiency, Lu et al. [105] developed a cascade heat recovery system based on an absorption heat pump for district heating, which achieved about 40% of primary energy savings compared to a conventional single gas-fired boiler system.

In experimental research, Yang et al. [106,107] tested a full-open absorption heat pump for total recovery of heat from flue gas, which recovered up to 178 % more heat than a single condensing system, though the achieved COPW was only up to 1.62. Similarly, Keil et al. [108] studied three customized absorption heat pumps in southern Germany, also observing a relatively low COPW in the context of heat recovery in district heating systems.

Heat recovery through compression heat pump

Alternatively, some research has focused on integrating compression heat pumps for heat recovery, as this technology is mature, robust, and widely available in the market. According to the IEA's heat pump program report (Annex 35) [28], the majority of existing heat pump projects employ compression technology, a trend also evident in studies mentioned in [29,109]. Futhermore, Xiao et al. [30] conducted a summary of heat pump applications in German district heating systems, revealing that over 70 % utilized compression technology.

There are different ways to integration compression heat pumps into heating networks. Sayegh et al. [110] described the possibility of incorporating compression heat pumps into district heating in terms of the placement, connection and operation modes. And Marguerite et al. [109] summarized the various ways to integrate compression heat pumps into district energy systems and provided examples of applications that have been implemented around the world. From the literature, two primary concepts emerge for integrating compression heat pumps for flue gas heat recovery in district heating:

Flue-Side Integration Concept: In this approach, the evaporator is directly or indirectly connected to the flue gas condenser via a heat exchanger. Jamil et al. [111] applied this concept to enhance the efficiency of a gas boiler, which showed an efficiency improvement of 11.47 % when reducing flue gas temperature from 120 °C to 30 °C. Shamsi et al. [112] presented a novel condensation system that combines an organic Rankine cycle and a compression heat pump to maximize the efficiency of a thermal power plant.

Network-Side Integration Concept: Here, the heat pump's evaporator is connected to the heating network's return flow. By cooling the return flow to a lower temperature level through the evaporator, the waste heat in the flue gas can be extracted directly by the cooled network. This also makes it possible to integrate additional energy sources like solar thermal, into the system. Zajacs et al. [113] investigated the feasibility and efficiency improvement of this concept on a natural gas boiler using a simple heat pump model, demonstrating its effective application in district heating systems.

Regarding biomass heating, the potential of heat recovery significantly depends on the fuel water content [114]. Higher water content in the fuel allows for greater heat recovery from the flue gases, influencing the design of the heat pump and its electricity consumption. This distinguishes the biomass boiler from the gas boiler. Hebenstreit et al. [115] assessed a quench

condensing system integrated with an heat pump in a biomass boiler, whereby an simple heat pump model with a fixed Carnot factor was applied. The study demonstrated that integrating heat pumps into biomass heat networks offers more substantial opportunities for enhancing fuel utilization rate compared to gas-fired heat networks.

2.3.4 Choice of heat pump

The choice between absorption and compression heat pumps for use in flue gas condensation plants is not straightforward and varies based on practical considerations. Practically, absorption heat pump technology is less frequently used in industrial applications compared to compression heat pumps based on the research in [29,30,116]. A significant factor influencing this choice is the higher investment cost of absorption heat pumps, which can be about 2.5 to 4 times greater than that of compression heat pumps [117]. This cost disparity is largely attributed to the more complex structure of absorption heat pumps, which limits their widespread application. According to [118] this is also partly because standard solutions for absorption heat pumps are less common in the market than for compression heat pumps. Additionally, Jaunegg [29] highlights that the operational requirements of absorption heat pumps, particularly the frequent use of hot water or steam, incur additional costs due to the need for specialized personnel.

Absorption heat pumps are particularly advantageous for high outputs (several MW) are ideal when hot water or steam above 130 °C is readily available [119]. However, in medium-capacity biomass heating networks, reliable heat sources at these driving temperatures are typically absent [21]. Previous studies by Gaderer [17,38,120,121] indicate that absorption heat pumps are less effective for flue gas heat recovery in medium-scale biomass district heating due to the requirements for high-temperature steam, their lower efficiency (COP ~ 1.7), and greater integration complexity.

To compare the feasibility of heat recovery by using compression and absorption heat pumps, Xu et al. [122] studied the two concepts under the same conditions. This study showed that compression heat pumps are more efficient, making them more effective for waste heat recovery due to their higher COP, which facilitates greater exergy recovery from waste heat. And Tan et al. [123] concluded that among all types of heat pumps, the performance of compression heat pumps is best when the ratio of user-side heat demand to

waste heat is greater than 0.5. Such ratio corresponds exactly with the research focus of this work.

In summary, compression heat pumps are generally more suitable for heat recovery from flue gas in biomass heating in the 1 MW to 10 MW power range. The preference for compression heat pumps in general heat pump projects [28,29,109,124] also reflects this trend, because of the comparatively low price of compression heat pumps and the advantages of standardization in terms of maintenance and spare parts availability. Thus, this work will focus on the use of electrically powered compression heat pumps, which can achieve a COP value between 2.9 and 6.0 depending on the temperature lift [125,126].

2.4 Small cogeneration technologies

As mentioned in Section 1.2, there are already several biomass heating networks in northern Europe [27] and Austria [28,29] that have integrated heat pumps for heat recovery. However, none of these networks are equipped with small cogeneration units for self-power supply. This is primarily due to the significantly lower electricity purchase price in these regions [127]. In contrast, in Germany, integrating small cogeneration units could be sensible and economically imperative to reduce the amount of electricity purchased from the grid. For this reason, research on the feasibility of integrating small cogeneration units will be an integral part in this work.

2.4.1 Available technologies

Various technologies can be considered for the cogeneration of electricity [34]. Small-scale devices can be categorized based on their capacity into micro Combined Heat and Power (µCHP), defined as having an electrical output of 50 kW_{el} or less, and small CHP, defined as having an electrical output of up to 500 kW_{el} [128]. For this research, the range of applicable technologies will be narrowed based on criteria such as development status, efficiency, and the capability for integration into a biomass heating plant. The ideal CHP technology should provide the necessary electrical power reliably and efficiently, while maintaining minimal complexity and cost. This subsection aims to evaluate and pre-select the most promising technologies for integration, without delving into detailed explanations of each technology.

Small steam rankine cycle

The steam Rankine cycle belongs to one of the mostly utilized technologies for electricity generation in the world [129], which is based on the traditional Clausius Rankine cycle using steam as working fluid. In small-scale applications, the steam Rankine cycle is characterized by low steam throughput. Due to the high expense of equipment, steam turbine are technically and economically viable only for outputs around 5 MW and above [130]. Consequently, in smaller-scale settings, volumetric machines like reciprocating and rotary expanders are often used instead of turbines [131]. This is due to the challenges associated with turbines in small applications, such as lower efficiency and higher investment costs [132].

In this context, the steam engine (SE) emerges as a suitable expander device for small-scale cogeneration, which can be constructed in reciprocating and rotary form. For example, Alanne et al. [133] demonstrated the feasibility of using a rotary steam engine for distributed generation with biomass combustion. Similarly, Badami et al. [134] conducted research on the preliminary design and controlling of a steam Rankine Cycle based on a reciprocating steam engine, indicating that electrical efficiencies of approximately 8 % to 14 % are achievable with proper control strategies.

When integrated into an appropriate biomass furnace, steam Rankine cycle offers the possibility to use biomass fuel with different moisture content and qualities, thus offering greater fuel flexibility [34]. The waste heat from the steam condenser is available at temperatures between 100 and 150 °C, which is suitable for local heating networks. Wood-fired reciprocating steam cogeneration units are commercially available [135], with electrical capacities ranging from 100 kW_{el} to approximately 1500 kW_{el}.

ORC

The Organic Rankine Cycle (ORC) is a also viable option for small-scale cogeneration, with its advantages over the steam Rankine cycle largely attributable to the properties of the working medium used [17,136]. ORC operates on the same principle as the steam Rankine cycle, but uses various organic media instead of steam. These media typically have lower boiling or condensing temperatures compared to water. The condensation temperature of ORC equipment usually ranges from 30 to 80 °C [137], depending on the working fluid selection and cooling media. A higher condensation temperature up to 90 °C can be achieved by using special working fluids, like butylbenzene [138].

Decentralized biomass cogeneration unit based on ORC technology have been implemented since the late 1990s [139]. Smale-scale biomass-based ORC cogeneration systems are now commercially available from vatious manufacturers [137], typically with electrical outputs ranging from 50 to 325 kW_{el}. These systems generally exhibit thermal to electrical power ratios of around 5:1 [140]. Similar to steam engine integration, ORC technology ensures high fuel flexibility when integrated into a compatible biomass furnace. In principle, ORC technology can be considered essentially state-of-the-art and has been used successfully so far with appropriate boundary conditions and technical design. Since the late 1990s, several hundred ORC plants have been realized worldwide. The profitability model for them is often provided by subsidy programs that include remuneration for power generation [141].

A notable limitation of ORC plants is their relatively low electrical efficiencies, typically between 17-20 % [142]. To facilitate effective cogeneration in heating networks, the condensation temperature in the Organic Rankine Cycle must reach 90 °C to maintain the requisite temperature level. This requirement restricts the selection to refrigerants that have higher critical points. Furthermore, these higher condensing temperatures lead to a increased heat output compared to the power output, resulting in a lower power-to-heat ratio.

Hot air turbine

Hot air turbines have also been utilized several times in the past in conjunction with biomass furnaces [17,120]. However, this technology presents complexities, particularly in terms of heat transfer and maintaining the necessary temperature levels. Typically, microturbines are converted to operate as hot air turbines. Due to the inherent complexity of the system, the initial costs are high, with efficiencies similar to those of fixed-bed gasifier CHP units. Currently, the technology is being implemented in an initial pilot project [143], achieving a thermal efficiency of 63 % and an electrical efficiency of 13 % were realized. Despite these advancements, the high costs and complexity of hot air turbines render them only marginally suitable for retrofitting purposes.

Stirling engine

Stirling engine is known as an external combustion engine, distinguished by its utilization of two pistons set at a phase angle to transfer the working fluid between spaces [144]. In this process, the working fluid is compressed in the cold cylinder and expanded in the hot

cylinder [145]. Similar to the steam engine, the Stirling engine derives heat from an external source, such as a biomass furnace. Here, hot flue gas from the biomass combustion chamber enters the Stirling engine heater at high temperatures. With an additional separate heat exchanger, the heat is transferred to the engine. The typical operating temperature for the engine's heat exchanger ranges between 700 and 800 °C. Within the engine, this heat is converted into mechanical work, while the lower temperature heat is either dissipated in the cooler or utilized as a low-temperature heat source (40-60 °C) [34].

One of the main challenges in integrating Stirling engines into biomass combustion is ensuring efficient heat transfer from the biomass combustion flue gas to the working gas of the Stirling engine [146]. To ensure optimal system efficiency, the flue gas should enter the heat exchanger at the highest possible temperature. However, this can lead to ash deposition issues in system components, affecting the heat exchanger's transfer efficiency [147].

Additionally, maintaining perfect sealing of the working gas within a Stirling engine poses a significant challenge, leading to increased maintenance costs. Compared to internal combustion engines, Stirling engines generally tends to be less efficient, with typical electrical efficiencies around 10 -12 % and thermal efficiencies about 60 %, which corresponds to a heat-to-electricity ratio of 5:1 or more [34]. In addition, Stirling engines require a warm-up period before starting, precluding immediate operation. Consequently, they are better suited for applications with steady, uniform operating speeds [148]. This technology is not recommended for powering the heat pumps with constantly changing demand.

Biomass gasifier engine CHP

Biomass gasifier engine cogeneration (GCHP), encompassing a fixed-bed biomass gasification unit for gas conversion and a gas engine for electricity and heat cogeneration, stands also as a promising decentralized technology. In the gasification unit, biomass fuel is converted into syngas, consisting of H_2, CO, CO_2, H_2O, CH_4, N_2, and residual coal [149]. The syngas subsequently flows into the gas engine unit, where it is combusted to generate electricity and heat.

Over the past decade, biomass GCHP has garnered increasing attention for its potential to achieve higher electrical efficiency compared to conventional biomass combustion units [150]. Recent developments have led to the commercialization of this technology for various

applications [151]. Several manufacturers, such as Spanner Re2 [152], Burkhardt [153], Hargassner [154], Fröling [155], Syncraft [156] and Urbas [157] have advanced this gasification technology, making it commercially available with power ranges from 10 kW_{el} to about 350 kW_{el}. The state of the art for the electrical efficiency of small-scale GCHP is between 16 and 36 %. [158]. Due to the high electrical efficiency, these technologies are well-suited to provide the electrical drive power for heat pumps in this proposed concept. Additionally, GCHP units can function either independently or in tandem with a heat pump as an additional base load heat generator in existing heating plants in summer, independent of the operation of the biomass boiler.

However, the GCHP units have special requirements in terms of fuel. The water content in the fuel should be 20 % or less, and the ash content should be as low as possible. Consequently, suitable input materials are limited to wood pellets or dried, low-bark forest chips.

2.4.2 Comparison of the cogeneration technologies

Based on the above review, a comparison of the mentioned decentralized technologies for the electricity supply is displayed in Table 2.

Table 2: Comparison of available µCHP and small CHP technologies.

Technology	***energy source***	***medium***	***electrical efficiency***	***heat temperature available***	***integration complexity***	***standard products available***
Steam Rankine Cycle	external heat source	water vapor	8 to 14 %	100 to 150 °C	high, integrated into furnace	yes
Organic Rankine Cycle	external heat source	organic medium	17 to 20 %	up to 90 °C	high, integrated into furnace with additional heat exchanger	yes
Hot air turbine	external heat source	air	approx. 13 %	approx. 130 °C		no
Stirling engine	external heat source	Helium or hydrogen	approx. 10 %	60 to 85 °C		no
Gasification CHP with gas Engine,	biomass	product gas from a gasification	16 to 36 %	80 to 500 °C	low, integrated separate and robust	yes

As seen from the table, GCHP has the lowest integration complexity from a technological point of view, due to its independence and robustness. Additionally, it boasts the highest electrical efficiency among the options and has mature market solutions. Despite its specific requirements on fuel quality, GCHP are considered a promising technology for this task.

Other standard products available in the market are ORCs and scale SRC. Both can be integrated biomass boiler. While the SRC is less efficient, it provides sufficient heating temperature for the heating network and can utilize a steam pipeline for direct heat exchange with furnace without an additional intermediate heat exchanger. The ORC achieves slightly higher electrical efficiency but requires special refrigerants to reach a heating temperature of 90 °C. Typically, heating of the working fluid in ORCs is conducted through an additional thermal oil circuit. This requires an additional intermediate heat exchanger and leads to efficiency loss.

The hot air turbine and Stirling engine, lacking proven products in the markets and exhibiting lower power generation efficiency, are less recommended. The hot air turbine can achieve a heating temperature of 130 °C but is not recommended due to high costs and complexity. The Stirling engine, with its lower efficiency and insufficient heating temperature for the network, is also not suitable for powering heat pumps.

In conclusion, ORC, small-scale SRC, and wood gasification CHP are identified as potentially viable technologies for providing the required electricity for heat pumps. Consequently, the focus of this work will be on integrating these three technologies, with their respective approaches to integration discussed in section 3.1.3.

3. Overview of the integration concepts and system analysis

This chapter gives an overview of the different integration concepts of heat pumps for waste heat recovery from flue gas. The first section outlines how the different system components, such as heat recovery components, heat pumps and different CHP units, are integrated into the system, along with their corresponding functions. To this end, detailed hydraulic diagrams of different systems are provided and described.

For the subsequent detailed analysis and evaluation of the various integration concepts, systems with different configurations and their system boundaries are defined and analyzed in terms of the mass energy flow in second section. First, based on the focus of this work, the optimization of the energy supply side, the boundaries of different systems are uniformly defined to make the various concepts studied in this work comparable. To better illustrate the difference in systems configurations, the mass and energy flows of each system are also displayed and analyzed. Among these, the traditional single boiler system is introduced as a baseline system. Other configurations include system with only integrated flue gas condensers, systems with heat pumps integrated in various connection variants, and systems that additionally integrate different CHP units.

3.1 Technical concepts of system integration

In this section, an overview of different concepts of integrating heat pumps and various types of CHP unis into biomass heating network is presented.

Before integrating a heat pump, various flue gas treatment and heat exchange equipment must be installed on the flue gas side to ensure effective heat recovery. This includes a flue gas cleaning system for dust removal, an economizer for sensible heat recovery, and a flue gas condenser for latent heat recovery. These components are installed independently of the heat pump integration. However, they are essential for direct heat recovery from flue gas and necessary to improve the reliability and economy of integrating the heat pump. The interconnection of these different components, determined by their function, will be described in Subsection 3.1.1.

For the integration of heat pumps, several studies, as referenced in [33,124,159,160], have been conducted to investigate efficient integration methods into heat networks. As mentioned in Subsection 2.3.3, integrating the heat pump into the biomass heating network

for heat recovery is possible at two points: either interconnection with the flue gas condenser or connection to the network's main return. Both can serve as heat sources for evaporators and be cooled to achieve effective flue gas condensation. In addition to the various ways of connecting the heat pump evaporator, there are also multiple variants for connecting the heat pump condenser to feed the "pumped" heat back into the network. A detailed description of these variants is introduced in Subsection 3.1.2.

In scenarios where onsite power generation is necessary for the heat pump, integrating a small-scale CHP unit into the system is a viable option. Various types of CHP technologies can be incorporated in different manners. A more detailed discussion on this integration will be provided in Subsection 3.1.3.

3.1.1 Integration of heat exchangers in flue gas path

Figure 10 shows an example of a modern biomass heating plant with a indirect-contact flue gas condensation system that includes an economizer, and a flue gas dehumidification unit.

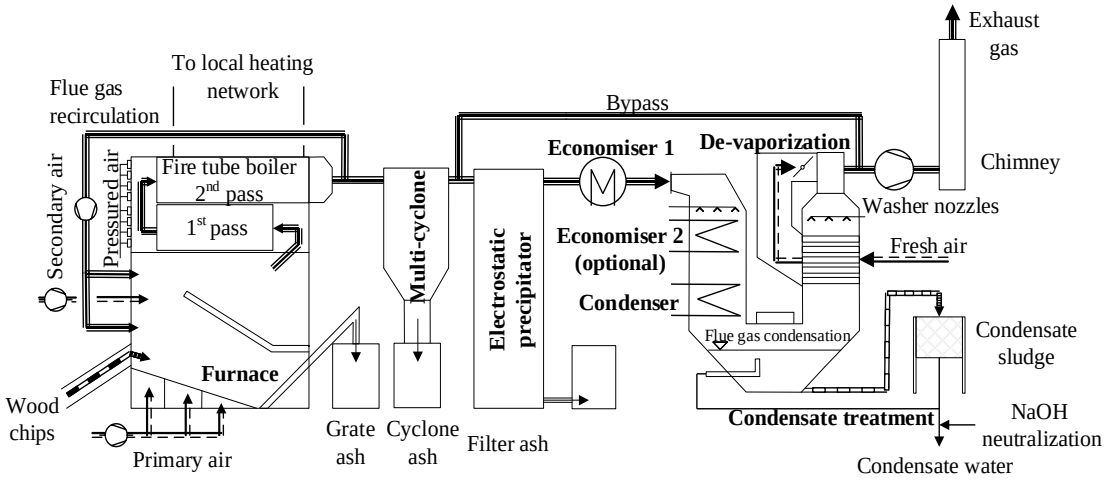

Figure 10: Biomass heating plant with dedusting, economizer, closed direct flue gas condenser and flue gas dehumidification (adapted from [17]).

In the flue gas path, the hot flue gas from the boiler, at approximately 180 °C, first passes through the gas cleaning unit, primarily used for dust removal, e.g., via an electrostatic precipitator. This prevents operational issues in downstream components. A bypass line should be installed before the gas cleaning unit in case of malfunctions, maintenance, etc.

The economizer (ECO) then cools the flue gas to a temperature above its dew point, allowing further extraction of sensible heat. The placement of the economizer before the flue gas condenser in the path is dictated by their respective functions. Additionally, the cooling process via the economizer occurs downstream of the flue gas cleaning unit rather than before it. This arrangement is crucial as the moisture and acid condensation in the flue gas at low temperatures can lead to corrosion, especially if ash has not been pre-filtered. Consequently, all components positioned downstream in this setup must be specifically designed to withstand both moisture and corrosive media [17].

After the economizer, the flue gas reaches the flue gas condenser at about 60 to 80 °C. If additional cooling can be achieved by passive condensation without a heat pump, it should be done upstream of the condensing heat exchanger. The economizer can be integrated into the U-shaped flue gas condensation system or an additional one can be installed upstream of the condensing bundle. At the condensing bundle, the water vapor in the flue gas condenses. In this process, the gas stream is deeply cooled to between 30 to 50 °C via the heat pump evaporator. The heat pump absorbs the condensation heat and raises it to a higher temperature level, and then feed it into the heating network.

Despite upstream de-dusting, it’s crucial to maintain sufficient, uninterrupted humidification of the heat exchanger surfaces to avoid corrosion. This can be achieved by additional quenching, i.e., injecting a small amount of water to saturate the flue gas [17], with quench spray nozzles located at both the inlet and outlet sides. The accumulated condensate flows into a catch basin beneath the condenser and is separated into sludge and water in a settling tank. Before exiting the condenser unit, if de-vaporization is necessary, the flue gas is mixed with fresh air in the de-vaporization unit and then discharged through the stack.

This U-shaped construction of the displayed condensation system typically has a lower height but a greater width. Alternatively, a tower shape can be selected, where the flue gas flow direction is not constrained to bottom-to-top. Biomass heating plants often use induced draft fans to either support or replace the chimney's natural draft, which simplifies exhaust gas cleaning. A horizontal flue gas condensation design is possible but not recommended, as it complicates ensuring reliable and consistent humidification of the entire condenser surface.

3.1.2 Integration of the heat pump for flue gas condensation

Various hydraulic circuits can be realized for integrating heat pumps, where the heat pump evaporator can be integrated either into the flue gas condenser or the network return [109]. Figure 11 exemplifies two hydraulic circuit diagrams for the integration of heat pumps for flue gas condensation, facilitating efficient utilization of waste heat from the flue gas condenser. Both circuits impose special demands on the heat pump design. To improve readability, the components on the flue gas path are simplified and the optional economizer in the flue gas condenser is omitted here.

As shown in the upper diagram, in the flue gas-side concept, the heat pump functions as a direct cooling unit for flue gas. Here, the heat pump evaporator directly extracts heat from the flue gas, cooling it to the desired exhaust gas temperature. In this case, the evaporation temperature of the heat pump should be lower than the target exhaust gas temperature, considering the temperature difference within the heat exchanger. Additionally, its evaporation capacity should match the heat output capacity of the condenser. Thus, the lower the target flue gas temperature, the greater the required power of the heat pump evaporator.

In the network-side concept, as illustrated in the lower diagram of Figure 11, the heat pump evaporator is connected to the network return flow. The return flow first passes through this 'active' heat exchanger to reach a lower temperature before entering the flue gas condenser. The evaporator draws heat from the network return, allowing for maximum heat extraction from the flue gas. The temperature of the cooled return flow into the condenser should also be lower than the target flue gas temperature, taking into account the heat exchanger temperature difference. Consequently, the evaporation temperature of the heat pump should be even lower. The diagram also indicates that the main return does not need to flow entirely through the heat pump evaporator. Instead, the interconnection allows for theoretically free adjustment of the mass flow using additional bypass valves or circulating pumps.

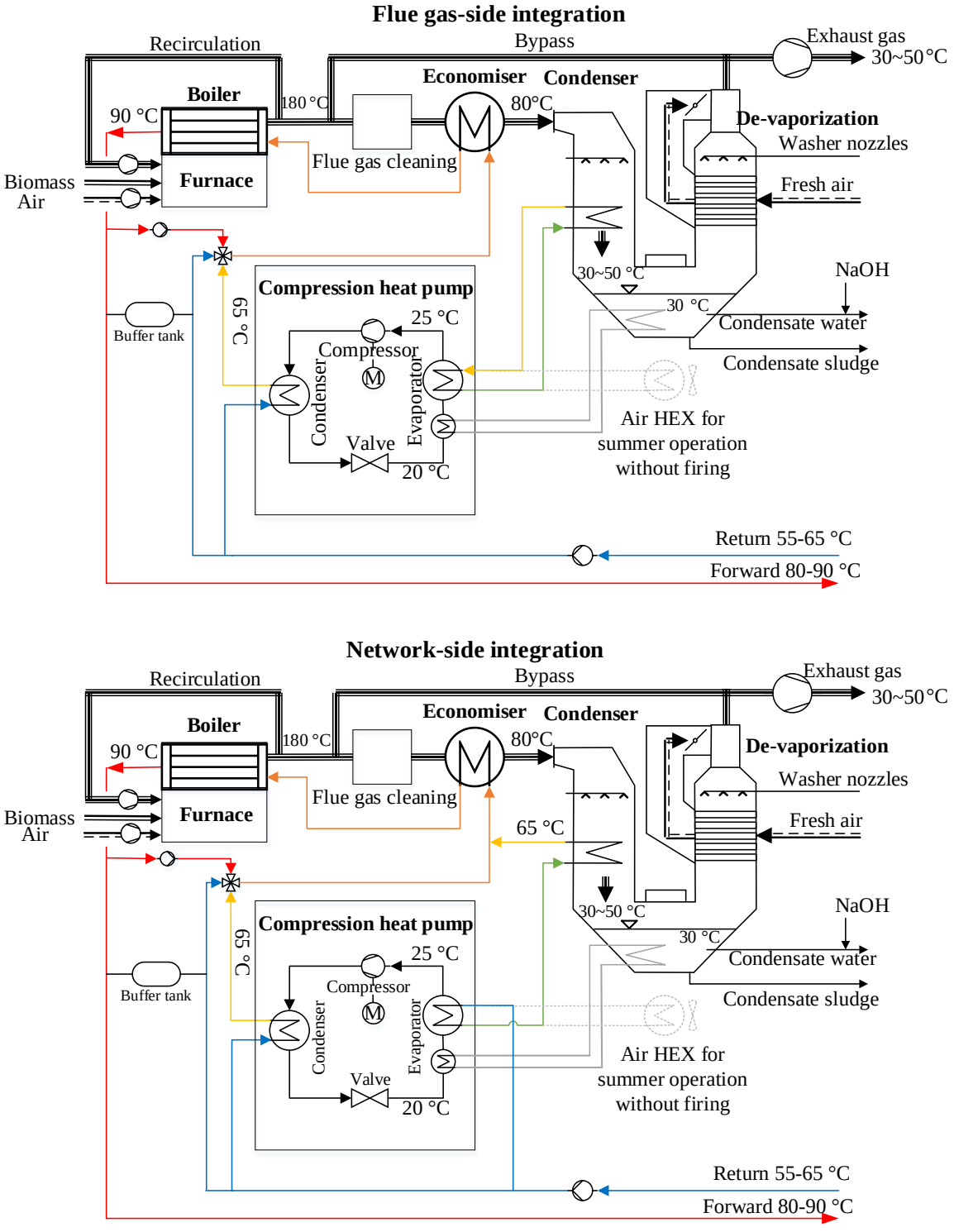

Figure 11: Hydraulic circuit diagram of the integration of a heat pump for flue gas condensation. Top: heat pump evaporator connected to the flue gas condenser (flue gas-side integration); Bottom: heat pump evaporator connected to the heat network return (network-side integration) (own illustration).

In both concepts, the heat absorbed by the evaporator is elevated to a higher temperature level and then released through the heat pump condenser. Beyond the various methods of connecting the heat pump evaporator, the heat pump condenser can also be connected in several ways to feed the 'pumped' heat into the network. Essentially, there are three distinct methods [161]. The heat pump condenser can be connected either to the network mains return, the preheated network return after the economizer, or directly to the network feed flow, depending on the supply temperature of the heat pump. The simplified diagrams of these different variants are presented in Figure 12.

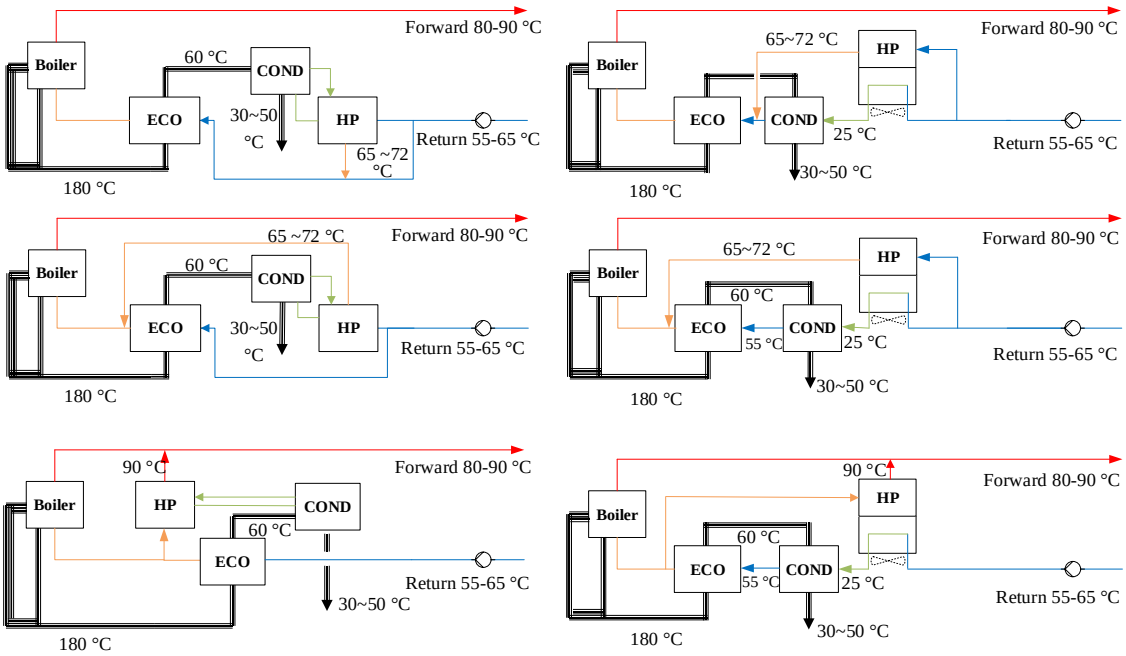

Figure 12: Simplified schemes of heat pump integration variants: (Lefts: evaporator connected to flue gas condenser, right: evaporator connected to with the mains return.) (Top: Feeding into the unheated mains return, Middel: Feeding into the preheated mains return, Bottom: Feeding into the mains feed flow.) (own illustration).

Among these three variants, the first, as depicted in the upper part of Figure 12, demonstrates the heat pump feeding into the network mains return. It is also the example shown in Figure 11. In this configuration, the heat pump heats a bypass from the mains return flow. This heated flow is then mixed at the multi-way valve with the main return flow and the bypass after the boiler. These combined flows are subsequently fed into economiser and the boiler. The bypass after the boiler is driven by a boost pump, which increases the flow through the economiser and boiler heat exchangers [162]. This increased flow mitigates the risk of deposits inside the heat exchangers and compensates for the disadvantages of the

increased return temperature. In this variant, the heat pump can operate at the best possible efficiency due to the lowest temperature lifts, which is especially advantageous for heat pumps.

In the second variant, heat is fed into the grid after the economiser. This variant is similar to the first variant. However, the efficiency of the heat pump in this configuration will be lower.

The third variant corresponds to a classic integration of a generator into a heating network. Here, the heat pump must provide the highest required temperatures. The respective return temperature and the required feed temperature in the network determine the temperature lift of the heat pump. This variant allows for the independent operation of the heat pump during summer when operating boilers at a low base load is not economical. However, this hydraulic circuit necessitates a significant temperature lift by the heat pump, which can be challenging for equipment manufacturers and impact the economics of operation. Special refrigerants and potentially multi-stage compression are potententially required to meet the temperature needs. Connecting multiple heat pumps in series to achieve higher temperature differentials is also a feasible approach.

3.1.3 Integration of small-scale cogeneration unit

The introduction of heat pump for an active condensation significantly increases electricity consumption. In this context, combining a small cogeneration is a favorable option to reduce electricity purchases from the grid. Based on the pre-analysis in Section 2.4, three promising cogeneration technologies are considered:

- Integration of a small-scale Steam Rankine Cycle (SRC) unit into the furnace.
- Integration of an Organic Rankine Cycle (ORC) unit into the furnace through an additional thermal oil heat transfer circuit.
- Integration of a separate gasification cogeneration (GCHP) unit.

These technologies are integrated into the system in different ways. The implementation of the integration of these three technologies will be described in the following paragraphs.

The manner in which the cogeneration units are integrated depends on the specific characteristics of the technology and is independent of the integration method of the heat

pumps. This means the approach to integration remains consistent across different heat pump connection methods. The implementation of these three cogeneration integration concepts will be elaborated based on the hydraulic diagram of the flue gas-side integration of the heat pump. To provide a clearer illustration of the cogeneration integration, other main components such as boilers, flue gas cleaning (FGC), heat exchangers, and heat pumps have been simplified in the diagram. The optional economizer in the flue gas condenser also has been omitted.

Integration of SRC unit

Figure 13 presents the hydraulic circuit of the integration of a steam rankine cycle into the system.

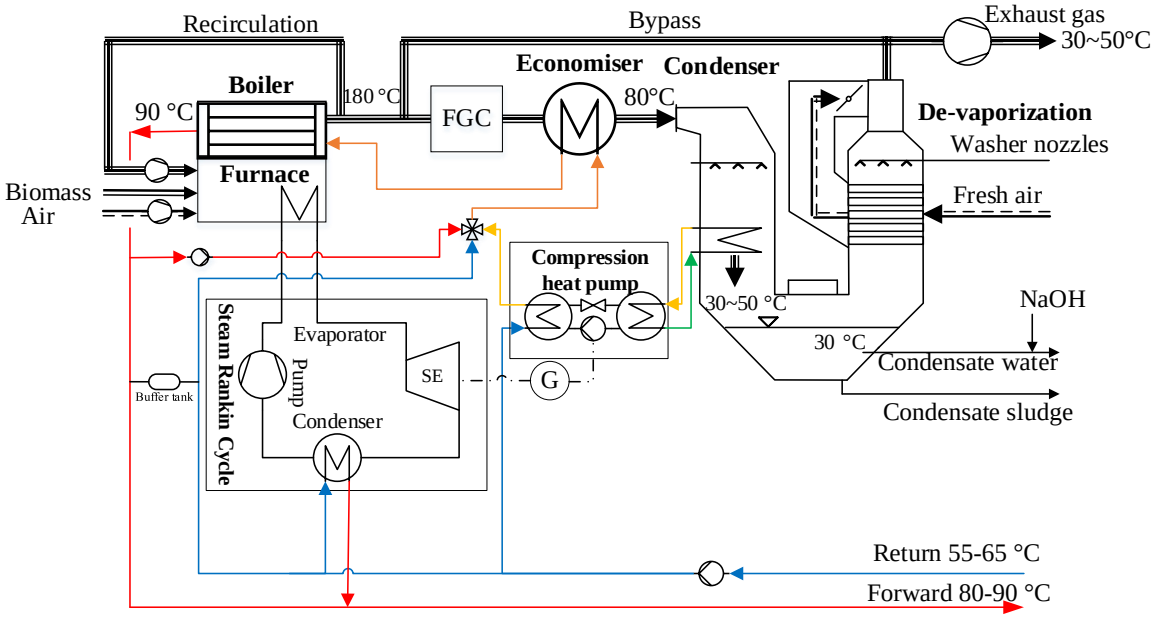

Figure 13: Hydraulic circuit diagram of the integration of the steam Rankine cycle based on steam engine for onsite power generation (own illustration).

The key advantage of integrating a SRC unit is that no additional heat source or firing systems are required. As illustrated in the diagram, the evaporator directly extracts heat from the combustion gas. Moreover, compared to GCHP units, the SRC offers greater fuel flexibility, as it can utilize wood with varying moisture contents and quality.

In designing the SRC, it is important to ensure that the steam condensing pressure and temperature are as low as possible, which is determined by the temperature level of the network. Conversely, the evaporating pressure and superheat temperature of the steam cycle

should be as high as possible, as these factors determine the electrical efficiency of the steam engine. To achieve this, the steam must be sufficiently superheated before expansion. Low steam pressures adversely affect the potential working capacity of the steam power process. For the system proposed in this work, a maximum pressure of 100 bar and a temperature of 450 °C, as recommended by Badmi et al. [134], have been chosen. These parameters represent a well-defined trade-off between high efficiency and the technical limitations of standard technology.

Integration of ORC unit

Different from the integration of a SRC unit, integrating an ORC unit into a biomass furnace necessitates an additional heat transfer circuit. This circuit transfers heat from the hot flue gas to the organic working fluid. The hydraulic circuit diagram for this integration is shown in Figure 14. Thermal oil is commonly used as the transfer medium in the intermediate heat exchanger. As a result, there is a loss of efficiency in the system due to the transfer of thermal oil.

Within the ORC cycle, the working fluid is initially heated by the heat transfer oil. After evaporation, it expands in the expander to drive the generator. The working fluid exiting the expander is then liquefied in the condenser. Similar to steam cycles, the condensing temperature of the ORC cycle is primarily determined by the supply temperature of the heating network. To directly utilize the condensing heat for local heating, the condensation temperature needs to be higher than the network's supply temperature. The minimum pressure within the device, i. e. condensing pressure in the ORC unit, should be higher than the ambient pressure to avoid air infiltration. Unlike steam cycles, the evaporation temperature and pressure in an ORC cycle are not only limited by equipment strength but also influenced by the physical properties of the Organic Working Fluid (OWF), such as its critical point and the enthalpy of evaporation. According to Xu et al. [163], the evaporating temperature should not exceed the critical temperature to avoid issues associated with a supercritical cycle. The higher the critical temperature of the OWF, the broader the temperature range for evaporation. Thus, in designing of the ORC unit, selecting the appropriate OWF is particularly critical, which has a significant impact on the system’s overall performance.

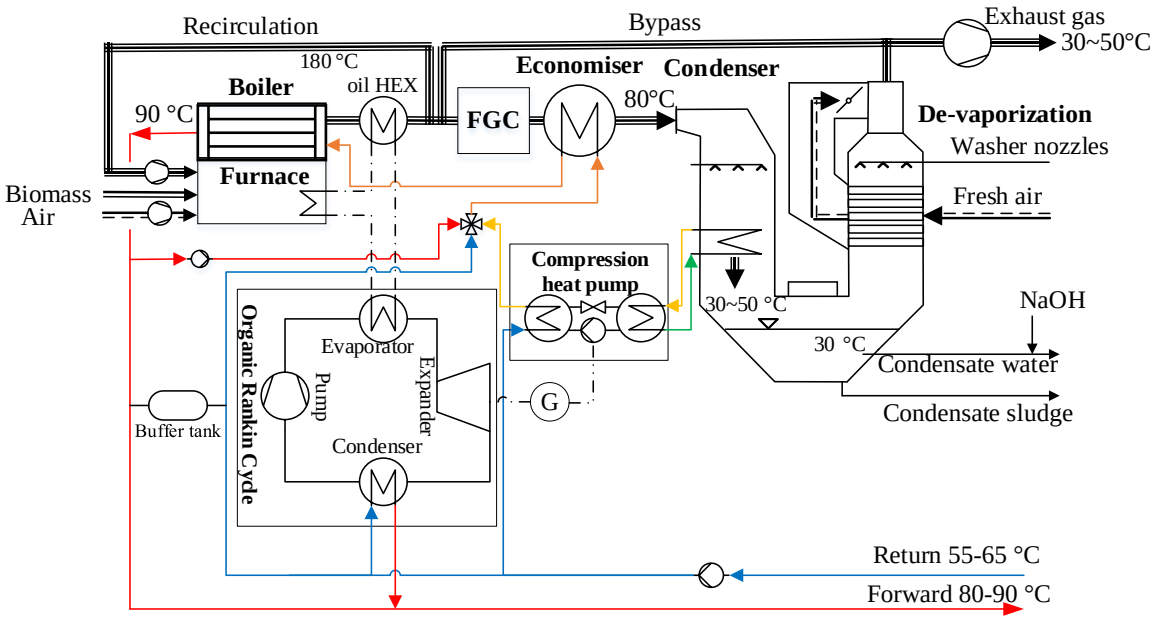

Figure 14: Hydraulic circuit diagram of the integration of the Organic Rankine cycle through an additional thermal oil heat transfer for onsite power generation (own illustration).

The selection process of OWFs has been extensively researched, with most OWFs being evaluated based on their thermodynamic properties and cyclic thermodynamic models. OWFs can be categorized into three types according to their properties in the isentropic expansion process: quasi-isentropic, wet, and dry fluid [164]. This classification is based on the saturation vapor curve in T-s (temperature-entropy) diagrams. A negative saturation vapor curve, indicative of a 'wet' fluid, can lead to droplet formation in the later stages of expansion [137]. Therefore, it is necessary to superheat the vapor at the expander inlet to prevent damage to the expander. In contrast, using dry fluid, with a positive saturation vapor curve, eliminates the need for steam superheating, as the steam can remain superheated even after expansion in the turbine. Additionally, using dry fluid, a recuperator can be employed to enhance the cycle's efficiency.

Based on a preliminary study of the characteristics of different OWFs, octamethyltrisiloxane (MDM) was chosen as the circulation medium in this work. The corresponding technical analysis will also be based on this selected working fluid.

Integration of gasification cogeneration unit

In Figure 15, the integration concept of the heat pump in combination with a gasification cogeneration (GCHP) unit is presented. In this variant, the biomass gasifier and the gas

cogeneration are treated as a combined cogeneration unit, capable of robust integration into the system independently of the biomass boiler.

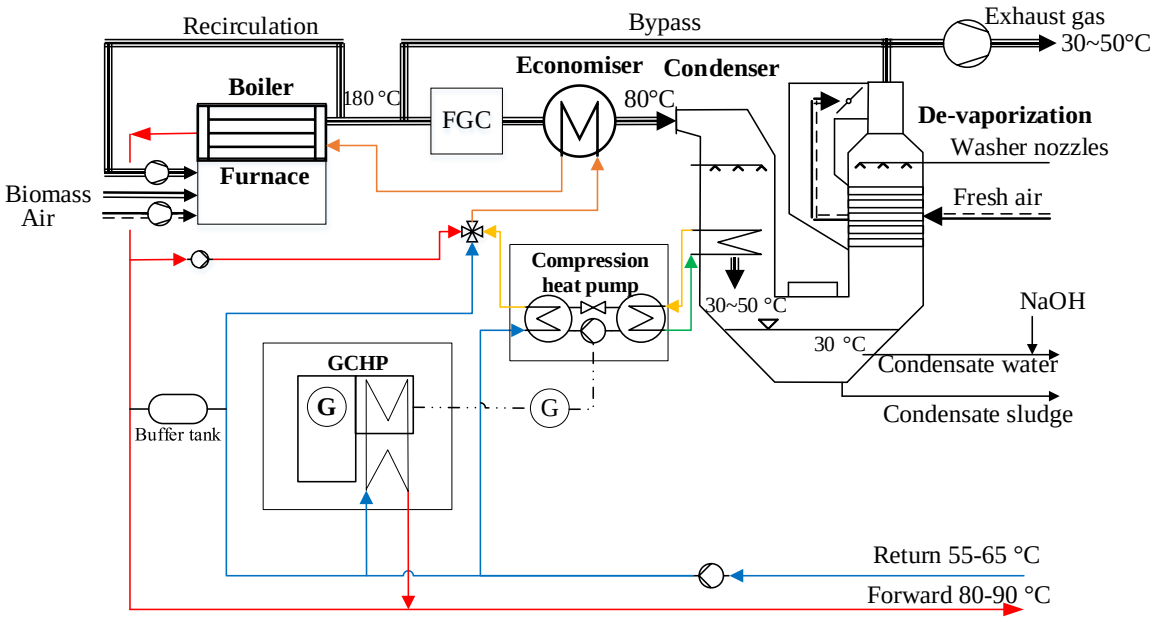

Figure 15: Hydraulic circuit diagram of the integration of the gasification CHP for onsite power generation (own illustration).

The major advantage of this solution is that the integration of a GCHP unit is less difficult compared to the integration of the SRC and ORC units. This "extra" equipment can be more robustly and independently integrated into the system. Additionally, when low-emission biogas is available, the biomass gasification unit can be omitted. Furthermore, the GCHP unit can function alone or in conjunction with the heat pump as an additional base load heat generator in the network for summer operation, independent of the biomass boiler's operation. However, due to the complexity of constructing the biomass gasification CHP unit itself, its initial cost is high, and thus its economic viability requires further analysis.

3.2 System definition and analysis

This section defines the systems to be studied under different concepts and provides a preliminary analysis in terms of mass and energy flows. To ensure comparability among the systems examined in this work, it is essential to define the system boundaries uniformly. The primary focus of this study will be on the primary heat network side of the biomass heat network, i.e., the energy supply system before the main heat exchange station, as illustrated in Figure 16.

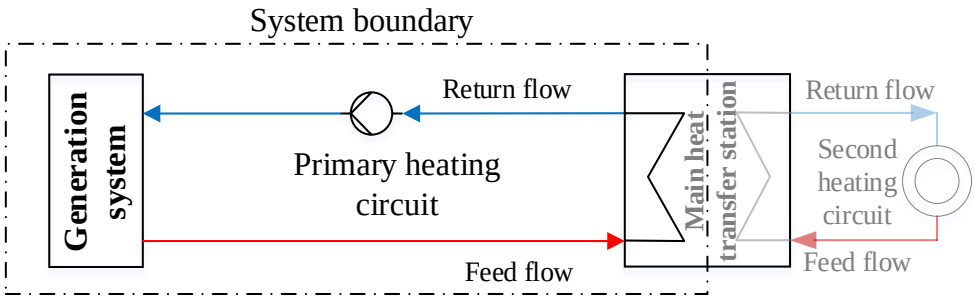

Figure 16: Definition of balance boundary of the studied systems (own illustration).

The principal distinction among the various integration concepts lies in the structure of the generation system. To evaluate the technical, economic, and environmental aspects of heat pump integration, the definition and boundaries of systems under different concepts are delineated. Moreover, to better illustrate the differences in system configurations, the mass and energy flows of each system are displayed and analyzed.

Baseline system

In this work, the traditional biomass heating system without flue gas condensation is defined as the baseline energy system for comparison purposes, where the heating supply of the network is covered solely by the boiler. The mass and energy flows of this system are shown in Figure 17.

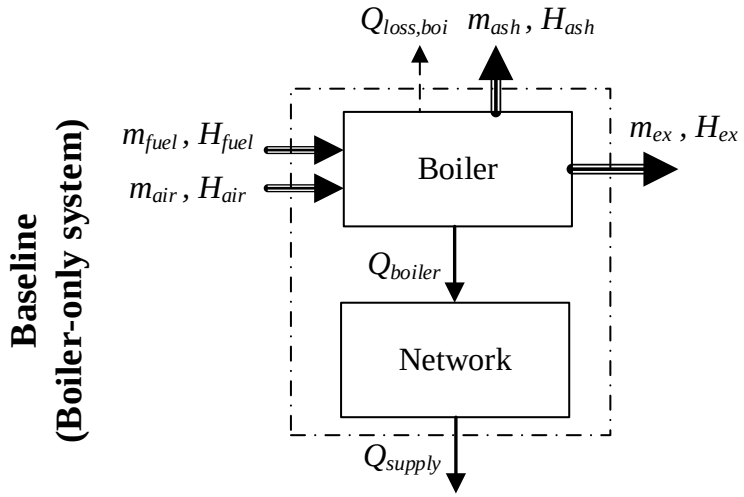

Figure 17: Mass and energy flow of baseline system (Boiler-only system) (own illustration).

In the diagram, thicker arrows represent the mass flows of the system inputs and outputs, along with the carrying enthalpies, such as fuel and air input into the system, and ash and exhaust gases output from the system. Solid lines represent the flow of energy achieved

through heat exchange, while dashed lines represent the heat loss from the boiler. The main components of the represented baseline system is the biomass boiler, including the combustion chamber. As shown in the figure, the mass and energy flow of the system is simple, without complex topology. Therefore, its design and operation are relatively simple, reflecting the status quo for most currently operating biomass heat networks in Europe. However, the absence of heat recovery components means that the exhaust gas exits the system at a higher temperature of about 180 °C, carrying a higher enthalpy, which results in decreased energy efficiency.

COND-only system

To investigate the necessity of integrating heat pumps, a system equipped only with heat exchangers for heat recovery (i.e., an economizer and a flue gas condenser) will also be examined. This system is defined as the COND-only system. The hydraulic diagram of this system refers to Figure 10, while the mass and energy flow are illustrated in Figure 18.

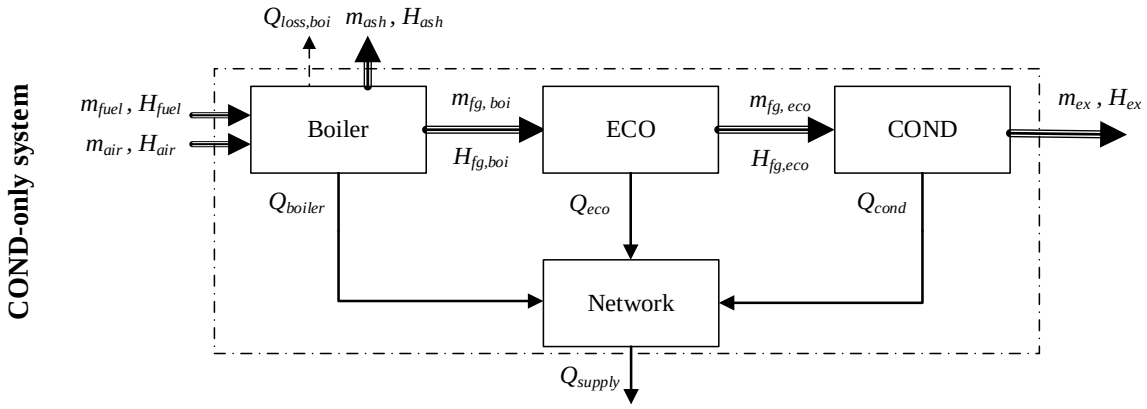

Figure 18: Mass and energy flow of flue gas condenser integrated system without heat pump (COND-only system) (own illustration).

The main components of this system, in addition to the biomass boiler, also include the heat recovery components. The system topology is more complex than that of the baseline system, but remains straightforward. As shown in the above diagram, the system generates three distinct energy flows that are fed into the network, with the recovered heat from the economizer and flue gas condenser utilized for pre-heating the network return.

Considering the system as a black box, the inputs and outputs across the system boundary remain the same as in the baseline system, including the input of biomass fuel and air, and

the output of exhaust gases, ash, and their associated enthalpies, as well as the heating energy supply and boiler losses. The temperature of the exhaust gas exiting the system boundary and the enthalpy it carries depend primarily on the return water temperature of the network. As noted in Section 2.2.3, if the network return temperature is above the flue gas dew point temperature, the latent heat in the flue gas cannot be effectively recovered by the flue gas condenser without auxiliary measures.

HP-integrated systems

To effectively recover the latent heat from the flue gas, heat pumps can be integrated into the system in various ways. The method of integrating the heat pump evaporator significantly impacts the system, with two primary connection methods: direct connection to the condenser and connection to the network to cool the flue gas, as described in Section 3.1.2. The hydraulic diagrams of both concepts can be found in Figure 11. For further analysis, systems employing these concepts are defined as the flue gas-side HP-integrated system and network-side HP-integrated system, respectively. For a clear illustration of the difference between both concepts, the mass and energy flows of the systems are displayed in Figure 19.

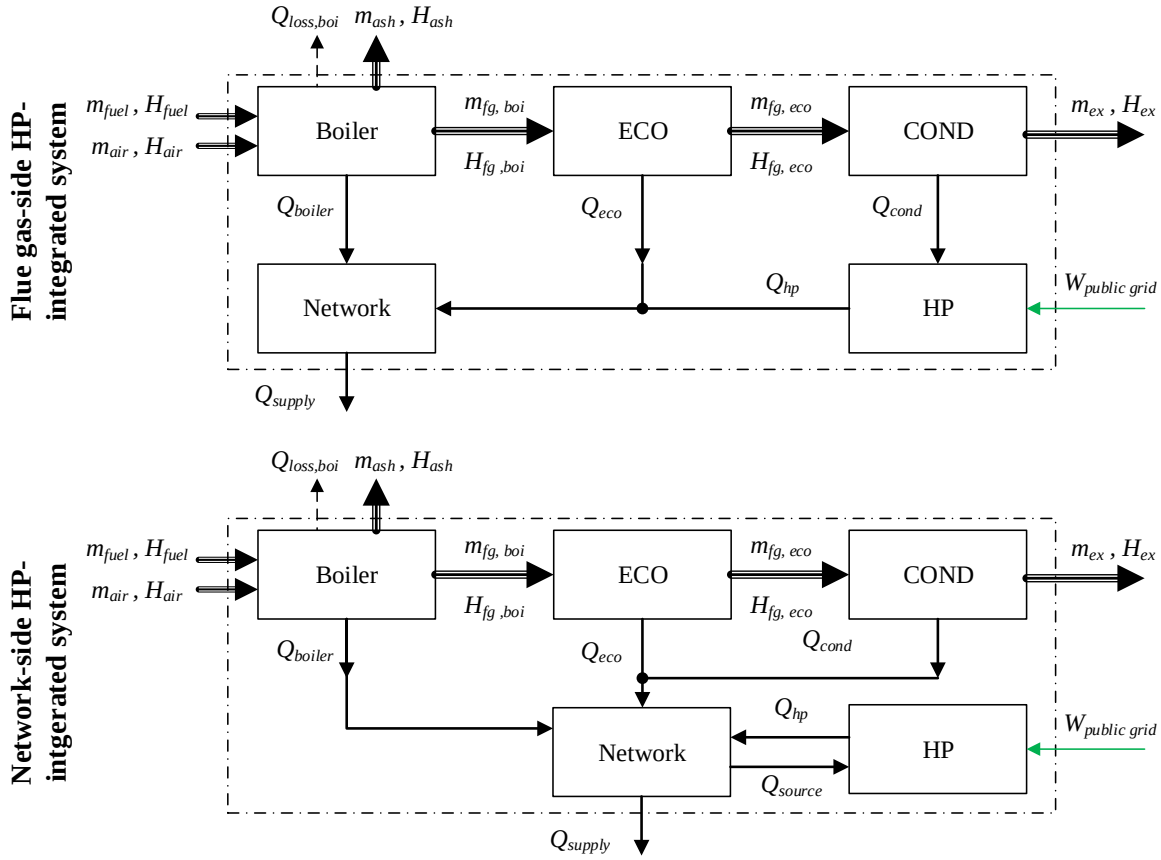

Figure 19: Mass and energy flow of the system with an integrated heat pump (Top: flue gas-side HP-integrated system; Bottom: network-side HP-integrated system) (own illustration).

The main components of both system configurations are the biomass boiler (including the combustion chamber), the economizer for sensible heat recovery, the flue gas condenser for latent heat recovery, and the heat pump for cooling and elevating the temperature of waste heat.

In both systems, the heat pump serves as both, a cooling device and an energy supply device. Both systems require the introduction of an additional energy input, as depicted in Figure 19 by the green arrows, which represent the electricity required to drive the heat pump. Externally, the input and output mass and energy flows appear similar for both systems, with an additional electrical input compared to the baseline system. The primary difference between these systems lies in the cooling objects (refer to Figure 11), resulting in different internal energy flows inside the system boundaries.

In the flue gas-side HP-integrated system, the heat pump directly cools the flue gas, by using additional electricity to raise the waste heat temperature in the flue gas to a usable

level. In this process, the heat flow from the condenser serves as the heat source for the heat pump. Therefore, only three heat flows are fed into the heat network: heat generated by the boiler, the economizer and the heat pump.

In the network-side HP-integrated system, the heat pump cools the flue gas indirectly by lowering the network return temperature below the flue gas dew point temperature. In this setup, the heat pump is not directly connected to the condenser and draws its heat source from the heating network. The heat output from the flue gas condenser is directly fed into the network, which leads to two additional internal heat flows compared to the flue gas-side HP-integrated system. Thus, there are five heat flows around the network, four as inputs from the four main components, and one as output, serving as the heat source for the heat pump. This leads to a more complex system topology.

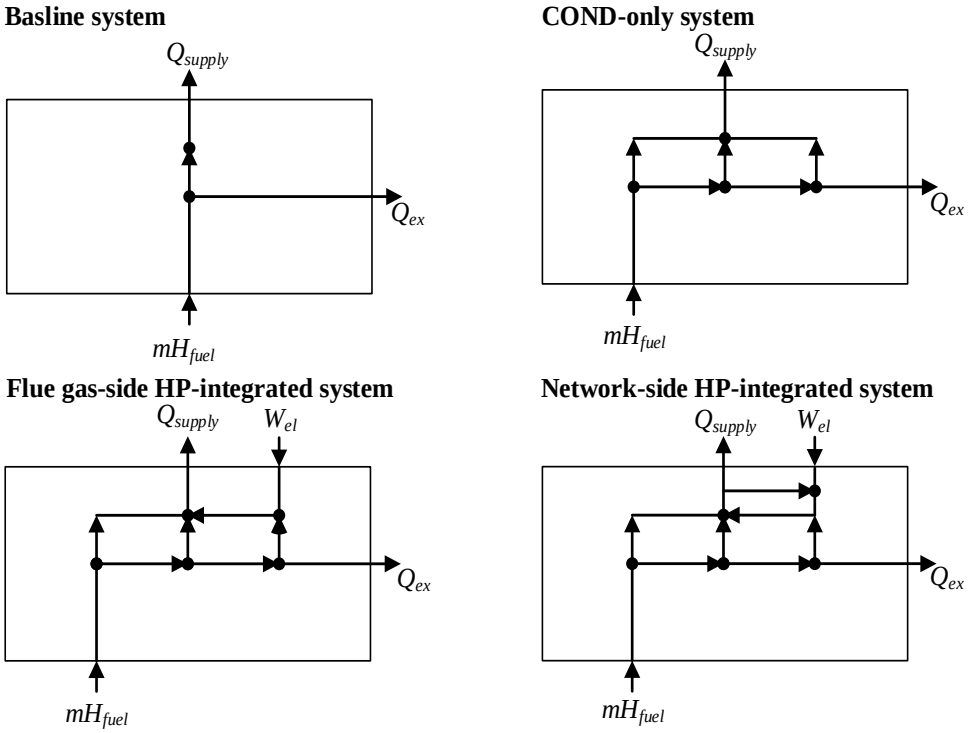

Figure 20: Opposite representation of the topologies of the HP-integrated systems compared to the baseline system and the COND-only system (own illustration).

An opposite representation of the topologies of both systems with integrated heat pumps compared to the baseline system and COND-only system is shown in Figure 20. Where each point represents a main system component, and the arrows indicate the direction of energy flow. It is evident from the figure that the topologies of the systems with integrated heat pumps are more complex than the two previously mentioned systems.

HP-CHP-integrated systems

To reduce external power input, additional integration of cogeneration can be considered to directly power the heat pump. Different concepts have been introduced in Section 3.1.3, including the integration of steam Rankine cycle (SRC), Organic Rankine cycle (SRC) and biomass gasification cogeneration (GCHP). The energy systems incorporating these integration concepts are defined here as the HP-SRC-integrated system, HP-ORC-integrated system, and HP-GCHP-integrated system, respectively. Figure 21 illustrates the corresponding mass and energy flows of these systems using examples of the flue gas-side integration of a heat pump. In this work, it is assumed that the cogeneration units solely supply the electricity demand of the heat pump excluding other devices, such as network pumps or lighting. Otherwise, additional power storage would be required to meet the real-time demand of these devices, which would further increase the initial investment and complexity of the system.

As shown in the figure, integrating different types of cogeneration units can eliminate the need for additional external power input to drive the heat pump. However, this integration also significantly complicates the internal energy flow of the system.

For instance, the HP-SRC-integrated system has two additional internal energy flows compared to the HP-integrated system. These include the heat generated by the CHP, which feeds into the network, and the electricity generated for the heat pump. This electric energy flow supplants the external power input, resulting in the system's inputs and outputs appearing the same as the baseline system from an external perspective. The energy flow of the HP-ORC integrated system is similar to the HP-SRC system, except that there is an additional intermediate energy exchange.

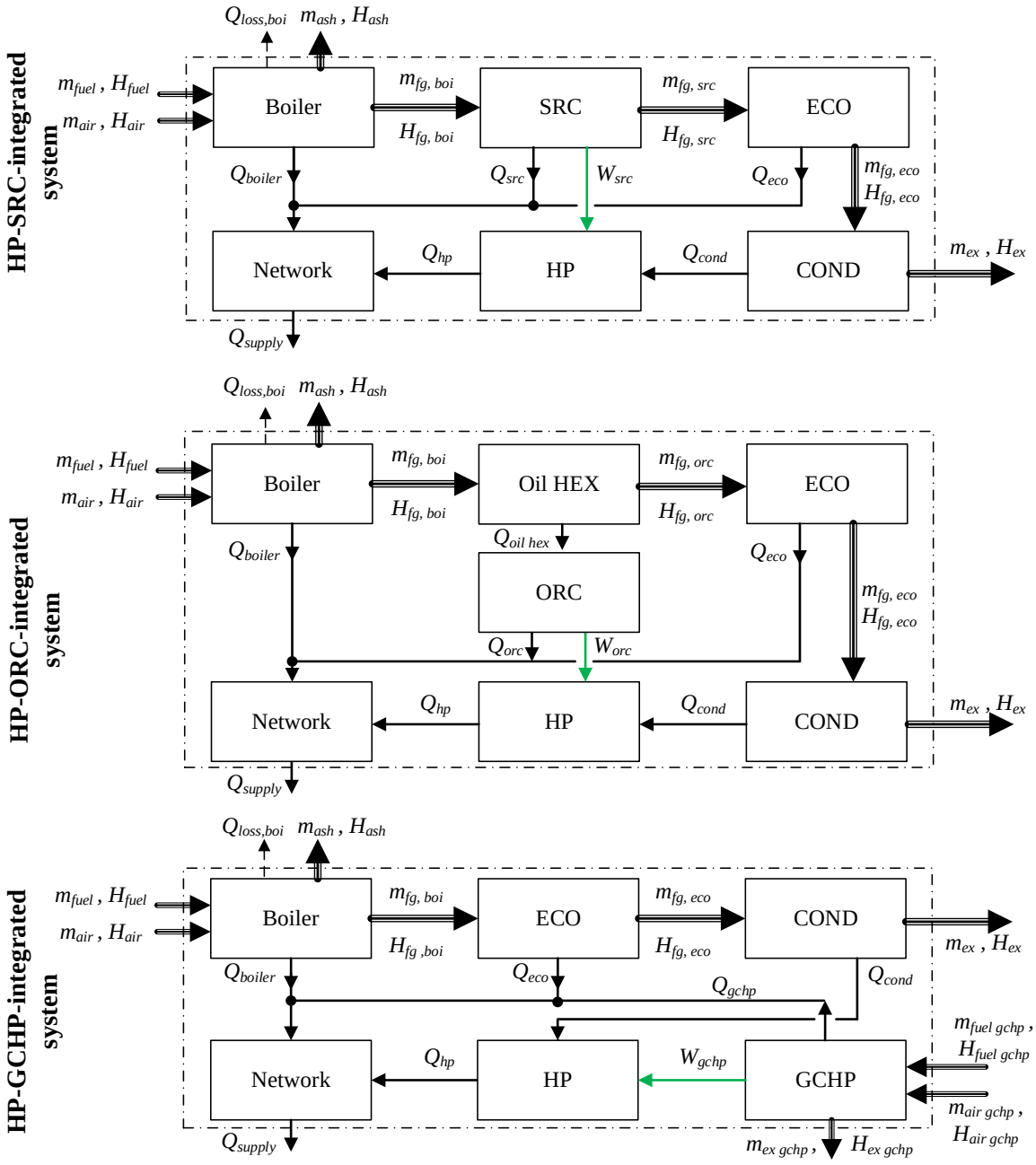

Figure 21: Mass and energy flow of the systems with an integrated heat pump and CHP units (Top: HP-SRC-integrated system; Middle: HP-ORC-integrated system; Bottom: HP-GCHP-integrated system) (own illustration).

In the HP-GCHP system, the integration of the GCHP unit is relatively robust and simple, with the electricity generated directly powering the heat pump and the heat generated being fed directly into the heat network. As depicted in Figure 21, the integration of the GCHP unit does not affect the mass and energy flow of the other components, except for the power supply to the heat pump, allowing the system to operate without impacting other

components. However, it requires additional fuel output. Consequently, resulting in additional input and output mass and energy flows to the system.

An opposite representation of the topologies of the systems with integrated heat pumps and CHP units is shown in Figure 22.

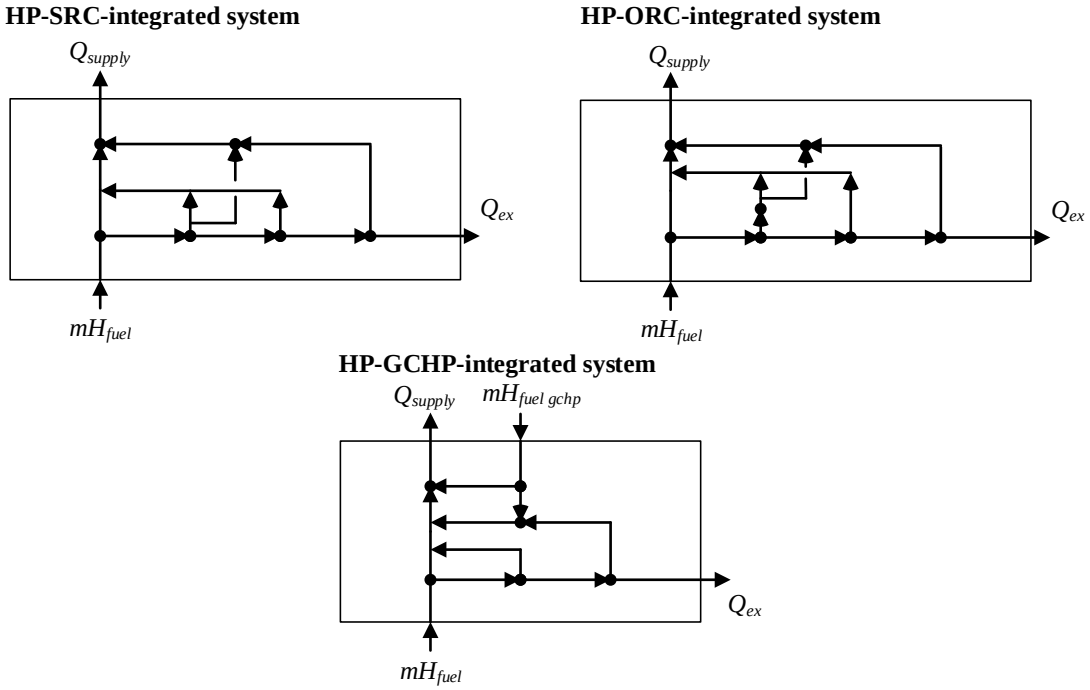

Figure 22: Opposite representation of the topologies of the HP-CHP-integrated systems (own illustration).

In all three CHP integration concepts, the CHP units are primarily electricity-conducted operated to satisfy the power demand of the heat pumps, since the operational control of the CHP unit is closely related to the operation of the heat pumps. Consequently, buffer tanks for heat storage will be necessary to maintain the balance of the heat network. The complexity of the system also increases significantly due to the addition of multiple components. This complexity places high demands on the planning and operation of the entire heating system, requiring careful consideration and management.

4. Methodology for system integration

To implement a comprehensive and transferable method for integrating heat pumps into biomass heating networks, a general simulation model is proposed in this chapter. The model enables the integration of the flue gas condenser and heat pump in biomass heating in different ways, as well as further integration of different types of small-scale cogeneration units to generate onsite electricity for the heat pump. A detailed description of the entire simulation model is carried out in the following sections.

Section 4.1 provides a detailed explanation of the thermodynamic model for each system component. These component models enable the simulation of the different integration concepts that can be applied in biomass heating networks.

Section 4.2 outlines the detailed procedures for integrating the various components of the system according to the selected integration concept. This section provides step-by-step instructions for connecting the modules in the simulation model.

To evaluate the integration concepts from thermodynamic, economic, and environmental perspectives, key performance indicators are defined in Section 4.3. These indicators allow for a comprehensive evaluation of the integration concepts and provide a basis for comparing the different integration options.

4.1 Modeling of System components

To accurately simulate the behavior of the different substances and components in the biomass heating network, the models were developed based on thermodynamic principles. The thermodynamic calculation aims to determine all significant energy and mass flows, which are critical for evaluating the performance of the system component. The main components of the system are the boiler with the combustion chamber, economizer, flue gas condenser, heat pump and different types of cogeneration technologies, including SRC, ORC and gasification cogeneration. In this work, the economizer is defined to recover sensible heat, while the flue gas condenser is primarily for recovering latent heat. Each component is modeled as an abstract object that has specific input and output parameters and can achieve some specific functions.

4.1.1 Combustion and boiler

In the combustion chamber, the incoming fuel and air undergo combustion, resulting in flue gas and ash. To regulate the temperature in the combustion chamber, a portion of the flue gases are typically recirculated. In this work, the combustion chamber, the boiler, and the precipitator are modeled together as a single unit. The mass and energy balance of which can be mathematically formulated as follows:

$$\sum_{s\in S_{in}} \dot{m}_s^{in} = \sum_{s\in S_{out}} \dot{m}_s^{out} \tag{17}$$

$$\dot{Q}_{boiler} + \dot{Q}_{loss} = \sum_{s\in S_{in}} \dot{m}_s^{in} * h_s^{in} - \sum_{s\in S_{out}} \dot{m}_s^{out} * h_s^{out} \tag{18}$$

where $\dot{Q}_{boiler}$ is the heat output of the boiler, which should be specified as a known parameter, and $\dot{Q}_{loss}$ is the heat loss via surface convection of the biomass boiler. The mass and energy flow of various substances *s* can be determined based on the combustion process. During combustion, the supplied fuel and air are converted into flue gas and ash, which contain various substances. The combustion equation based on dry fuel can be expressed as follows:

$$\begin{gathered} C_xH_yN_zS_uCl_vO_wAO_s + \\ \lambda\left(x+\frac{y}{4}+u-\frac{w}{2}\right)\left(O_2+\frac{0.79}{0.21}N_2\right) \rightarrow \\ (x-k)CO_2 + kCO + \frac{y}{2}H_2O + uSO_2 + \\ ((\lambda-1)\left(x+\frac{y}{4}+u-\frac{w}{2}\right)+\frac{k}{2}-j)O_2 + \\ (\frac{0.79}{0.21}\lambda\left(x+\frac{y}{4}+u-\frac{w}{2}\right)+\frac{z-j}{2})N_2 + \\ jNO_2 + vCl + sAO \end{gathered} \tag{19}$$

This formula enables the systematic calculation of the molar proportions of the individual substances and their enthalpy values. The fuel composition in this formula should be given as input, which can be obtained from the supplier or analyzed in the laboratory.

To solve the energy balances, the temperature-related thermal enthalpy h_s^{th} and the chemically bound enthalpy $h_s^{chem.}$ of the substance should be considered. The exact thermal enthalpy values can be determined using the thermodynamic library CoolProp [165], which provides accurate representations of various thermodynamic parameters of pure and pseudo-

pure fluids based on two given thermodynamic state variables. The thermal enthalpy h_s^{th} can be mapped by the pressure p_s and temperature T. And the chemically bound enthalpies $h_s^{chem.}$ are determined based on the lower heating value lhv_s of substance *s*:

$$h_s = h_s^{th} + h_s^{chem.} = h_s(p_s, T) + lhv_s \; \forall \; s \in S_{in}, S_{out} \tag{20}$$

In practice, the most significant limitation in the energy assessment for biomass heating systems is often the accurate determination of fuel consumption $\dot{m}_f$, since it is typically estimated based on the approximate daily burned volume of the fuel, which can be inaccurate. Therefore, it is essential to determine the fuel consumption through a detailed simulation based on the solved mass and energy balance:

$$\dot{m}_f = \frac{3600 * \left(\dot{Q}_{boiler} + \dot{Q}_{loss}\right)}{\sum_{s \in S_{in}}(h_s^{*th} + h_s^{*chem.}) - \sum_{s \in S_{out}}(h_s^{*th} + h_s^{*chem.})} \tag{21}$$

where enthalpy values h_s^* of all substances are based on 1 kg of burned wet biomass fuel. For calculating the heat loss via surface convection of the biomass boiler $\dot{Q}_{loss}$, a simplified model was suggested by Gaderer [21] and adapted for this study, which is detailed in Appendix B.

4.1.2 Heat exchanger

This section sets up the modules of the various heat recyclers, such as economizers, flue gas condensers, as well as air preheaters, which all belong to the category of heat exchanger (HEX) devices. Heat recycler like flue gas condensers are available in both direct and indirect contact systems, as mentioned in Section 2.2.1. In direct contact systems, the cooling water is exposed to the flue gas and used as heat source for the heat pump outflow or directly for heating the network. The condensation water is removed with the cooling water together. In indirect contact system, shell-and-tube and plate heat exchangers are typically used for condenser and economizer, with the condensation water being removed separately.

When the exiting flue gas temperature is lower than the dew point, it signifies that the saturated partial pressure of the vapor at the outlet point in the flue gas is lower than the actual partial pressure of the vapor at the inlet. This discrepancy results in the formation of condensation water from the flue gas. The mass and energy balance within a HEX can be described as follows:

$$\sum_{s \in S_{fg}^{in}} \dot{m}_s^{in} = \sum_{s \in S_{fg}^{out}} \dot{m}_s^{out} + \Delta\dot{m}_c \mid \dot{m}_{clt}^{in} = \dot{m}_{clt}^{out} \tag{22}$$

$$\sum_{s \in S_{fg}^{in}} \dot{m}_s^{in} * h_s^{in} + \dot{m}_{clt}^{in} * h_{clt}^{in} = \sum_{s \in S_{fg}^{out}} \dot{m}_s^{out} * h_s^{out} + \Delta\dot{m}_c * h_c + \dot{m}_{clt}^{out} * h_{clt}^{out} \tag{23}$$

Where $\dot{m}_{clt}^{in}$ and $\dot{m}_{clt}^{out}$ represent the in- and outlet mass flow of the cooling medium, respectively. And $\Delta\dot{m}_c$ is the mass flow of condensation water in the exiting, which can be determined as follows, in relation to the molar amount of dry flue gas $\dot{n}_{fg,dry}^{tot}$.

$$p_{H2O,sat}^{out} = e^{\frac{-5{,}098 + 0{,}051 * t_{fg}^{out}}{1 + 0{,}0043 * t_{fg}^{out}}} \tag{24}$$

$$p_{H2O}^{in} = \frac{\dot{n}_{H2O}}{\dot{n}_{fg,wet}^{tot}} * p_{fg}^{in} \tag{25}$$

$$p_{H2O}^{out} = min\left(p_{H2O,sat}^{out}, p_{H2O}^{in}\right) \tag{26}$$

$$\Delta\dot{m}_c = \frac{p_{H2O}^{in} - p_{H2O}^{out}}{p_{fg}^{in} - p_{H2O}^{in}} * \dot{n}_{fg,dry}^{tot} * M_{H2O} \tag{27}$$

Where p_{H2O}^{in}, p_{H2O}^{out} and $p_{H2O,sat}^{out}$ represent the heat exchanger inlet water vapor partial pressure, the outlet actual water vapor partial pressure and the outlet saturated water vapor partial pressure, respectively. Among these, equation (24) is an empirical formula based on the steam table as a T(p) fit according to [17].

To solve the balances of the heat exchanger, the flue gas composition $\sum_{s \in S_{fg}^{in}} \dot{m}_s^{in}$ and the amount of wet flue gas $\dot{n}_{fg,wet}^{tot}$ should be provided as input or calculated by the combustion boiler model. Additionally, the inlet and outlet temperatures of the heat exchanger should be set. The determination of the enthalpy h_s of substance *s* may also refer to equation (20).

By balancing the mass and energy flows, the performance of the heat exchanger can be determined:

$$\dot{Q}_{hex} = \sum_{s \in S_{fg}^{in}} \dot{m}_s^{in} * h_s^{in} - \sum_{s \in S_{fg}^{out}} \dot{m}_s^{out} * h_s^{out} - \Delta\dot{m}_c * h_c \tag{28}$$

4.1.3 Heat pump

In this section, the heat pump model is presented, which considers the thermodynamic cycle at different temperature levels, with different refrigerants. The simplified scheme with four main components is shown in Figure 23.

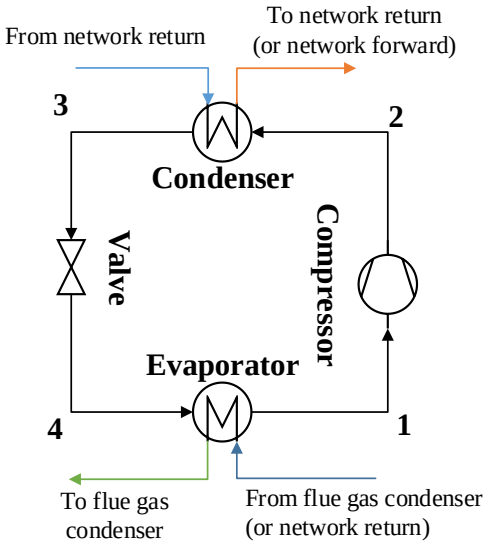

Figure 23: Simplified scheme of the heat pump model (own illustration).

For initializing the heat pump unit, following input parameters shall be specified:

- Source temperature T_{source}^{in}, T_{source}^{out}, e.g., inlet and outlet temperature of the flue gas in the flue gas condenser at the heat pump evaporator side.
- Sink temperature of the heat pump T_{sink}^{in}, T_{sink}^{out}, e.g., inlet and outlet temperature of the network at the heat pump condenser side.
- Available heat flow from the heat source $\dot{Q}_{source}$
- Selected refrigerant *ref*.

The default parameters, such as minimal temperature differences and isentropic efficiency, are listed in Table 3. Using these input parameters, the state of the different points in the thermodynamic cycle and the required size of the different subcomponents can be calculated.

Table 3: Default parameters for the design of the heat pump.

Parameters	***Default values***
Minimal temperature difference between source outlet and evaporating ΔT_e	$5K$
Minimal temperature difference between sink outlet and condensing ΔT_c	$5K$
Compressor isentropic efficiency η_{is}	80 %
Compressor mechanical efficiency η_m	95 %
Compressor electrical efficiency η_{el}	95 %
Valve isolation efficiency η_{iso}	95 %
HEX efficiency η_{hex}	94 %

Thermodynamic cycle

The evaporation and condensation temperature of the cycle can be defined by source and sink temperature, where temperature difference in heat exchangers should be considered. From this, the evaporation and condensation pressure can be determined by the CoolProp database [165].

1→2: The compression model calculates the required compression work based on the given input and output pressures. With the defined evaporating temperature T_e and superheating ΔT_{sh}, as well as the pressure, other thermodynamic parameters at the compressor inlet point can be mapped. The ideal compression process is isentropic, meaning the entropy at the ideal outlet should match that at the inlet. With the entropy and pressure value, the ideal outlet point can be determined:

$$(h, s, q)_1 = map(p_e, T_1, ref.) \tag{29}$$

$$s_{2,is} = s_1 \tag{30}$$

$$(h, T, q)_{2,is} = map(p_c, s_{2,is}, ref.) \tag{31}$$

Real processes invariably involve some entropy gain during compression, which can be described by the isentropic efficiency. The isentropic efficiency of a compressor is defined as the ratio of the work input in an isentropic process to the work input in the actual process for the same inlet and outlet pressures [166]. This often varies from the manufacturer data.

In general, it is complex to calculate, which requires the use of partly spatial models with numerous empirically determined parameters for quantifying the total irreversibility in the circuit [167]. To reduce the complexity of the model, a fixed isentropic efficiency is assumed for the analysis, which is also used in [168]. After calculating the specific enthalpy at the real outlet point, other thermodynamic parameters at that point can also be determined:

$$h_2 = h_1 + \frac{h_{2,is} - h_1}{\eta_{is}} \tag{32}$$

$$(T, s, q)_2 = map(p_c, h_2, ref.) \tag{33}$$

2→3: The condensing model enable the determination of the heating output of the heat pump. The inlet point of the condenser corresponds to the outlet point of the compressor, and the condenser outlet point can be determined by the sink temperature. In the model, it is assumed that the refrigerant is subcooled to the inlet sink temperature, considering the temperature difference in the heat exchanger. This allows the subcooled refrigerant to absorb more heat from the source.

$$(h, s, q)_2 = map(p_c, T_3, ref.) \tag{34}$$

3→4: The valve in the heat pump enables the control of the flow rate of the refrigerant released into the evaporator and is intended to regulate the superheat of the vapor leaving the evaporator [169]. The refrigerant temperature drops below the flue gas temperature after passing through it. Ideally, the specific enthalpy does not change during the isenthalpic process. However, in reality, there can be some enthalpy losses due to insufficient insulation.

$$h_4 = h_3 * \eta_{iso} \tag{35}$$

$$(q)_4 = map(h_4, T_e, ref.) \tag{36}$$

4→1: After passing through the valve, the refrigerant re-enters the evaporator with low enthalpy. Upon evaporation, the refrigerant is heated and then circulates back into the compressor.

The calculation procedure for the thermodynamic cycle is summarized in Table 4.

Table 4: Calculation procedure for the thermodynamic cycle.

Nodes	***Known parameters***	***Solved parameters***
init	$T_e = T_{source}^{out} - \Delta T_e$ $T_c = T_{sink}^{out} + \Delta T_c$ π_{max}, *refrigerant*	p_e, p_c
1"	T_e, p_e, q=1	-
1	$p_e, T_1 = T + \Delta T_{sh}$	h_1, s_1, q_1
2	p_c, s_1, η_{is}	h_2, T_2, q_2
2"	p_c,q=1	$h_{2"}, s_{2"}$
2'	p_c,q=0	$h_{2'}, s_{2'}$
3	$p_c, T_3 = T_e - \Delta T_{sc}$	h_3, s_3, q_3
4	h_3, T_e, η_{iso}	h_4, s_4, q_4

Energy flows

With the defined cycle, the refrigerant flow rate $\dot{m}_{ref}$ and energy flows, like the available heat supply $\dot{Q}_{sink}$ and the required electrical power P_{el} can be determined as follows:

$$\dot{m}_{ref} = \frac{\dot{Q}_{source} * \eta_{hex}}{h_1 - h_4} \tag{37}$$

$$\dot{Q}_{sink} = \dot{m}_{ref} * (h_2 - h_3) * \eta_{hex} \tag{38}$$

$$P_{el} = \frac{\dot{m}_{ref} * (h_2 - h_1)}{\eta_m * \eta_{el}} \tag{39}$$

Where η_{hex}, η_m and η_{el} represent the heat exchange efficiency, compressor mechanical efficiency, and compressor electrical efficiency, respectively.

For the evaluating the performance of the heat pump, the Coefficient of Performance (COP) can be calculated based on the heat supply and the electricity demand, following Equation (11).

4.1.4 Rankine Cycle

This subsection set up the model of the Rankine Cycle, which is applicable to both SRC and ORC units. By varying the chosen working medium, along with the working pressure and temperature, the thermodynamic cycles can be simulated, allowing for the analysis of electrical efficiency. The SRC or ORC consists of Evaporator, Expander, Condenser and Pump. For an ORC unit, a recuperator is also often employed to improve the cycle efficiency, when dry OWF is used. The design of the thermodynamic cycle is analogous to that of the heat pump process. A simplified scheme of the model is shown in Figure 24.

Similar to the heat pump model, the following input parameters should be specified:

- Source temperature $T^{in}_{source,rc}$, $T^{out}_{source,rc}$, e.g., inlet and outlet temperature of the heat source
- Sink temperature $T^{in}_{sink,rc}$, $T^{out}_{sink,rc}$, e.g., inlet and outlet temperature from network
- Necessary power requirement for the operation of the heat pump
- Selected working medium *wf*.

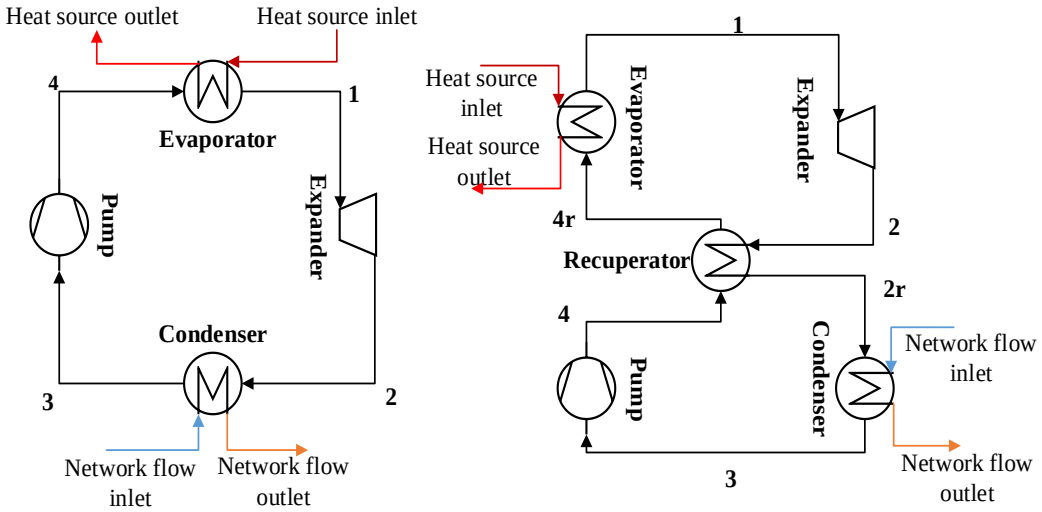

Figure 24: Simplified schematic of CHP unit based on Rankine cycle (Left: SRC or ORC without recuperator, right: ORC with recuperator) (own illustration).

The default parameters, e.g., minimal temperature differences and isentropic efficiencies are listed in Table 5. Using these parameters, the state of the different points in the thermodynamic cycle and the required size of the various subcomponents can be determined.

Table 5: Default parameters for the design of the Rankine Cycle.

Parameters	***Default values***
Minimal temperature difference inside heat exchanger ΔT_{hex}	$5K$
Expander isentropic efficiency η_{is} [134,170]	75 %
Mechanical efficiency η_m [134]	95 %
Pump efficiency η_{pump} [171]	70 %
Electrical generator efficiency (including inverter) η_{eg} [170]	92 %
HEX efficiency η_{hex}	94 %

Thermodynamic cycle

For the ORC design, to prevent issues caused by a supercritical cycle, the maximum possible evaporation temperature is set below the critical temperature. For the SRC design, a maximum pressure of 100 bar and a temperature of 450 °C, as suggested by Badmi et al. [134], are chosen. These parameters represent a balance between high efficiency and the technical limitations of standard technology. The process of identifying each point is detailed below. The calculation of each state point depicted in Figure 24 is outlined as follows.

1→2: Similar to the compression process, there is an entropy increase in the actual expansion process. The default value of the isentropic efficiency of the expansion process η_{is} is set to 0.7 for both steam engine [134] and ORC expander [170] in this model, reflecting the current status of both technologies. With this parameter, the enthalpy of the expander exit point can be calculated.

$$h_2 = h_1 - (h_1 - h_{2,is}) * \eta_{is} \tag{40}$$

2→(2r→) 3: In a simple cycle without a recuperator, the working fluid flows directly into the condenser after expansion. The entry point of the condenser is exactly the same as the exit point of the expander. When using dry working fluid, it is possible to install a recuperator to improve the efficiency of the circuit. In this case, the working fluid flows to the recuperator after expansion. The minimum exit point $2r$ on the recuperator source side is determined by the condensation temperature T_c, which can be defined as

$$T_{2r,min} = T_c + \Delta T_{hex} \tag{41}$$

The exit point of the working fluid on condenser is defined as the point of saturated liquid at the condensation temperature T_c, and pressure p_c,. The condition can be determined by calling the CoolProp database.

3→4: The pump maintains both the pressure and the mass flow of the working fluid. The condensed liquid from the condenser is pumped to the required evaporation pressure. The pumping work should also be taken into account when calculating the output and efficiency of the ORC unit [171].

4→ (4r→) 1: After pumping, the working fluid enters the recuperator or directly the evaporator as an unsaturated liquid under high pressure. The maximum temperature at the recuperator's sink side outlet cannot exceed the source inlet side's temperature minus the heat exchanger's temperature difference:

$$T_{4r,max} = T_2 - \Delta T_{hex} \tag{42}$$

The maximum available recovered specific enthalpy is:

$$\Delta h_r = \min\left(h_2 - h_{2r,min}, h_{4r,max} - h_4\right) \tag{43}$$

Table 6: Calculation procedure for the thermodynamic cycle of the ORC or steam plants.

	Points	***Known parameters***	***Solved parameters***
	init	$T_{e,max} = \min(T_{crit}, T^{in}_{source,rc} - \Delta T_e - \Delta T_{sh})$ $T_{c,min} = T^{out}_{sink,rc} + \Delta T_c$ $p_{e,max}, \pi_{max}, wf$	$p_e = min(f(T_{e,max}), p_{e\_max})$ $T_e = f(p_e)$ $p_c = max(f(T_{c,min}), p_e/\pi_{max})$ $T_c = f(p_c)$
Without recuperator	1"	$T_e, p_e, q=1$	-
	1	$p_e, T_1 = \min(T_{1,max}, T_e + \Delta T_{sh})$	h_1, s_1
	2	p_c, s_1, η_{is}	h_2, T_2, s_2, q_2
	2"	$p_c, q=1$	$h_{2"}, s_{2"}$
	3(2')	$p_c, q=0$	h_3, s_3
	4	p_e, s_3, η_{is}	h_4, s_4, q_4
Recuperator	2r	T_4, p_c	T_{2r}, s_{2r}
	4r	T_2, p_e	T_{4r}, s_{4r}

Based on the recovered specific enthalpy, the specific enthalpy of the recuperator's exit points on the source and sink side and other states can be calculated. The calculation procedure for each point of the Clausius-Rankine cycle is recorded in Table 6.

Energy flows

Energy flows are crucial in determining the efficiency. The required electrical power for the heat pump, serving as an input, allows for the calculation of the working fluid's mass flow rate:

$$\dot{m}_{wf} = \frac{P_{el}}{\eta_m * \eta_{eg} * (h_1 - h_2) - (h_4 - h_3)/\eta_{pump}} \tag{44}$$

The various energy flows are determined using the following equations:

$$\dot{Q}_{source} = \dot{m}_{wf} * (h_1 - h_{4r})/\eta_{hex} \tag{45}$$

$$P_{el,eg} = \dot{m}_{wf} * (h_1 - h_2) * \eta_m * \eta_{eg} \tag{46}$$

$$\dot{Q}_{sink} = \dot{m}_{wf} * (h_{2r} - h_3) * \eta_{hex} \tag{47}$$

$$P_{el,pump} = \dot{m}_{wf} * \frac{h_4 - h_3}{\eta_{pump}} \tag{48}$$

The electrical and thermal efficiency of the cogeneration unit can be calculated as follows:

$$\eta_{el} = \frac{P_{el,eg} - P_{el,pump}}{\dot{Q}_{source}} \tag{49}$$

$$\eta_{th} = \frac{\dot{Q}_{sink}}{\dot{Q}_{source}} \tag{50}$$

4.1.5 Wood gasifier CHP

An other possibility to provide the necessary power for the heat pump operation is through a small biomass gasifier cogeneration unit (GCHP). In this model, the GCHP is considered as an integrated device that includes a gas conversion component and a gas engine unit for power and heat generation [172]. In the biomass gasification unit, the fuel is first converted into syngas consisting of H_2, CO, CO_2, H_2O, CH_4, N_2, and residual coal. [149]. The gas conversion efficiency $\eta_{gasifier}$ is assumed to be 0.85 in the model, which is state of the art [151]. The syngas subsequently enters the gas engine unit and is burnt to generate electricity

and heat. The mass and energy balances of the gasifier cogeneration unit (GCHP) are analogous to the boiler model.

The partial load behaviors of gas engine units vary greatly. Electrical, thermal and overall efficiencies depend on various factors such as manufacturer, network temperature, modulation z, and most importantly, the rated power $P_{el,n}$ of a GCHP. In ref. [173], two general formulas are established for calculating the electrical efficiency η_{el} and thermal efficiency η_{th} of a gas engine CHP units, based on a variety of product data from gas engine CHP manufacturers, which had been proven by Koch et al. [174] to be applicable to biogas engine cogeneration as well.

$$\eta_{el} = 0.27 + 0{,}1089 * (z - 0.33) + 0{,}0255 * \Big(log\big(P_{el,n}\big) - log(50)\Big) \tag{51}$$

$$\begin{aligned}\eta_{th} = {} & 0.61 - 0.0746 * (z - 0.33) - 0.0255 * \big(log\big(P_{el,n}\big) - log(50)\big) \\ & -0.002 * (T_{return} - 45) - 0.00175 * \big(T_{feed} - 90\big)\end{aligned} \tag{52}$$

where z is the modulation of the cogeneration.

$$z = \frac{P_{el}}{P_{el,n}} \tag{53}$$

Based on these equations, the power to heat ratio of the cogeneration σ can be determined:

$$\sigma = \frac{\eta_{el}}{\eta_{th}} = f\big(P_{el,n}, z\big) \tag{54}$$

In this work, the power output of the GCHP $P_{el,gchp}$ should be decided by the simulated power demand of the heat pump, and therefore be provided as an input parameter in the GCHP module. The power to heat ratio σ then allows the calculation of its thermal output $\dot{Q}_{th,gchp}$:

$$\dot{Q}_{th,gchp} = \frac{P_{el,gchp}}{\sigma} \tag{55}$$

The overall efficiency of the GCHP η_{gchp} would be the product of the gas conversion efficiency and the total efficiency of biogas engine CHP:

$$\eta_{gchp} = \eta_{gasifier} * (\eta_{el} + \eta_{th}) \tag{56}$$

With the obtained values $P_{el,gchp}$, $\dot{Q}_{th,gchp}$, η_{gchp}, the fuel demand of the *GCHP* $\dot{m}_{f,gchp}$ can now be determined by:

$$\dot{m}_{f,gchp} = \frac{\left(\dot{Q}_{th,gchp} + P_{el,gchp}\right)}{\eta_{gchp} * H_{fuel,gchp}} \tag{57}$$

4.1.6 Heat network

In this study, the focus is on the primary heating cycle of the networks before the heat transfer station. This cycle is characterized by the measured heating demand of the primary cycle (which encompasses the heat losses in the secondary heating cycle), along with the main grid return and forward temperatures. Due to the short lengths of the pipes in the primary cycle, heat loss is considered negligible. The flow rate in this context is expressed as follows:

$$\dot{m}_{main}^{net} = \frac{\dot{Q}_{demand}}{T_{feed}^{net} - T_{return}^{net}} \tag{58}$$

4.2 System integration

Depending on the selected concept and required input parameters, different modules can be initialized and connected based on their interconnection of the mass and energy flows. The devices to be integrated include system components such as heat exchanger (e.g., economizer, flue gas condenser), heat pump and cogeneration units. The integration process for the heat exchanger, which cools the flue gas, and the heat pump, which assists the condensation, is described in subsection 4.2.1. The process for integrating the cogeneration units to power the heat pumps is described in subsection 4.2.2. Subsection 4.2.3 describes the solving procedure of the system's energy balance, allowing for simulation of the system as an integrated unit.

4.2.1 Integration procedure of heat pump

An overview of the approach to integrate the different heat exchangers and heat pump into the system, as well the interconnection of the mass and energy flows of different modules, is displayed in Figure 25.

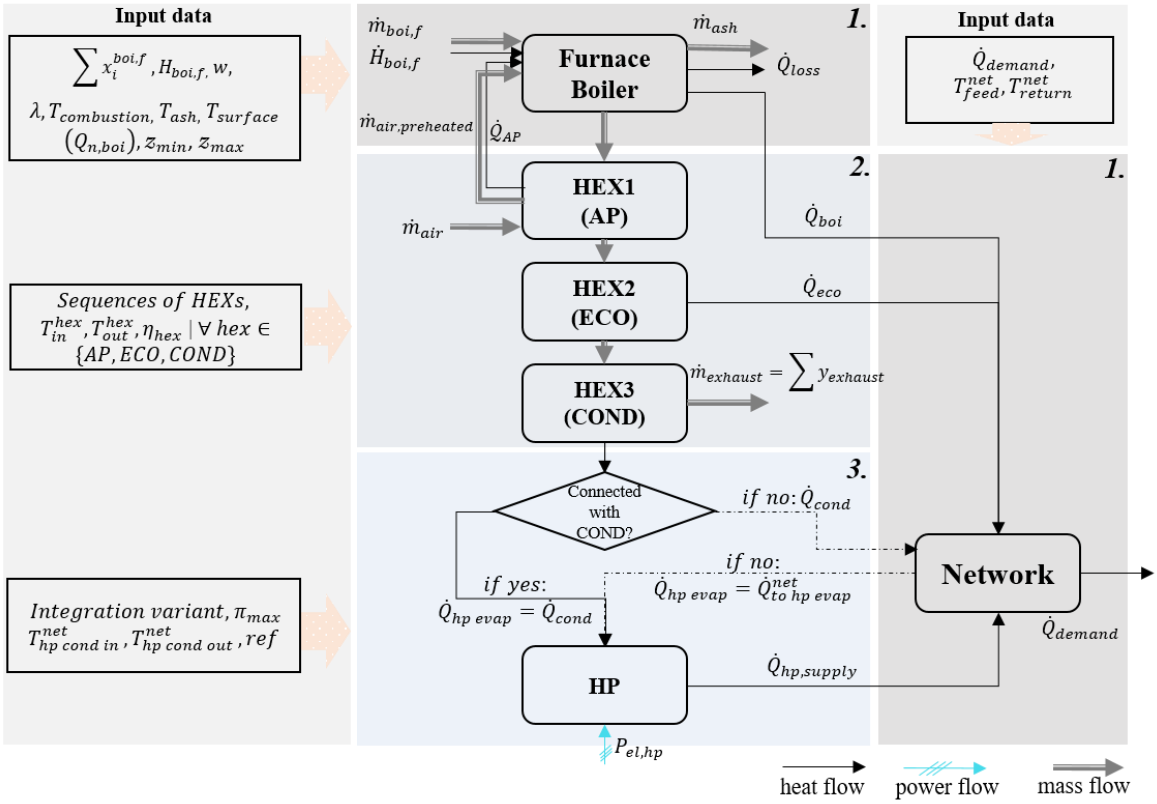

Figure 25: Flow chart of the integration process of heat exchangers and heat pump.

1. Model initialization

For the initialization of the whole system simulation model, the network pipeline and the biomass boiler models should first be initialized.

Initialization of the network model: The annual network demand time series $\dot{Q}_{demand}^{t}$ as well as the required network temperatures, i.e., network return temperature T_{return}^{net} and feed forward temperature T_{feed}^{net}, should be specified.

Initialization of the boiler model: This begins with setting up the fuel data, which includes the type of biomass being used (e.g., wood chips or pellets or self-defined), the fuel element composition $\sum x_i^{boi}$, as well as the water content w, and fuel lower heating value $H_{boi,f}$. Following this, other parameters of the boiler should be specified. If the existing boiler in the heating network remains to in operation, its historical technical data, including the boiler nominal heat output $Q_{n,boi}$, the combustion air ratio λ, combustion temperature $T_{combustion}$, ash temperature T_{ash}, surface temperature $T_{surface}$, should be provided. With these input parameters, the mass and energy balance within the boiler model can be solved.

For an assessment of the historical actual operation of a specific biomass heating network, the performance profile of the boiler $\dot{Q}_{boi}^{t}$ can be determined from measurements and used as input. If the boiler is equipped with a cogeneration unit, e.g., ORC, the furnace total performance will be:

$$\dot{Q}_{furnace}^{t} = \dot{Q}_{boi,th}^{t} + \frac{P_{gen,el}^{t}}{\eta_{gen.el}} \tag{59}$$

In scenarios that the existing boiler is being replaced or if the boiler nominal heat output $Q_{n,boi}$ is not available, the nominal heat output of the boiler should be determined iteratively by solving the whole system model. For accuracy, it is recommended to use a small-time interval for the network demand data $\dot{Q}_{demand}^{t}$, such as one hour, to account for fluctuations in demand throughout the day and year.

To ensure accurate simulation of biomass heating systems, it is crucial to account for both mass and energy balances as well as the operating constraints of the biomass boilers. These constraints include the part-load operating thresholds and the minimum full utilization hours (FUH_{min}) of the boilers. The part-load operating thresholds refer to the minimum and maximum heat outputs at which the boiler can operate efficiently. These thresholds are critical for system performance and should be considered during the simulation. The FUH_{min} for the biomass boilers is the minimum number of equivalent hours that the boiler should run at full load annually. This constraint ensures optimal utilization of the boiler. These operating constraints should be incorporated as input parameters to model the performance of the biomass heating system accurately:

$$z_{boi,min} \leq \frac{\dot{Q}_{boi}^{t}}{Q_{n,boi}} \leq z_{boi,max} \quad \forall \quad t \in S_t \tag{60}$$

$$\int \dot{Q}_{boi}^{t}\, dt \geq Q_{n,boi} * FUH_{min} \; \forall \quad t \in S_t \tag{61}$$

where $z_{boi,min}$ and $z_{boi,max}$ stand for the minimal and maximal operating modulation of boiler, respectively. The integrals are calculated numerically over a year. dt denotes the time interval of the demand time series S_t.

2. Integration of the heat exchangers

To initialize the heat exchanger model, the inlet- and outlet temperatures of flue gas for each type of heat exchanger T_{in}^{hex}, T_{out}^{hex} should be set as predetermined values. Additionally, the inlet gas composition $\sum y_{fg,in}^{hex}$ should be determined. To get this value, the sequences of different types of heat exchangers must be first defined. In this sequence, the economizer must be connected before the flue gas condenser to prevent condensation in the economizer. Various installation and placement options for the air preheater can be considered in the model, including:

- No installation of an air preheater
- Installation before the economizer and condenser
- Installation after the economizer and before the condenser
- Installation after the economizer and condenser

Once the sequence of heat exchangers is established, they can be integrated to the boiler. The inlet flue gas composition and enthalpy of the most upstream of these heat exchangers is identical to the flue gas composition coming out of the boiler, which can be obtained from the boiler model. The outlet flue gas of the upstream heat exchanger is also identical to the inlet flue gas of the next heat exchanger. Thus, using the calculated flue gas composition from the boiler model, the outlet flue gas composition $\sum y_{fg,out}^{hex}$ and the heat output $\dot{Q}_{hex}$ of each heat exchanger can be solved.

3. Integration of the heat pump

After integrating heat exchangers for heat recovery, the heat pump can be integrated depending on the chosen connection variant. It is crucial to ensure that the heat pump is sized as small as possible for a given flue gas outlet temperature to avoid unnecessary investments.

In the flue gas-side integration variant, the heat pump directly extracts heat from the flue gas. Hence, the heat source for the heat pump evaporator $\dot{Q}_{hp\,evap}$ originates from the output of the flue gas condenser:

$$\dot{Q}_{hp\,evap} = \dot{Q}_{cond} \tag{62}$$

To cool the flue gas to the targeted exhaust temperature, the capacity of the heat pump evaporator should match that of the flue gas condenser. Consequently, the inlet gas temperature of the flue gas condenser $T_{cond\,in}^{fg}$ should be as low as possible to minimize the size of the heat pump.

In the network-side integration variant, where the heat pump evaporator is connected to the mains return, the heat output of the flue gas condenser $\dot{Q}_{cond}$ is directly fed into the network. The heat pump draws heat from the mains return. The size of the heat pump evaporator $\dot{Q}_{hp\ evap}$ can be adjusted within a certain range depending on the requirements. This can be achieved by varying the diverted network water flow to the heat pump evaporator $\dot{m}_{to\ hp\ evap}^{cooled\ net}$. The setting of the cooled return flow temperature $T_{to\ cond}^{cooled\ net}$ depends on the target outlet gas temperature of flue gas condenser $T_{cond\ out}^{fg}$.

$$\dot{Q}_{hp\ evap} = \dot{m}_{to\ hp\ evap}^{cooled\ net} * c_p * \left(T_{return}^{main\ net} - T_{to\ cond}^{cooled\ net}\right) \tag{63}$$

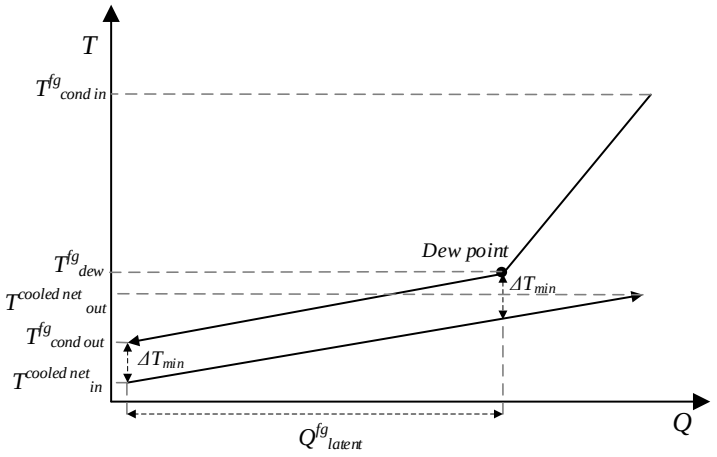

Figure 26: Pinch analysis of the flue gas condensation process.

It is important to maintain a minimum flow rate of the cooling water to the evaporator $\dot{m}_{to\ hp\ evap}^{cooled\ net}$, as a higher flow rate would necessitate a larger heat pump capacity at the given inlet and outlet water temperature of the evaporator. However, to ensure effective waste heat recovery, it is equally essential to ensure that the flow rate of the cooling water does not fall below a certain limit. Pinch analysis, as shown in Figure 26, indicates that the heat capacity of the cooling water flow should not be less than the heat capacity of the flue gas during condensation. To balance these factors and achieve efficient waste heat recovery while minimizing the heat pump size, the following constraints are applied based on a pinch analysis:

$$\frac{\dot{Q}_{fg,latent}}{c_p\left(T_{dew}^{fg} - T_{cond\ out}^{fg}\right)} \leq \dot{m}_{to\ hp\ evap}^{cooled\ net} \leq \dot{m}_{main}^{net} \tag{64}$$

Where $\dot{Q}_{fg,latent}$ is the recoverable latent heat from the flue gas. T_{dew}^{fg} and $T_{cond\ out}^{fg}$ indicate the dew point of the flue gas and the flue gas outlet temperature of the condenser, respectively.

From Equation (64) it can be derived that the lowest amount of bypassed network water flow $\dot{m}_{to\ hp\ evap}^{cooled\ net}$ depends on the recoverable latent heat $\dot{Q}_{fg,latent}$ and dew point of the flue gas T_{dew}^{fg} at a specified $T_{cond\ out}^{fg}$. The pinch analysis in Figure 26 also indicates that the inlet temperature of the flue gas to the condenser in this variant don't need to be as low as possible. For this reason, the economizer before the flue gas condenser is not mandatory.

When selecting the heat pump supply temperature for either integration variant, it's important to ensure that this temperature cannot fall below the minimum value so that the heat can be efficiently fed into the network. The limit value of the heat pump supply temperature T_{hp} depends on the maximum possible water mass flow from network to the heat pump condenser , i.e., the total mass flow of the mains return network $\dot{m}_{main}^{net}$ and the inlet sink temperature of the heat pump $T_{hp\ cond\ in}^{net}$.

$$\frac{\dot{Q}_{hp}}{\dot{m}_{main}^{net} * c_p} + T_{hp\ cond\ in}^{net} \leq T_{hp} \tag{65}$$

Where $T_{hp\ cond\ in}^{net}$ is usually identical to the main network return temperature T_{return}^{net}. And the heat supply of the heat pump $\dot{Q}_{hp}$ shall be obtained by iterative calculation.

After setting the operating temperature and mass flow parameters, the appropriate refrigerant can be selected based on the chemical and physical properties, safety risks, and environmental factors, as described in Section 2.3.1.

With these steps completed, the heat pump model can be initialized. Subsequently, the required electricity demand $P_{hp,el}$ and heat output $\dot{Q}_{hp}$ of the heat pump can be calculated based on the thermodynamic cycle.

4.2.2 Integration procedure of cogeneration units

After initializing the heat pump model and determining the power demand, a cogeneration unit can be integrated into the system. This could either be a Rankine Cycle-based cogeneration unit integrated into the boiler furnace or a gasification cogeneration (GCHP) unit integrated independently into the system. An overview of the integration procedure of

various cogeneration units are represented in Figure 27, using the flue gas-side concept as examples.

In scenarios where a SRC or an ORC unit is to be integrated, the heat source of the cycle shall be covered by the boiler furnace, which leads to an additional heat flow $\dot{Q}_{to\ chp}$ ($\dot{Q}_{to\ src}$ or $\dot{Q}_{to\ oil\ hex}$) out of boiler model. In this case, the furnace total performance will be the summary of the boiler output and the heat flow to the congenator. The required heat flow can be calculated by initializing the cogeneration models.

To initialize the Rankine Cycle model, the maximal allowed evaporating temperature $T_{e,max}$ and pressure $p_{e,max}$, as well as the cycle working fluid wf, shall be specified as input. These inputs determine the evaporating temperature and pressure of the cycle. The condensing temperature is defined by the network temperatures, i.e. the sink temperature. By determining the operation temperature and working fluid, the thermodynamic cycle can be initialized, and the electrical and thermal efficiencies calculated. Then, based on the simulated power demand of the heat pump $P_{hp,el}$, the required heat demand from the boiler $\dot{Q}_{to\ chp}$ and the heat supply for the network $\dot{Q}_{chp}$ ($\dot{Q}_{src}$ or $\dot{Q}_{orc}$) can be solved. For the ORC unit, the heat loss of the oil heat exchanger should also be considered.

It should be noted that small-scale SRC unit and ORC unit usually have lower electrical efficiency at a higher condensing temperature up to 90 °C. To cover the heat pump power demand, increased furnace heating performance is required. However, this leads to a larger flue gas volume, and therefore more waste heat, as well as a higher power demand for its heat recovery by the heat pump. It's possible that the electricity generated by the CHP unit may not cover the increased electricity demand for waste heat recovery. The minimal possible electrical efficiency of the SRC and ORC unit can be defined as follows:

$$\eta_{el,min} = \xi/(COP - 1) \tag{66}$$

Where ξ is the ratio of heat performance of the flue gas condenser $\dot{Q}_{cond}$ to the furnace heat performance $\dot{Q}_{furnace}$, which can be calculated by simulation. This value is considered constant when the fuel data and operating parameters of the boiler and flue gas condenser remain unchanged. The derivation of this formula is detailed in Appendix D. When the cycle electrical efficiency falls below this limit, the integration of the cogeneration unit is deemed unsuitable for powering the heat pump.

In scenarios, where a GCHP unit is to be integrated, additional fuel is required. To initialize the GCHP model, fuel data (such as fuel type (e.g. pellet) and fuel element composition x_i^{gchp}, fuel heating value $H_{f,gchp}$) and the technical specifications (such as combustion air ratio λ, minimal and maximal modulation z_{min}, z_{max}) for it should be set up, analogous to the boiler model. Using the simulated power demand of the heat pump $P_{hp,el}$, the required electricity production $P_{el,gchp}$ can be quantified. Then, the empirical electrical efficiency $\eta_{el}(P_{el,n}, z)$, thermal efficiency $\eta_{th}(P_{el,n}, z, T_{return}^{net}, T_{supply}^{net})$, thermal output $\dot{Q}_{th,gchp}$ and the fuel demand $\dot{m}_{f,gchp}$ of the GCHP unit can be determined.

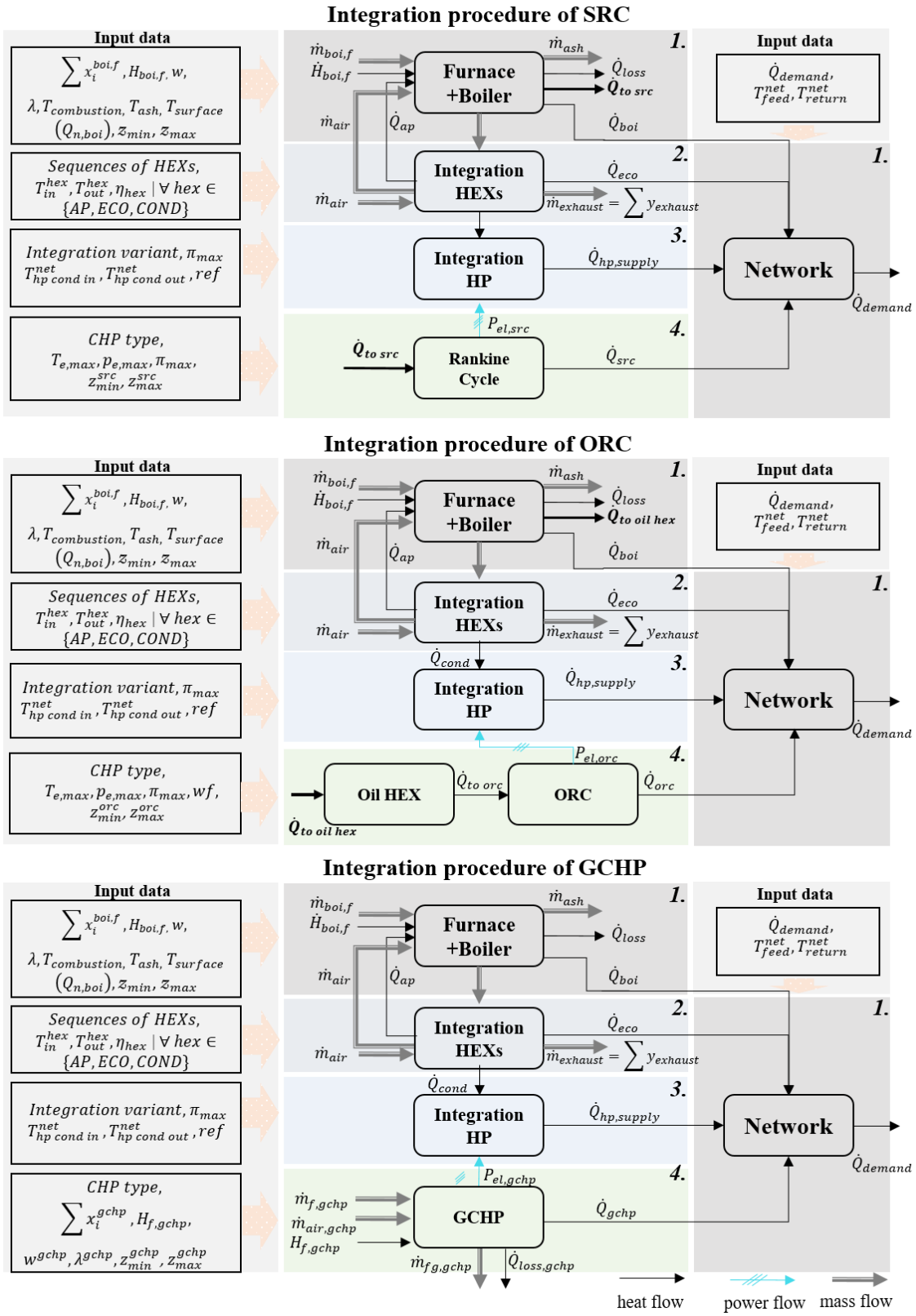

Figure 27: Flow chart of the integration processes of various cogeneration units.

4.2.3 Solving energy system

Once the main components are integrated and the selected system configuration is initialized, the next step involves determining the energy flows and sizes of the components. This is achieved by solving energy balance equations based on the network demand.

In the flue gas-side concept, the total heat demand of the heat network will be supplied by the biomass boiler $\dot{Q}_{bio\ boi}$, the economizer $\dot{Q}_{eco}$, the heat pump $\dot{Q}_{hp}$, the CHP unit $\dot{Q}_{chp}$ and possibly an additional peak load boiler $\dot{Q}_{pl\ boi}$, which can be expressed as:

$$\dot{Q}_{demand} = \sum_{i \in \{bio\ boi, eco, hp, chp, pl\ boi\}} \dot{Q}_i \tag{67}$$

In the network-side concept, the heat flows will include heat input from the boiler, the economizer and the heat pump, as well as the heat input from the flue gas condenser $\dot{Q}_{cond}$ and the heat extraction from the network $\dot{Q}^{net}_{to\ hp\ evap}$ by the heat pump evaporator.

$$\dot{Q}_{demand} = \sum_{i \in \{bio\ boi, eco, cond, hp, chp, pl\ boi\}} \dot{Q}_i - \dot{Q}^{net}_{to\ hp\ evap} \tag{68}$$

The nominal capacity of the various components corresponds to the maximum required performance of the individual components:

$$Q_{n.i} = f_{size} * \max_{t \in S_t} \{\dot{Q}_{i,t}\} \ \forall\ i \in \{bio\ boi, eco, cond, hp, chp, pl\ boi\} \tag{69}$$

where S_t denotes the set of time series over a year, and f_{size} is the size factor in the actual design, which is usually equal to or greater than 1 to ensure that the maximum output can be guaranteed.

4.3 Evaluation indicators

For evaluating the different systems, some key performance indicators (KPIs) are defined in this section. The analysis is conducted from three perspectives: energetical, economical as well as environmental. These KPIs will provide a comprehensive assessment of each system's performance, encompassing efficiency, cost-effectiveness, and environmental impact.

4.3.1 Technical indicator

To describe the overall energy performance of a system with different types of energy inputs, the indicator "figure of merit" was suggested by Rosen et al. [175] and Wirtz et al. [176] for indicating the overall efficiency of an integrated system. This is determined by the ratio of annual total energy supply and the sum of energy inputs into the system. For the systems studied, it can be defined in a uniform form as:

$$f_{lhv,sys} = \frac{\int (\dot{Q}_{demand} + P_{surplus}) dt}{\int (\sum_{i \in \{bio\ boi, gchp, pl\ boi\}} \dot{m}_{f,i} * H_{f,i} + P_{el\ from\ grid}) dt} \tag{70}$$

The integrals are calculated numerically over a yearly time period, where dt denotes the time interval of the demand time series. The total energy produced primarily satisfies the heat demand of the network $\dot{Q}_{demand}$. In case where surplus electricity $P_{surplus}$ is generated and fed into the power grid, it should also be considered. Otherwise, this value is zero. The energy input includes the fuel energy consumption of the biomass boiler, peak load boiler, and possibly the GCHP unit (based on the lower heating value (*lhv*)). Additionally, auxiliary electricity $P_{el\ from\ grid}$ from power grid is required to drive the heat pump,if no cogeneration is installed or its operation is limited.

The exergy efficiency of the system, considering the quality of energy expenditures, can be expressed as:

$$f_{ex,overall} = \frac{\int (\sum_{c \in \{bio\ boi, hp, hexs, chp, pl\ boi\}} \dot{Q}_c \left(1 - \frac{T_0}{T_{c,supply}}\right) + P_{surplus}) dt}{\int (\sum_{i \in \{bio\ boi, gchp, pl\ boi\}} \beta_{f,i} * \dot{m}_{f,i} * H_{f,i} + P_{el\ from\ grid}) dt} \tag{71}$$

where the T_0 and $T_{c,supply}$ represent the ambient temperature and the supply temperature of the component *c* at a specific time slot. The β_f defines the "merit of the fuel" [177], which describes the quality of the fuel for exergy analysis. For wood, this value is estimated to be about 1.15 in [177].

4.3.2 Economic indicator

The levelized cost of heating production (*LCOE*) of the entire system is chosen as the criterion to evaluate the economic feasibility of the concepts. This criterion indicates the normalization of the annualized cost to the total annual supply E_{supply}^{year} and can be expressed as:

$$lcoe = \frac{TAC^{year}}{E_{supply}^{year}} = \frac{CAPEX^{year} + OPEX^{year}}{\int (\dot{Q}_{demand} + P_{surplus}) dt} \tag{72}$$

Where TAC^{year} represents the total annualized cost of the system, which consist of the annualized capital cost $CAPEX^{year}$ and the annual operating cost $OPEX^{year}$. These values are determined using the annuity method, considering the net present value following the German guideline VDI 2067 [178]. A higher *LCOE* indicates greater payout and a correspondingly poor economic feasibility of the entire integrated system.

The annualized capital cost $CAPEX^{year}$ denotes the annualized costs of the system over its entire service life. The value is obtained from the initial investment I_c for each component c with the respective annualization factor $a_{inv,c}$ according to the VDI 2067:

$$CAPEX^{year} = \sum_{c \in \{bio\ boi, ap, eco, cond, hp, gchp, pl\ boi\}} I_c * a_{inv,c} \tag{73}$$

The investment costs for the main components in the heating plant can be represented as functions in the model. These costs, including those for a biomass boiler (comprising the furnace, boiler, pumps, electrics, etc.), air preheating, economizer, and flue gas condensation, are estimated using the WDesign database [51], under consideration of the Chemical Engineering's Plant Cost Index (CEPCI) [179] change from 2004 to 2021. For estimating the costs of industrial heat pumps for flue gas heat recovery, the research by Pieper et al. [27] is adopted. To account for the installation costs, an installation factor of 1.3 is also applied to all components. These default cost functions are listed in Table 20 in Appendix E.

The annual operating cost consists of the fixed operating cost $OPEX_{fix}^{year}$ and variable operating cost $OPEX_{var}^{year}$:

$$OPEX^{year} = OPEX_{fix}^{year} + OPEX_{var}^{year} \tag{74}$$

Where the fixed operating cost $OPEX_{fix}^{year}$ comes from the annual expense for maintenance, staff, emission control, etc., which can be estimated by a fixed factor $f_{o\&m}$ related to the investments:

$$OPEX_{fix}^{year} = \sum_{c \in \{bio\ boi, ap, eco, cond, hp, gchp, pl\ boi\}} I_c \cdot f_{o\&m,c} \tag{75}$$

The default values of $f_{o\&m}$ can also be found in Table 20 in Appendix E.

The $OPEX_{var}^{year}$ consist of the performance-related costs, such as fuel costs for the biomass boiler and the GCHP unit, electricity costs from the grid, and costs for ash disposal and cleaning:

$$OPEX_{var}^{year} = \int \Big(\sum_{i=bio\ boi,gchp,pl\ boi} c_{f,i} \cdot \dot{m}_{f,i} H_{f,i} + c_{el} \cdot P_{el,from\ grid} + c_{ash\ \&\ cleaning} \cdot \sum_{i=bio\ boi,gchp} \dot{Q}_i \Big) dt \quad (76)$$

where $c_{f,i}$, c_{el}, $c_{ash\ \&\ cleaning}$ represent the energy specific costs of fuel, electricity, ash disposal and cleaning, respectively. The default values of which are also listed in Table 21 in Appendix E.

4.3.3 Environmental indicators

In the various systems considered, different forms of energy are consumed, which can significantly influence the environmental impact of these concepts. The following equations are applied to evaluate how the equivalent primary energy demand and CO2 emissions change with the implementation of the concepts:

$$e_{CO2,sys} = \frac{\int (\sum_{i=bio\ boi,gchp,pl\ boi} \dot{m}_{f,i} * H_{f,i} * f_{CO2_{f,i}} + P_{el\ from\ grid} * f_{CO2_{el}}) dt}{\int (\dot{Q}_{demand} + P_{surplus}) dt} \quad (77)$$

$$e_{PE,sys} = \frac{\int (\sum_{i=bio\ boi,gchp,pl\ boi} \dot{m}_{f,i} * H_{f,i} * f_{PE_{f,i}} + P_{el\ from\ grid} * f_{PE_{el}}) dt}{\int (\dot{Q}_{demand} + P_{surplus}) dt} \quad (78)$$

Where, the e_{CO2} and e_{PE} represent the specific CO2 emissions and specific primary energy demand of the system based on per unit of energy supply, respectively. And $f_{CO2_{i,f}}$ denotes the CO_2 emission factors for different fuels used and $f_{CO2_{el}}$ represents the CO2 emission factor for electricity from the public power grid. The CO2 emission factors reported by the Federal Environment Agency in 2020 [180] are used as the default reference values for Germany (detailed in Table 22 in the Appendix E).

5. Development of the optimization framework

In general, selecting of the appropriate concept and planning a biomass energy system with the integration of multiple devices is a complex process. To ensure diligent selection of the proposed concepts and to maximize the benefits of the selected system, developing an optimization approach at the system level is necessary. This approach should simultaneously consider the technical, economic, and environmental impacts as well as the interactions between the system components. Furthermore, the various connection variants of the heat pump and its parameter selection make the optimization approach a feasible and recommended solution for achieving the optimal design of the entire system.

This chapter presents the optimization framework, which aims to find the best combination of the variable decision variables to simultaneously minimize the levelized cost of energy production and specific CO_2 emission, while still improving system efficiency.

5.1 Selection of optimization approach

Generally, there are two ways to formulate an optimization problem [181]. The first is to express the optimization objective and boundary conditions in a linear or non-linear manner, usually depending on the level of refinement of the modelling. This approach is recognized as mixed-integer programming (MIP). Where mixed integer linear programming (MILP) is known as state-of-the-art for energy system optimization. This approach is attractive when a problem can be linearly described, requiring a trade-off between the level of detail and computational time [182]. The formulated optimization problem can be then solved using solvers, such as cbc, glpk, cplex or gurobi [183,184]. However, if complex non-linear constraints are unavoidable in the formulation, the problem becomes a mixed-integer non-linear problem (MINLP), posing challenging due to its high complexity [185].

Alternatively, the second approach involves conducting optimization based on a complex simulation model that relies on exact formulas for each component, generally yielding more accurate results [186]. This simulation-based optimization approach decouples the modelling task from the optimization task [187]. Therefore, this approach is widely employed in commercial software (e.g., Aspen-HYSYS, TRNSYS) coupled with optimization algorithms. Optimization of this approach is typically performed by heuristic algorithms, which are derivative-free and suitable for highly complex non-linear models

[188]. Among these algorithms, the genetic algorithm is a well-known technique inspired by the biological evolution process [189]. Since it uses evaluation functions to quickly search for different combinations of input variables, rather than by derivation [190], facilitating its coupling with various nonlinear complex models.

For the concepts studied in this thesis, complex thermodynamic processes, such as combustion, gas cooling and heat pump cycles, need to be considered to explore the potential for heat recovery. The design of such heat pump integrated biomass heating systems is complex and nonlinear due to the thermodynamic processes and interconnections of components. Given these complexities, the simulation-optimization approach emerges as the more suitable approach for addressing the optimization problem in this work.

Accordingly, the simulation-based optimization approach is employed in this thesis to assist in selecting an appropriate concept and optimizing the parameter selection of the system. To this end, the proposed simulation model for the integration of HP and CHP into biomass heating networks from Chapter 4 is utilized, which considers thermodynamic processes and interactions between system components. This simulation model will be combined with an independent genetic optimization algorithm. By identifying the optimization objectives and the range of the decision variables to be optimized, a multi-objective optimization of the system can be performed to find the most optimal system design.

In the present context, the optimization objectives are identified as techno-economic or environmental indicators. The decision variables are the selectable integer and continuous design parameters of the system components, such as the operating air ratio of the boiler, the connection method of the heat pump, and the design parameters of its thermal cycle, as well as the refrigerant selection. The proposed framework can serve as a supportive decision-making tool for evaluating the techno-economic and environmental potential of integrating heat pumps into biomass heating networks, and for optimizing the parameter design of different system components. The following section introduces the workflow of the framework and the mathematical formulation of the optimization problem.

5.2 Overview of the optimization framework

Figure 28 shows the workflow of the optimization framework, which is coupled with the proposed simulation model.

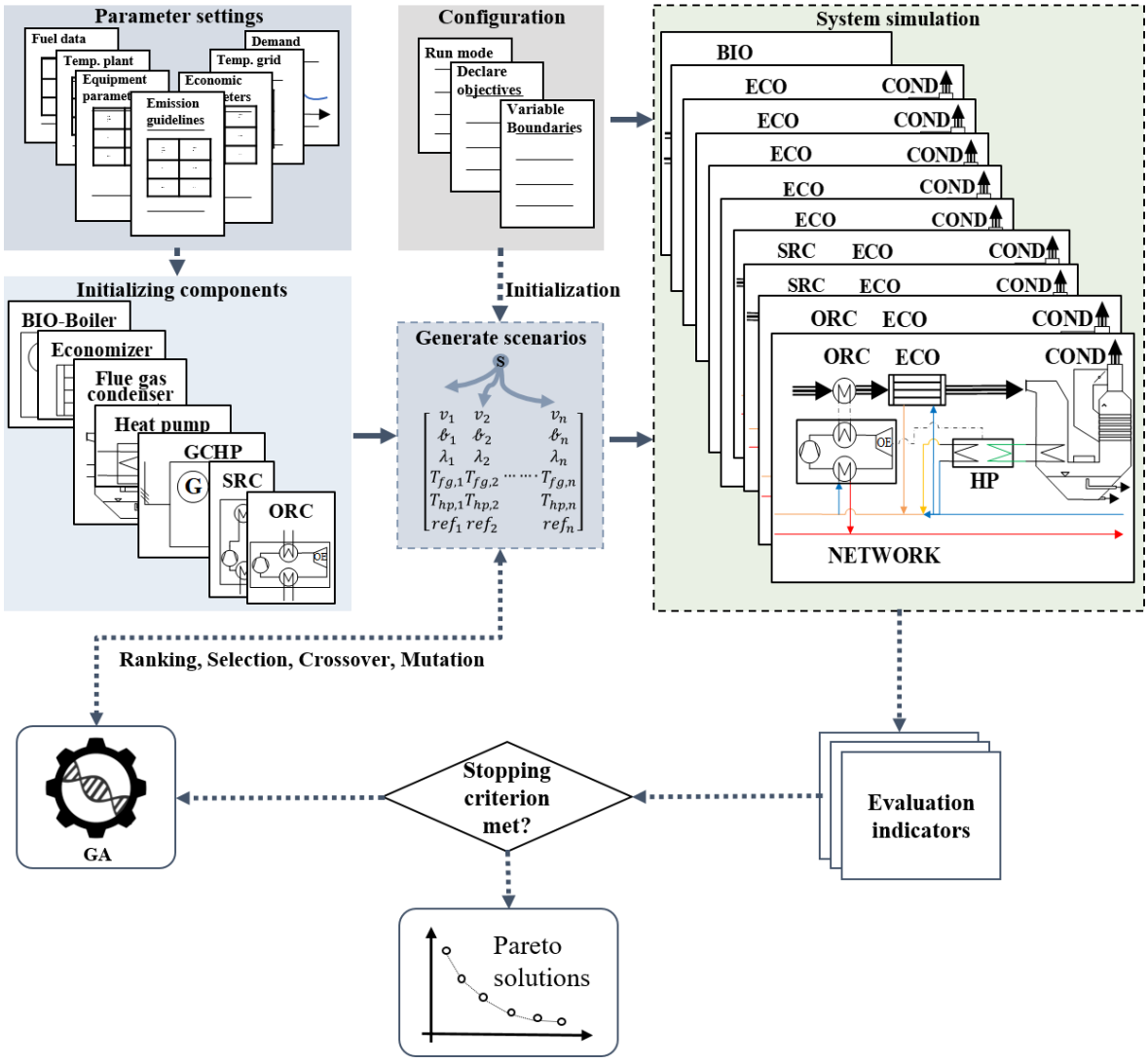

Figure 28: *Working flow of the simulation-optimization framework.*

The optimization framework starts with the initialization of the main components and the simulation template. Within this framework, the input parameters of the simulation model are categorized into two groups: **initialization parameters** and **decision variables**.

Initialization parameters are essential data required to optimize the assignment of values to decision variables. These parameters are declared before the optimization process to initialize the components. They are typically predetermined by factors such as customer requirements, technical limitations, environmental factors, and economic conditions. In this

work, the required initialization parameters include the technical requirements of network and predefined parameters for system component design, fuel characteristics, air temperature and humidity, and the economic and environmental parameters. Initializing these parameters enables the generation of the simulation template.

Decision variables, in contrast, are parameters whose final values should be obtained through optimization. In this work, the decision variables that can be chosen by designers include the air ratio of the biomass boiler λ, the connection variant of the heat pump $\mathscr{v}$, the target exhaust gas temperature T_{ex}, the heat pump supply temperature T_{hp}, the selected refrigerant of the heat pump $ref.$, and the integer decision variable $\mathscr{b}$ to indicate whether and what type of CHP unit is integrated for self-power supply. These variables are subject to boundary conditions and must to be declared prior to optimization. The final goal of the optimization is to obtain the optimal combination of these variables, which provide decision support for the final design of the integrated system. Each combination of decision variables constitutes a scenario.

An overview of the required initialization parameters and the decision variables can be found in Table 7.

Table 7: Overview of the required initialization parameters and decision variables for the optimization.

Initialization parameters	Technical requirements of network	$\dot{Q}^t_{demand}$, T_{return}, T_{feed}
	Fuel characteristics	*fuel type*, $\sum x_i$, w, H_f
	Predefined parameters for system component design	$T_{combustion}$, T_{ash}, $T_{surface}$, z_{min}, z_{max}, T^{hex}_{in}, T^{hex}_{out}, ξ_{hex}, $\xi_{gasifier}$ *FUH, etc.*
	Air temperature and humidity	T^t_{air}, d^t_{air}
	Economic parameters	I_c, $f_{o\&m,c}$, $c_{i,fuel}$, c_{el}, $c_{ash\ diposal}$, $c_{cleaning}$
	Environmental parameters	$f_{CO2_{i,fuel}}$, $f_{CO2_{el}}$, $f_{pe_{i,fuel}}$, $f_{pe_{el}}$
Decision variables		$\mathscr{v}$, $\mathscr{b}$, λ, T_{ex}, T_{hp}, $ref.$

Following the initialization process, the optimization objectives, the run mode of the optimization procedure, and the constraints of the decision variables should be declared according to the mathematical formulation outlined in Section 5.2.1. The optimization procedure can be executed in multithreading mode to leverage the computing power of multiple cores and expedite the optimization process.

To commence the optimization procedure, a predetermined number of scenarios should be initialized based on the boundaries of the decision variables. These scenarios comprise the initial population of the genetic algorithm. The simulation model of the system will be invoked based on these defined scenarios and the initialized components. Subsequently, the required energy performances and the necessary size of various components will be computed based on the simulation model. Based on the technical results, various evaluation indicators can be determined and given as fitness evaluation criteria for the genetic algorithm. Depending on the evaluation results, the genetic algorithm will generate new scenarios with higher fitness. These newly generated scenarios will serve as new population as input for the next iteration. This process will continue until the termination condition is met, such as reaching the maximum number of evolutionary generations. At the end of the optimization, the set of Pareto optimal solutions will be obtained, and the corresponding optimal solutions will be output.

5.2.1 Mathematical formulation

The general mathematical formulation of this optimization problem is proposed as follows:

$$\min_{\vec{x}}\{f_1(\vec{x}), f_2(\vec{x})\}$$

$$s.t.\ g(\vec{x}) = 0$$

$$\vec{x} = vector(\mathscr{v}, \mathscr{b}, \lambda, T_{ex}, T_{hp}, ref.)$$

$$x_i \in [lb_i, ub_i] \mid \forall\ x_i \in \{\lambda, T_{ex}, T_{hp}\}$$

$$\mathscr{v} \in \{0, 1\}$$

$$\mathscr{b} \in \{0, 1, \dots, n\}$$

$$ref. \in \{0, 1, \dots, m\} \tag{79}$$

Where $f_1(\vec{x})$ and $f_2(\vec{x})$ are objective functions, representing the evaluation indicators of the systems. For example, these two objective functions can be chosen as the economic indicator $lcoe$ and the environmental indicator e_{CO2}, respectively. And $\vec{x}$ indicates the vector of the decision variables $vector(\mathcal{v}, \mathcal{b}, \lambda, T_{ex}, T_{hp}, ref.)$ of the optimization problem, i.e., the scenario. Among them, $\mathcal{v}$ is a binary variable representing the connection variant of the heat pump. The other variables, such as air ratio λ, the target exhaust gas temperature $\mathcal{T}_{ex}$ and the heat pump supply temperature $\mathcal{T}_{hp}$ are the continuous variables that can vary between their respective lower boundary lb and upper boundary ub. And the variable $ref.$ and $\mathcal{b}$ are integer variables, representing the choice among the m optional refrigerants and the type of CHP unit to be installed, respectively. The equivalence constraint $g(\vec{x}) = 0$ represents the mass and energy balance constraints for the entire system, implemented by the entire simulation model presented in Section 4.2. This constraint declares the system's technical requirements and ensures that the demand of the network is met.

In multi-objective optimization (MOO) problems, finding a single solution that optimizes each objective simultaneously can be challenging due to potential conflicts between economic and environmental objectives. To solve this problem, the weighted sum method [191,192] is applied, which yields a set of optimal points as Pareto solutions. The Pareto solutions reflect a balance between the optimum of the two objectives, i.e., the trade-off between economics and environmental impact. Using the weighted sum method, the objective can be reformulated as a composite objective function:

$$\min_x ws = \sum_{i=1,2} \alpha_i \widehat{f}_i(\vec{x})$$

$$\sum_{i=1,2} \alpha_i = 1 \;\; \alpha_i \geq 0 \tag{80}$$

where α_i is the non-negative scalar weight of each single objective function, with the sum of all weights equaling to 1. Here the $\widehat{f}_i(\vec{x})$ represents the normalized objective, which is defined as:

$$\widehat{f}_i(\vec{x}) = \frac{f_i(\vec{x}) - f_i^{ut}}{f_i^{na} - f_i^{ut}} \; \forall \, i = 1, 2 \tag{81}$$

where f_i^{ut} and f_i^{na} represent the utopia points and pseudo nadir points of the i corresponded $f_i(\vec{x})$.

A utopia point is a point in the objective space where the objective function reaches its optimal value, which represents the approximate minimum value of the corresponding indicator. And a pseudo-nadir point is a point in the space of the objective where it reaches its pseudo-worst value, which is the approximate maximum value of the indicator [193]. These points are employed as anchor points [194] for the normalization. In this study, these anchor points are defined as the extreme points when $\alpha_i = 1$, which corresponds to the individual minimum of each objective $f_i(\vec{x})$. The determination of these points and the implementation of the genetic algorithm is explained in Section 5.2.2.

5.2.2 Optimization procedure

Figure 29 illustrates the detailed procedure of the optimization framework, utilizing a genetic algorithm (GA). The objective of the optimization is to identify a Pareto-optimal solution set, representing a balance between the various objectives, such as economic efficiency and environmental sustainability.

To solve the optimization problem, the first step is to calculate the anchor points by solving the optimization of each single objective. At the start, with $\alpha_1 = 1$, the framework calculates the utopia points for the first objective function $f_1(\vec{x})$, typically associated with economic performance, identifying the minimum attainable values for this objective. Simultaneously, the nadir points of the second objective function $f_2(\vec{x})$ are determined, which represents the maximum values. The framework then switches $\alpha_1 = 0$ to compute the reverse, obtaining the utopia points for $f_2(\vec{x})$ and the nadir points for $f_1(\vec{x})$. These calculations establish the anchor points, which define the extremities of each objective's feasible range.

Once the anchor points are established, the algorithm proceeds to normalize the objective functions using the formulation described in Eq. (81). This normalization ensures that the objectives are dimensionally consistent and can be compared directly, which is crucial for multi-objective optimization. By varying weighting factor α_1 in steps of a certain magnitude (e.g. 0.1) within the range 0 to 1, a set of the Pareto solutions, the non-dominated solutions that represent the best trade-offs between conflicting objectives, can be computed.

The optimization procedure with a specific α_1 can be summarized as follows:

1. Initialization scenarios

The optimization with a specific α_1 starts with generating *n* scenarios that consists of the decision variables as the initial population. In genetic algorithms, the decision variables of the optimization problem are encoded as "genes," and each individual in the population is represented as a "chromosome", i.e., vector of genes. And each chromosome is treated as a scenario — a vector of decision variables that lies within the constraints of the problem, which represents a possible system design.

2. Simulation

Once the scenarios are initialized, the framework simulates each scenario by calling an underlying model that calculates the values of the objective functions for each decision variable. In this multi-objective optimization problem, this often involves evaluating performance across different criteria, such as levelized cost, environmental impact, or energy efficiency.

3. Fitness Evaluation

After simulation, the algorithm calculates the "fitness" of each scenario by assessing how well it performs with respect to the normalized objective functions $\widehat{f}_i(\vec{x})$. The fitness function is crucial, as it determines which scenarios are likely to be passed on to the next generation.

4. Evolutionary Process

The core of the genetic algorithm lies in its evolutionary process, which iteratively refines the population of scenarios through selection, crossover, and mutation. These operations are designed to emulate natural selection, enabling the algorithm to evolve higher-quality solutions over successive generations. This process is conducted by a python package scikit-opt [195].

a. Ranking: The fitness values of all scenarios are ranked. Solutions that perform better, i.e., have a higher fitness score, are given higher rankings. This ranking determines which scenarios are more likely to be selected as "parents" for the next generation.

b. Selection: The selection process chooses a subset of scenarios from the population based on their rankings. Various selection strategies can be applied, such as roulette-wheel selection, tournament selection, or rank-based selection. The rank-based selection is applied

in this framework. Scenarios with better fitness scores have a higher probability of being selected as parents.

c. Crossover: Once the parent scenarios are selected, the algorithm performs crossover, combining the genes (decision variables) from two or more parent chromosomes to create new "child" scenarios. This process simulates reproduction in nature, where offspring inherit traits from both parents. Crossover can occur in several forms, such as single-point crossover, multi-point crossover, or uniform crossover.

d. Mutation: After crossover, the newly generated child scenarios undergo mutation. Mutation introduces random changes to the genes (decision variables) of the children with a certain probability. This ensures genetic diversity in the population and prevents the algorithm from becoming stuck in local optima. Mutation can involve altering individual decision variables by a small random value or swapping gene positions.

5. Test for Convergence

After the evolutionary steps, the algorithm checks whether the stopping criterion is met. The stopping criterion could be based on various factors, such as the number of iterations, the rate of improvement of the best scenario.

If the stop criterion is met: The algorithm terminates and returns the best solution(s) found, along with the corresponding decision variables. The final Pareto-optimal solutions are plotted, allowing the decision-maker to visualize the trade-offs between the objectives.

If the stop criterion is not met: The algorithm generates a new population by replacing the parent chromosomes with the newly generated children. The process then loops back to the Step 2 to conduct new simulations, where the new population is evaluated, and the cycle continues.

6. Store Pareto Point

Throughout the optimization process, the algorithm stores the Pareto solutions. Each α_1 produces a Pareto point, which is stored. By varying the value of α_1, a set of Pareto points are generated. These Pareto points form the "Pareto front", which visualizes the set of optimal solutions where no single objective can be improved without worsening another.

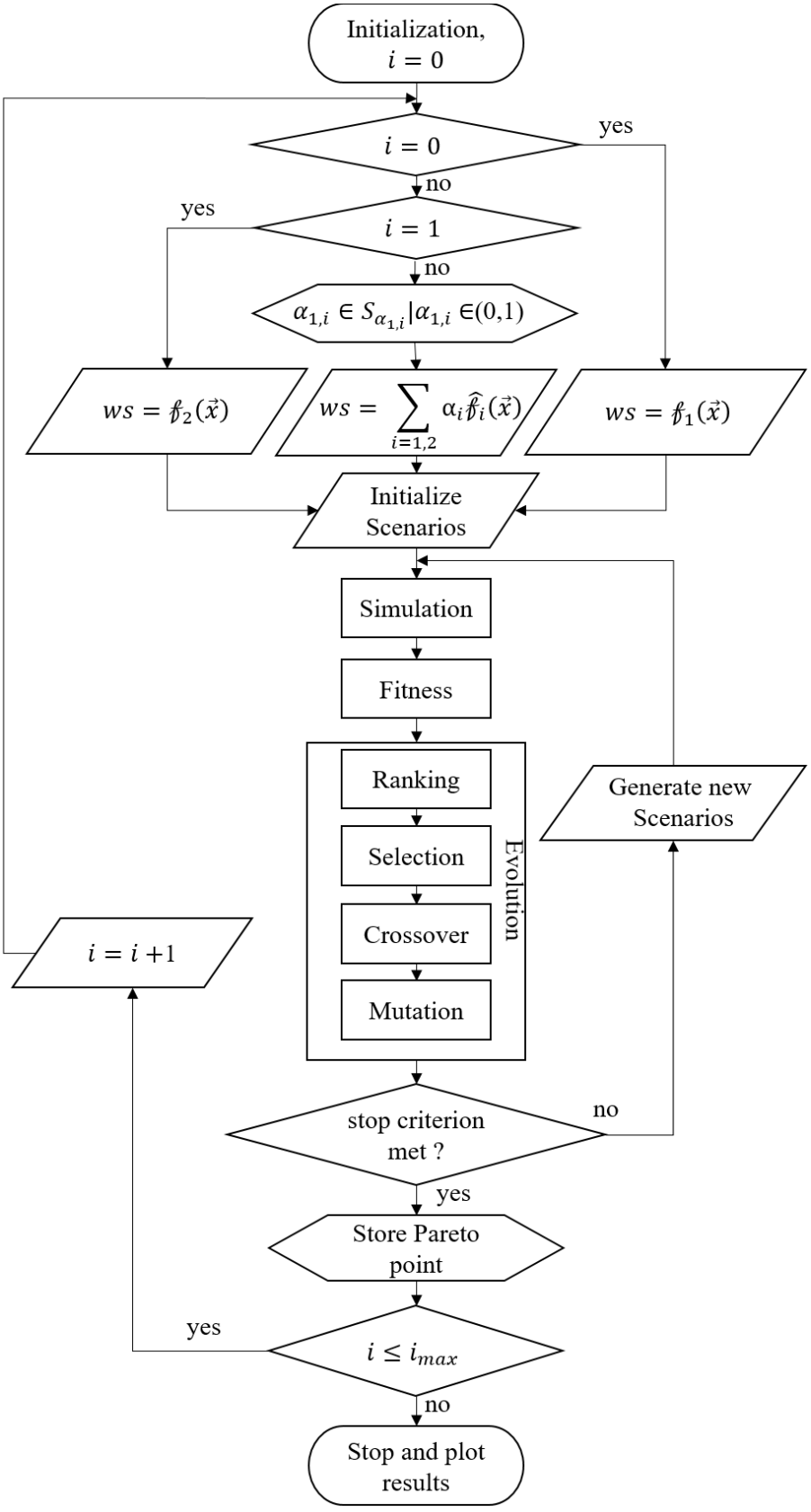

Figure 29: Flowsheet of the optimization algorithm.

6. Description and Analysis of selected heating networks

For the verification of the proposed method in this thesis and the evaluation of the various concepts of heat pump integration, three biomass heating networks (BHNs) were selected for investigation.

Two of these networks are anonymized biomass heating networks in Austria, both equipped with heat pumps using different connection variants. The first network represents a typical biomass heating system with a flue gas-side integrated heat pump (e.g., the flue gas-side HP-integrated system), while the second represents a typical biomass heating system with a network-side integrated heat pump (e.g., the network-side HP-integrated system).

In addition, a standard biomass heating network located in Germany, without flue gas condensation and heat pump, was selected as a focus to investigate the feasibility of different integration concepts in Germany. The selection of this network is particularly relevant due to its adverse experience with flue gas condensation prior to 2001, without the integration of heat pumps. Insights from this third network regarding potential issues associated with flue gas condensation provide valuable information on the risks and possible weaknesses of flue gas condensation technology.

6.1 Technical information

6.1.1 Description of the first biomass heating network

The first BHN was commissioned in Austria in 2006 to provide heating for 300–320 households. The biomass furnace has a nominal heat output of 4.5 MW. The biomass boiler nominal output at full load is 3730 kW. The nominal efficiency, as given in the manufacturer's documentation, is 87 % [196]. Besides the boiler, it is also equipped with an ECO tower, which has an air preheater and an economizer directly after the boiler. Additionally, there is a flue gas condensation unit integrated with a compression heat pump. The nominal technical data of this BHN are detailed in Table 8. The simplified hydraulic circuit of the network is shown in Figure 30. In addition to the biomass-fired equipment, there is an oil-fired boiler with a nominal thermal output of 6 MW, serving as a backup unit that operates during peak load, breakdowns and repairs phases.

Table 8: Technical data of the first biomass heating network.

Parameter	Value	Unit
firing system		
nominal thermal output furnace	4.50	MW
nominal thermal output boiler	3.73	MW
nominal efficiency	87.00	%
max. fuel mass flow (w = 60 %)	2862	kg/h
air preheater (before economizer)		
nominal thermal output AP	220	kW
economizer		
nominal thermal output ECO 1 in the tower	624	kW
flue gas condensation		
nominal thermal output ECO2	960	kW
nominal thermal output condenser	500	kW
heat pump		
nominal thermal output heat pump	761	kW
nominal electrical demand heat pump	160	kW
refrigerant	R717	

At the plant side, the hot flue gas first flows through the biomass furnace and then into the boiler following combustion. There, the flue gas releases part of its thermal energy to the flow of the local heating network. The flue gas then flows into the tower, which consists of an air preheater, economizer, and a compressed air cleaning unit. After purification by the electrostatic precipitator, the flue gas enters the condensation unit, where the second economizer (ECO2) and the condenser are located. Quenching spray nozzles are positioned on both the incoming and outgoing sides. The accumulated quench and condensation water flows into the sump below the condenser, where it is separated into solid and liquid phases in a sedimentation tank. Before exiting the condenser unit, the flue gas is mixed with heated fresh air in the devaporization unit and then flows out of the stack.

At the network side, the heat pump evaporator is connected to flue gas condenser bundle and is controlled by a pump and a mixing valve. The mains return temperature is first raised in ECO 2, then further increased by the heat pump condenser. The heat pump is followed by the mains boost pumps, which increase the flow through the ECO 1 and boiler heat

exchangers. The increased flow decreases the risk of deposits inside the heat exchangers and raises the return temperature. After passing through ECO 1, the mains water flow then enters the biomass furnace boiler. Upon exiting the boiler heat exchanger, the mains water flow reaches the feed temperature level.

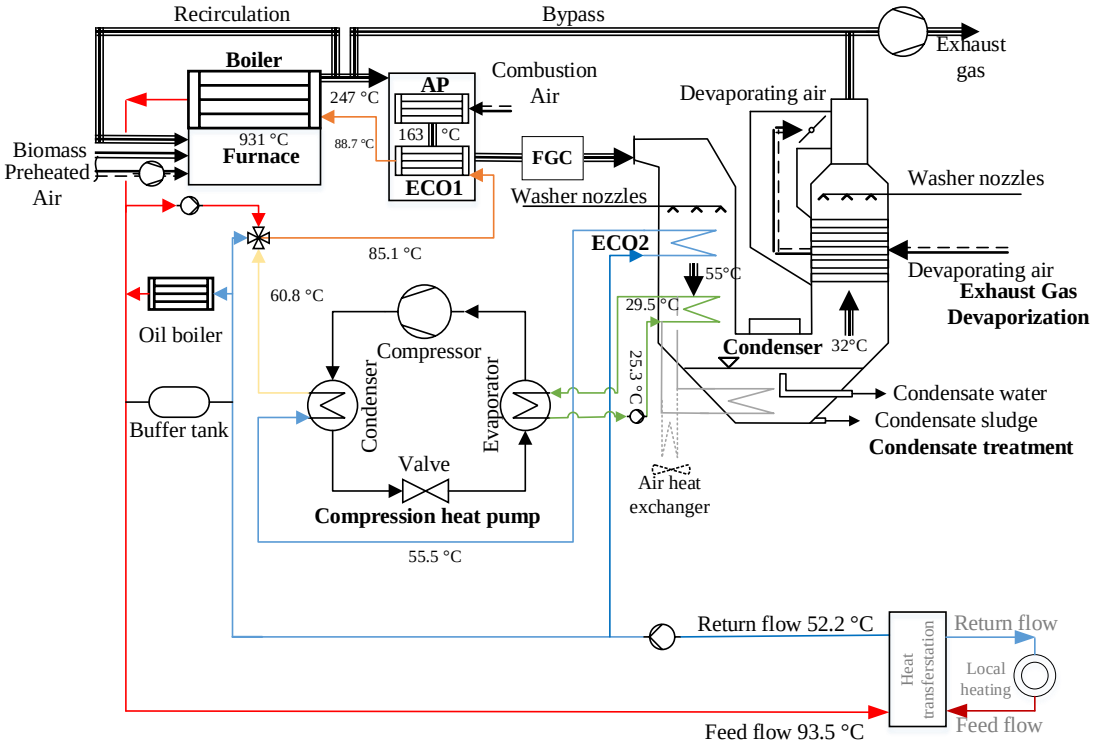

Figure 30: Hydraulic circuit diagram of the first biomass heating network with flue gas-side integrated heat pump (own illustration).

6.1.2 Description of the second biomass heating network

The second network under investigation was established in Austria in 1996 for about 500–550 customers [197]. Technical information regarding this network is available in Table 9. This network includes two biomass boilers, both fired by a mixture of wood chips and bark. Boiler 1, the larger of the two, is dedicated to wintertime use. Boiler 2, the smaller one, is combined with an integrated ORC for electricity production, which has a rated electrical output of 600 kW_{el} and two integrated economizers. The electricity generated is exclusively fed into the power grid. In addition to the biomass boilers, there is an oil-fired boiler that serves as backup equipment or as a peak load device, to provide heat in case of malfunction in both biomass boilers. There are also three series-connected buffer storage

tanks, with a total water storage volume of 210 m^3, which serve as buffering devices to balance fluctuations in heat network demand and cover peak loads.

The heat pump, commissioned in 2012, consists of four refrigeration circuits with a total of eight compressors, with two modules connected in series per refrigeration circuit. The refrigerant used is R236fa and is assigned to safety group A1, indicating low toxicity and low flame spread [198].

Table 9: Technical data of the second biomass heating network.

Parameter	Value	Unit
biomass boiler 1		
nominal thermal output boiler 1	5000	kW
ORC biomass boiler 2		
nominal thermal output boiler 2	3000	kW
nominal electrical output boiler 2	600	kW
Condensation plant		
nominal thermal output condenser	2000	kW
heating surface	416	m^2
Heat pump		
nominal thermal output heat ump	1000	kW
nominal electrical demand heat pump	177	kW
refrigerant	R236fa	

Figure 31 shows the schematic diagram of the second BHN. Biomass boiler 2, equipped with ORC unit, is utilized up to the maximum permissible electricity generation. The remaining heat load is covered by biomass boiler 1. Consequently, the utilization ratio of biomass boiler 1 was generally lower than that of biomass boiler 2.

The flue gas from biomass furnace 1 passes through boiler 1 and is then cleaned in the multi-cyclone precipitator. The cyclone is followed by the induced draft fan. The flue gas from the first firing system is combined with the flue gas from the second firing system upstream of the electrostatic precipitator. The flue gas from biomass furnace 2 first passes through boiler 2 with integrated thermal oil economizer and hot water economizer. These economizer cools the flue gas to about 180 °C. In the thermal oil economizer, the thermal oil for heating ORC working fluid is preheated before it enters boiler. The hot water economizer directly heats the network. Both economizers can be separated from the flue gas

path by the bypass. A detailed display of boiler 2 with an integrated ORC unit and 2 economizers can be found in Appendix C.

After the flue gas streams from the two biomass furnaces are combined, they enter the electrostatic precipitator, followed by the flue gas condensation with integrated air preheating. The air preheating is arranged in the flue gas flow direction after the condensation. Here, the preheated air serves as both primary and secondary air for combustion. After passing through the air preheater, the exhaust gases continue into the chimney.

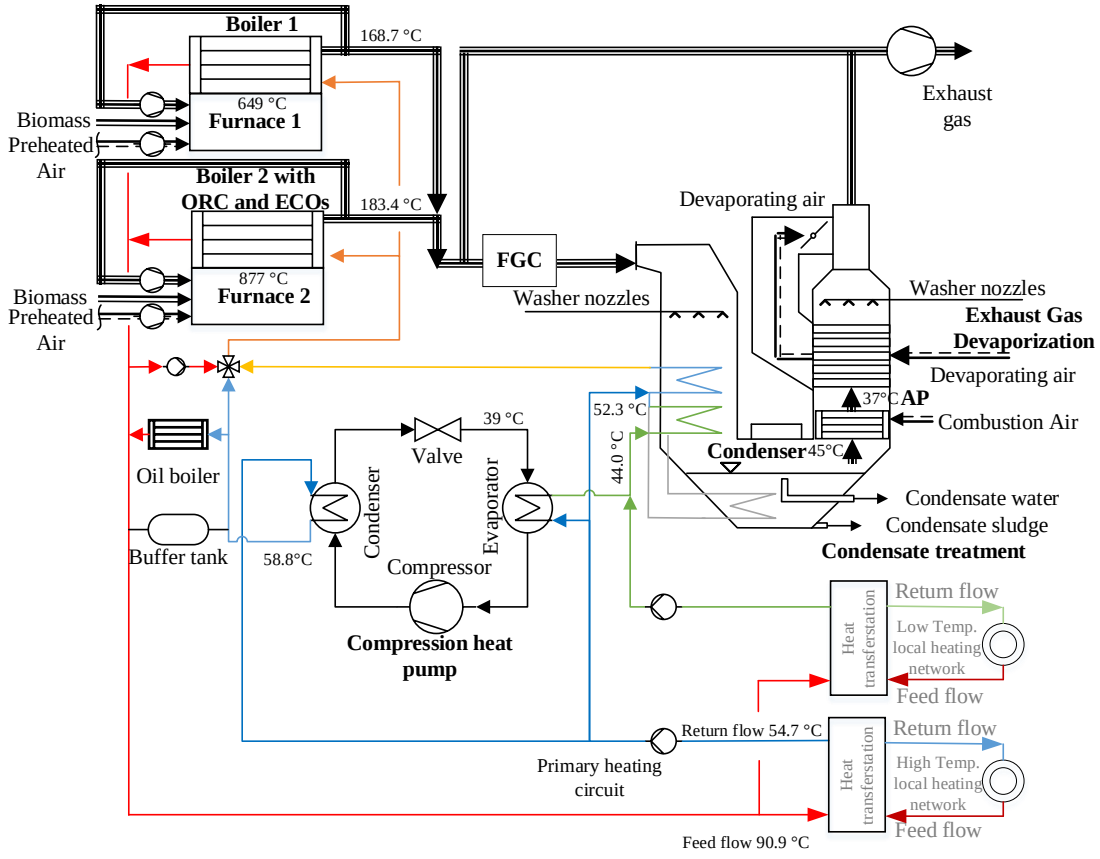

Figure 31: Hydraulic circuit diagram of the second biomass heating network with network-side integrated heat pump (own illustration).

The process of the network side starts with the mains return. This heating network has two different heating circuits: one with a high return temperature (HT-RF) and another with a low return temperature (LT-RF). A branch of the HT-RF leads to the heat pump evaporator, while another branch is pumped to the economizer bundle upstream the condenser bundle. The water from the evaporator is mixed with the NT-RF, also flows into the economizer

bundle. The combined flow from the economizer bundle then merges with the flows from the heat pump condenser and the booster pump.

Subsequently, the network water flows into both boilers. After reaching the heating supply temperature, there is a branch to the buffer storage tanks. These tanks can be charged during periods of low demand or in preparation for large peak loads. Following this, the network water is pumped into the district heating network by the network pumps.

6.1.3 Description of the third biomass heating network

The third BHN was commissioned in 1996. This network experienced problems with flue gas condensation since its commissioning, primarily due to corrosion caused by inadequate heat engineering design. During the commissioning years, significant changes in heat demand were observed. Consequently, the boiler was operated at an average daily load of 1.2 MW_{th} in wintertime, despite having a nominal capacity of 3.0 MW_{th}. In addition, the boiler output fluctuated strongly despite a buffer storage volume of 40 m^3. As a result, the flue gas condenser, which was made of V4A (stainless steel) material, often had to be significantly down-regulated. During the low-load periods, malfunctions, and summer operation, the flue gas condensation was turned off. In consequence, corrosion on the heat exchanger bundles progressed rapidly. Within two years of commissioning, all heat exchanger bundles of the flue gas condenser had to be replaced due to rusting. Due to this reason, the flue gas condenser was dismantled in 2001. Besides, as the load in summer was too low for the operation of boiler 1, the biomass boiler 2 with a nominal heat output of 600 kW_{th} was installed in 2001, which has been has been mainly used during the summer. Table 10 shows the technical data of this heating network.

Table 10: Technical data of the third biomass heating network.

Parameter	Value	Unit
firing system 1		
nominal thermal output furnace 1	3800	kW
nominal efficiency furnace 1	79	%
biomass boiler 1		
nominal thermal output boiler 1	3000	kW
firing system 2		
nominal thermal output furnace 2	750	kW

nominal efficiency furnace 2	80	%
biomass boiler 2		
nominal thermal output boiler 2	600	kW
condensation (de-installed in 2001)		
nominal thermal output condenser	875	kW

The hydraulic circuit of this network since 2001 is displayed in Figure 32, which is notably simpler than the other two BHNs investigated. Both biomass furnaces are equipped with secondary air fans, in addition to primary air supply, to ensure efficient combustion. The flue gases are cleaned by a cyclone and, after branching off the recirculation, are transported to the stack by the induced draft fan.

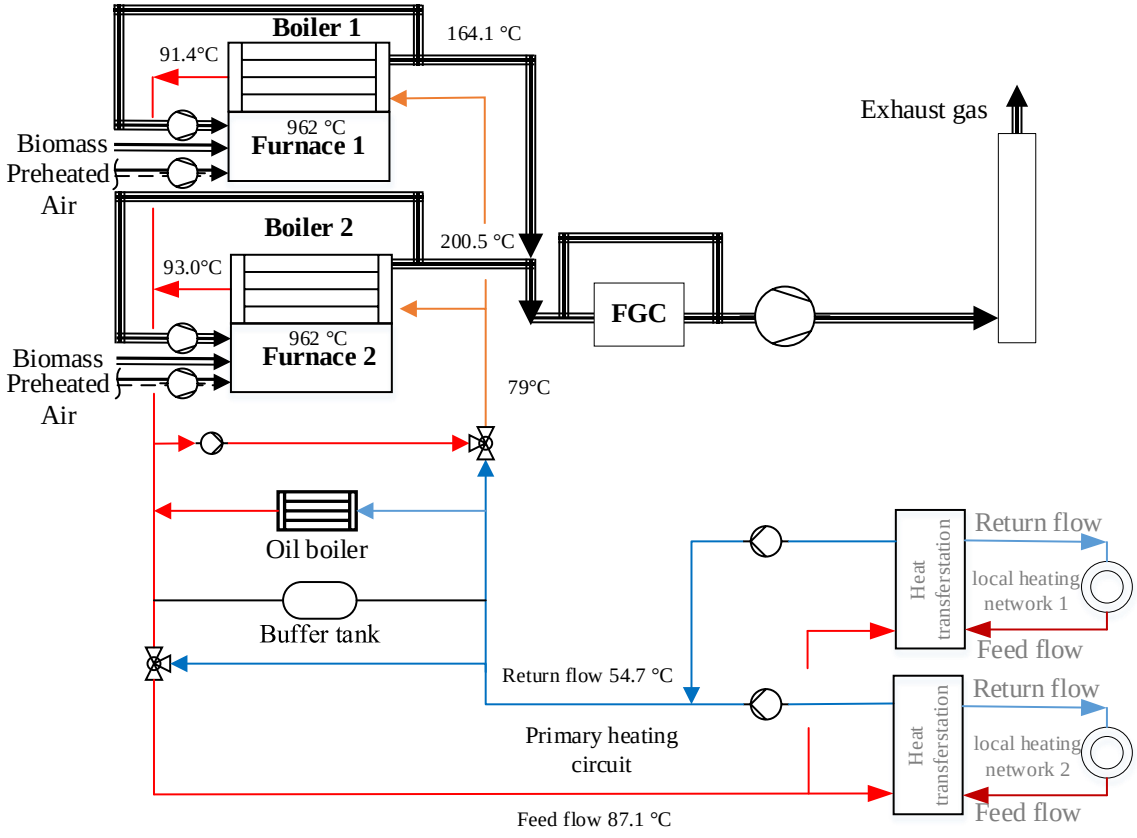

Figure 32: Hydraulic circuit diagram of the third biomass heating network without flue gas condenser and heat pump (own illustration).

During the winter period, biomass boiler 2 is not in operation. All heat demand in winter is provided by biomass boiler 1. The feed flow of the boiler reaches a three-way mixer, where it is mixed with the flow from the 40 m^3 buffer storage tank. The mixture flow then passes through another three-way mixier where it is combined with the return flow before

splitting into two secondary local networks. In addition to the biomass boilers, an oil-fired boiler with a rated thermal output of 3.2 MW operates as a backup unit during peak load, breakdown and maintenance phases.

6.2 Input data and analysis

To evaluate the heat pump integration concepts, various operating parameters were continuously measured from the three heating networks. These data sets are instrumental in validating the proposed method and in providing a better assessment of historic operating situations. In addition, fuel compositions used in the networks were determined based on the laboratory analysis for a more accurate evaluation. In this section, the data used for simulation are introduced, and a preliminary analysis of the investigated networks is conducted.

6.2.1 Fuel analysis

Given that the heat recovery potential is highly dependent on the fuel composition, especially the water and hydrogen content, fuel samples were collected from the three investigated networks and experimentally analyzed in the laboratory. As mentioned in Section 4.1.1, the compositions can be used as the database for calculating fuel energy consumption and efficiency. The results of the experimental analysis are presented in Table 11. The conversion of the compositions from dry fuel to wet fuel is as follows:

$$x_{i,wet} = x_{i,dry} * \left(1 - \frac{w}{100}\right) \tag{82}$$

Table 11. Experimental analyzed fuel compositions of the investigated networks in the laboratory

Parameter	**BHN1**	**BHN2**	**BHN3**	**Unit**	**Methods**
Total water content	30	47.4	25.8	ma% wet fuel	DIN EN ISO 18134-2:2017-05
higher heating value (*hhv*)	20300	19900	20400	kJ/kg dry fuel	DIN EN ISO 18125:2017-08
lower heating value (*lhv*)	18670	18600	19100	kJ/kg dry fuel	DIN EN ISO 18125:2017-08
Ash content	0.6	1.9	0.7	ma% dry fuel	DIN EN ISO 18122:2016-03
Total chlorine content	0.03	0.013	0.009	ma% dry fuel	DIN EN ISO 16994:2016-12
Carbon	50.6	50.5	50.9	ma% dry fuel	DIN EN ISO 16948:2015-09
Hydrogen	6.2	6.1	6.3	ma% dry fuel	DIN EN ISO 16948:2015-09
Nitrogen	0.24	0.24	0.24	ma% dry fuel	DIN EN ISO 16948:2015-09
Total sulfur content	0.009	0.011	0.01	ma% dry fuel	DIN EN ISO 16994:2016-12
Oxygen	42.4	41.3	41.8	ma% dry fuel	DIN EN ISO 16993:2016-11

6.2.2 Analysis of the operating data

Historical operating data was extensively collected from the three investigated BHNs. Only data relevant to efficiency were selected, based on the hydraulic circuits. These data are categorized into two types: performance data and temperature data.

With an observation period of more than one year for each BHN, daily average values over a year were determined during this duration. During the actual measurement process, anomalies or missing data often occurred for technical reasons, e.g., sensor damage or anomalies or interruptions in the operation. In the context of this thesis, apparent anomalies and missing data were processed through normal distribution and random forest methods, which improves the plausibility of the analysis results. The processed data of each BHN are visualized and analyzed in this subsection. The mean temperatures in winter at different measurement points are illustrated in the hydraulic circuits shown in Figure 30 to Figure 32.

6.2.2.1. Analysis of the first biomass heating network

Operating data from the first BHN was recorded over a period of 13 months. Considering the maximum observation period of approximately oneyear, daily average values were determined. For the analysis, data from the periods between 01.07.2018 – 30.06.2019 were selected.

Temperature data

Figure 33 shows the temperature data in the first BHN. The average furnace temperature over the year was 931 °C. The flue gas temperature directly downstream of the boiler had an average temperature of 247 °C. The flue gas successively passed through the boiler, air preheater, economizers, precipitator, and condensation components. Between the air preheater and economizer in the eco tower, the flue gas temperature in winter averaged 163 °C. After passing through ECO 1 and ECO 2, the temperatures dropped sharply to 55 °C before reaching the heat exchanger for the HP-evaporator. Since temperature data between ECO 1 and ECO 2 are not available, these two components are analyzed as a single compact economizer The average drop in ECO in winter was 103 K. Compared to the economizer, the flue gas in the condenser was cooled by only 21 K.

Figure 34 displays the forward and return temperatures at various points on the grid side. It can be noticed that the heat pump was operated only in winter, with the cooling water temperature at the evaporator-side averaging 25.3 °C at the outlet and 29.5 °C at the inlet. The average mains forward and return temperatures over the year were 53.8 °C and 91.6 °C, , respectively, and 52.2 °C and 93.5 °C in the winter period. Initially, the network return temperature was raised to about 55.5 °C by ECO 2, then flowed into the heat pump condenser, exiting at 59.1 °C. This resulted in a temperature increase of 3.6 K. After passing through the mains boost pumps, the return temperature rose to 85.3 °C. Before entering the boiler, it was further heated to 88.7 °C by ECO 1.

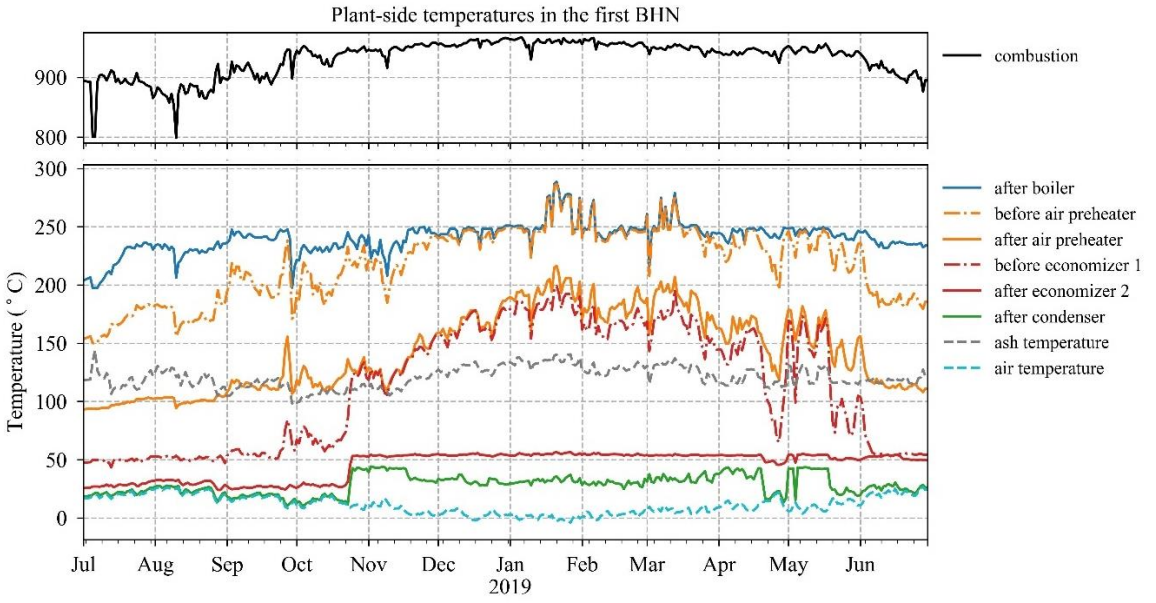

Figure 33: Temperatures of the plant-side in the first biomass heating network

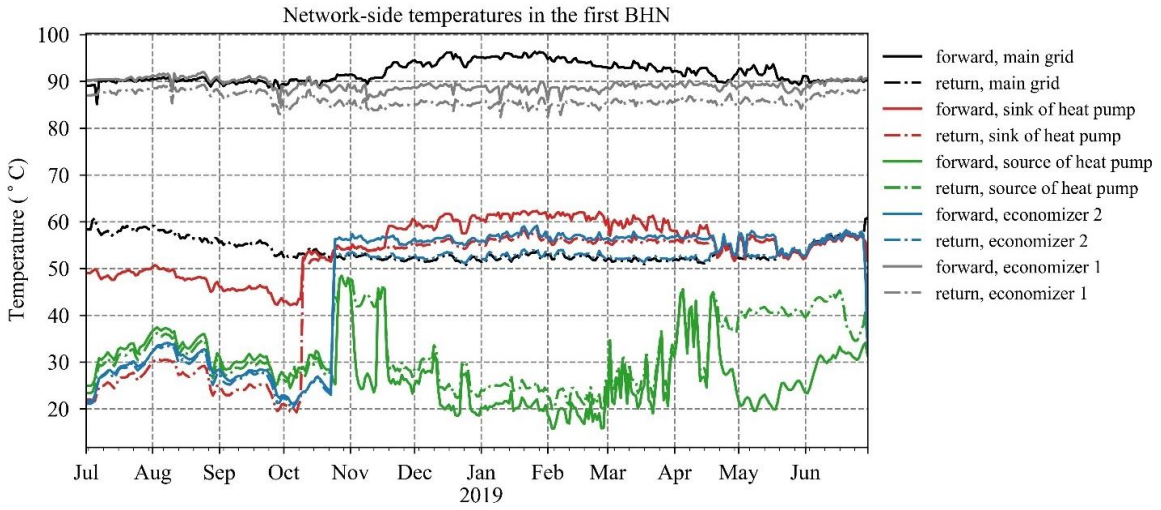

Figure 34: Temperatures of the grid-side in the first biomass heating network.

Performance analysis

Figure 35 shows the thermal outputs of the main heating supply components of the first BHN, including the boiler, economizer, and heat pump. The biomass boiler has an average annual heat output of 1862 kW_{th}. This corresponded to a 50 % utilization of the boiler and an annual full load hour of 4372 h. The economizer and the heat pump provided 7.1 % and 6.8 % of the total heat generation, respectively. During the year, the peak demand for the entire BHN was 4.7 MW_{th}, at which point the boiler operated at its rated output and the economizer and heat pump collectively contributed 20.4 %.

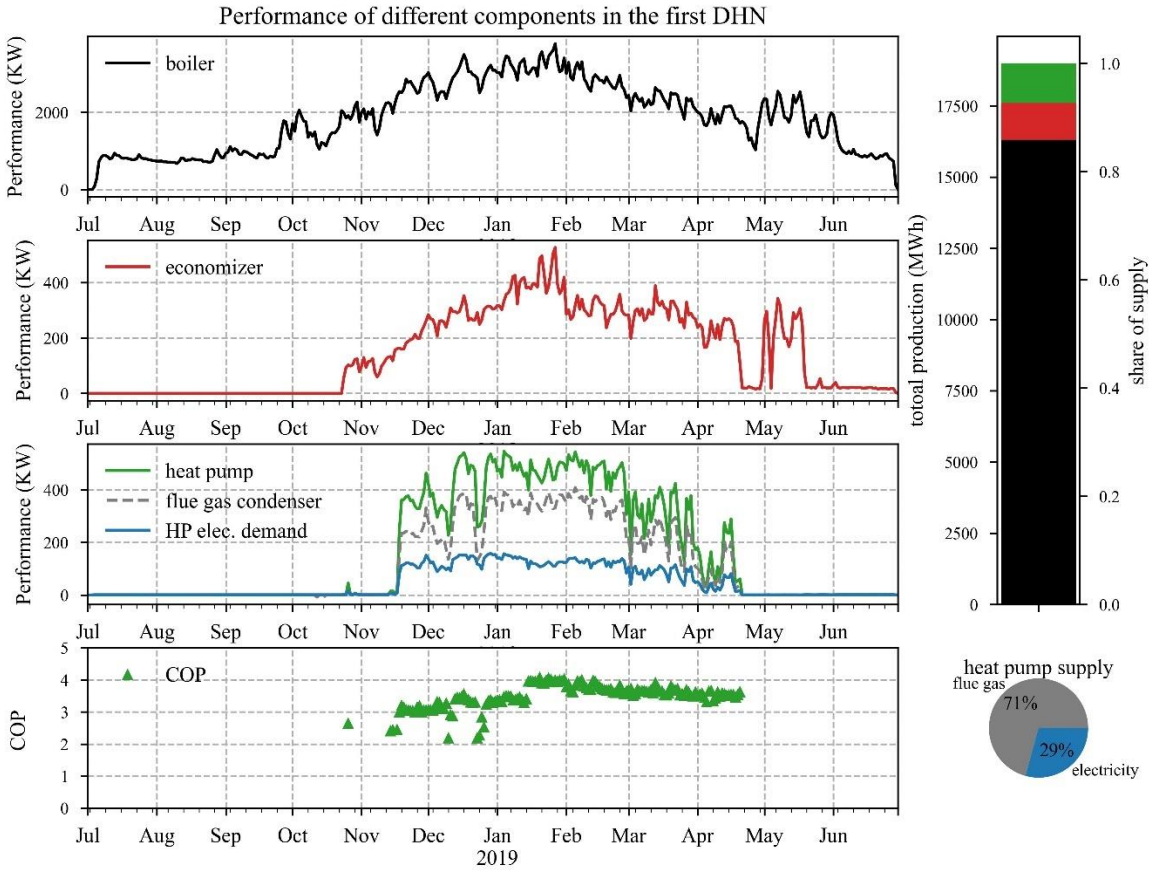

Figure 35: Performances of different components in the first biomass heating network.

The graph also indicates that the economizer and the heat pump were operated only in winter. The reason for this is the lower heat demand in summer. The economizer had an average heat output of 265 kW_{th} during operation, while the combination of flue gas condenser and heat pump had an average output of 383 kW_{th}. This corresponded to annual full load hours of only 2030 h for the economizer and 1811 h for the heat pump, indicating low utilization rates of the equipment.

For a detailed analysis of the flue gas condenser and heat pump, the respective performances and the calculated COP values are also displayed in the figure. The analysis shows only a slight difference in heat recovery performance between the flue gas condenser and the economizer, despite the much lower gas temperature drop in the former. The high performance of the flue gas condenser was contributed by the latent heat of the water vapor in the flue gas. The COP of the heat pump ranged between 3 and 4. According to the information provided by the BHN operator, the heat pump is equipped with a COP controller. This controller ensures that the heat pump operates only upon achieving the minimum COP value.

6.2.2.2. Analysis of the second biomass heating network

For the second BHN, daily average performance data are available for the period from July 1st 2013 to June 30th 2018. From these data, a daily average time series for a sample year was compiled, as illustrated in the subsequent graphs.

Temperature data

Figure 36 shows the temperature data in the second BHN. As shown in the graph, biomass boiler 2 operated over the entire year with an average combustion temperature of 877.0 °C. The average flue gas temperature after passing through the ECOs was 183.4 °C. Biomass boiler 1 operated only from mid-September to mid-May, exhibiting a significantly lower average combustion temperature of 649.3 °C, and an average flue gas temperature of 168.7 °C. After mixing and de-dusting, the flue gas from both boilers entered the flue gas condensation unit and was cooled to 45 °C before flowing to the air preheater.

The grid-side temperatures of the BHN are displayed in Figure 37. The average forward temperature was 90.9 °C. A portion of the high-temperature mains return flow, approximately 55 °C, was first cooled by the heat pump. This cooled flow was then mixed with the low-temperature mains return, resulting in a mixing temperature of 44 °C before the condenser inlet. By recovering the waste heat, the return was raised to approx. 52.3 °C and then fed into the main network again. On the other side, the heat absorbed by the heat pump from the network was raised to a higher level and also fed back to the main network. The heating supply temperature of the heat pump averages about 58.8 °C.

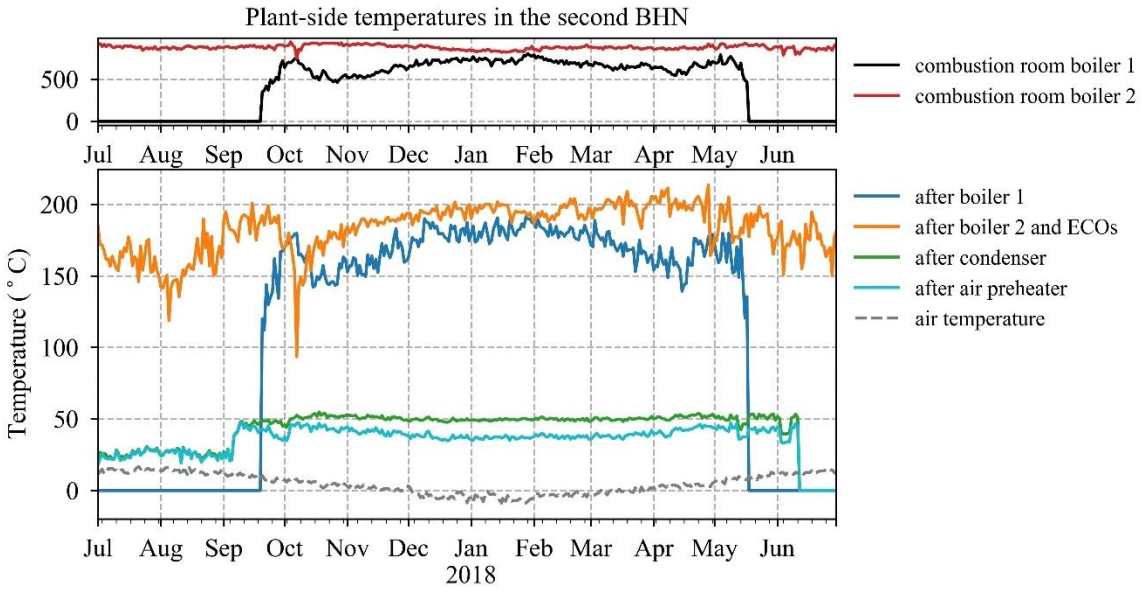

Figure 36: Temperatures of the plant-side in the second biomass heating network.

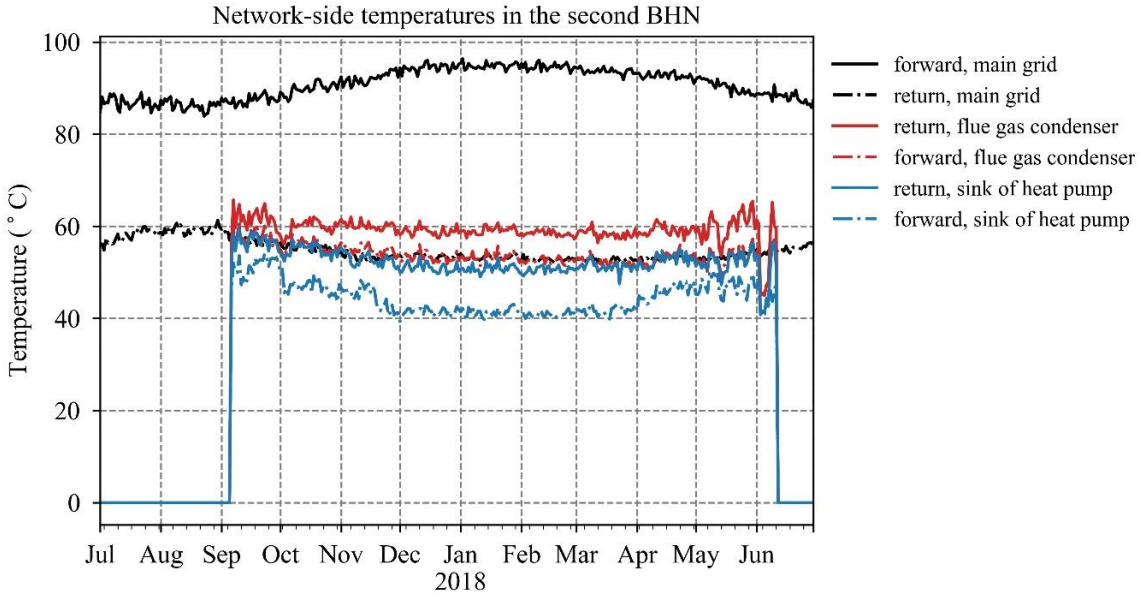

Figure 37: Temperatures of the grid-side in the second biomass heating network.

Performance analysis

Figure 38 illustrates the power and heat output of this BHN. Biomass boiler 1 had an average output of 1954 kW_{th} from mid-September to mid-May, while biomass boiler 2 generated an average of 2196 kW_{th} heat and was operated over the year. This resulted in utilization rates of 24.2 % for biomass boiler 1 and 73.2 % for biomass boiler 2. The ORC unit of biomass boiler 2 generated an average electrical output of 438 kW_{el}.

In the period from the beginning of September to the end of May, the flue gas condensation operated with an average heat output of 984 kW_{th}. The heat pump was operational from the early October to mid-May, with an average output of 744 kW_{th}. This corresponded to 3480 full operation hours. As depicted in the graph, the COP values of the heat pump lay on approx. 5.0, which is higher than those in the first BHN. To operate the heat pump, an average electrical power demand of 186 kW_{el} form public power grid and a thermal demand of 558 kW_{th} from the heating network were required.

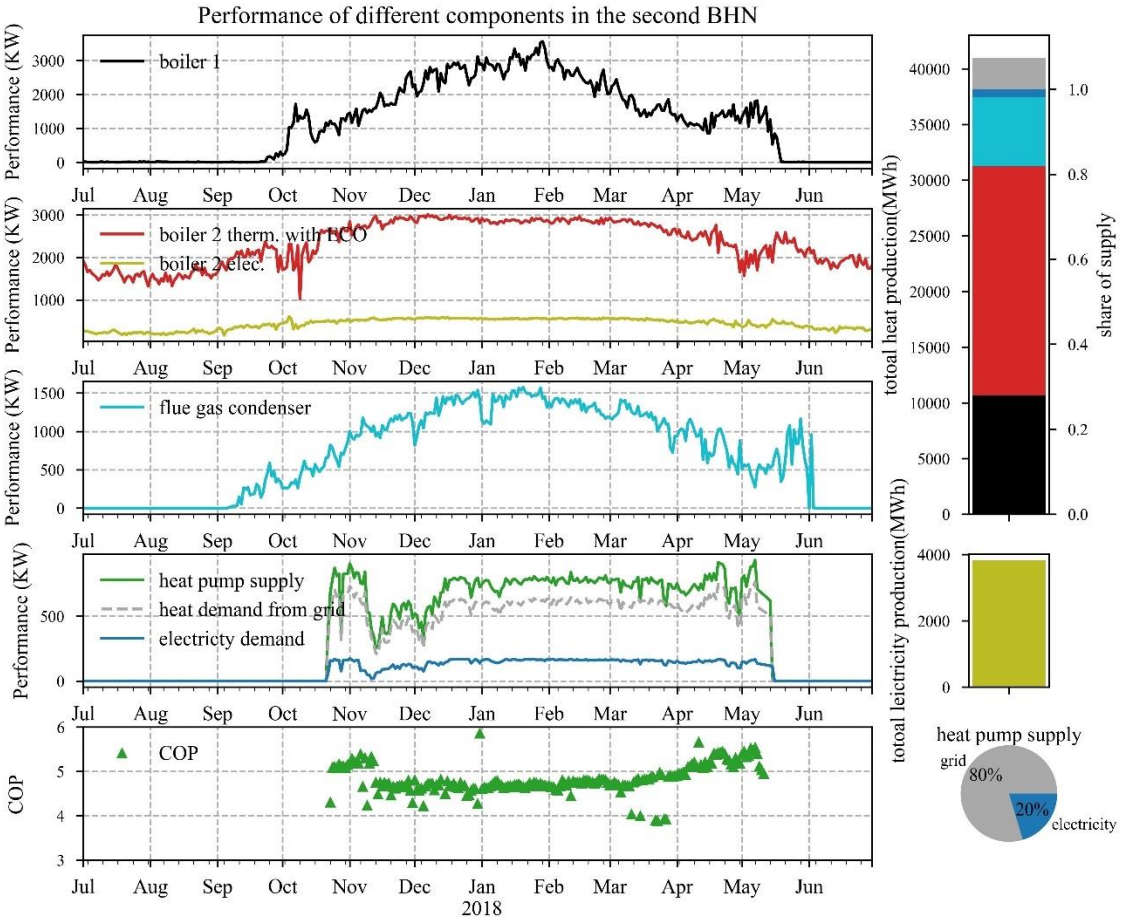

Figure 38: Performances of different components in the second biomass heating network.

6.2.2.3. Analysis of the third biomass heating network

For the third heating network, the hourly average data from July 1st 2018 to June 30th, 2019 is analyzed. To make it comparable with the other two heat networks, their daily average data during this period will be displayed and analyzed in the following.

Temperature data

The temperature data from the boilers and network over the recorded period are displayed in Figure 39 and Figure 40.

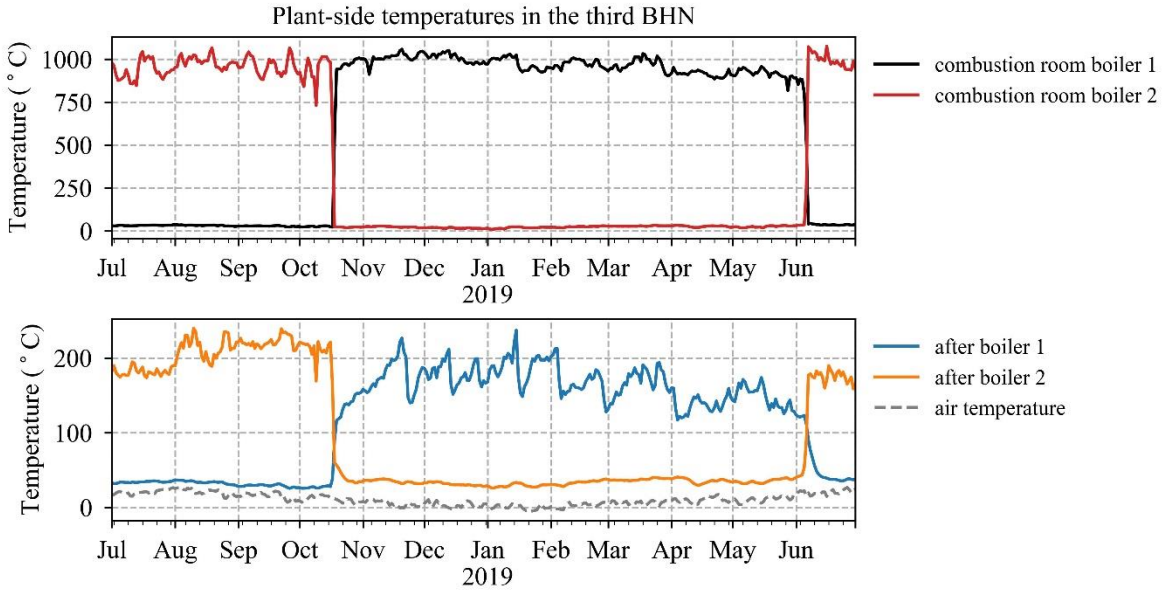

Figure 39: Temperatures of the plant side in the third biomass heating network.

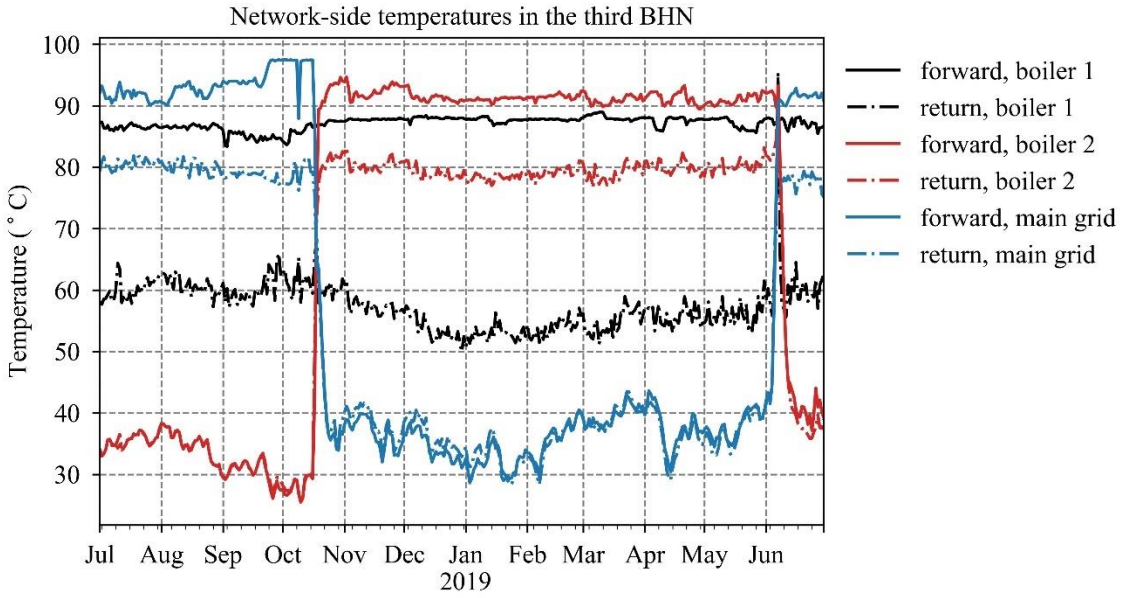

Figure 40: Temperatures of the grid side in the third biomass heating network.

Figure 39 reveals that both biomass boilers in this heating network did not operate simultaneously. The average combustion temperatures of biomass boilers 1 and 2 were nearly identical, both lay on 962 °C. The average gas temperature after boiler 1 was

164.1 °C, showing significant fluctuations, whereas it was 200.5 °C after boiler 2. To mitigate these fluctuations, an improvement in the boiler control system is suggested. Figure 40 shows the forward and return temperatures of this BHN, which indicates an average forward temperature of 87.1 °C and a return temperature of 57.3 °C.

Performance analysis

Figure 41 illustrates the heat generation by the boilers in the third BHN. The graph indicates that the highest daily average demand reached only 1470 kW_{th}. This value represented only 49 % of the nominal heat output of biomass boiler 1. The average heat output of biomass boiler 1 in wintertime was only 989 kW_{th}, which corresponded to 33 % of the nominal capacity, indicating a yearly utilization rate of only 21 %. In summer, biomass boiler 2 was operated instead of biomass boiler 1. Its average output reached up to 493 kW_{th}, equivalent to 82 % of the nominal capacity. However, due to the limited operating time, the full operating hours were only 2640 h, which corresponded to a utilization rate of just 30 %. The comparison of the rated capacity of thie BHN with its daily average demand clearly indicates that the plant is significantly oversized..

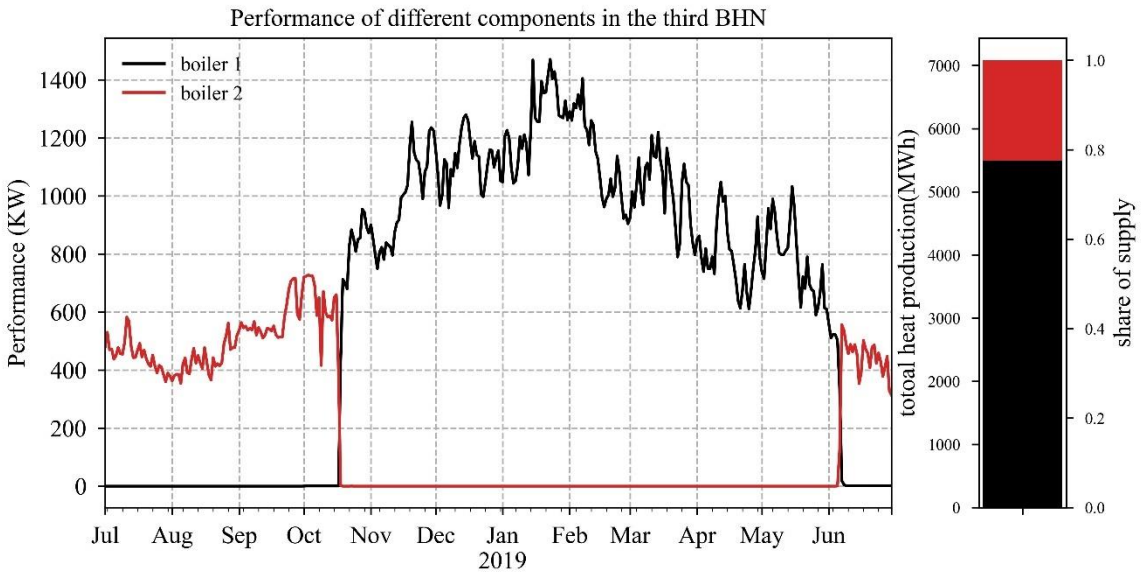

Figure 41: Supply of the main components in the third biomass heating network.

7. Evaluation and discussion of investigated biomass heating networks

To ensure an accurate evaluation of the performance of a biomass heating system, precise determination of fuel energy consumption is essential. This is often challenging due to inaccuracies in measurement of biomass weight. To solve this issue, a detailed simulation based on measured operating data can provide more precise results. In this study, the fuel composition and the heating value were analyzed in the laboratory (See Section 6.2.1). The fuel consumptions are iteratively calculated through simulations based on measured operating data (See Section 6.2.2). Based on this, the calculation of the overall efficiency and specific CO2 emission of the studied networks can be also performed.

To conduct accurate calculations of the fuel consumption and system efficiency, the general model proposed in Section 4.1 is employed, where the selected BHNs are implemented based on their real hydraulic circuits (See Section 6.1).

7.1 Model implementation and validation

The validation of the proposed methodology involves comparing the measured and simulated performances of the key components for heat recovery in the first and second BHNs, including heat pumps, economizer, and flue gas condenser. By utilizing the measured parameters such as analyzed fuel data, measured temperatures, and boiler performances as input data, the performances of the heat pumps, economizer as well as flue gas condenser can be simulated by the model for comparison with actual measured values.

Figure 42 shows the comparison between the simulated and measured results of the two biomass heating networks in Austria, each equipped with integrated heat pumps in different configurations. In the first BHN, the simulated results of the heat pump correspond well with the actual measured values, with an average deviations of 20 kW. This corresponds to 2.7 % of the heat pump capacity. The graph indicates that the deviation of the data is minor. Similarly, in the second BHN, the simulated performance curve of the heat pump closely resembles the measured one, with an average deviation of 37 kW, which corresponds to 3.7 % of the nominal heat output. The heat pump in the second BHN operated in the period from November to mid-May. Most of the data points are also less than 5% off.

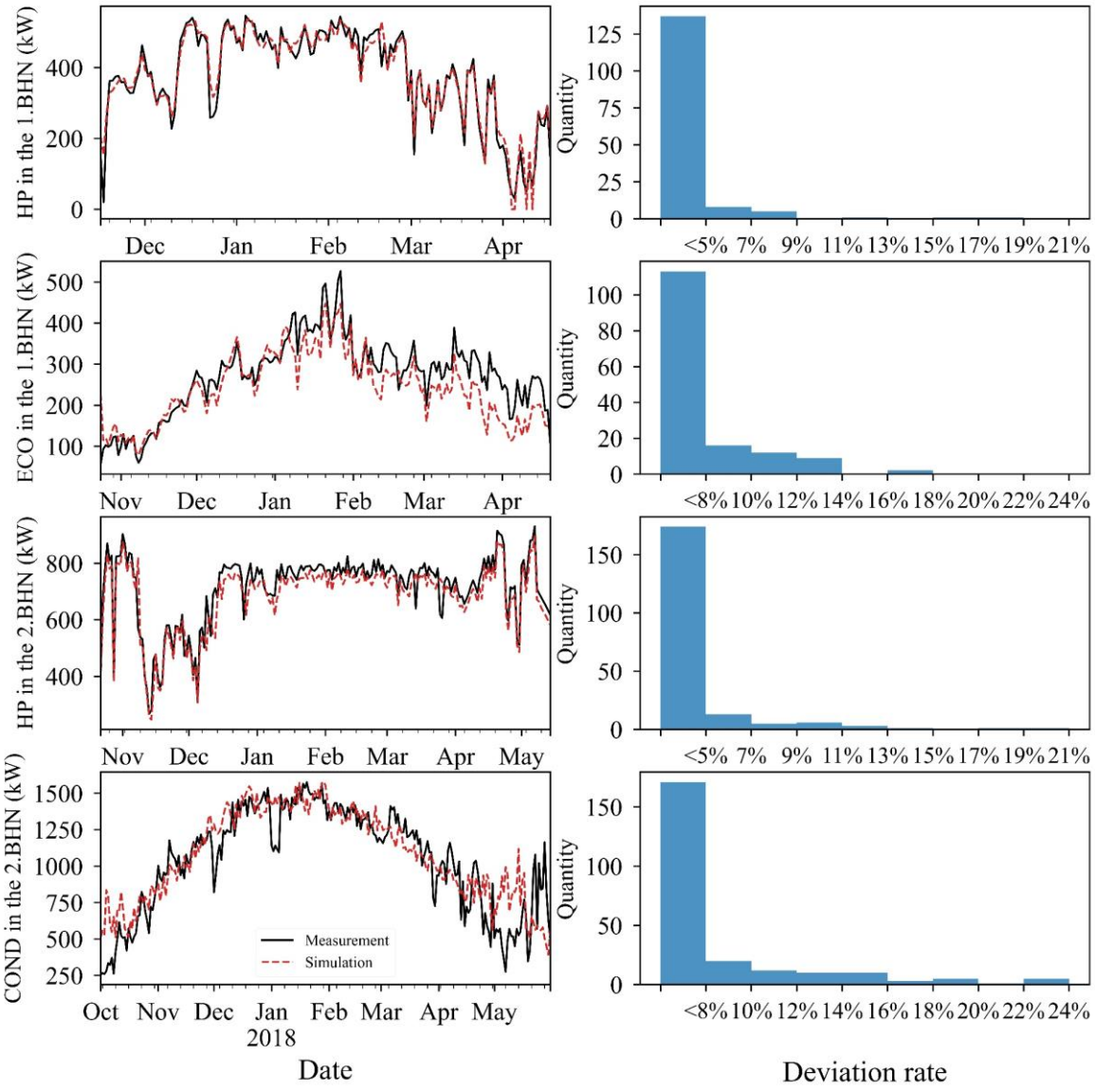

Figure 42: Validation of the simulation results of the 1st and 2nd BHN.

The simulation results and the measured results of the economizer (ECO) for the first BHN and the condenser (COND) in the second BHN appear to be less consistent compared to those of the heat pumps. However, the deviations of most data points are also mainly below 8 %. These discrepancies arise from various factors. A primary reason could be the assumptions made about input parameters in the model, such as the efficiencies of the heat exchangers. In the simulation model, heat exchanger efficiencies are assumed to be 94 %. But in reality, it can vary depending on the types of construction and operating conditions. Another important cause can be the measurement errors of temperatures and performance data. Another significant factor could be measurement errors in temperature and performance data. For instance, in the first BHN, the two economizers (ECO1 and ECO2)

were treated as a single entity due to a lack of measurement data between them, leading to the neglect of temperature loss between the two ECOs. Moreover, the performance of economizers is highly sensitive to the exit temperature of ECO2. With the high latent enthalpies of vapor in the flue gas, even a minor temperature deviation of 0.5 K can cause a significant difference in the heat exchangers performance. In the second BHN, the mixed flue gas temperatures after both biomass boilers had to be estimated due to the lack of sensors, which introduced further uncertainty. Additionally, the measured performance of the condenser in the second BHN showed minor anomalies in December, January, and May due to unidentified operational issues. This also leads to higher deviation. Despite these challenges, the overall results can be considered reliable, as the deviations of most data points are mainly below 8 % when validated against the respective input temperatures.

7.2 Simulation-based evaluation of the biomass heating networks

7.2.1 Energetical evaluation

Through modelling, the boiler efficiency and system overall efficiency, referred as “figures of merit”, can be determined. The calculated technical indicators of the three investigated BHNs are shown in Figure 43 to Figure 45. Determining the boiler efficiencies and system overall efficiencies allows to evaluate these biomass heating systems under investigation.

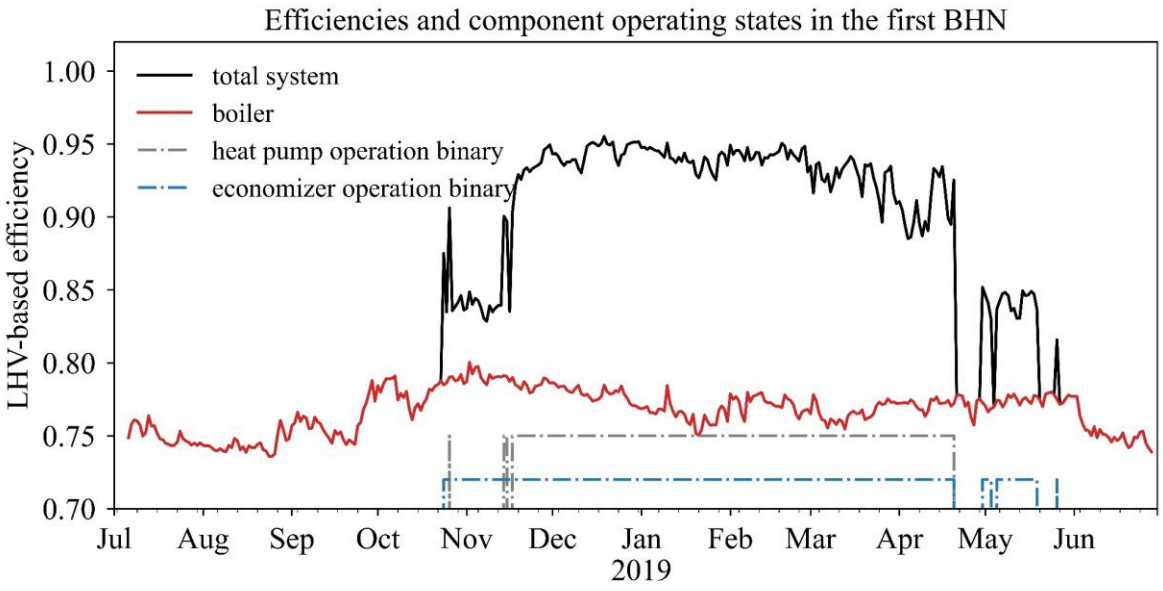

Figure 43: Efficiencies and component operating states in the first biomass heating network.

Figure 43 shows the efficiencies and operation states of ECO and heat pump in the first biomass heating network. Where the solid black line represents the system overall efficiency, i.e., the total heat supplied divided by the total input energy in the form of fuel and electricity. The red line represents the boiler efficiency. The blue dotted line indicates operation state (on/off) of the ECO and the grey dotted line indicates the operation state of the heat pump. In the first BHN, Both the heat pump and ECO are switched off in summer due to the low heat demand [199]. Therefore, the system overall efficiency is the same as the boiler efficiency. Analysis of the remaining period shows that the operation of ECO increased the total efficiency by about 8 – 10 %. By integrating the flue gas condenser and the heat pump, a further increase of the system efficiency of about 10 % was achieved, leading to an total overall efficiency increase up to 20 %.

While the first BHN represents the variant of the flue gas-side HP-integrated system , the second BHN represents the variant of the network-side HP-integrated system. Figure 44 shows the efficiencies and operation states of flue gas condenser and heat pump in the second BHN. Where the solid black line also denotes the system overall efficiency. The red line represents the average efficiency of both boilers in this BHN, while the green line and cyan line represent the efficiency of boiler 1 and boiler 2, respectively. The blue dotted line indicates the operation state of the flue gas condenser and the grey dotted line operation state of the heat pump.

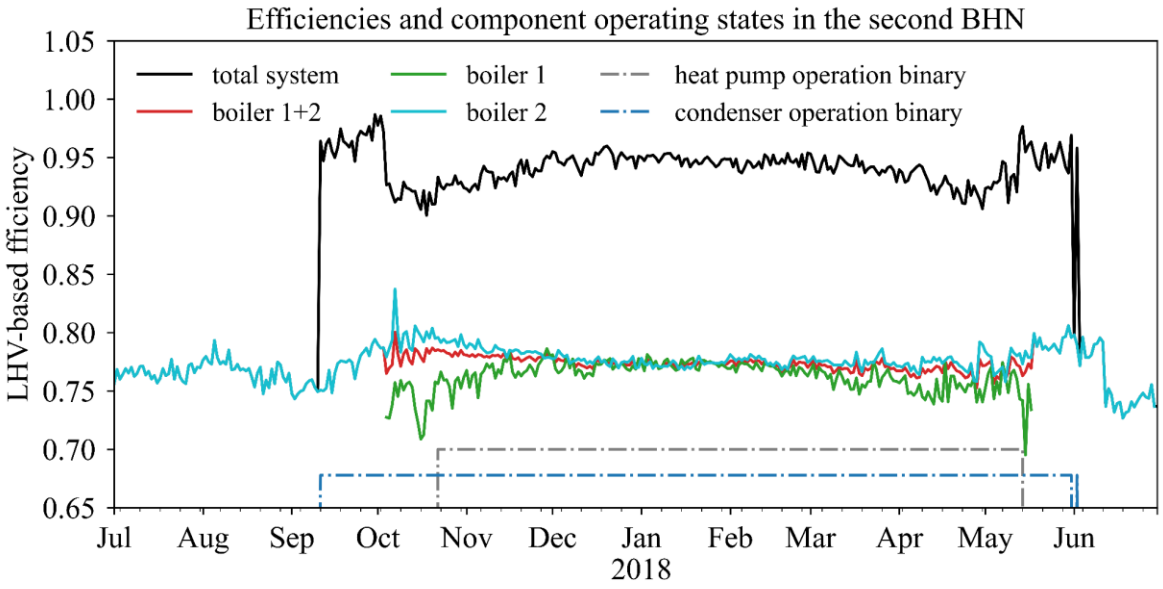

Figure 44: Efficiencies and component operating states in the second biomass heating network.

From the graph, it is evident that the incorporation of flue gas condenser and heat pump with network-side connection can significantly increase the system efficiency by about 17 %. The peculiarity of this BHN is that the heat network has a low-temperature network return at about 38 °C, in addition to the high-temperature network return. During periods of low heat demand (i.e., early September to October and mid-May to early June), the low amount of waste heat available in the flue gas can be efficiently recovered through the low-temperature network return, eliminating the need to operate the heat pump. As a result, the system's efficiency during these periods is remarkably increased, even beyond the core winter season.

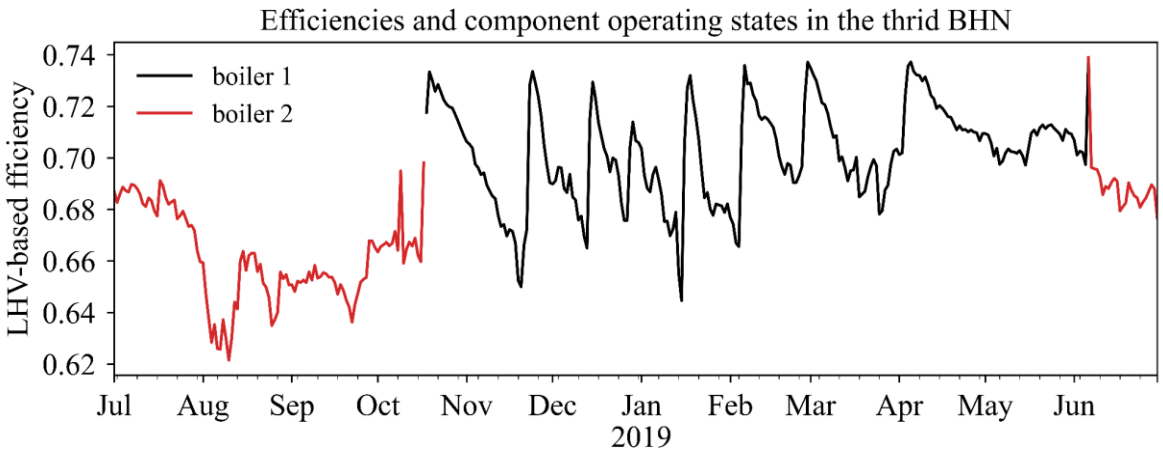

Figure 45: Efficiencies and operating states of the two biomass boilers in the third biomass heating network.

In Figure 45, the efficiency of the two biomass boilers over the year in the third BHN is displayed. A comparison with the first two BHNs reveals that the operation of the third BHN is notably inefficient. The maximal efficiency of the BHN observed over the year is about 73.6 %. The efficiency varies significantly due to changes in flue gas temperature from the boilers. Considering the total energy supply and total fuel demand, the average efficiency of the heating network is 69.2 %, markedly lower than that of the other two BHNs.

7.2.2 Environmental evaluation

To investigate the environmental impact of the heat pump integration concepts, the specific primary energy demand and CO_2 emissions of the two BHNs with integrated heat pumps are analyzed. As the calculation basis, the legally binding primary energy factors and

CO_2 emission factors of Austria from the OIB guideline 6, edition 2019 [200] are used as reference values.

Table 12: Reference values of primary energy and CO2 factors in Austria [200].

Energy source	f_{PE} *in* kWh_{PE}/kWh	$f_{CO2,equ}$ *in g* CO_2 */kWh*
electricity mix	1,02	227
wood chips 1.000 kW	0,1	17

Figure 46 and Figure 47 show the calculated environmental evaluation indicators of both BHNs with integrated heat pumps. The graphs indicate that the specific equivalent CO_2 emissions and the primary energy demand in the first BHN decreased significantly during early and late summer due to the operation of the economizer. A similar pattern is observed in the second BHN, where the condenser directly cools the low-temperature network return without the need for the heat pump, resulting in improved system efficiency without external power input and a consequent reduction in primary energy consumption. In wintertime, the operation of the heat pump at both BHNs led to a notable increase in the environmental indicators.

This effect is primarily due to the significant difference in CO2 emission and primary energy factors between the current electricity mix and forest wood chips, as detailed in Table 12. Although the integration of the heat pump reduces the need for biomass fuel, it necessitates additional electricity for active condensation. Only when the ratio of the heat pump COP to the boiler efficiency is larger than the ratio of the CO_2 factors of electricity to wood chip, the integration of the heat pump will have a positive environmental effect, which can be expressed as follows:

$$f_{CO2,el} < f_{CO2,fuel} * \frac{COP}{\eta_{boiler}} \tag{83}$$

From this equation it can be inferred that this negative environmental impact will be reduced if the electricity emission factor of the public grid decreases, for example, through an increased share of renewable energy generation in the future.

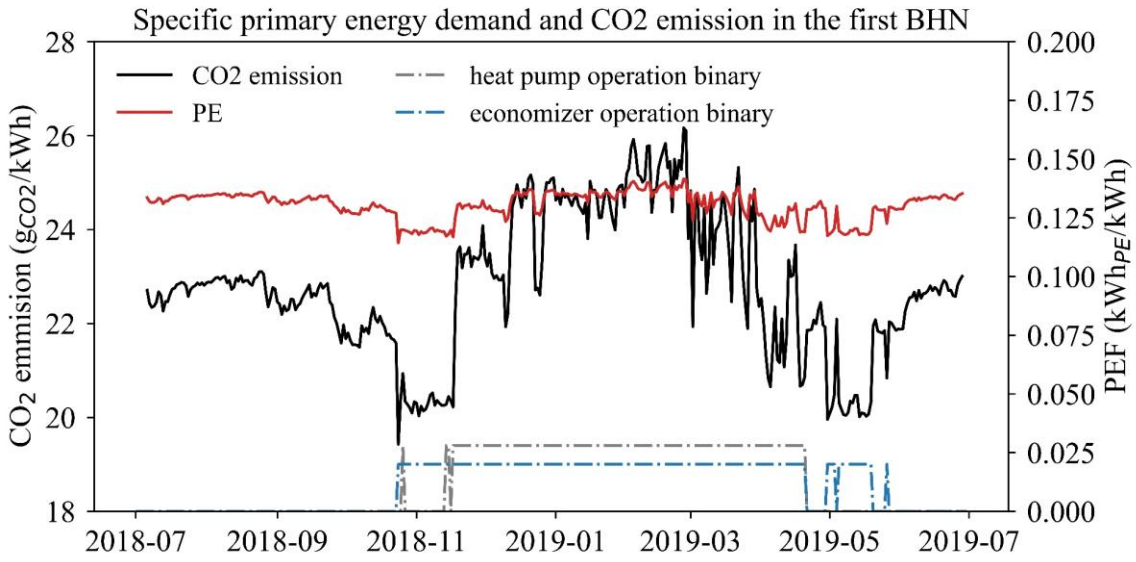

Figure 46: Specific primary energy demand and CO_2 emissions the first biomass heating network.

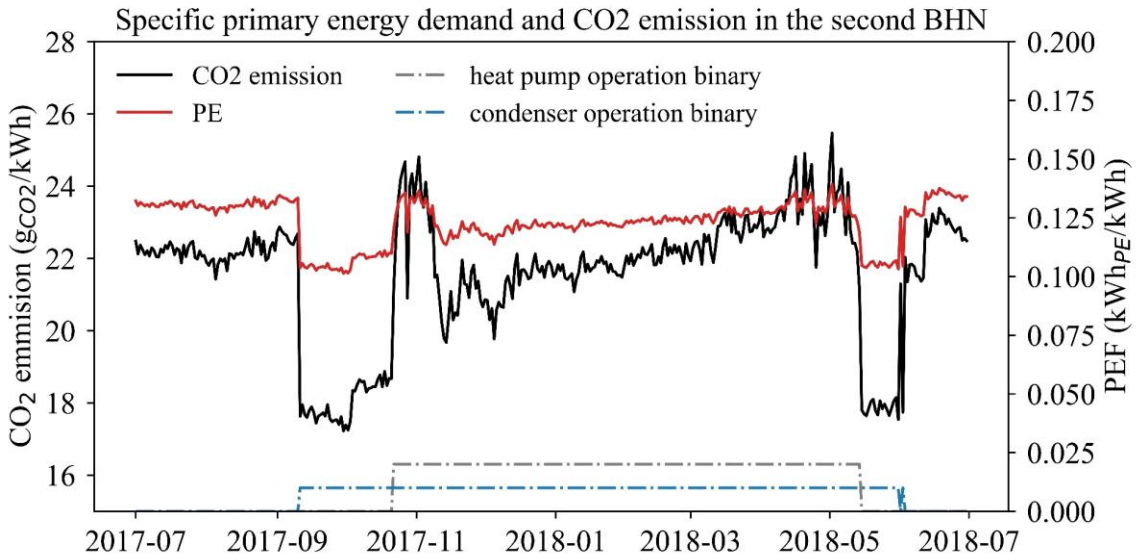

Figure 47: Specific primary energy demand and CO_2 emissions the second biomass heating network.

7.3 Comprehensive comparison and discussion of investigated biomass heating networks

For a comprehensive comparison of the three BHNs investigated, Table 13 summarizes the differences based on the technical information, operational data obtained, as well as the simulation results presented in the previous Chapter.

Regarding the commissioning years of the flue gas condensation, it can be noted that they correspond to the commissioning year of each heating network. This indicates that the flue

gas condensation was an integral part of the system from the time the network was commissioned. The commissioning year of the heat pump in the second BHN differs from the commissioning year of the network. While in the first BHN, the heat pump has already been implemented since commissioning of the network. A possible reason for the early integration of the heat pump in the first BHN could be its later commissioning year, coinciding with more advanced developments in biomass heating technology. Notably, the third BHN does not include a heat pump.

By utilizing the economizer and flue gas condensation with heat pump, an increase in the system overall efficiency of 17.8 % for the first BHN and 17.4 % for the second BHN was achieved during the winter months. When comparing these two networks, it's observed that the contribution of recovered heat to the total heat supply in the second BHN is significantly higher than that in the first one. This is attributed to the higher utilization rate of flue gas condensation and the heat pump in the second BHN, with the full utilization hours being almost double that of the first BHN. It is also noteworthy that the second BHN exhibits a significantly higher Coefficient of Performance (COP) for the heat pump, due to the lower temperature increase in its system. As shown in Table 13, the flue gas temperature after the flue gas condensation (related to the evaporating temperature) in the second BHN is significantly higher than in the first, while the difference in heat pump supply temperature (related to the condensing temperature) between the two BHNs is mere 0.3 K. However, a higher exhaust gas temperature also indicates a lower fuel utilization rate and, consequently, a lower overall system efficiency. An analysis of how the exhaust gas temperature and heat pump supply temperature affect the COP and system overall efficiency will be discussed in the next chapter.

Comparing to the other two BHNs, the third BHN has a significantly lower average efficiency of 69.2 %. The primary reason for this low boiler efficiency is the increased residual oxygen content in the exhaust gas. This is approximately three times higher than that of in the first BHN. Through calculation (Eq. (7)), it can be calculated that the combustion air ratio is around 3.0. This value is significantly above the optimum air ratio of 1.4 to 1.8. This discrepancy is attributed to the oversizing of the biomass boiler. Consequently, the biomass furnace of the third BHN is currently unsuitable for efficient flue gas condensation, as high excess air leads to a lower dew point temperature. To effectively implement the concept of flue gas condensation, optimization of combustion is necessary,

which would involve reducing the air ratio. This could be achieved by improving the control of combustion air entering the furnace and enhancing the flue gas recirculation.

Table 13: Comparison of the three studied biomass heating networks.

Parameter	*BHN 1*	*BHN 2*	*BHN 3*	*Unit*
Commissioning year of the BHN	2006	1996	1995	
Commissioning year of the COND	2006	1996	1995 dismantled 2001	
Commissioning year of the heat pump	2006	2012	HP not available	
System configuration	flue gas-side HP integration	network-side HP integration	baseline (before 2001 COND-only)	
Fuel water content	30	47.4	25.8	Ma%
Nominal output biomass boiler	3000	5000 + 3000	3000 + 600	kW
Boiler utilization rate	44,9	24.2 / 73.2	22.1 / 25.8	%
Flue gas temperature after boiler	247	169 / 373	164.1/200.5	°C
O_2 content in exhaust gas	5.43	unknown	14.1	%
Gas temperature after condensation	32	45	-	°C
Network average demand	2245	4290	818	kW
Network full utilization rate	43.9	47.7	27.3	%
Mains return temperature	53.8	55	79.0	°C
Mains feed temperature	91.6	90.9	92	°C
Heat pump supply temperature	59.1	58.8	-	°C
COP heat pump	3.5	5.1	-	-
Annual full utilization hours of flue gas condensation and heat pump	1811	3460	-	h
Contribution of recovered heat to total heat supply	14.1	19.5		%
Annual average efficiency of boiler	80.0	77.2	69.2	%
System efficiency increase in wintertime	17.8	17.4	-	%
Maintenance costs COND	annual cleaning	annual cleaning	10 h/week (before dismantling)	
Maintenance effort HP	annual maintenance	annual maintenance	HP not available	
Susceptibility to faults compare with other components	identical	significantly lower	above average	

Furthermore, when planning a new flue gas condensation system for the third BHN, it is crucial to consider the consistently low heating demand of the network. This implies that the capacity of the new flue gas condensation system should be significantly smaller than the one installed in 1995, which was dismantled in 2001 due to corrosion and operational problem. Moreover, the operational experience from this BHN prior to 2001 also indicates that the corrosion problems must be prevented in the technical planning and operation of any new condensation systems:

A primary concern is the exposure of the heat exchanger bundles in the flue gas condensation and the upstream economizer to flue gas. To mitigate potential corrosion, these heat exchanger bundles should be made of higher-quality stainless steel. Moreover, unlike the other two BHNs, this BHN currently lacks an electrostatic precipitator. The installation of an electrostatic precipitator upstream of the flue gas condenser would be beneficial in reducing the dust load on the heat exchangers, thereby enhancing the effectiveness of the flue gas condensation. If emission regulations become more stringent, installing an electrostatic precipitator will become essential.

A second issue concerns the negative effects of fluctuating return temperatures on the flue gas condensation process. Since condensation primarily occurs at temperatures below approximately 55 °C, fluctuating temperatures that alternate above and below this threshold can lead to intermittent condensation states. This fluctuation can result in condensate formation on heat exchangers, subsequently causing dried-out, salt-containing ash deposits (such as KCl and NaCl) to accumulate on the surfaces of the condenser bundle. These deposits can lead to corrosion on stainless steels, rapidly deteriorating the heat exchanger bundle. To counteract this, a heat pump can be employed to stabilize these fluctuating return temperatures. The low cooling temperatures provided by heat pumps ensure continuous condensation of the flue gas, effectively preventing the formation of dried-out deposits on the heat exchanger surfaces and thereby reducing the risk of corrosion. Operational experiences from the first and second BHN have demonstrated that integrating a heat pump not only effectively improves the fuel utilization rate but also ensures reliable, long-term operation of the flue gas condenser.

8. Thermodynamic analysis of the heat pump cycle

This chapter aims to investigate the impact of technical parameters on the integration of heat pump and to develop optimal heat pump circuits. For this purpose, a thermodynamic analysis based on the first BHN is conducted. The technical data of the equipment used can be found in Table 8. To evaluate the influence of the technical parameters, the boiler is assumed to operate at its rated heat output. Additionally, the exhaust gas is assumed to contain 220 mg/Nm^3 of CO and 200 mg/Nm^3 of NO_x, corresponding to the limits set by the 44th BlmSchV in Germany [201], with a reference O_2 content of 11 %*vol*. The flue gas temperature exiting the boiler is set at 180 °C. There is a temperature reduction of 20 K after the air preheater and 100 K after the economizer. The flue gas then reaches the condensation bundle at 60 °C, where it is cooled by the heat pump to the target exhaust gas temperature. The default value of the target exhaust gas temperature is assumed to be 30 °C. The network flow and return are set at 90 °C and 55 °C respectively, with the average ambient temperature being 15 °C. The default values of various operating parameters used in the analysis are listed in Table 14.

Table 14: Default operating parameters for the c analysis of heat pump integration.

Parameter	Value	Unit
CO in exhaust gas	220	mg/Nm^3_{dry}
NOx in exhaust gas	200	mg/Nm^3_{dry}
O_2 reference	11 %	$vol.\%_{dry}$
Excess air	1.6	-
Combustion temperature	900	°C
Boiler surface temperature	200	°C
Flue gas temperature after boiler	180	°C
Flue gas temperature after air preheater	160	°C
Flue gas temperature after economizer	60	°C
Target exhaust gas temperature	30	°C
Ash temperature	100	°C
Air temperature	15	°C
Main network return temperature	55	°C
Main network supply temperature	90	°C
Heat pump supply temperature	65	°C

In the following, the impact of the target exhaust gas temperature, heat pump supply temperature, and choice of refrigerant on heat pump design and overall system efficiency under different conditions will be examined.

8.1 Analysis of target exhaust gas temperature

In a standard heating plant, the overall efficiency increases as the exhaust gas temperature decreases. However, when a heat pump is integrated into the system, its power consumption also affects the overall efficiency. As mentioned in Chapter 4, the evaporation temperature of the heat pump depends strongly on the target exhaust gas temperature after flue gas condenser. A lower target exhaust gas temperature results in a lower evaporation temperature of the heat pump, which leads to lower heat pump efficiency and, in turn, affects the overall efficiency.

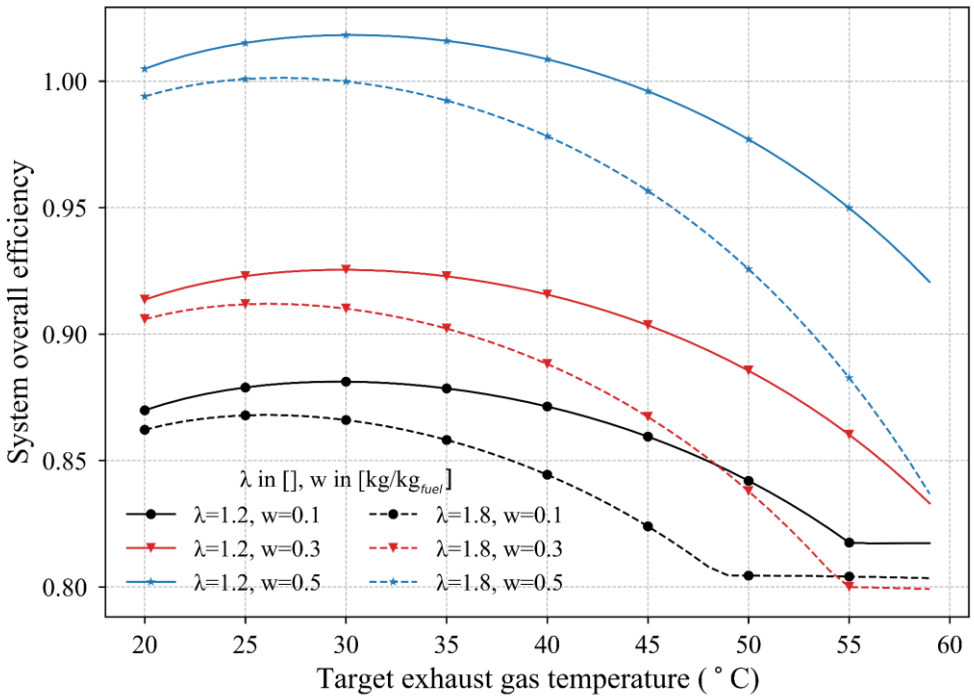

Figure 48: LHV-based system overall efficiency as a function of target exhaust gas temperature at different air ratios and fuel water contents w in kg/kg$_{fuel}$ (at a constant heat pump supply temperature of 65 °C).

Figure 48 indicates that the system overall efficiency based on the lower heating value does not always increase with decreasing exhaust gas temperature. At an air ratio of 1.2, the highest efficiency points appear at an exhaust gas temperature of around 30 °C. If the exhaust gas temperature drops further, the overall efficiency will also decrease. This is due to the

unavoidable power consumption of the heat pump. At a very low exhaust gas temperature, the energy saving potential is already so low that the power consumed for heat recovery has a negative effect on the system.

The diagram also demonstrates that, as the exhaust temperature varies, the maximal achievable overall efficiency also depends on the air ratio and the fuel water content. A higher air ratio (λ) decreases the maximal achievable overall efficiency since the higher air volume increases the exhaust gas volume, leading to higher heat loss to environment. By increasing the λ value, the optimum exhaust gas temperature shifts to the left. The figure also clearly shows that the maximal overall efficiency is significantly higher at a higher fuel water content *w* than at a lower one. This is due to the high latent heat of the steam in the flue gas. The greater the quantity of water in the fuel, the more energy can be recovered. Therefore, the overall efficiency also increases with the increase in water content.

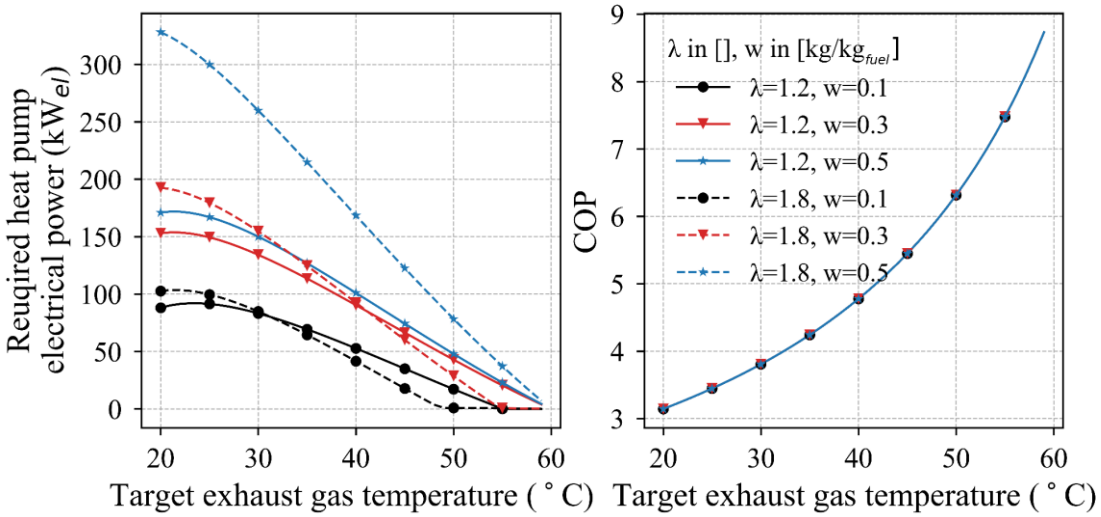

Figure 49: Required heat pump electrical power demand and COP as a function of target exhaust gas temperature at different air ratios and fuel water contents w in kg/kg$_{fuel}$ (at a constant heat pump supply temperature of 65 °C).

A lower exhaust gas temperature means a high recovery potential, but also higher temperature lift requirements for the heat pump. Therefore, the electrical power required for the recovery of waste heat at a lower temperature level also increases with an increased target exhaust gas temperature, as shown in Figure 49. The graph indicates that the electrical power required by the heat pump increases rapidly as the exhaust gas temperature falls. This is accompanied by a sharp drop in the COP. Higher power requirements coupled with a lower

COP value also mean higher investment costs and poor operating conditions, even though more energy can be recovered from the exhaust gas.

In addition, at higher levels of fuel water content, the electrical power requirements of the heat pump are significantly higher because of the higher amount of waste heat to be recovered. Moreover, it is noticeable that at lower exhaust gas temperatures, a lower air ratio achieves higher system overall efficiency, but with less power demand for heat pumps. Therefore, based on the above analysis, the fuel water content and air ratio also need to be considered when selecting the exhaust gas temperature.

8.2 Analysis of heat pump supply temperature

As described in Section 3.1.2, it is possible to feed the heat from the heat pump into the heat network in different ways, e.g., into main network return, the preheated network after economizer, or directly into the network feed flow. The feeding variant of the recovered heat determines the required heat pump supply temperature to be selected.

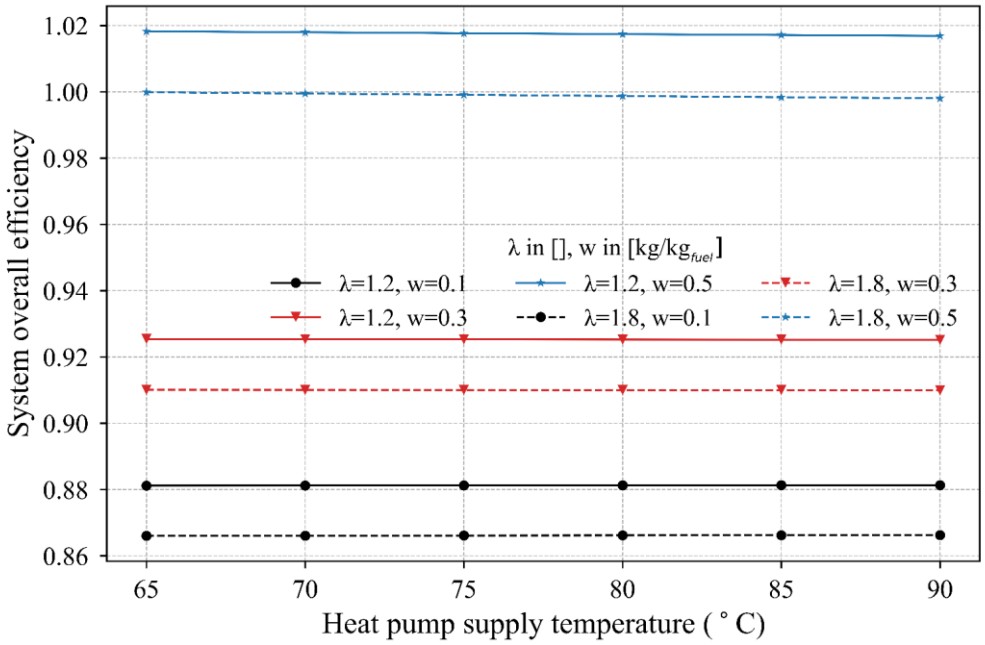

Figure 50: LHV-based overall system efficiency as a function of heat pump flow temperature at different air ratios and fuel water contents w in kg/kg$_{fuel}$ (at a constant target exhaust gas temperature of 30 °C).

Figure 50 and Figure 51 present the system overall efficiencies, the required heat pump electrical power demand, and the COP, at different heat pump supply temperatures. Figure

50 shows that the change in heat pump supply temperature has no significant effect on system overall efficiency. However, as the heat pump supply temperature increases, the power requirements of the heat pump also increase significantly. This is due to the increased temperature lift between the evaporator and the condenser, resulting in a sharp drop in the COP.

It is also important to note that at a fixed exhaust gas temperature, the heat available from the flue gas condenser remains constant. To fully recover the heat at a lower COP value, the required heat pump electrical power increases, as do the dimensions of the heat pump. This trend is more pronounced at higher fuel water contents. Although from a technical point of view, a higher heat pump supply temperature has no significant impact on the overall system, it leads to larger heat pump sizes, higher investment costs, and more significant power input. Therefore, when designing the heat pump, the supply temperature should only be selected as high as necessary. However, it is crucial to ensure that the heat supply temperature must not fall below the minimum value, so that all the heat can be fed into the heat network, as described in Section 4.2.1.

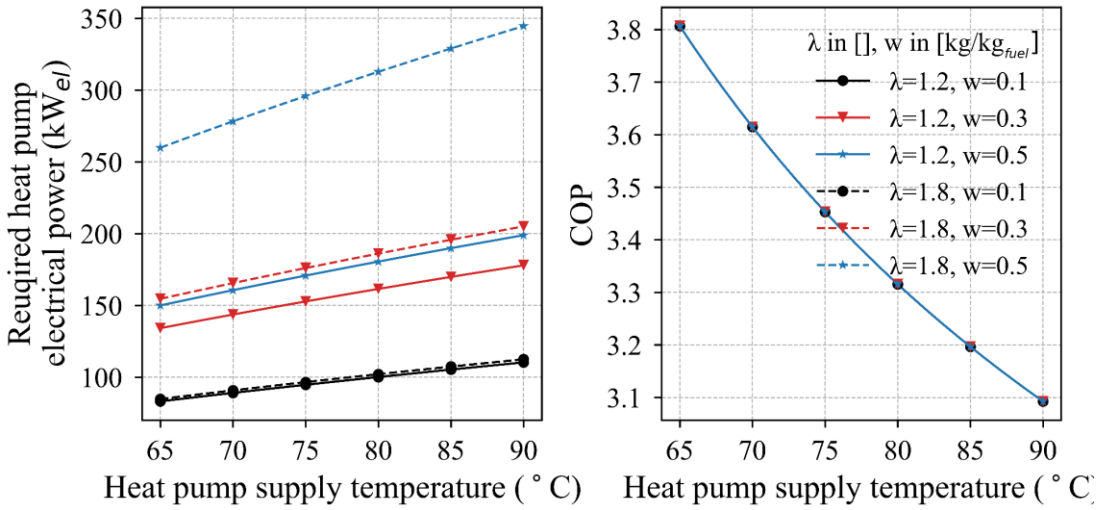

Figure 51: Required heat pump electrical power demand and COP as a function of heat pump supply temperature at different air ratios and fuel water contents w in kg/kg$_{fuel}$ (at a constant target exhaust gas temperature of 30 °C).

8.3 Analysis of the refrigerant selection

The selection of the refrigerant is crucial for the application scenarios studied in this thesis. A preliminary analysis of different refrigerants' properties, such as their evaporating temperatures at ambient pressure and critical points, was conducted. Based on the preliminary analysis, the following refrigerants were found to be suitable for the application scenarios:

- R134a, which is the most commonly used refrigerant [202].
- R717 and R236fa, which were used in the two real-world cases investigated in this thesis (See Section 6.1).
- And R290, R600a, and R1234yf, which were recommended in [203] for their low GWP (Global Warming Potential).

Figure 52 shows the results of varying the exhaust gas temperatures for different heat pump temperature lifts and refrigerants. From the figure, it is evident that the choice of refrigerant strongly affects the COP of the heat pump and, in turn, the electricity demand. However, the choice of refrigerant has no significant effect on system efficiency. This is because the fuel utilization remains constant at a constant exhaust gas temperature and the system overall efficiency is only influenced by the electricity consumed by the heat pump. Although there are differences in electricity consumption, they are, however, very small relative to the total energy consumption of the system. Nevertheless, due to the high price and environmental impact of electricity, the choice of refrigerant is still important.

Figure 52 also highlights the differences in the COP values for both low- and high-temperature increases. As can be seen in the graphs, R236fa performs well at high target exhaust gas (heat source) temperatures, while R717 performs better at lower temperatures. However, R236fa, with the highest GWP value [204] of all the refrigerants considered, can cause environmental damage. R717 is in the safety group denoting increased toxicity (B2L) [205].

As an alternative, R600a behaves well at different exhaust temperatures and temperature increases. Compared to R600a, the COP values are significantly lower with R290 and R1234yf. It is also noticeable that R1234yf does not perform well at low exhaust temperatures with large temperature increases, due to the low critical temperatures of these refrigerants. Thus, the R600a refrigerant might be a better alternative to R236fa and R717

than R290 or R1234yf. However, even when using R600a, it should be noted that R600a belongs to the "highly flammable"(A3) group 13]. The most used refrigerant, R134a, is not recommended due to its high GWP number and relatively low COP values.

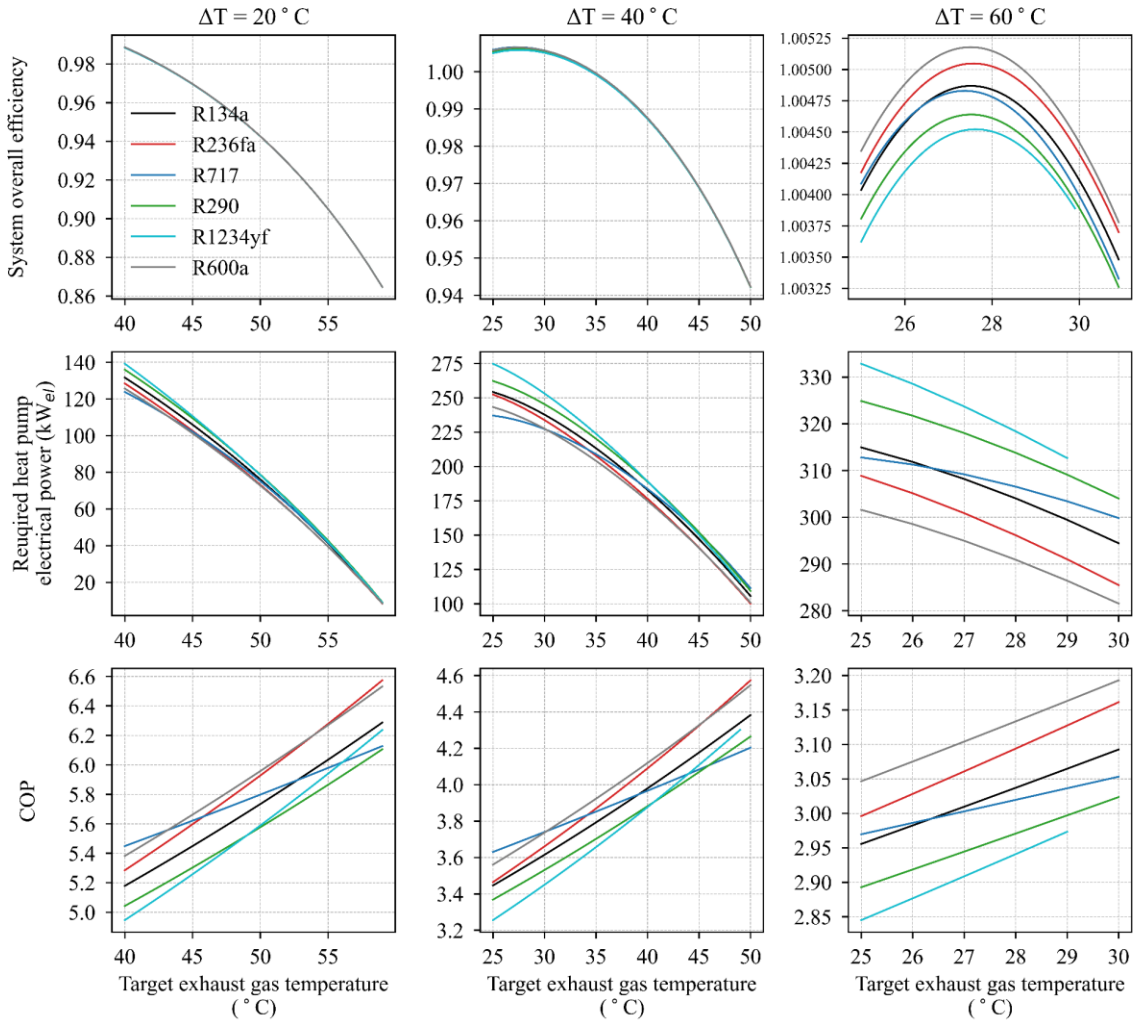

Figure 52: LHV-based system efficiencies, required heat pump power demand and COP, as a function of target exhaust gas temperature for various temperature lifts and refrigerants selection.

9. Techno-economic analysis of the heat pump integration concepts

To conduct a study in Germany and an in-depth analysis of the heat pump integration concept, both integration variants are implemented in the third BHN through the proposed method. Considering the service life and oversizing of the heating plant in the third BHN, the biomass boilers should be modernized with reduced nominal thermal output according to the heating network operator. The concepts investigated in this thesis offers the possibility to install a smaller biomass boiler than the old one, as the heat pump can cover part of the heat demand. This also helps prevent malfunctions of the boiler due to low utilization rates.

Three renovation scenarios are considered in this chapter:

1. Baseline system: Renovation with a boiler without ECO, COND, and HP
2. Flue gas-side HP-integrated system: Renovation with a smaller boiler with ECO and COND, and a flue gas-side integrated heat pump
3. Network-side HP-integrated system: Renovation with a smaller boiler with ECO and COND, and a network-side integrated heat pump

For the design of different systems, it is assumed that the future heating load, ambient temperature, and humidity will remain at the same hourly average values as in the historical years. To meet the original temperature requirements of consumers, it is also assumed that the supply and return temperatures of the network will maintain historical averages. In addition, the minimum annual full utilization hours for designing the integrated biomass heating system (including biomass boiler, heat recovery equipment and heat pump) is set at 5500 hours to ensure efficient operation. The existing oil-fired backup boiler and the 40 m^3 buffer storage will cover the remaining heating demand, including peak load demand, and demand during biomass boiler malfunctions. The average hourly and daily operating data, including heating load, weather data, and network temperatures, can be found in Figure 73 in Appendix F.

Besides, considering that the supply chain of biomass fuel has geographical limitations, it is also assumed that the fuel composition for the biomass boiler remains the same as in previous years. The default value for excess air during combustion is 1.6. The CO and NO2 content of the exhaust gas also follows the limit values of the 44th BlmSchV [201]. The flue

gas temperature directly downstream of the boiler is 180 °C and is cooled to the lowest possible temperature in the ECO via the main return flow.

For designing the heat pump cycle, it is assumed that the flue gas is cooled to 30 °C in the flue gas condenser by default, unless specifically noted otherwise. The inlet water temperature of the heat pump condenser is the same as the network return water temperature, and the heat pump supply temperature is set at 65 °C by default. As refrigerant, R600a is chosen from the case study, as recommended in Chapter 8.

In this chapter, these scenarios are investigated under the given assumptions from a technical and economic point of view, where the two integration variants are compared, and the influence of the technical and economic parameters is analyzed. Since the economic feasibility of the measures is crucial in the decision-making process for network operators. The comparison and analysis can provide an overview of the differences between the renovation variants and help in deciding.

9.1 Comparison of technical and economic results of the heat pump integration concepts

9.1.1 Comparison of component capacities and investments

The comparison of necessary equipment capacities and investment costs for different renovation scenarios is presented in Figure 53. The left graph illustrates the required nominal capacities of various components in different renovation concepts. It can be observed that the biomass boiler should have a capacity of around 1200 kW in the baseline scenario, with designed annual full utilization hours of 5500 h. In the other two scenarios, the required size of the biomass boiler is significantly reduced due to the integration of the heat recovery components and heat pump. When comparing these two scenarios, it is noticeable that the required heat pump capacity is significantly higher in the network-side integration scenario compared to the flue gas-side integration scenario. This difference comes from the required cooling capacities for the different heat sources. In the flue gas-side integration scenario, where the heat pump is directly connected to the flue gas condenser, the evaporator capacity should be equal to the capacity of the flue gas condenser. In the network-side integration scenario, where the evaporator of the heat pump is connected to the main return, the lowest amount of diverted mains flow to the evaporator depends on the recoverable latent heat and dew point. In this case study, the dew point is 53.3 °C, which is lower than the mains return

temperature. This results in a larger heat pump dimension than in the flue gas-side integration case.

The different equipment sizes also lead to different investment costs. The cost structures with different concepts are also shown in the right graph of Figure 53. The diagram indicates that the investment costs are lowest in the baseline scenario, with the biomass boiler accounting for the majority of the investment. The integration of the heat recovery components in the other two scenarios significantly increases the total investment costs, even though the required boiler size is much smaller. The total investment in the network-side integration scenario is slightly higher than in the other due to the difference in heat pump capacity. In the flue gas-side integration scenario, the investment in the heat pump accounts for 8.1 % of the total investment, while the share of the heat pump in the network-side integration scenario is up to 10.5 %.

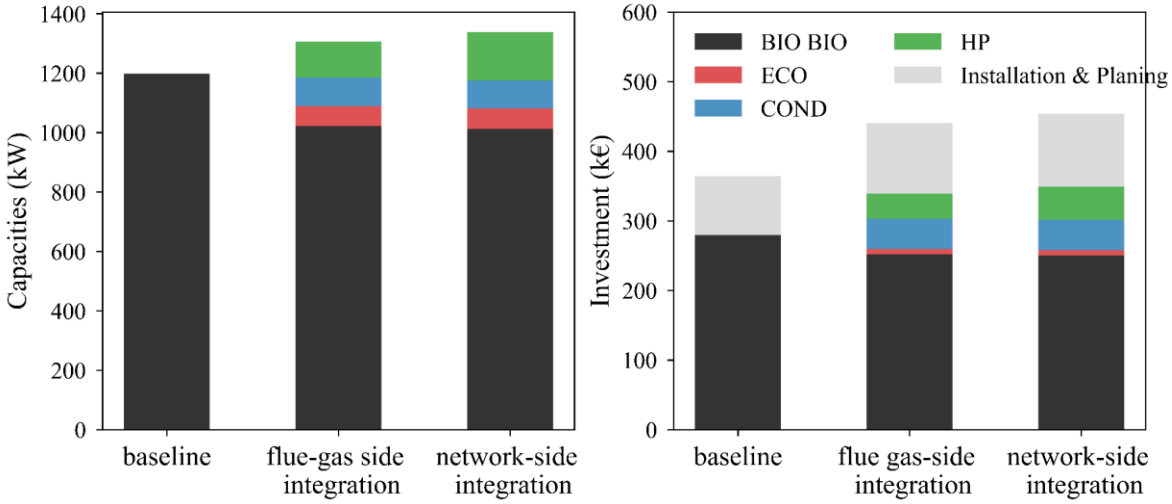

Figure 53: Required capacities and investment costs of various components for different renovation scenarios.

9.1.2 Comparison of energy supply and operating costs

Through the simulation with the historic curve, the annual energy supply curve by the different components in the three scenarios under consideration can be obtained, which are illustrated in the form of the duration line in Figure 54.

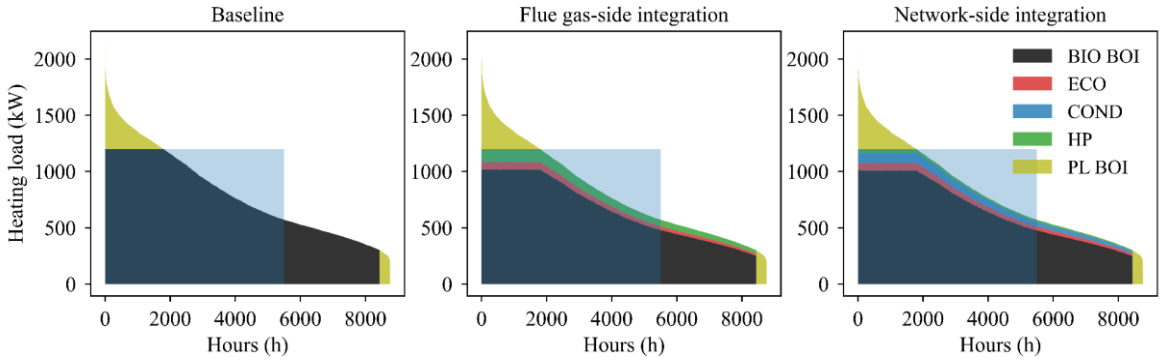

Figure 54: Annual duration line of the energy supply by the different components in the three scenarios.

For a more detailed analysis, the annual total contributions of the components' energy supply and the biomass fuel consumption of the system are presented in Figure 55. From the figure lefts, it can be seen that the demand of the heating network is completely covered by the biomass boiler and the peak load boiler in the baseline scenario, resulting in the highest the fuel consumption. In the flue gas-side integration scenario, the economizer contributes 5.3 % and the heat pump 9.2 % of the total heat demand, respectively. Among the contribution of heat pump, 534 MWh comes from the heat recovery of the flue gas condenser and 155 MWh from the electricity consumption. This results in an annual performance factor of 4.35. The integration of the heat pump reduces biomass fuel consumption by 15.5 % compared to the baseline scenario. The network-side integration scenario shows the specific feature of the energy supply by the heat pump. In this case, the heat pump extracts 735 MWh of heat from the network and feeds 928 MWh of heat at a higher temperature into the network. This results in a net energy supply of 193 MWh, which comes from the difference between heat injection and extraction.

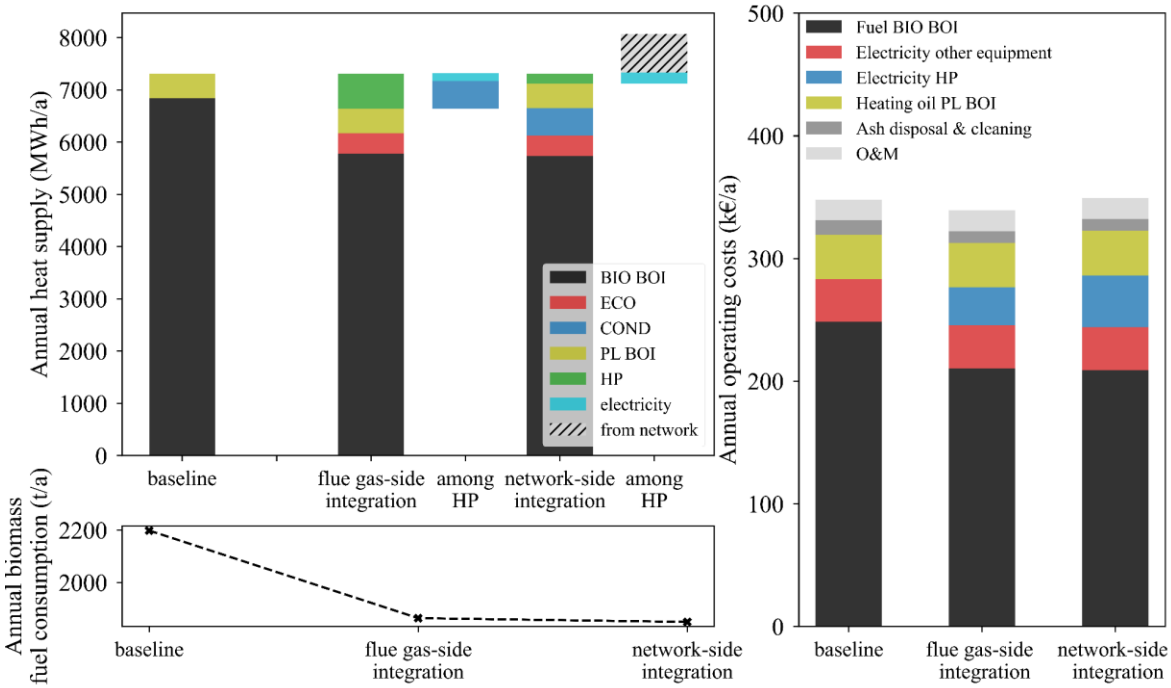

Figure 55: Comparison of energy supplies, fuel consumption and operating costs of the different renovation concepts.

The different operating behaviors of the components also lead to the different operating costs. As shown on the right side of Figure 55, the operating costs in the flue gas-side integration scenario slightly drop due to the heating recovery. Despite the significantly higher electricity price than that of biomass fuel, the good annual performance of the heat pump is expected to reduce the operating costs of the total system. However, the total operating costs in the network-side integration scenario, are higher than that in the baseline scenario, due to the higher electricity consumption, while its fuel consumption is almost the same as in the flue gas-side integration scenario. This results in increased operating costs for heat recovery.

9.1.3 Comparison of evaluation indicators

Based on the analysis presented above, the energetical, economic, and environmental indicators can be determined for the different scenarios. In this section, these evaluation indicators are compared, as listed in Table 15.

Table 15 clearly shows that the LCOE in the baseline scenario is 54.61 €/MWh, with an energy efficiency of only 81.89 %, indicating that it is the least favorable option. By

implementing the heat pump integration concepts, the overall energy efficiencies increase to 93.36 % in the flue gas-side integration scenario and 93.30 % in the network-side integration scenario, respectively. Due to the smaller heat pump size and lower electricity demand, the flue gas-side integration concept has proven to be a more economical solution, while the LCOE in the network-side scenario has slightly increased compared to the baseline scenario.

The table also shows that the variable operating cost of the system accounts for the majority of the heat production cost. Although the investment cost in the flue gas side integration scenario is higher than in the baseline scenario, the overall economic feasibility of the system is still improved due to the reduction of the variable operating costs. However, since electricity prices are much higher than biomass fuel prices, the operating costs in the network-side scenario become higher than in the baseline scenario, making its total heat production costs higher than in the baseline scenario.

Table 15: Comparison of the different evaluation indicators for different renovation scenarios.

	baseline	flue gas side-integration	network side - integration	unit
spec. CAPEX	5.31	6.18	6.33	€/MWh
spec. fix. OPEX	2.38	2.41	2.44	€/MWh
spec. var. OPEX	46.92	45.67	47.07	€/MWh
LCOE	54.61	54.26	55.84	€/MWh
$f_{lhv,sys}$	81.89 %	93.36 %	93.30 %	-
$e_{PE,sys}$	0.36	0.36	0.37	MWh_{PE}/MWh
$e_{CO2,sys}$	50.44	54.92	57.80	kg_{CO2}/MWh

Regarding environmental performance indicators, both integration concepts have a negative impact on the environment. The high CO_2 factor of electricity from the power grid leads to a sharp increase in specific CO_2 emissions, rising from 50.44 kg_{CO2}/MWh to 54.92 kg_{CO2}/MWh and 57.80 kg_{CO2}/MWh, respectively. Therefore, in terms of CO_2 emissions, both heat pump integration concepts prove to be less advantageous due to the electricity consumption in this case study, if the electricity is sourced directly from the public power grid.

In summary, both heat pump integration concepts enhance the energy efficiency of biomass heating networks. However, they also have negative impacts on the environment. Among the studied cases, the flue gas-side integration concept emerges as a more promising option due to its lower operational heat costs and higher energy efficiency, despite

necessitating higher initial investment costs. Nonetheless, a critical consideration in this approach is the source of electricity, which needs to be carefully chosen to minimize the environmental impact.

9.2 Analysis of the impact of technical parameters

This section aims to examine the influence of technical input parameters on the feasibility of integrating heat pumps. These parameters play a critical role in determining the technical and economic viability of the integration concepts. This analysis can ensure that the concepts are not only energy-efficient but also cost-effective implemented under given conditions.

9.2.1 Target exhaust gas temperature and heat pump supply temperature

First, the impact of heat pump temperature levels on the technical and economic feasibility is analyzed. Figure 56 displays the correlations between system overall efficiencies and *LCOE* at varying flue gas temperatures and HP-supply temperature. The results show that the selection of temperature level in the design of the heat pump has a strong impact on the economic viability. In this case study, the flue gas-side integration concept consistently proves to be more favorable than the network-side integration under varying exhaust gas temperatures.

The analysis of the trend of the lines indicates that the overall efficiency in both heat pump integrated systems increases with the lowering of exhaust gas temperatures, when the temperature is obove 30 °C. However, if the temperature becomes too low, the heat pump operation will impact the overall efficiency negatively, consistent with the thermodynamic analysis presented in Section 8.1. In contrast, the LCOE increases consistently with the decrease of the exhaust gas temperature set point, as the heat pump dimension needs to be increased due to the higher temperature rise. This leads to higher investment and electricity costs, despite recovering more energy from the flue gas. Therefore, the energetical optimal exhaust gas temperature for this case study would be around 30 °C for both scenarios, as presented in the results. In the range below 30 °C, both the LCOE and the efficiency increase as the exhaust gas temperature set point is lowered, indicating that a set point under 30 °C is not viable from either a technical or economic perspective.

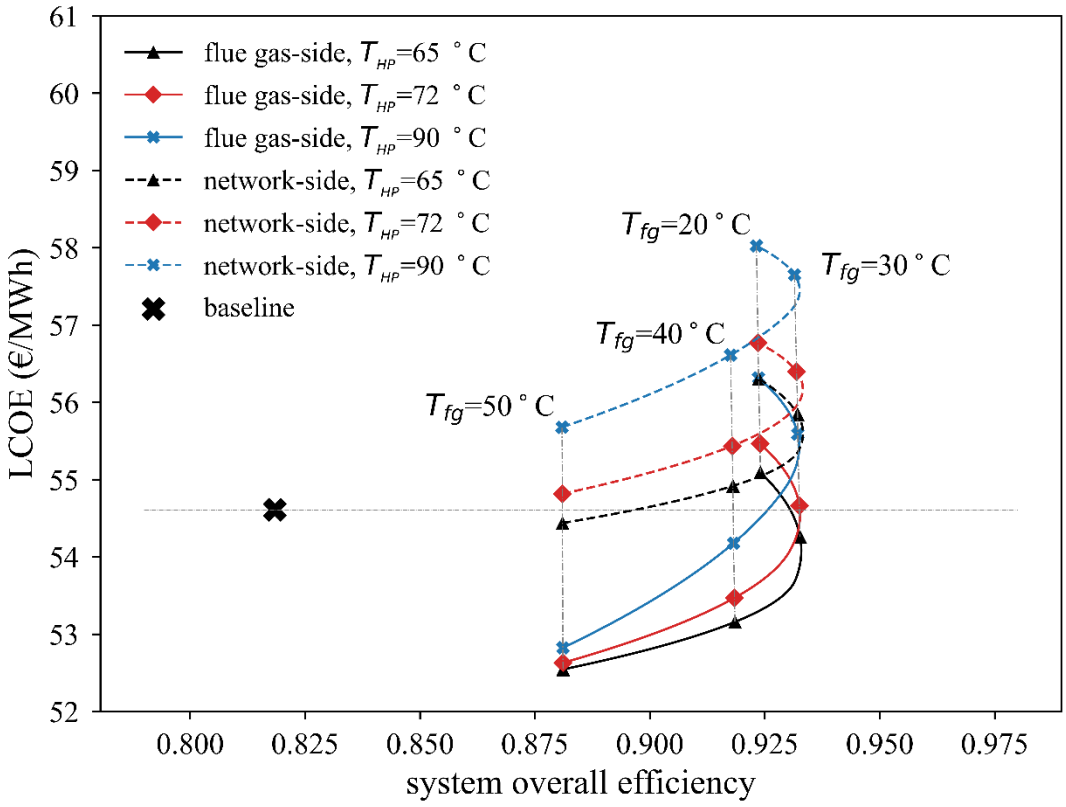

Figure 56: Correlations between overall efficiencies and LCOE of both heat pump integration concepts with varying target exhaust gas temperatures and HP-supply temperatures.

The figure also indicates that, although the system efficiency drops sharply at high exhaust gas temperatures, it remains significantly higher than in the baseline scenario. Both heat pump integration concepts can be implemented cost-effectively in practice by identifying the appropriate exhaust gas temperature setpoint. In this case study, the flue gas-side integration proves to be economically beneficial when the exhaust gas temperature is above 30 °C. Furthermore, the analysis reveals that increasing the HP heating temperatures has no remarkable influence on overall efficiency but negatively impacts economics. Thus, it is advisable to keep HP heating temperatures as low as possible during planning the heat pump.

9.2.2 Fuel water content and annual full utilization hours

When planning the heat pump integration concepts for biomass heating, it is crucial to consider the potential variations in fuel water content and the minimum full utilization hours of the equipment.

Figure 57 presents the curves of overall efficiency and LCOE for different scenarios as a function of fuel water content, considering various full utilization hours of the biomass heating. It is assumed that the heating value and fuel price based on the dry substance of the fuel remain constant. The exhaust gas temperature is set at 30 °C and the heat pump is supplied at 65 °C.

As depicted in the left figure, an increase in water content leads to a higher overall system efficiency when integrating a heat pump, while the overall system efficiency of the baseline scenario decreases. This indicates that a higher water content presents greater potential for overall system efficiency improvement using an integrated heat pump. The efficiency improvement is comparable in both the flue gas-side and network-side integration scenarios. A similar trend is observed when considering the different full utilization hours.

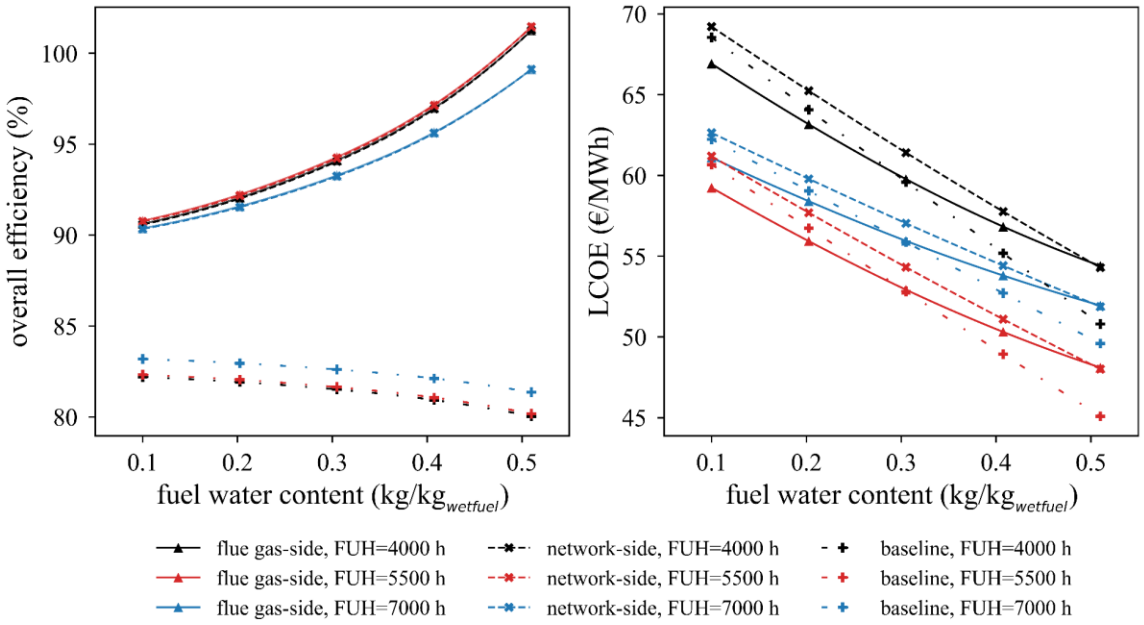

Figure 57: Analysis of overall efficiency and LCOE for different scenarios as a function of fuel water content at different full utilization hours of the biomass boiler.

The right figure in Figure 57 illustrates that in all scenarios, the cost decreases rapidly as fuel water content increases. However, if fuel water content exceeds 0.3 kg/kg$_{wetfuel}$, integrating the heat pump on the flue gas side will no longer be cost-effective, despite the higher potential for efficiency improvement. Furthermore, the graph demonstrates that the difference in heating cost between the network-side and flue gas-side integration scenarios gradually decreases. At a fuel water content of 0.5 kg/kg$_{wetfuel}$, the costs of both options are

similar, but both are above the baseline cost. Therefore, at higher fuel water contents, both heat pump integration concepts are unfavorable in terms of cost.

Figure 58 illustrates the impact of full utilization hours on overall system efficiency and LCOE for an integrated biomass heating system, considering different fuel water contents. As shown in the left panel, both excessively low and high full utilization hours of the biomass boiler affect the overall system efficiency negatively. This effect arises because the designed full utilization hours influence the rated heat output of the biomass boiler, thereby affecting the proportion of the load that can be covered by the biomass heating. he influence of varying full utilization hours on the energy supply for this heat network is further depicted in Figure 59, using the duration curve. Additionally, Figure 74 in Appendix G provides a detailed view of how the integrated biomass heating system covers the total demand at different FUHs.

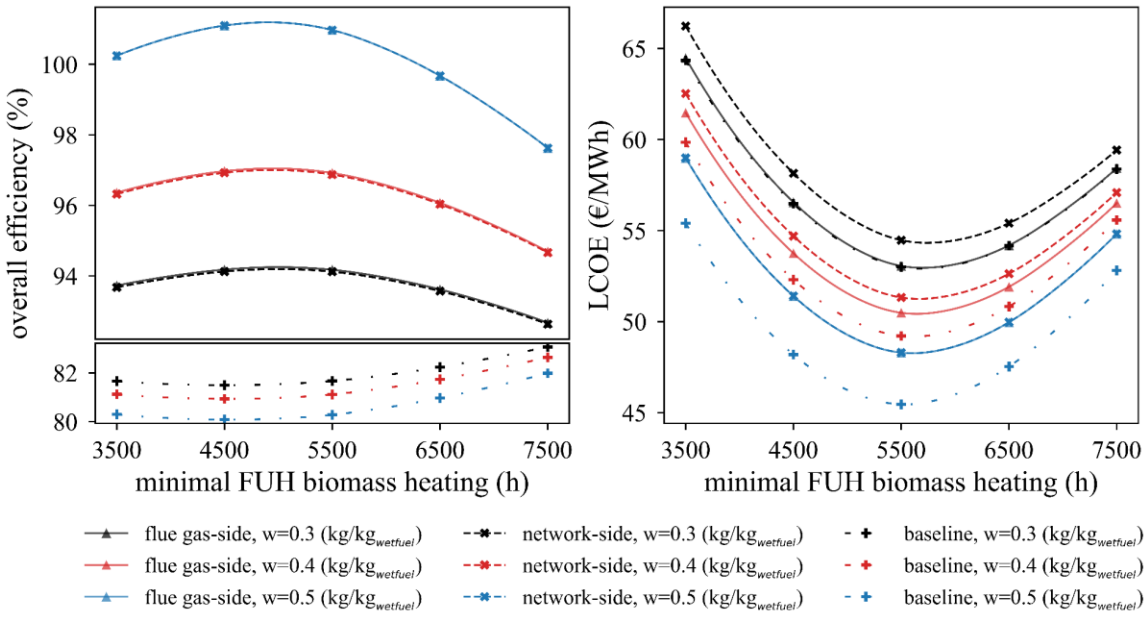

Figure 58: Analysis of overall efficiency and LCOE for different scenarios as a function of full utilization hours of the biomass boiler at different fuel water contents.

As demonstrated in Figure 59, setting the designed full utilization hours too high results in a relatively low required rated heat output for the biomass boiler. This leads to a higher reliance on the backup fossil fuel boiler for peak loads. On the other hand, setting the designed full utilization hours too low leads to an excessively high required rated heat output for the biomass boiler, making it infeasible for the biomass boiler to operate during summer. Consequently, base load heating during this period must also be provided by the backup oil boiler. In both scenarios, the contribution of the biomass heating system is diminished, and

the amount of heat recoverable by the heat pump is reduced, thereby decreasing the overall system efficiency. Therefore, choosing an appropriate number of full utilization hours is crucial. In the case study, the optimal overall system efficiency is achieved with full utilization hours amounting to approximately 5000 hours.

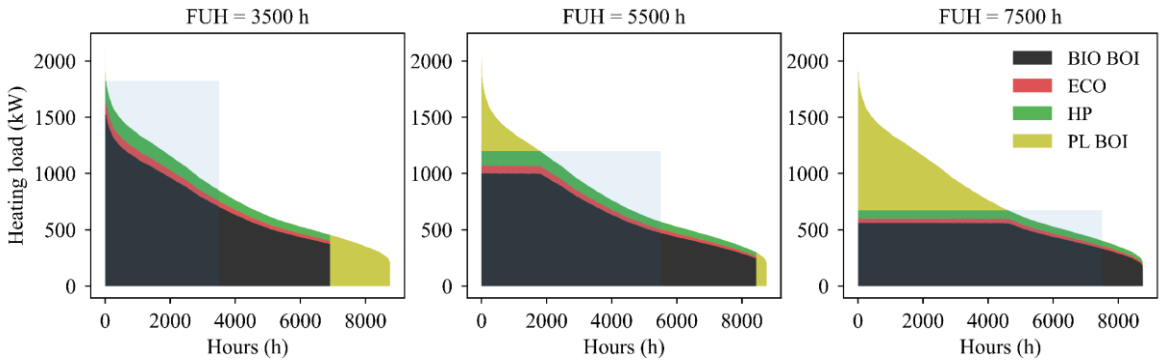

Figure 59: Annual duration line of the energy supply by the different components with different FUH in the flue gas-side integration scenario.

The impact of different full utilization hours on the LCOE of the heating system is also shown in the right panel of Figure 58. Both extremely low and high full utilization hours also have negative impacts on the system's economic feasibility. Significantly lower full utilization hours necessitate larger biomass boilers and increased reliance on oil-fired boilers during low loads in summer (as illustrated in Figure 59). This requirement leads to higher investment costs and increased operating expenses due to the higher price of heating oil compared to biomass, thus elevating the LCOE. Conversely, excessively high full utilization hours require a smaller biomass boiler, resulting in more frequent reliance on backup fossil fuel boilers during peak loads. This increased dependence also drives up operating costs, raising the system's LCOE. Therefore, selecting an appropriate number of full utilization hours is also crucial for minimizing the LCOE of the system. In the case study, the optimal full utilization hours are identified to be around 5500 hours for achieving the lowest cost.

9.3 Analysis of the impact of economic parameters

This section presents an assessment of the economic viability of various integration concepts is conducted by analyzing the impact of fluctuating economic parameters. The aim is to investigate how price uncertainties, particularly in fuel and electricity, affect the economic outcomes of these concepts. As indicated in Table 15, the variable operating costs, primarily fuel and electricity costs, constitute the most substantial proportion of the LCOE.

These costs emerge as the crucial determinants that influence the economic feasibility of the concepts. To demonstrate the impact of these factors, Figure 60 (a) and (b) display how changes in fuel and electricity prices affect the heating production costs.

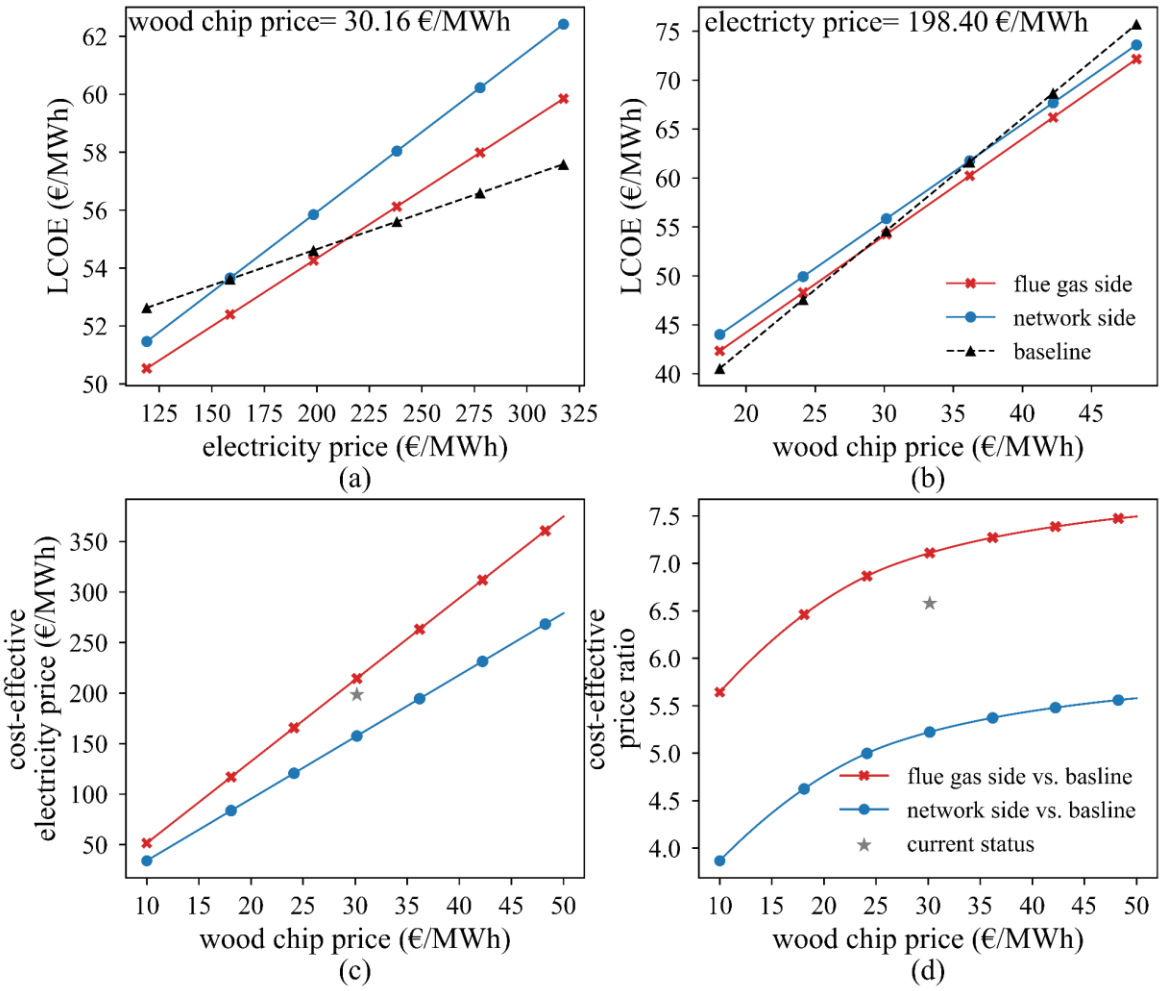

Figure 60: Analysis of LCOE of both heat pump integration concepts at different electricity and fuel prices (a and b) and cost-effective electricity price and ratio compared to baseline scenario with varying fuel prices (c and d).

Graph *a* decipts that both heat pump integration scenarios are significantly impacted by fluctuations in electricity prices. At the current fuel price of 30.16 €/MWh, the LCOE of the flue gas-side integration concept decreases by 1.91 €/MWh for every 20 % reduction in electricity price in the present case study. In comparison, the LCOE of the network-side integration concept decreases by 2.26 €/MWh, indicating that this option is more sensitive to changes in electricity prices.

It is noteworthy that if the electricity price increases to around 200 €/MWh, the gas-side integration concept will become more expensive than the baseline scenario, and the cost difference will further escalate with rising electricity prices. Conversely, if the electricity price drops to around 135 €/MWh, the network-side integration concept becomes economically viable relative to the baseline concept. The variation in LCOE in the baseline scenario is attributed to the consumption of electricity by general equipment in the heating network, including lighting and pumps.

Apart from the electricity price, the price of biomass fuel plays an even more crucial role in the economic viability, as the heat demand is met primarily by biomass fuel. As seen in graph *b*, the baseline scenario is more sensitive to biomass fuel price than both heat pump integration scenarios. With increasing fuel prices, using heat pumps becomes more cost-effective compared to the baseline scenario, assuming constant electricity prices. Therefore, the more expensive the biomass fuel, the more significant the heat utilization from the fuel becomes.

To investigate the correlations between the fuel and electricity prices, a sensitivity analysis was conducted to identify the highest economically feasible electricity price for implementing the integration concepts at various fuel prices. The results of this investigation are displayed in Figure 60 (*c*) and (*d*). Analysis of the graph reveals that the economically viable highest electricity price increases with rising fuel prices. In other words, as the fuel price increases, the economically feasible ratio between electricity and fuel prices also increases. Given the possibility of a substantial increase in fuel prices in the future, both integration concepts will likely be economically viable. A comparative analysis between the two integration concepts shows that the flue gas-side integration scenario exhibits greater elasticity and tolerance to variations in fuel and electricity prices. This is evidenced by the fact that the economically viable maximum price ratio in the flue gas-side integration scenario consistently exceeds that of the network-side integration scenario.

10. Techno-economic analysis of the HP-CHP integration concepts

The analysis in Chapter 9 indicated that the high price and high CO_2 emission factor associated with the electricity from the public grid might render the heat pump integration concepts less attractive. To mitigate dependence on external power supplies due to heat pump power consumption, the integration of additional components for self-generating electricity can be considered. In this chapter, three pre-selected possibilities of small-scale cogeneration technologies, as introduced in Section 3.1.3, are integrated into the system. To perform the analysis, the following scenarios are defined:

1. Baseline system: Renovation with a boiler without ECO, COND, and HP
2. HP-only system: Renovation with a smaller boiler with ECO and COND, and a flue gas-side integrated heat pump
3. HP-ORC system: Renovation with a smaller boiler with ECO and COND, a flue gas-side integrated heat pump and an ORC unit for cogeneration
4. HP-SRC system: Renovation with a smaller boiler with ECO and COND, a flue gas-side integrated heat pump and a SRC unit for cogeneration
5. HP-GCHP system: Renovation with a smaller boiler with ECO and COND, a flue gas-side integrated heat pump and a GCHP unit for cogeneration

The baseline and HP-only systems are chosen as comparison scenarios. Descriptions and analyses of the mass and energy flow of these predefined systems can be found in Section 3.2. The design of these systems employs the same assumptions presented in Chapter 9. In all scenarios, the heat pump is integrated on the flue gas side by default.

In the HP-ORC system, the refrigerant MDM (Octamethyltrisiloxane) is selected as the working fluid and a recuperator is utilized [206,207]. For the HP-GCHP system, a gasification efficiency of 85 % is assumed for the GCHP unit. [151,208]. As the biomass gasifier of the GCHP unit has specific requirements concerning the fuel: its water content should be lower than 20 %, and the ash content should be as low as possible. The optimum fuel water content for the gasification process is about 10 % [209]. As a result, only wood pellets or dried and low-bark forest chips are suitable as input materials. For this case study,

the standard wood pellet from the data bank of WDesign [210] is selected, with its elemental composition of which is shown in Table 23 in Appendix F.

10.1 Comparison of technical and economic results of the HP-CHP integration concepts

10.1.1 Comparison of component capacities and investments

The upper part of Figure 61 presents the required nominal capacities of the different components for heat recovery and cogeneration units in various scenarios. As observed in the figure, the integration of cogeneration units significantly affects the dimensions of the boiler, heat exchanger, and heat pump. Specifically, the integration of cogeneration units in the HP-ORC and HP-SRC systems necessitates a greater biomass furnace capacity compared to the HP-only system. The reason for this is that the biomass furnace serves as the heat source for both the SRC and ORC cycles.

Moreover, the sizes of heat recovery equipment, such as the economizer and heat pump, are nearly identical between the HP-ORC and HP-SRC systems, resulting in similar electrical power capacity of the cogeneration units in both scenarios. However, due to the relatively low electrical efficiency of the steam engine-based SRC cycle, the SRC unit has a rated thermal output of 145 kW with a power-to-heat ratio of 0.2, while the ORC unit has a rated thermal output of 113 kW with a power-to-heat ratio of 0.26. The HP-GCHP system necessitates a biomass boiler with a lower rated furnace capacity, where the energy input of the GCHP unit comes from additional biomass pellets. Additionally, it has a lower rated thermal output compared to the other two scenarios with cogeneration units. The power-to-heat ratio of the GCHP unit is 0.58, which is more than twice that of the ORC option.

The cost structure of the different scenarios is depicted in the lower part of Figure 61. This graph reveals that the investment costs increase to varying degrees compared to the HP-only scenario due to the integration of cogeneration units. The HP-ORC system incurs the highest investment cost, with its total costs escalating from 441 k€ for the HP-only system to 682 k€, which is nearly twice of the investment cost of the baseline system. The majority of the investment increase is attributable to the cost of the ORC unit. In contrast, the investment cost of the HP-SRC system, featuring a steam engine, only rises to 598 k€, as the ORC equipment is much more expensive than steam cycle equipment. Among the three

scenarios with cogeneration units, the HP-GCHP system experiences the smallest increase in investment cost, totally approximately 574 k€, which is marginally less than the HP-SRC system.

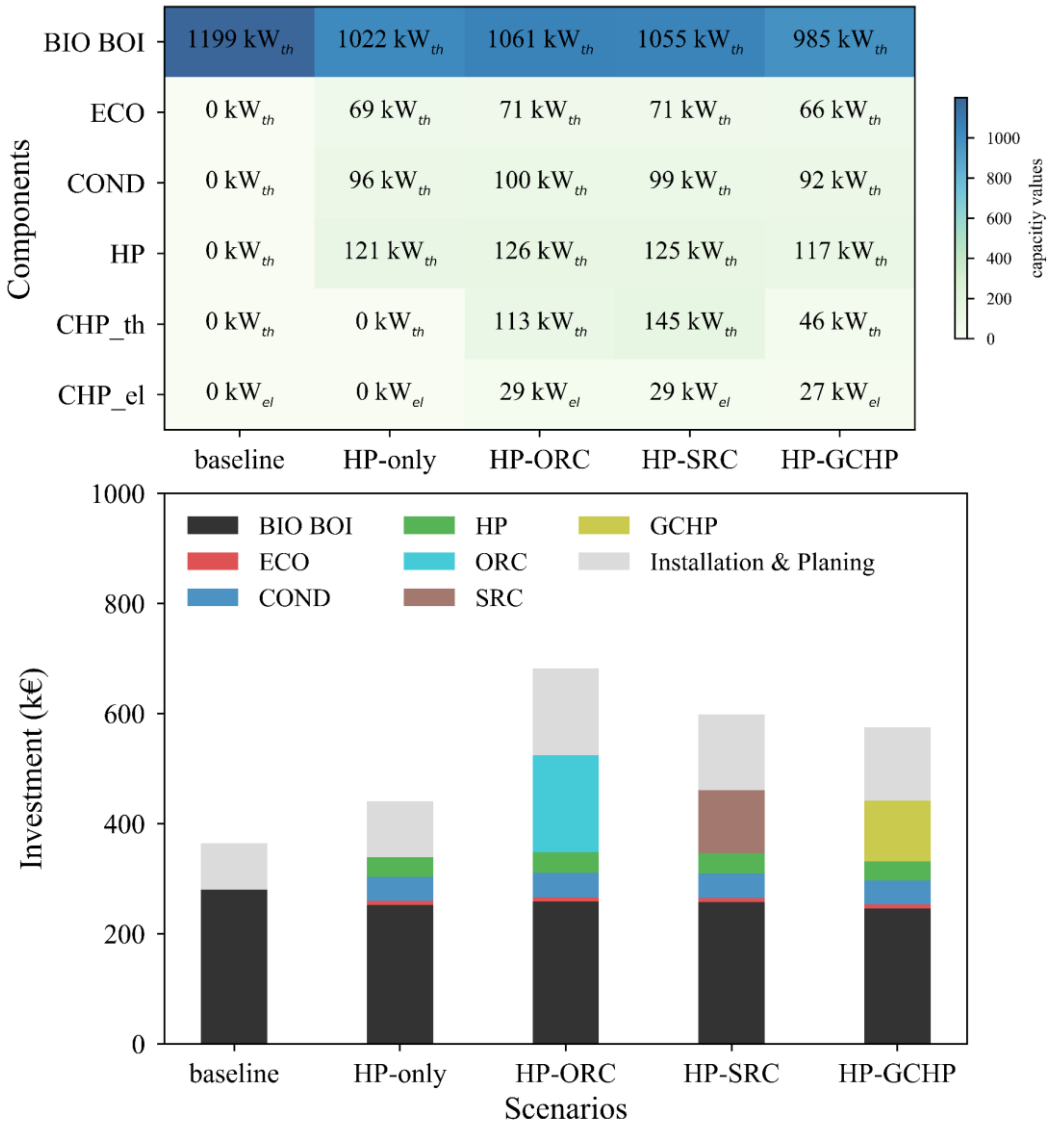

Figure 61: Required capacities and investment costs of various components for different renovation scenarios with and without CHP units.

10.1.2 Comparison of energy supply and operating costs

Figure 62 presents an analysis of the annual energy supply structure, the energy consumption of different components, and the composition of annual operating costs for

various integration scenarios. The upper left graph reveals that the further integration of a cogeneration unit leads to a more complex energy supply structure. Specifically, in the HP-ORC and HP-SRC systems, the direct heating contribution of biomass boiler is significantly reduced, as part of its heat output serves as heat source to the ORC and SRC cycles. This heat is partially converted into electricity through the cycle, and partially returned as heat, which is indirectly fed back into the heat network. The direct heat supply from the biomass boilers in the HP-ORC and HP-SRC systems accounts for only 72.3 % and 69.9 %, respectively, of the total demand (7059 MWh). This reduction is attributable to the lower power-to-heat ratio of both cogeneration technologies. This means that more heat needs to be extracted from the biomass furnace for the same amount of electricity generation, which reduces the proportion of direct heat supply by the biomass boiler. In contrast, the HP-GCHP system has a higher contribution by the biomass boiler due to the higher power-to-heat ratio of the GCHP unit.

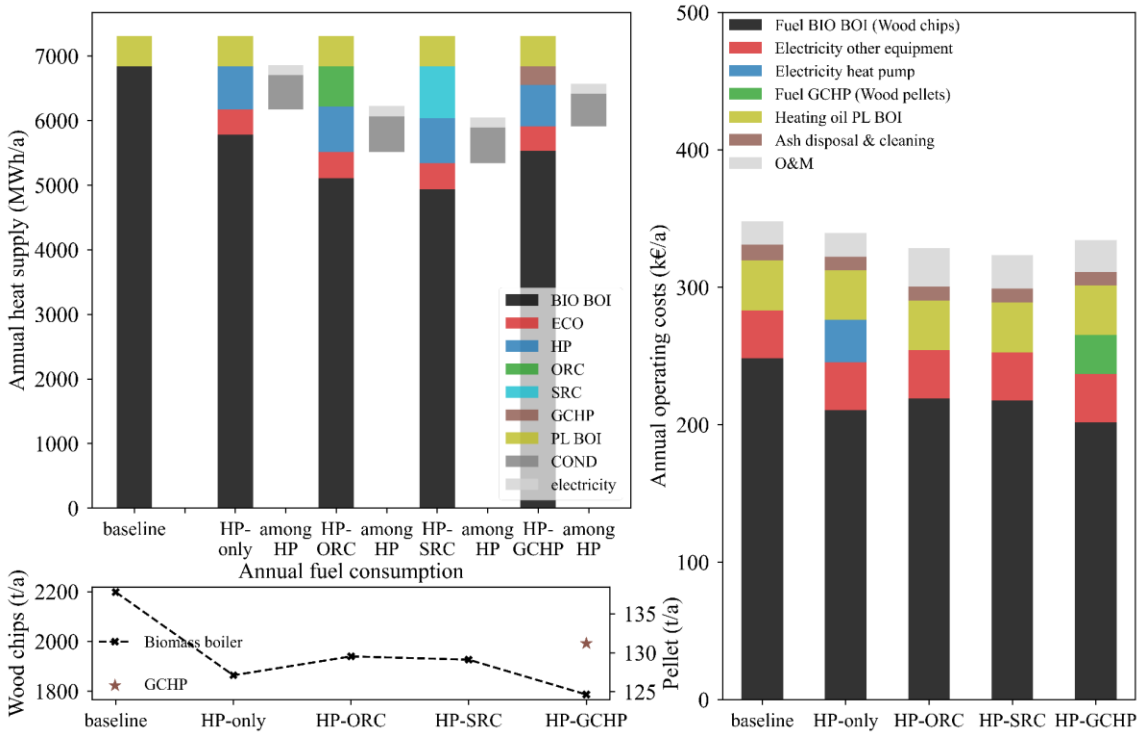

Figure 62: Comparison of energy supplies, fuel consumption and operating costs of the different renovation concepts with and without CHP units.

The lower left graph in Figure 62 illustrates the fuel consumption for different scenarios. The consumption of biomass wood chips in the HP-ORC and HP-SRC systems has significantly increased compared to the HP-only scenario, yet it remains lower than the

baseline system. The HP-GCHP system shows the lowest consumption of biomass wood chips, which is only 81 % of the baseline system. However, in addition to biomass wood chips, it also consumes 131 t of biomass pellets, which are more expensive.

In all three scenarios with integrated cogeneration units, operating costs are significantly reduced as the electrical demand of heat pump is covered by biomass fuel. The results on the right side of Figure 62 indicate that the cost of biomass pellets required for GCHP is relatively high due to the high fuel requirement. Consequently, the operating cost reduction in the HP-GCHP scenario is only marginal.

10.1.3 Comparison of the evaluation indicators

Various evaluation indicators for HP-CHP integration concepts can be derived from the obove analysis. As shown in Table 16, the additional integration of cogeneration units results in a slight decrease in the overall energy efficiency compared to the HP-only system, but still remains approximately 10 % higher than the baseline system.

Moreover, the table indicates that the high investment costs of the cogeneration units may eventually lead to an increase in the levelized heat production cost, despite their effective reduction of operating costs. Among the three systems with integrated cogeneration units, the HP-ORC system exhibits the highest increase in the LCOE, rising from 54.26 €/MWh to 55.74 €/MWh, followed by the HP-GCHP system with 55.48 €/MWh. In contrast, the LCOE of the HP-SRC system has slightly decreased to 53.94 €/MWh.

Table 16: Comparison of the different evaluation indicators for different renovation scenarios with and without CHP units.

	baseline	HP-only	HP-ORC	HP-SRC	HP-GCHP	nit
spec. CAPEX	5.31	6.18	9.17	8.14	8.13	€/MWh
spec. fix. OPEX	2.38	2.41	3.98	3.43	3.30	€/MWh
spec. var. OPEX	46.92	45.67	42.59	42.37	44.05	€/MWh
LCOE	54.61	54.26	55.74	53.94	55.48	€/MWh
$f_{lhv,sys}$	81.89 %	93.36 %	91.84 %	92.41 %	91.62 %	-
$e_{PE,sys}$	0.36	0.36	0.33	0.333	0.33	MWh_{PE}/MWh
$e_{CO2,sys}$	50.44	54.92	47.70	47.56	48.34	kg_{CO2}/MWh

Conversely, the table highlights significant improvements in environmental indicators due to the integration of additional cogeneration units. In terms of primary energy demand and CO_2 emissions, all three scenarios with cogeneration units perform better than both the HP-only scenario and the baseline scenario. The primary energy demand is reduced from about 0.36 to 0.33 MWh_{PE}/MWh in all these scenarios, resulting in an overall reduction of 9 % in primary energy demand. A similar trend is observed in CO2 emissions, which are reduced by approximately 15 % compared to the HP-only scenario upon integrating cogeneration units. Therefore, the additional integration of CHP units for onsite electricity supply is preferred from the environmental point of view under the current emission factor of the electricity mix.

10.2 Analysis of the impact of technical parameters

As previously discussed in Section 9.2, changes in the heat pump operating temperatures, particularly the target exhaust gas temperature, can lead to varying electricity demands. This also results in different design and operational conditions of the cogeneration units, ultimately affecting the techno-economic feasibility of the integration concepts. Besides, parameters such as biomass fuel water content and the full utilization hours of the integration systems also play a crucial role in determining the feasibility. This section will address the impact of these technical parameters on the further integration of cogeneration units in terms of the overall efficiency $f_{lhv,sys}$ and levelized heat production costs LCOE of the systems.

10.2.1 Target exhaust gas temperature

Figure 63 illustrates the changes in overall efficiency and LCOE for different HP-CHP integration concepts at varying target exhaust gas temperatures. The heat pump supply temperature is set at 65 °C. As shown in the figure, all three scenarios with integrated cogeneration units exhibit slightly lower system overall efficiency compared to the HP-only system across different exhaust gas temperatures. The system overall efficiency of each scenario reaches the maximum when the exhaust gas temperature is around 30 °C. Among these, the HP-ORC system consistently shows the highest LCOE, making it the least economically favorable option at the same exhaust gas temperature. In Contrast, the HP-SRC system maintains the lowest LCOE among the three CHP-integrated scenarios, and its

economic viability surpasses that of the HP-only scenario when the exhaust gas temperature drops below 37 °C

Furthermore, although the integration of cogeneration units may result in a decrease in economic performance compared to the HP-only scenario, selecting an appropriate exhaust gas temperature can still improve both the efficiency and economic viability of the system relative to the baseline system. Theoretically, it is possible to achieve system optimization in terms of efficiency, economic and environmental feasibility by further integrating cogeneration units compared to the baseline system. A detailed discussion will be carried out in Chapter 11 based on the proposed optimization approach.

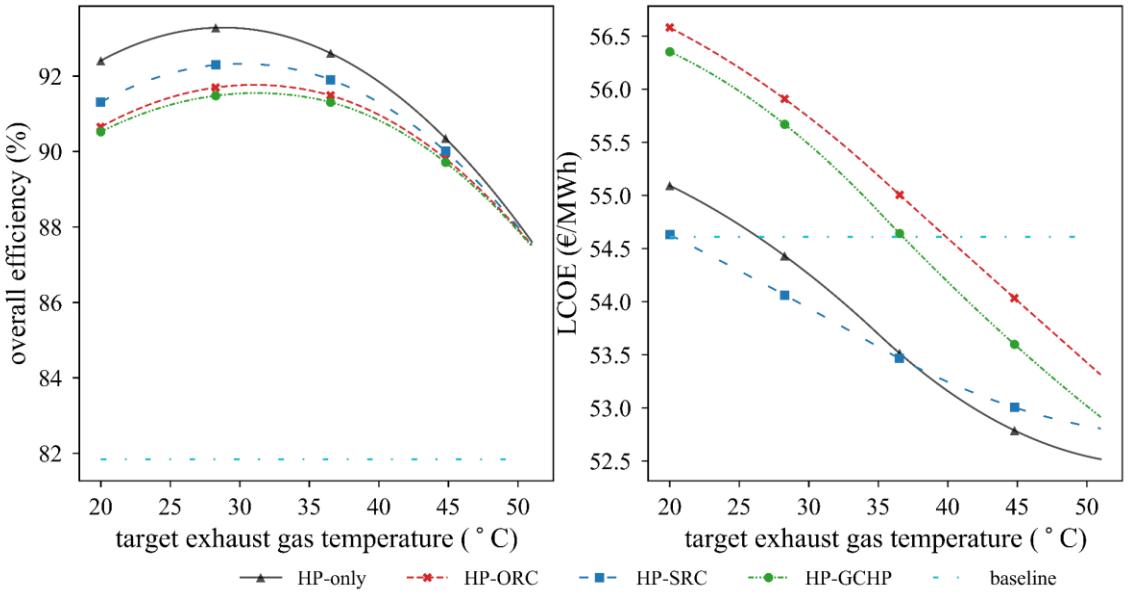

Figure 63: Correlations between overall efficiencies and LCOE of different HP-CHP integration concepts with varying target exhaust gas temperatures at HP-supply temperature of 65 °C.

10.2.2 Fuel water content and annual full utilization hours

Figure 64 presents the analysis of the overall efficiency and LCOE for different HP-CHP integration concepts at various fuel water contents. The left graph demonstrates that while all scenarios employing heat recovery techniques show a trend of efficiency improvement with increasing fuel water contents, the additional integration of cogeneration units results in a smaller overall efficiency gain compared to the HP-only system. As the fuel water content increases, the difference with the HP-only system becomes more significant.

The right graph indicates that fuel water content has a significant impact on the cost of different scenarios. The HP-SRC and HP-ORC system, along with the baseline system, are more sensitive to the water content of wood chips, as they solely rely on wood chips for energy. With an increase in wood chip water content, fuel prices decrease, leading to a corresponding reduction in LCOE. Notably, the HP-SRC system becomes more economical than the HP-only system when the fuel water content exceeds approximately 0.2 $kg/kg_{wet\ fuel}$. Similarly, the HP-ORC system is more economical than the HP-GCHP system when the fuel water content surpasses 0.3 $kg/kg_{wet\ fuel}$.

From this analysis, it is evident that fuel water content has varying impacts on different HP-CHP integration concepts. Thus, it is essential to consider the fuel water content when selecting the most appropriate cogeneration technologies for on-site power supply of heat pumps.

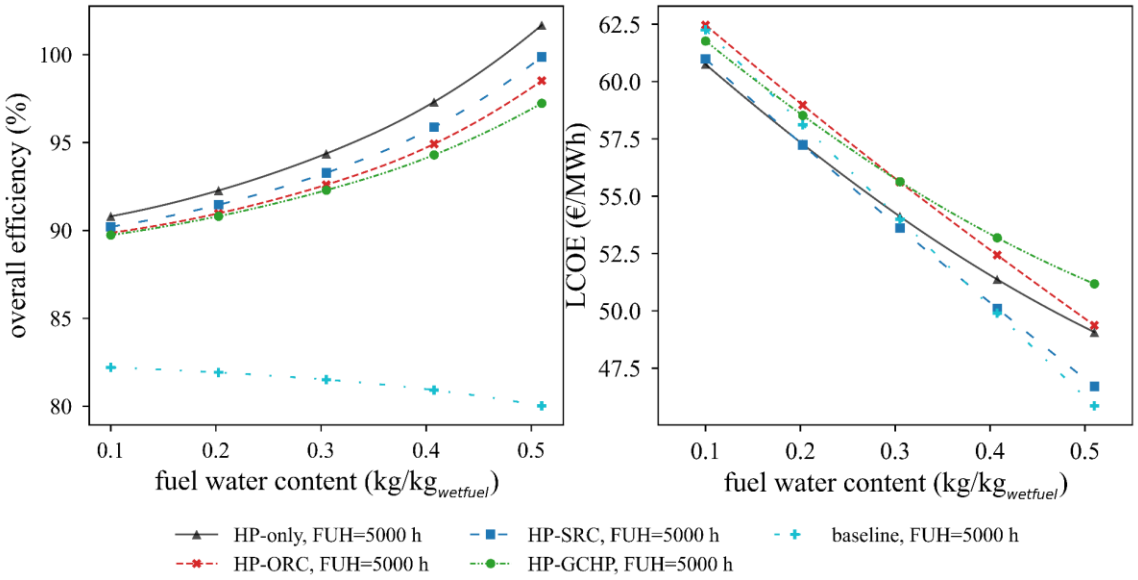

Figure 64: Analysis of overall efficiency and LCOE for different HP-CHP integration scenarios as a function of fuel water content at the full utilization hours of 5000 h.

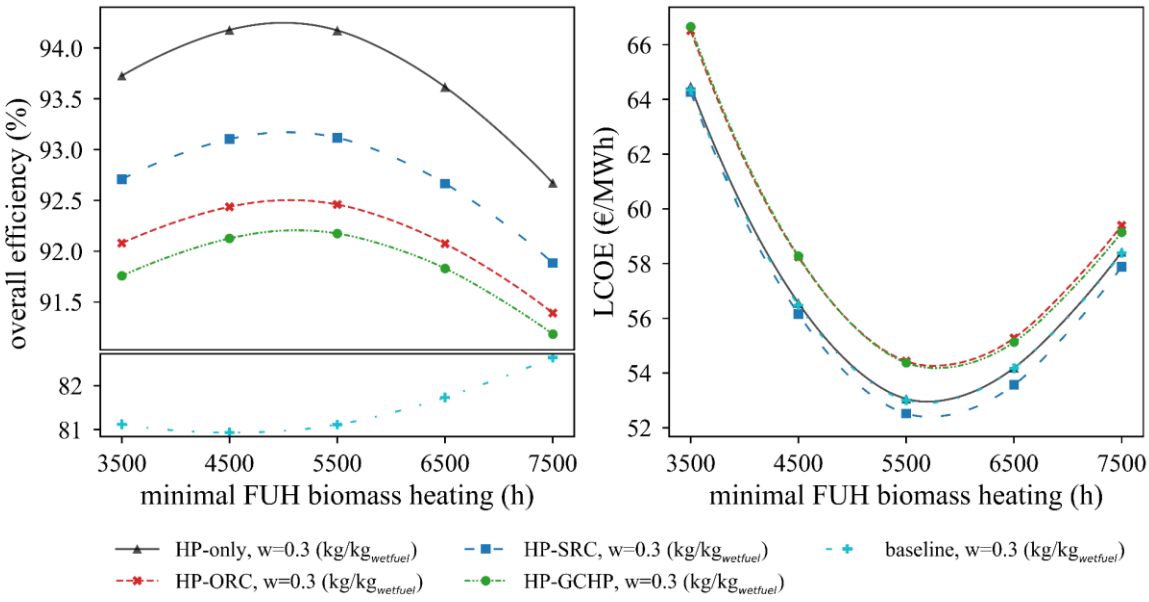

Figure 65: Analysis of overall efficiency and LCOE for different scenarios as a function of full utilization hours of the biomass boiler at fuel water content of 0.3 kg/kg$_{wet\ fuel}$.

Figure 65 illustrates the changes in system overall efficiency and LCOE across different HP-CHP integration concepts with varying annual full utilization hours (FUH). The figure shows that the variation trend for different scenarios equipped with cogeneration units is consistent with that of the HP-only integration scenario. This suggests that the optimal FUH value is minimally affected by the installation of cogeneration units.

10.3 Analysis of the impact of economic parameters

This section analyzes the impact of variations in electricity and fuel prices on the economic viability of different HP-CHP integration concepts. It is assumed that fluctuations in the biomass pellet price are approximately proportional to those in wood chip prices. Figure 66 illustrates how the LCOE varies with different electricity prices (graph a) and different wood chip prices (graph b). Graph a indicates that the trend of LCOE of the different HP-CHP systems with varying electricity prices is consistent with the baseline system, with all curves remaining parallel. This is because, after integrating the cogeneration units, the electricity price only affects the cost of electricity for the general equipment of the heating network. As a result, the sensitivity of LCOE to electricity prices is reduced.

When the wood chip price is kept at 30.16 €/MWh, systems with integrated cogeneration units become increasingly economically advantageous compared to the HP-only system as

the price of electricity climbs. At an electricity price of about 250 €/MWh, the economic feasibility of the HP-GCHP system exceeds that of the HP-only system. When electricity price further increased to about 270 €/MWh, the economic feasibility of the HP-ORC system will also exceed that of the HP-only system.

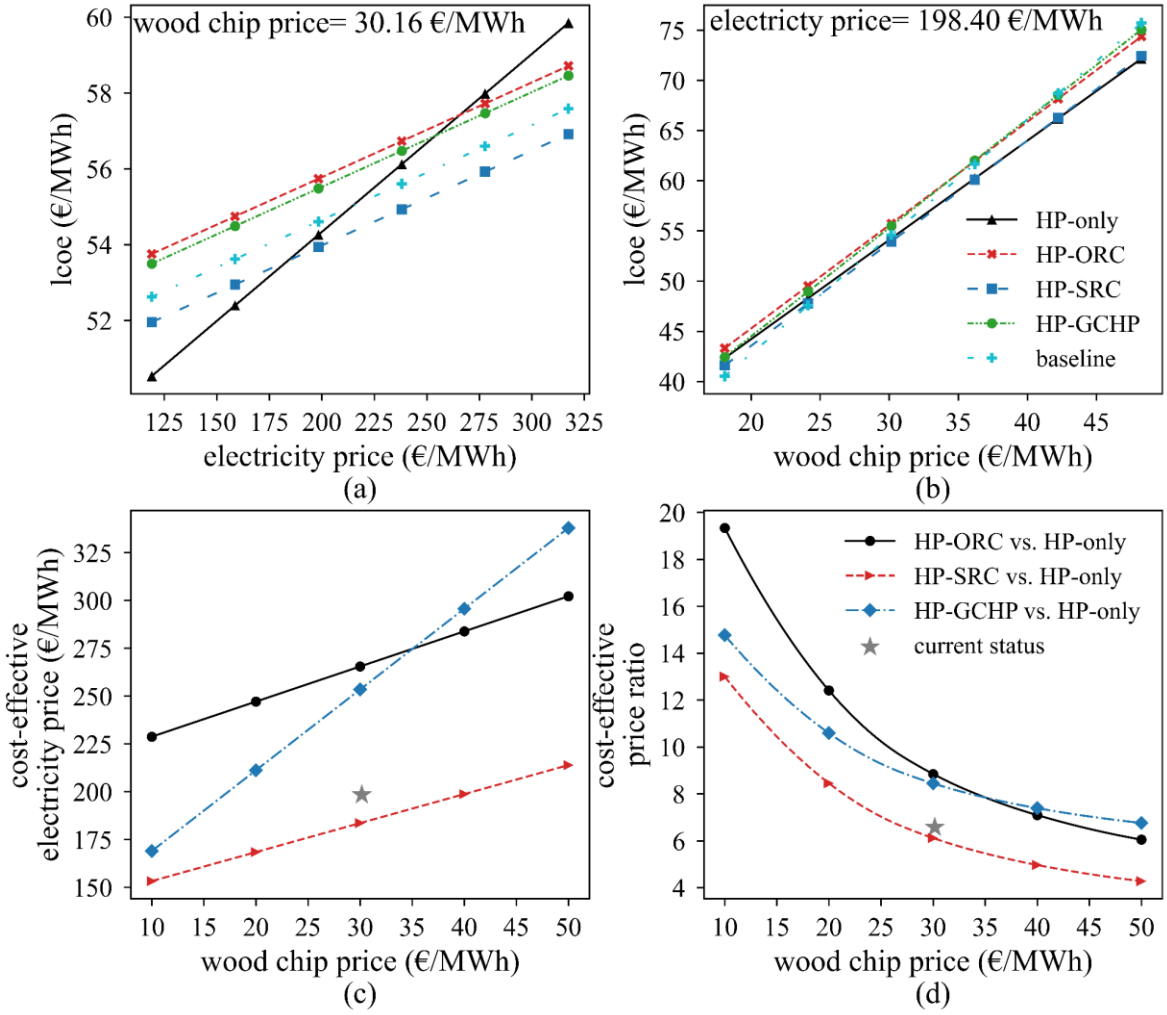

Figure 66: Analysis of LCOE of different HP-CHP integration concepts at different electricity and fuel prices (a and b) and cost-effective electricity price and ratio compared to HP-only scenario with varying fuel prices (c and d).

Graph b shows that the systems with integrated cogeneration units exhibit only slightly greater sensitivity to fuel prices than the HP-only system. When the electricity price remains constant, the HP-only scenario remains the most economical across different fuel prices. Nevertheless, compared to the baseline scenario, the sensitivity of these three systems with integrated cogeneration units to biomass fuel prices is still significantly lower. This reduced sensitivity is attributable to the reduced use of biomass fuels.

To identify the feasible power-to-fuel price ratios that are suitable for integrating additional cogeneration units in comparison to the HP-only system, the bounds of cost-effective electricity price, as well as the electricity-to-fuel price, are calculated for different wood chip prices. The results are demonstrated in graph c and d of Figure 66. For any given cogeneration technology, the integration is more economical compared to HP-only system only if the electricity price or the electricity-to-fuel price ratio exceeds the value indicated by the curve, assuming a constant fuel price.

11. Implementation of system optimization

11.1 Input data specification

To implement the optimization approach proposed in Chapter 5, the third BHN is conceptualized to be upgraded to an integrate system that include an integrated heat pump and potentially an integrated cogeneration unit for onsite power generation, as outlined in Section 3.1.3. For comparison, the conventional renovation concept with a new biomass boiler without flue gas condensation is considered as the baseline. To initialize the optimization process, various initialization parameters such as demand and temperature data for the network, along with the range of the decision variables, are required as input for the framework, as described in Section 5.2.

For this case study, it is assumed that the future heating load, ambient temperature, and humidity will remain constant at the same hourly averages as in the previous years. To satisfy the consumer temperature requirements, the supply and return temperatures of the network will also maintain their historical averages. As the system pre-configuration, the assumptions in Chapter 9 and Chapter 10 will be adopted to initialize the parameters.

11.2 Optimization configuration

This case study both flue gas-side and network-side connections for heat pump evaporators. The selection of the connection concept is adopted as binary input variable, where $\mathscr{v} = 0$ indicates the flue gas-side concept and $\mathscr{v} = 1$ indicates the network-side concept. If a cogeneration unit is to be integrated into the system ($\mathscr{b} \neq 0$), the heat pump power supply will primarily come from self-generated electricity. In the absence of a cogeneration unit ($\mathscr{b} = 0$), the local public grid will fully supply the electricity power. Another decision variable is the air ratio λ for combustion, which ranges from 1.2 to 2.7 [211,212].

The thermodynamic design of the heat pump primarily depends on the target exhaust gas temperature T_{ex} that affects the evaporation temperature, the heat pump supply temperature T_{hp} that affects the condensation temperature, and the choice of refrigerant that impacts the performance of the heat pump. In this case study, the threshold of the target exhaust gas temperature is set between 25 °C and 50 °C, considering the room temperature and the dew

point temperature of the flue gas. The heat pump supply temperature is set between 65 °C and 90 °C, considering the heat network constraints [213,214] and temperature requirements, with a precision of 0.1K. The refrigerant selection involves a preliminary analysis of various refrigerants' properties, particularly their evaporating temperatures at ambient pressure and critical points. The final refrigerants selected for the optimization in this case study include the most commonly used refrigerant R134a [202], the refrigerants R717 and R236fa used in the two real-world cases studied in this thesis, and the refrigerants R290, R600a, and R1234yf recommended in [203] for their low GWP.

Table 17 summarizes the ranges for all decision variables and provides an overview of their mapping and precision. For configurating the optimization algorithm, the run mode is set to multi-threading optimization to accelerate the computation. The population size of the genetic algorithm is established at 100, and the maximum iteration number of generations is 100. The non-negative scalar weight α_1 vary in equal intervals from 0 to 1, with a granularity of 0.1.

Table 17: Thresholds of the decision variables for this study.

Type	**Decision variable**	**Ranges**	**Precision/ Mapping**	**unit**
Continuous	λ	1.2: 2.7	0.1	-
	T_{ex}	25: 50	0.1	°C
	T_{hp}	65: 90	0.1	°C
Discrete	$\mathscr{v}$	{0, 1}	{flue gas-side, network-side}	-
	$\mathscr{b}$	{0, 1, 2, 3}	{not integrate CHP, SRC, ORC, GCHP}	-
	$\mathscr{r}\mathscr{e}\mathscr{f}$	{0, 1, 2, 3, 4, 5}	{R134a, R600a, R236fa, R717, R1234yf, R290}	-

11.3 Optimization results and discussions

11.3.1 Optimization results

Figure 67 displays the Pareto optimization results derived from the optimization framework proposed in Chapter 5, where each point around the curve represents an optimal solution corresponding to different values of the non-negative scalar weight α_1. The combinations of the decision variables in the set of Pareto solutions, corresponding to various α_1 values, are detailed in Table 18. It is noted that some optimization results for similar α_1 values are too close to each other, resulting in an overlap of some points in the figure.

For a detailed analysis, three scenarios are selected from these results and compared with the baseline scenario, which is also depicted in Figure 67. Where the minimal cost scenario (cyan dot) represents the scenario where only economic indicators are prioritized as the optimal design target, corresponding to $\alpha_1 = 1$. While the minimal emission scenario (blue dot) represents the scenario focusing solely on environmental indicators as the design target, corresponding to $\alpha_1 = 0$. And the trade-off scenario (green dot) represents the balanced scenario where both economic and environmental indicators are given equal weight, corresponding to $\alpha_1 = 0.5$. These scenarios are highlighted in Figure 67, respectively.

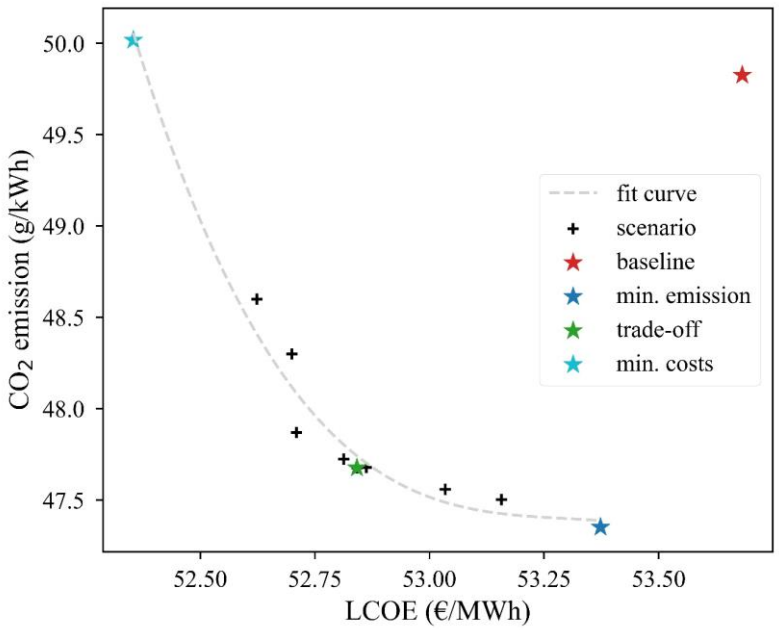

Figure 67: Pareto optimal solutions of the studied case.

Table 18: Optimal combinations of the decision variables of the Pareto solutions.

Alpha 1	0	0.1	0.2	0.3	0.4	0.5	0.6	0.7	0.8	0.9	1
HP integration	flue gas-side	flue gas-side	flue gas-side	flue gas-side	flue gas-side	flue gas-side	flue gas-side	flue gas-side	flue gas-side	flue gas-side	flue gas-side
CHP type	SRC	SRC	SRC	SRC	SRC	SRC	SRC	SRC			
air ratio	1.2	1.2	1.2	1.2	1.2	1.2	1.2	1.2	1.2	1.2	1.2
exhaust gas temperature (°C)	35.0	44.5	43.5	43.5	40.4	43.5	39.4	47.0	45.7	45.3	50.0
HP supply temperature (°C)	65.0	65.0	65.0	65.0	65.1	65.0	65.0	65.0	65.2	65.3	65.0
refrigerant	R717	R236fa	R600a	R236fa	R717	R600a	R236fa	R717	R717	R600a	R600a

Table 18 reveals that the integration of a cogeneration unit is not recommended in the minimal cost scenario ($\alpha_1 = 1$), where only economic indicators are considered as the optimization objective. In this scenario, the target exhaust gas temperature should be set at the maximum of its allowed range, which results in a smaller heat pump size and a higher COP value. As shown in Figure 67, this scenario offers a distinct economic advantage over both the baseline scenario and the optimized scenarios.

In the minimal emission scenario ($\alpha_1 = 0$), the integration of a cogeneration unit contributes positively to emission reduction. Compared to the baseline scenario, this scenario reduces CO_2 emissions by about 2.5 g/kWh, which corresponds to a reduction of 5 %. Additionally, its LCOE is also reduced compared to the baseline scenario, by 0.34 €/MWh. In this case, the optimal exhaust gas temperature is around 35°C, with R717 chosen as the refrigerant.

For the trade-off option, the sum of the two normalized objective functions with equal weights is used as the final objective function. As shown in Figure 67, this alternative scenario is significantly more favorable than the baseline scenario in terms of both economic and environmental indicators. Meanwhile, integrating a cogeneration unit remains favorable under this scenario. However, the optimal exhaust gas temperature increases to 43.5 °C.

It is noteworthy that the flue gas-side integration concept is recommended for all three solutions discussed here, and the air ratio remains at 1.2. A detailed techno-economic analysis of the selected solutions is conducted in Section 11.3.2.

11.3.2 Techno-economic and environmental analysis

Figure 68 outlines the evaluation indicators for the four selected scenarios from technical, economic, and environmental perspectives, including overall efficiency, LCOE, and specific CO_2 emissions. The graph indicates that the baseline scenario is inferior not only in terms of economic and environmental benefits compared to the other scenarios, but also regarding lower energy efficiency. Compared to the baseline scenario, the minimal cost scenario and the trade-off scenario are both about 8 %-points[4] more energy-efficient, and the minimal emission scenario has an energy improvement of about 9%-points.

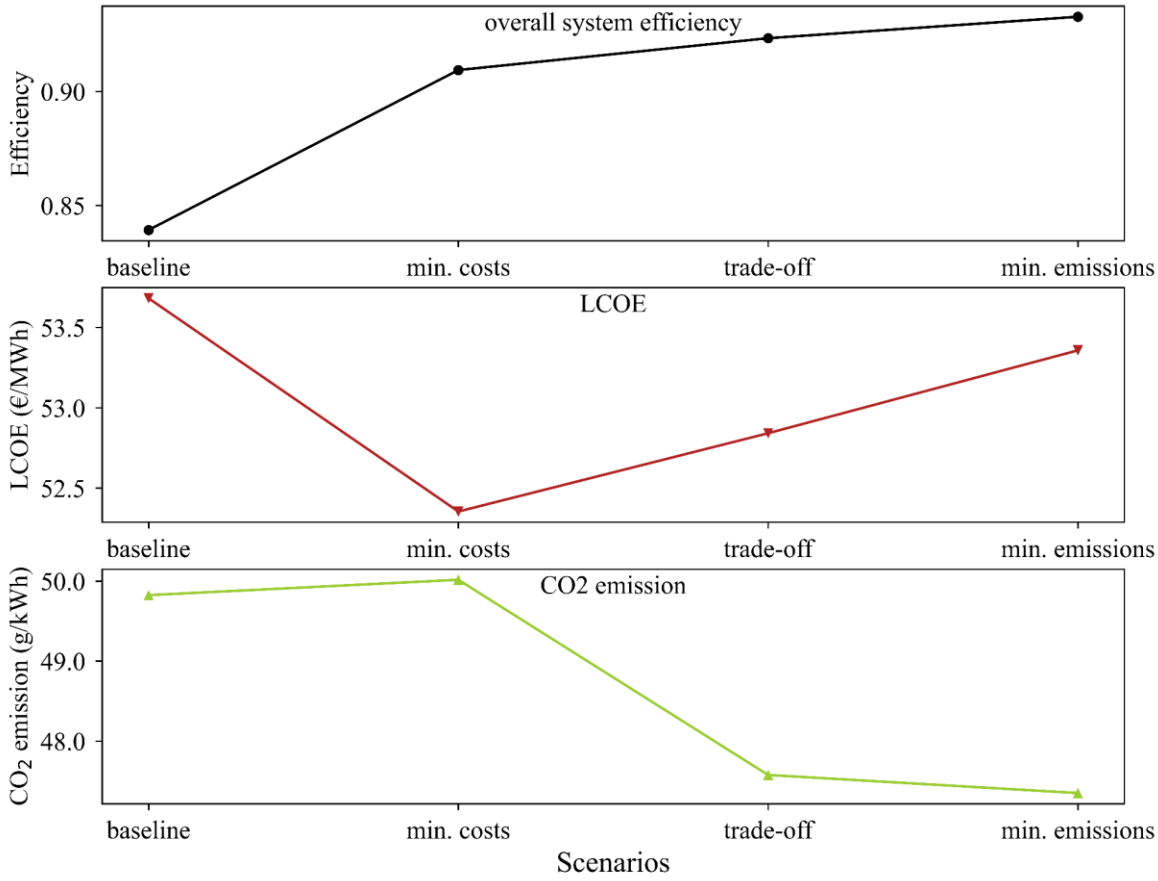

Figure 68: Comparison of the technical, economic, and environmental evaluation indicators of the selected scenarios (upper: overall system efficiency, middle: levelized costs of heat production, bottom: specific CO_2 emission).

[4] absolute difference in energy efficiency

A detailed analysis of the technical, economic, and environmental aspects is presented below:

Technical analysis

For a more in-depth technical analysis of each scenario, the system energy expenditure and energy supply for each scenario are presented in Figure 69, while Table 19 shows the rated installed capacity of the main components in each scenario.

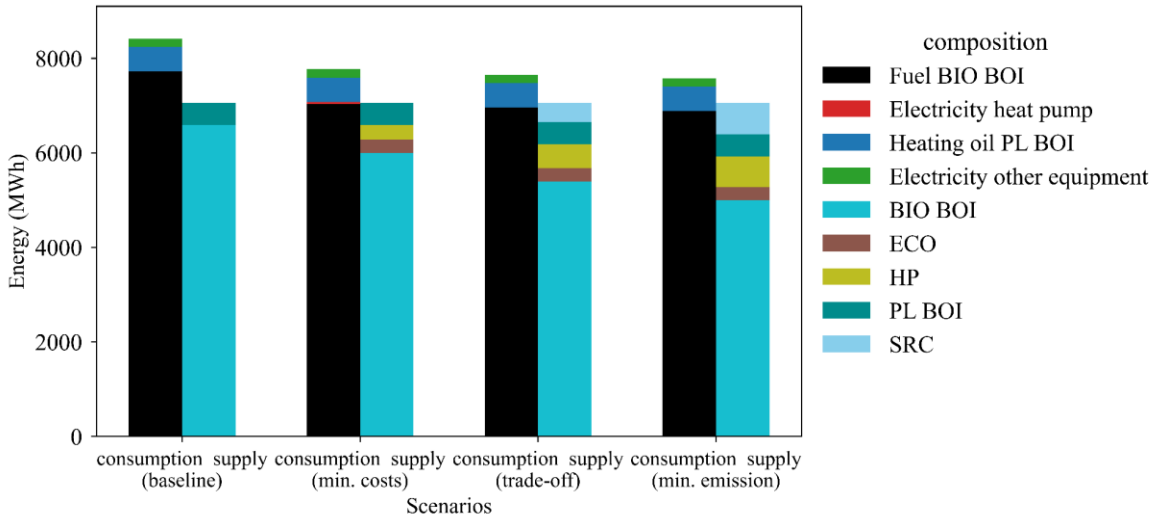

Figure 69: Structures of the energy expenditures and energy supplies of the four selected scenarios.

Table 19: Nominal capacities of different components.

Capacities	Baseline	min. costs	Trade-off	min. emission	unit
BIO BOI	1199	1096	1083	1071	kW_{th}
COND	0	53	81	98	kW_{th}
ECO	0	52	51	51	kW_{th}
HP	0	60	94	120	kW_{th}
CHP_{th}	0	0	77	123	kW_{th}
CHP_{el}	0	0	16	25	kW_{el}

As seen from the figure, the biomass boiler (BIO BOI) in the baseline scenario has the highest fuel consumption, approximately 7722 MWh/a. The heat demand of the network of 7059 MWh/a is met solely by the biomass boiler and the peak load boiler (PL BOI). For this scenario, the low consumption to output ratio leads to a low system energy efficiency. To

guarantee the heating performance over the year, the biomass boiler should have an installed capacity of 1199 kW_{th}.

Due to the benefits of the heat pump, the system efficiency in the minimal cost scenario is increased, and its fuel consumption was reduced by 689 MWh/a, which is 9 % of the consumption in the baseline scenario. In this scenario, the heat pump expends 42 MWh of electricity, which is almost negligible compared to the total energy consumption, while providing 318 MWh of heat demand, accounting for 4.5 % of the total demand. The annual performance exceeds 7. The main reason for such a high heat pump efficiency is its low difference between evaporation and condensation temperatures, which is only 15 °C, as shown in Table 18. In addition to the heat pump, the economizer can provide a part of the heating load, which contributes about 4.0 % of the total demand. To achieve the target heat recovery rate, the required nominal capacity of the heat pump is 60 kW_{th}, combined with a flue gas condenser with 53 kW_{th}, and an economizer with 52 kW_{th}. As a result of the contribution of the heat recovery components, the required nominal boiler capacity can be reduced from 1199 kW_{th}. to 1096 kW_{th}.

In the trade-off scenario, the energy input to the system remains primarily wood chips and there is no more electrical input. However, the total fuel consumption is reduced considerably compared to the baseline scenario due to heat recovery. Because the system is equipped with a SRC based cogeneration unit, the electricity for the heat pump is obtained completely from self-sufficient production. The fuel consumption of the boiler is 6957 MWh/a, which is 90 % of the baseline scenario, which is similar to the least cost scenario. However, since the SRC-based cogeneration unit requires heat from the biomass boiler, it reduces the net heat output of the boiler. In this variant, the heat demand covered by the boiler is 5393 MWh, which corresponds to 76.41 % of the total demand. For the remaining demand, 4% is supplied by the ECO, 7.2 % by the boiler, and 5.9 % by the SRC. The nominal electrical power of the cogeneration is 16 kW_{el}, which needs to be sufficient to cover the electrical power demand of the heat pump.

In the last option, the minimal emission scenario, which is also equipped with a cogeneration unit, the target exhaust gas temperature is reduced from about 50 °C to 35 °C. As a result, the required nominal capacity of the flue gas condenser and heat pump doubles as the working temperature difference of the heat pump increases. Correspondingly, the rated electrical power of the CHP unit increases to 25 kW_{el}. With the increased amount of

recovered heat, the overall system efficiency is also effectively improved. In this context, the biomass boiler capacity decreases further to 1071 kW_{th}, due to the increase in the contribution of other system components. In terms of energy consumption and supply, both the boiler fuel consumption and its share of heating supply are further diminished. The wood chip consumption for the biomass boiler is reduced to 6880 MWh, which accounts for a 11 % reduction compared to the baseline scenario. On the energy supply side, the contribution of biomass boiler is correspondingly reduced to 71 % of the total annual load, while the heat pump supply is increased to almost 10 % due to the recovery of the waste heat at low temperatures. The heat pump COP decreases to 3.3 in this scenario, due to the higher temperature difference between evaporation and condensation compared to the other two scenarios. The heat supply from the cogeneration unit increases to 667 MWh, or 9.45 % of the total demand, due to the increased electricity generation for the heat pump.

From the above results and analysis, it can be observed that the share of heat supplied by the biomass boiler decreases from left to right in the four scenarios mentioned above. The change in system efficiency is inversely correlated with this. In general, the integration of heat pumps can effectively improve overall system efficiency and reduce the energy consumption of the entire system. By comparing the minimal cost scenario and the trade-off scenario, it can be found that the further integration of the cogeneration unit has little effect on system efficiency, when the heat pump operating temperatures remain constant. When comparing the minimal emission scenario with other scenarios, it can be observed that the amount of wood chip fuel required by the boiler is further reduced, since more heat is covered due to the lower exhaust gas temperature. However, the rated capacity of the SRC-based cogeneration unit in the minimal emission scenario improve as the heat pump electricity demand grows. This results in higher investment in the system and makes the economic feasibility of this scenario open to discussion. In the following, a detailed economic analysis of the system is discussed.

Economic Analysis

Figure 70 displays the cost structure of the four scenarios, where the inner ring at the top shows the share of CAPEX and OPEX , and the outer ring illustrates the detailed percentages of various components. CAPEX includes the capital costs of the different system components, including biomass boilers, heat exchangers, heat pumps, and CHP unit, while OPEX consists of the energy purchase costs plus cleaning and maintenance costs. The

absolute values of the total annualized costs and levelized costs for each component are shown in the bar diagram below.

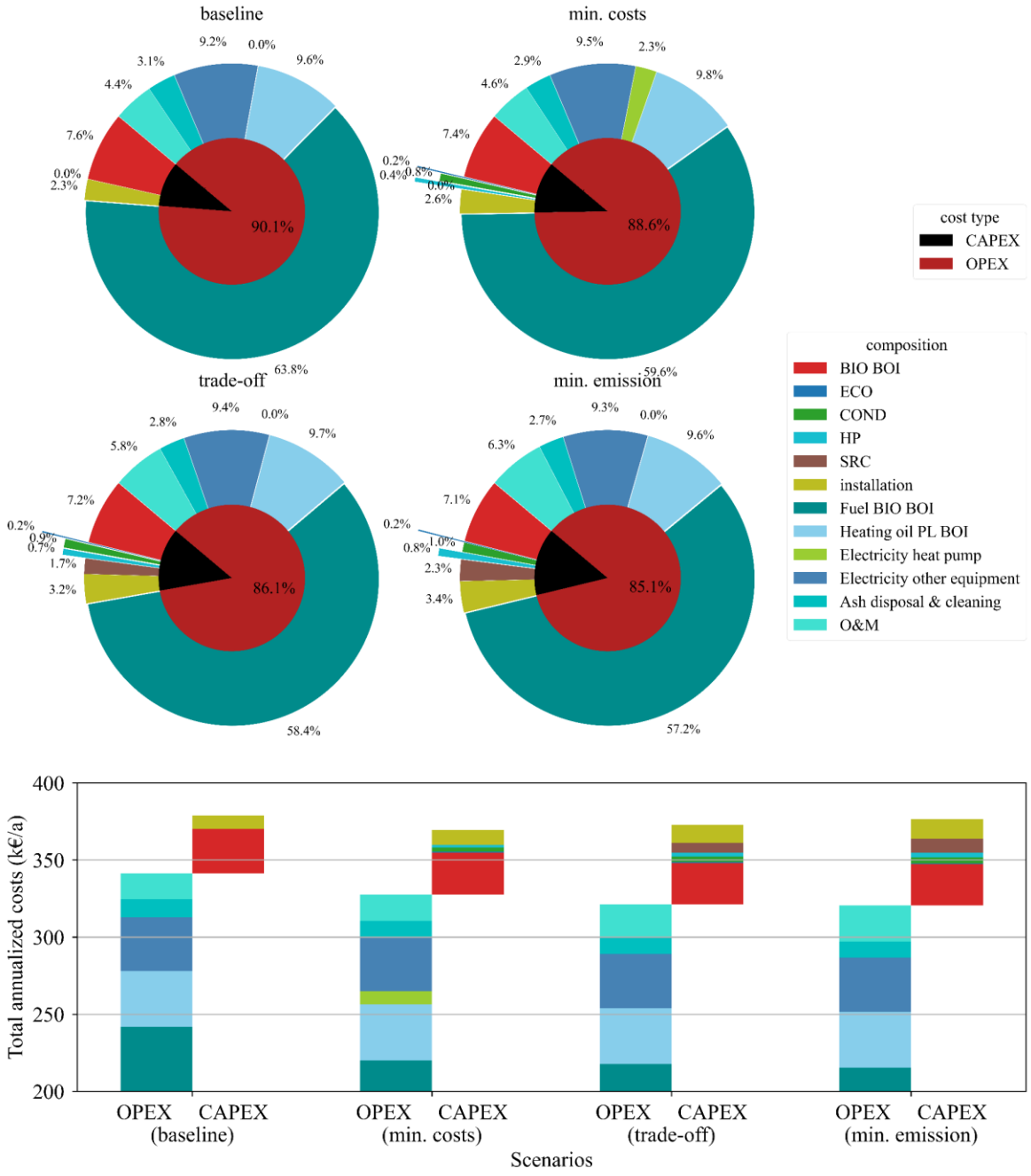

Figure 70: Costs structures of the four scenarios (upper graph:inner: CAPEX vs. OPEX, outer: costs from various compositions).

It can be noticed from the graph that the capital cost share is significantly smaller than the operating cost for all four scenarios. The baseline scenario has the lowest capital cost share of 9.9 %, amounting to an absolute value of approximately 37 k€/a. Due to the lowest

system efficiency, this scenario has the highest operating cost among all the scenarios at 342 k€/a. Among these costs, 242 k€/a for biomass fuel accounts for the largest share of 63.8 % of the total cost.

With the integration of the heat pump and heat exchangers, the capital cost of the minimal cost scenario increases to 42 k€/a, representing 14.4 % of the total annualized cost. The investment costs of the biomass boiler decreased slightly in absolute terms, but its share remained almost the same, while the rest of the investment came from the heat recovery equipment, of which the flue gas condenser and the heat pump accounted for 0.8 % and 0.4 % of the total costs, respectively. Benefiting from the heat recovery in the exhaust gas, the operating costs in this scenario are reduced to 327 k€/a. The share of biomass fuel for the boiler decreases from 63.8 % to 59.6 %. The expenditure on electricity for the heat pump amounts to 9.5 k€/a, with a share of only 2.3 % of the total.

In the trade-off scenario, the capital cost increases to 52 k€/a due to the integration of the SRC unit, which is 24 % more than the minimal cost scenario. The capital cost of the CHP takes up 1.7 % of the total annualized costs, and its relative share of the total investment cost stands at 12.1 %. While the capital costs increase, the annual operating costs of this scenario have slightly decreased compared to the minimal cost scenario, reaching 321 k€/a. Among the operating costs, the expenditure on fuel for the biomass boiler is 218 k€/a, representing 58.4 % of the total costs. while the fixed operating costs, i.e., the O&M costs for the system components, increase from 4.6 % in the minimal cost scenario to 5.8 % in the trade-off scenario, which is primarily attributed to the maintenance of the CHP unit.

Among all these scenarios, the minimal emission scenario has the highest capital cost of 14.9 % of the total cost. Due to the increase in the capacity required for the integrated system components, the annualized capital cost of this scenario increases to 56 k€/a, 33 % more than that of the minimal cost scenario. This includes 9 k€/a for the CHP unit, which represents 15.4 % of the total investment cost, and more than a third of the investment cost of the biomass boiler. Investments in the flue gas condenser and heat pump also increased to 3.8 k€/a and 3.1 k€/a, accounting for 1.0 % and 0.8 % of the total costs, respectively. The operating costs in this scenario identical with the trade-off scenario. Overall, this scenario is the most economically disadvantageous due to its high capital costs.

Environmental Analysis

For a comprehensive system analysis, environmental performance must also be considered alongside technical and economic feasibility. First, it can be inferred from the previous analysis that the integration of heat pumps and heat exchangers alone cannot contribute to the reduction of the carbon emission of the system. As shown in Figure 71, all emissions caused by heat production in the baseline scenario originate from the combustion of wood chips. Among all scenarios, although wood chips are the most consumed, CO_2 emissions generally arise from the peak-load boiler and general electricity use for other equipment, such as pumps. But since these consumptions are fixed, the difference in total emissions across scenarios comes primarily from the amount of wood chips consumed and the electricity used to drive the heat pump.

In the minimal cost scenario, although the wood chip consumption is reduced by 690 MWh, an additional 42 MWh of electricity is consumed for driving the heat pump. Due to the higher carbon emission factor of 366 g_{CO2}/kWh of electricity from the public grid, the total carbon emissions in this scenario exceed those of the baseline.

In contrast, the minimal emission scenario shows a decrease in the system's economic feasibility with the integration of the cogeneration unit (see Figure 68), yet it results in a significant reduction in overall system emissions. Compared to the baseline scenario, this scenario reduces CO_2 emissions by 5 %, yet the levelized costs of heat become higher than minimal cost scenario.

As a trade-off, the target exhaust gas temperature is set higher to reduce the required capacity of the heat pump and cogeneration unit. This is achieved at the expense of efficiency to ensure both low cost and low emissions. The trade-off scenario results in a 4.5 % reduction of CO_2 emissions compared to the baseline solution, while also ensuring the affordability of the system. Due to the low emission factor of wood chips, the integration of the cogeneration unit results in a significant reduction in the CO_2 emissions of the electricity required by the heat pump, thereby decreasing the overall CO_2 emissions of the system. Thus, the integration of cogeneration units allows for lower CO_2 equivalent emissions at the expense of certain affordability, while ensuring a higher system energy efficiency in the biomass heating network.

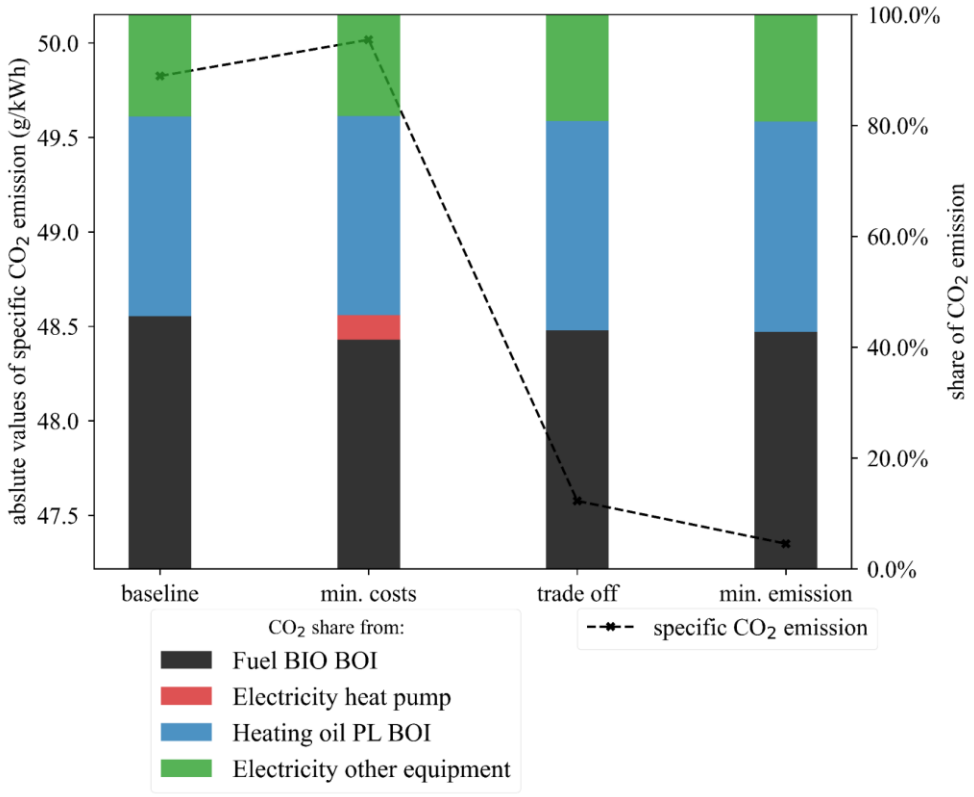

Figure 71: Analysis of CO_2 emission in various scenarios.

Based on the analysis of the aforementioned three aspects, it can be concluded that the proposed design approach of the integrated system significantly increases system overall efficiency while fulfilling the same heating demand. Utilizing the simulation-optimization framework, decision-makers can adopt the appropriate system design solutions according to their specific requirements. In the presented case study, integrating a cogeneration unit for self-power generation is not recommended for the minimal cost scenario, as the high investment and maintenance costs of the cogeneration unit can undermine the economic viability of the system. However, the cogeneration unit can effectively provide electricity for the heat pump and reduce the CO_2 emissions of the overall system. As a trade-off, the target exhaust gas temperature can be adjusted to a higher value, which reduces the required heat pump capacity and the corresponding CHP capacity, thus reducing the investment cost of the system. The cogeneration technology recommended for this case study is the SRC unit. This trade-off scenario is recommended when the balance between economic and emission goals is to be met, which enables the simultaneous achievement of an optimal system in techno-economic and environmental aspects.

12. Conclusion and outlook

In this thesis, a general approach for integrating compression heat pumps into biomass heat networks for heat recovery is proposed and analyzed starting from the real laboratory, taking into account the different connection variants. For this purpose, **Chapter 2** introduces the technologies of the system components involved in this research, including their fundamental principles and the current state of art. **Chapter 3** outlines how different system components can be integrated into the system. It defines the systems with different integration concepts and analyses the complexity of the different systems based on their mass and energy flows.

For implementing these integration concepts, a detailed simulation is proposed in **Chapter 4**. The proposed model allows for the integration of heat pumps either into a flue gas condenser or into the return flow, facilitating innovative integration of flue gas condensing technology with heat pumps into networks with high return temperatures. Additionally, the model also accommodates the integration of a cogeneration unit for powering the heat pump. Furthermore, key figures are established to evaluate the integration concepts from thermodynamic, economic and ecological perspectives. To facilitate simulation-based multi-objective optimization, the proposed simulation model is coupled with a genetic algorithm (**Chapter 5**). This optimization framework enables the optimal integration of heat pumps and their self-power generation units, taking into account the thermodynamic processes and the interactions between the system components, as well as the techno-economic performance and environmental impact.

To verify the proposed simulation model and evaluate the effectiveness of integrating heat pumps in real-world scenarios, three biomass heating networks are investigated, as detailed in **Chapter 6**. This chapter provides comprehensive information of these biomass heat networks (BHN), including their system configurations, technical parameters, and operating data. Among these networks, two have already been equipped with compression heat pumps using different integration methods, while the third network represents a typical conventional BHN in Germany without flue gas condensation and heat pump. This network had previously experienced problems with flue gas condensation due to the lack of integration of heat pumps.

For validation purposes, measured data of the first and second networks are fed into the model, enabling the simulation of both networks. The simulated results in **Chapter 7** show minor deviations from the measured values at the respective input parameters. Besides, Chapter 7 also provides a comparative analysis of the three biomass heating networks with respect to their energy efficiency and the effectiveness of their flue gas condensation systems. The evaluation based on the real operating data yielded the following results:

- The comparison of the three investigated cases reveals that the integration of heat pumps in the first two BHNs increases total efficiency (related to the lower heating value) by over 17%. In contrast, the third BHN displays significantly lower average efficiency due to its oversized biomass boiler and high excess air, making it unsuitable for flue gas condensation.
- The analysis of the operating data indicates that the full utilization rate of the heat recovery equipment in the first and second BHNs is low, which affectes the economic viability.
- Due to the electrical energy consumption of the heat pump, the integration leads to higher specific equivalent CO2 emissions and primary energy demand for the whole system under current emission factor from the electricity mix.
- The comparative analysis of three investigated biomass heating network showes that flue gas condensation in combination with a heat pump can operate reliably over the long term. Since condensation only occurs at temperatures below about 55 °C, the operation of the flue gas condenser is affected by fluctuating operating temperatures. Utilizing a heat pump helpes to stabilize the fluctuating return temperatures, ensuring consistent condensation.
- The analysis also highlighted technical challenges in designing a flue gas condensation system, such as preventing corrosion and stabilizing fluctuating return temperatures.

Chapter 8 presents a thermodynamic analysis focusing the impact of technical parameters on the heat pump design and on the overall biomass district heating system, using the hydraulic diagram and technical parameters of the first investigated BHN as an example. The analysis identifies several crucial technical parameters, such as the target exhaust gas temperature, heat pump supply temperature, and choice of refrigerant, due to their significant

impact on heat pump design. The analysis under various conditions led to several key conclusions:

- The overall efficiency of a biomass district heating system with an integrated heat pump is not solely dependent on the exhaust gas temperature, unlike standard biomass heating systems. Instead, the electrical power demand of the heat pump is also a critical factor affecting overall efficiency. Consequently, the system's overall efficiency does not always increase as the exhaust gas temperature decreases. Fuel water content and air ratio are additional factors influence the effectiveness of heat pump integration. Thus, these factors must be carefully considered in the design process.
- The supply temperature of the heat pump has a minimal impact on the overall performance of the system. However, it does significantly affect the size of the heat pump. Higher flow temperature necessitate larger heat pump dimensions, which results in increased investment and operating costs. Therefore, the selected supply temperature for a heat pump should be only as high as necessary, to avoid incurring excessive system costs.
- The choice of refrigerant does not have a significant effect on the system overall efficiency. However, it does affect the COP of the heat pump. The analysis indicated that refrigerant R236fa performs best at high target exhaust gas temperatures, while R717 performs better at low temperatures. R600a is suitable for both temperature levels and, based on its properties, it is the recommended for the case studied in this analysis.

For better comparison and in-depth analysis of the heat pump integration concepts, **Chapter 9** represents a comprehensive techno-economic analysis of two different heat pump integration concepts based on the third biomass heating network. Following the integration approaches proposed in Chapter 4, both different integration concepts,i.e., the flue gas-side integration and network-side integration, are implemented by simulation. The analysis in this chapter showed that:

- Both integration concepts can improve the system efficiency by over 10%. In the flue gas-side integration scenario, operating costs are significantly reduced, although investment costs increase due to the integration of heat recovery components. Consequently, the levelized heat production costs are reduced.

- Analysis of various technical parameters reveals that exhaust gas temperature has a significant influence on both the system overall efficiency and heating production costs. Setting an appropriate exhaust gas temperature can enable both integration concepts to be implemented more cost-effectively. From a techno-economic perspective, the heat pump supply temperature should also be designed to be as low as possible.
- Further investigation into different fuel water contents indicates that both integration concepts are more favorable from an energy perspective at higher fuel water content, though less cost-effective. Additionally, choosing the correct full load utilization hours for the integrated biomass heating system is crucial. Values that are too low or too high could adversely affect the system efficiency and economic viability. In the case studied, the optimal range for this parameter is identified as between 5000 and 5500 hours.
- Finally, the analysis of the economic parameters indicates that the economic viability of both integration concepts is sensitive to the ratio of the electricity price to biomass fuel price. The higher the fuel price, the higher the price ratio will also be. Since fuel prices are likely to rise sharply in the future, both concepts are deemed economically viable under such circumstances.

Furthermore, **Chapter 10** focuses on analyzing the techno-economic feasibility of integrating additional cogeneration units for onsite electricity supply for the heat pump.

- The techno-economic analysis reveals that the integration of additional cogeneration units may not always be economically feasible, primarily due to the high investment costs. For the studied case, only the HP-SRC integration scenario is more economical than the HP-only scenario, based on the given assumptions. However, incorporating low carbon self-power generation unit can effectively reduce CO_2 emissions and primary energy demand, considering the high CO_2 emission factor of grid electricity. In these three HP-CHP integration scenarios, the primary energy demand is reduced by approximately 9 % and CO_2 emissions by approximately 15 %.
- The analysis of the impact of various technical parameters reveals that all HP-CHP integration concepts can be implemented more economically by identifying the appropriate exhaust gas temperature. Additionally, changes in the fuel water content of the boiler affect the different HP-CHP integration concepts differently. This factor must be considered when selecting the most suitable CHP technology for onsite power

generation. In contrast, the optimal value of annual full utilization hours of the integrated system are not affected by CHP integration.

- The analysis of the economic parameters indicates that the sensitivity of the different integration scenarios of cogeneration units to the electricity price is reduced compared to the HP-only scenario. Under the current fuel price, higher electricity prices increase the viability of integrating additional cogeneration units.

Chapter 11 focuses on testing the capabilities of the proposed optimization framework through a case study based on the third biomass heat network. This network, due to its long service life and inefficient operation, was chosen for renovation. By varying the weights of the objective functions, a set of Pareto optimal solutions and their corresponding combinations of decision variables were obtained. Among these optimization results, three feasible scenarios are investigated in detail: the minimal cost scenario, the minimal emission scenario, and the trade-off scenario. The detailed analysis of these scenarios shows that:

- The integration of heat pumps can effectively improve the overall system efficiency and bring economic benefits to the system. In scenarios where environmental indicators are not a priority, the exhaust gas temperature should be set as high as possible, yet below the gas dew point temperature, to optimize economic benefits.
- The further integration of a cogeneration unit can effectively reduce the equivalent CO_2 emissions of the entire system. However, under the conditions assumed in the study, integrating a cogeneration unit was not recommended for scenarios focused solely on economic indicators. This is due to the high initial capital costs associated with cogeneration units.
- When aiming to satisfy both economic and emission targets, a balanced trade-off between these two indicators is suggested. This option ensures efficiency gains while simultaneously reducing heat costs and equivalent CO_2 emissions of the system, achieving a harmonious balance between economic viability and environmental sustainability.

In summary, this thesis develops a transferable methodology for optimizing biomass heating networks (BHN) through innovatively integratng heat pumps (HP) and, if necessary, cogeneration units for onsite-power supply. Besides, this thesis demonstrates the possibility of integrating heat pumps into biomass heating networks to ensure the effective utilization of biomass resources while satisfying the economic and environmental viability. The success

of this integration depends on careful selection of design parameters. The prices of biomass fuel and electricity are crucial factors affecting the economic viability of the integration concepts.

The proposed simulation model and optimization framework allow decision-makers to achieve an optimal system design, considering the given constraints and the chosen objectives. Depending on the optimization objectives, the optimal system configuration, as well as the best combination of design parameters for the system components, can be determined.

The increased complexity due to the integration of multiple system components presents a challenge and an opportunity for further research. Future studies could explore the general operation modes of system equipment for safer and more economical operation. Additionally, the detailed analysis suggests that fuel and electricity prices, along with emission factors, significantly impact the optimization results. Investigating the specific effects of various fuel and electricity sources and their price dynamics on optimization results could be a valuable direction for future research.

Appendix

Appendix A. Determination of U-value of an indirect-contact flue gas condenser

From the basics of heat transfer, it is known that the value of *U* is determined from the thermal circuit, using an analogy between thermal and electrical circuits. It is determined jointly by the heat transfer coefficients of the different layers. Among them, the convective heat transfer coefficient between the flue gas and the condenser tube is the key factor that usually produces the largest errors in the heat exchanger analysis. The convective heat transfer coefficient must be solved by empirical correlations, which usually has an error of 10 % to 30 %, and sometimes worse [55].

To determine this value, the dimensionless parameter Nusselt number (*Nu*) is often used as an important parameter [215], which represents the ratio of convective to conductive heat transfer at the boundary and defined as:

$$Nu = \frac{\alpha * L_{char.}}{\lambda_{fg}} \quad 1.$$

Where α is the heat transfer coefficient for the convective heat transfer between the condensing bundle and flue gas, which is a key parameter in determining the overall heat transfer rate. λ_{fg} is the thermal conductivity of the flue gas. $L_{char.}$ is the characteristic length of the heat exchanger, dependent on the geometry of the system under consideration [216].

Nußelt number depends on the properties of the fluid. These properties can also be summarized as dimensionless groups of numbers, such as the Prandtl number (*Pr*) and Reynolds number (*Re*), Jacob number (*Ja*), etc. For designing the flue gas condenser, Zhang et al. [217] established a dimensionless formula to address the correlation among the *Nu*, *Re*, *Ja.*

$$Nu = f(Re, Ja) = C * Re^m * Ja^n \quad 2.$$

The Reynolds number *Re* in this formula can be expressed as:

$$Re = \frac{u * L}{\nu} \quad 3.$$

Where *u* is the velocity of the flue gas, ν is the kinematic viscosity of the flue gas (m^2/s), and *L* is the characteristic length of the flue gas flow over the condensation bundle.

The Jacob number *Ja* is used to describe the heat transfer during phase transitions. For flue gas condensation it can be determined as the relative ratio of latent heat to sensible heat of flue gas in different conditions. Wang et al. [218] provided a modified equation for *Ja* to account for the driving force of the concentration difference between the mainstream flue gas and the condensing interface, which can be adapted as:

$$Ja = \frac{\left(x_{H20,fg,in} - x_{sat\ H20,fg,cond}\right) * r}{\rho * c_p * (T_{fg,in} - T_{fg,cond})} \quad 4.$$

Where $x_{H20,fg,in}$ represents the water vapor content of the flue gas entering the condenser (kg_{H20}/m^3_{fg}), $x_{sat\ H20,fg,cond}$ represents the saturated water vapor content at the average temperature of the condensing surface (kg_{H20}/m^3_{fg}). $T_{fg,in}$ and $T_{fg,cond}$represent the entering temperature of the flue gas in the condenser and the average temperature of the condensing surface (°C), respectively. *r* represents the latent heat of condensation of water vapor (kJ/kg). c_p represents the specific heat capacity of water (kJ/kgK).

The *m* and *n* in Equation 2. represent the exponential factors corresponding to *Re* and *Ja* number, respectively. These two values need to be obtained through a series of experimental measurements to accurately define the function.

Appendix B. Simplified model for calculating heat losses of a biomass boiler.

Average surface temperature:

$$T_{ave} = \frac{T_A + T_r}{2} \quad 5.$$

Isobaric coefficient of thermal expansion of air:

$$\beta = \frac{1}{T_{ave} + 273.15} \quad 6.$$

Dynamic viscosity of air:

$$\gamma = -312.66 + 447.22 * e^{\frac{T_{ave}}{495.76}} \quad 7.$$

Thermal conductivity of air:

$$\lambda = 24.14 + 9.07 * 10^{-2} * T_{ave}{}^{0.952} \quad 8.$$

Prandtl number of air:

$$Pr = 0.72 - 9.62 * 10^{-4} * T_{ave}{}^{0.57} \quad 9.$$

Surface of the heat generator:

$$A = (4 + 1.3 * P_h)^{0.5} * f_h \quad 10.$$

Overflow:

$$l = (0.8 + 0.09 * P_h)^{0,5} * f_{hr} \quad 11.$$

Grashof number:

$$Gr = \frac{9.81 * \left(l^3 * \beta * (T_A - T_r) \right)}{(\nu * 0.0000001)^2} \quad 12.$$

Rayleigh number:

$$ra = Gr * Pr \quad 13.$$

Auxiliary function $f_{(Pr)}$:

$$f(Pr) = \left(1 + (0.492 / Pr)^{\frac{9}{16}}\right)^{-\frac{9}{16}} \quad 14.$$

Nusselt number:

$$Nu = \left(0.825 + 0.387 * \left(ra * f_{(Pr)}\right)^{\frac{1}{6}}\right)^2 \quad 15.$$

Heat transfer coefficient:

$$\alpha = Nu * \lambda * \frac{0,001}{l} \quad 16.$$

Heat loss:

$$\dot{Q}_{loss} = \frac{\alpha * A * (T_A - T_R)}{1000} \quad 17.$$

Appendix C. Detailed representation of boiler 2 with integrated ORC unit and economizers

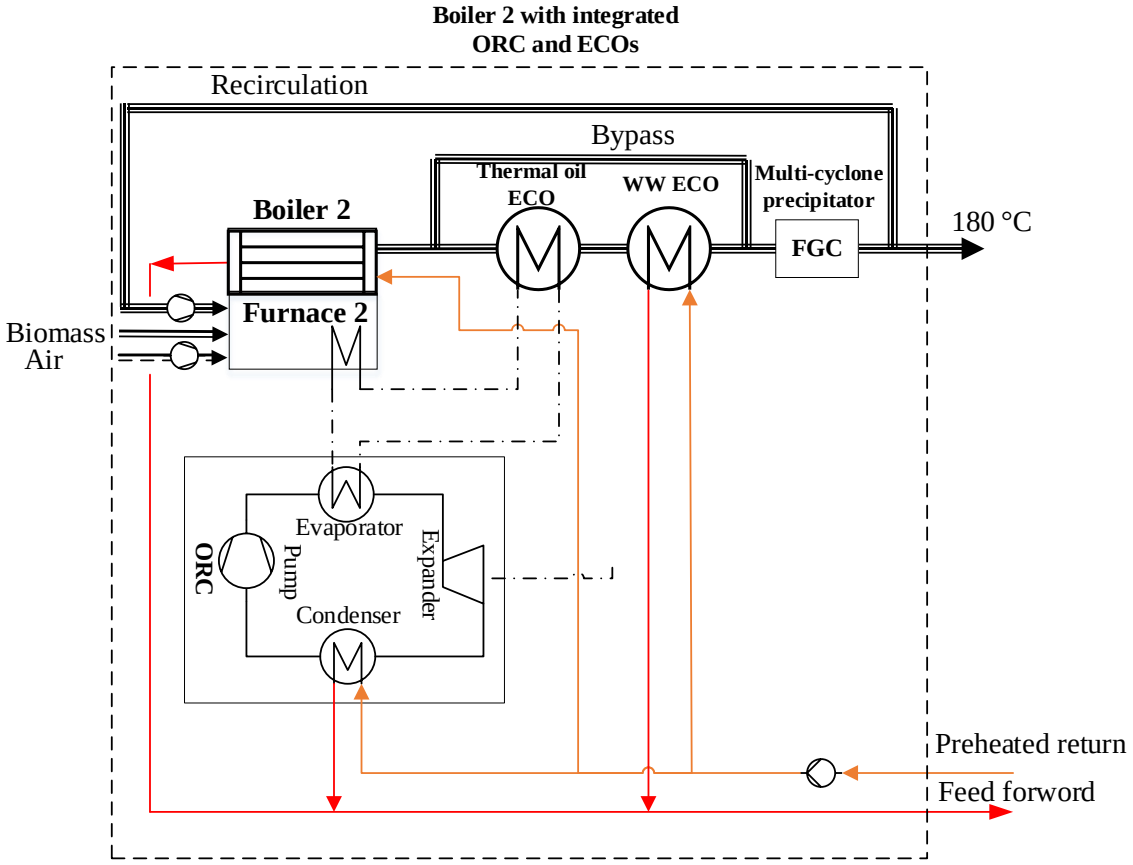

Figure 72: Detailed representation of Boiler 2 with integrated ORC unit and two economizers.

Appendix D. Derivation of the minimal allowed electrical efficiency of the Rankine cycle

From thermodynamics, it is known that the ratio ξ, representing the heat performance of the flue gas condenser $\dot{Q}_{cond}$to the furnace heat performance $\dot{Q}_{furnace}$, can be considered constant when the fuel data and the operating parameters of the boiler and flue gas condenser remain unchanged. This is because the specific enthalpy change of the flue gas in furnace and in flue gas condenser remains constant in this situation. A change in the performance of the furnace indicates an increase in the fuel input and thus a proportional increase in the performance of the condenser:

$$\xi = \frac{\dot{Q}_{cond}}{\dot{Q}_{furnace}} = \frac{\dot{m} * \Delta h_{cond}}{\dot{m} * \Delta h_{furnace}} \approx constant \qquad 18.$$

The heat performance of the flue gas condenser $\dot{Q}_{cond}$ and the furnace heat performance $\dot{Q}_{furnace}$ can be determined as follows:

$$\dot{Q}_{cond} = P_{el} * (COP - 1) \quad 19.$$

$$\dot{Q}_{furnace} = \dot{Q}_{boi} + \dot{Q}_{to\,rc} = \dot{Q}_{boi} + \frac{P_{hp,el}}{\eta_{el}} \quad 20.$$

Where P_{el} represents the electrical demand of the heat pump. η_{el} is the electrical efficiency of the Rankine Cycle. $\dot{Q}_{boi}$ is the boiler heat output, which should be greater than or equal to 0. In worst case the boiler output can be 0. With these equations, It can be deduced that:

$$P_{hp,el} * (COP - 1) = \left(\dot{Q}_{boi} + \frac{P_{hp,el}}{\eta_{el}}\right)\xi \quad 21.$$

$$P_{hp,el} * (COP - 1) \geq \frac{P_{hp,el}}{\eta_{el}}\xi \quad 22.$$

$$\eta_{el} \geq \frac{\xi}{COP - 1} \quad 23.$$

Appendix E. Default parameters for the simulation model

Table 20: Investment costs [27,210,219], operation costs factor and lifetime of [220] the main components.

Components	Investment (€/unit)	operation costs factor	lifetime(a)
Biomass firing	$2011 * P_n{}^{0,6658}$	0.06	15
Economizer	$841 * P_n{}^{0.4786}$	0.02	20
Flue gas condenser	$4253 * P_n{}^{0.4730}$	0.02 with heat pump 0.08 without heat pump	20
Air preheating	$1105 * P_n{}^{0.3663}$	0.02	20
Flue gas pipe surcharge	$107 * P_{n,firing}{}^{0.6378}$	0.02	15
Heat pump	$350 * P_n{}^{0.93}$	0.025	20
Gasifier CHP	$6941 * P_{n,gchp}{}^{0.791}$	$0.1336 * P_{n,gchp}{}^{-0.284}$	15
Installation factor	1.3 for all components		

Table 21: Prices for the calculation of variable operating costs.

	Costs (€/MWh)	**Ref**
wood chips price in 2021	$32.15 - 34.33 * (w - 0.2)$	[221]
Pellets price in 2021 (w=0.1)	48.3	[222]
Electricity price in 2021	198.4	[223]
Ash cleaning and disposal price	1.7	[224]

Table 22: Reference values of the CO_2 factor [180,225].

Energy source	**CO_2 factor (g/kWh)**
Wood chips	20
Pellet	27
Electricity mix	366

Appendix F. Input parameters for the case studies

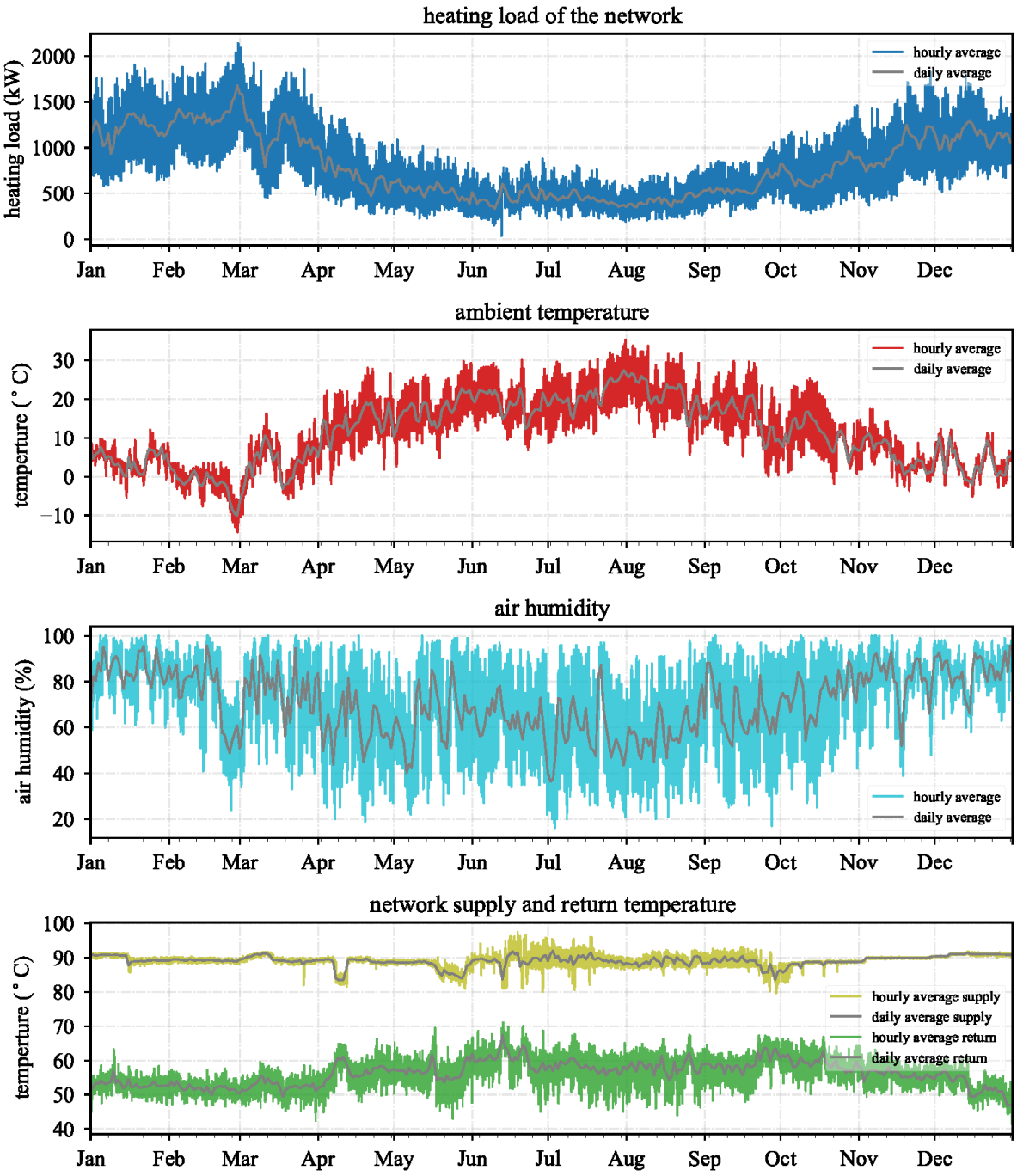

Figure 73: Input data for case study: historic heating load, weather data and network temperatures of the investigated biomass heating network.

Table 23: Element compositions of chosen fuel for GCHP.

Parameter	**Wood pellets for GCHP**	**Unit**
Total water content	10	Ma% wet
Higher heating value (HHV)	19.73	kJ/kg dry
Lower heating value (LHV)	18.35	kJ/kg dry
Ash content	1.0	Ma% dry
Total chlorine content	0.0090	Ma% dry
Carbon	50.0	Ma% dry
Hydrogen	6.3	Ma% dry
Nitrogen	0.10	Ma% dry
Total sulfuric content	0.0250	Ma% dry
Oxygen	42.57	Ma% dry

Appendix G. Supplementary charts for analysis

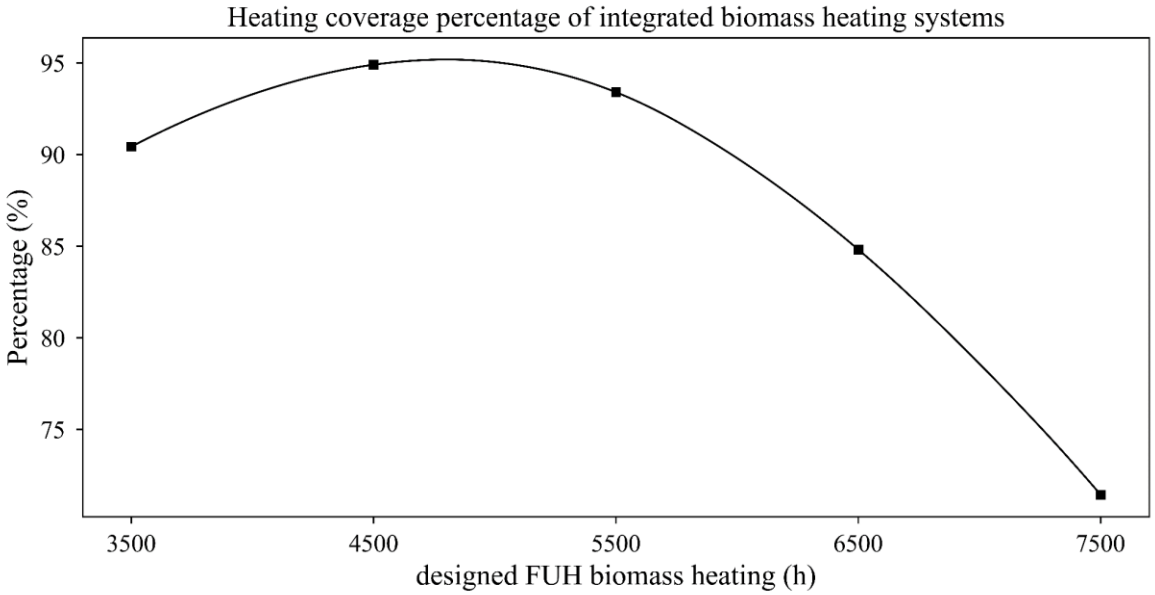

Figure 74: Heating coverage percentage of integrated biomass heating systems with different in the three scenarios considered in Section 9.2.2..

References

[1] T.A. Boden, G. Marland, and R.J. Andres, Carbon Dioxide Information Analysis Center (CDIAC) Datasets, 2010.

[2] Ian Tiseo, Historical carbon dioxide emissions from global fossil fuel combustion and industrial processes from 1750 to 2020, 2021. https://www.statista.com/statistics/264699/worldwide-co2-emissions/ (accessed 21 February 2022).

[3] Rebecca Lindsey, Luann Dahlman, Jessica Blunden, Climate Change: Global Temperature, 2021. https://www.climate.gov/news-features/understanding-climate/climate-change-global-temperature (accessed 21 February 2022).

[4] M. Meinshausen, N. Meinshausen, W. Hare, S.C.B. Raper, K. Frieler, R. Knutti, D.J. Frame, M.R. Allen, Greenhouse-gas emission targets for limiting global warming to 2 degrees C, Nature 458 (2009) 1158–1162. https://doi.org/10.1038/nature08017.

[5] The Paris Agreement, United Nations Climate Change, 2015.

[6] Europäische Kommission, Lage der Union: Fragen und Antworten zum Klimazielplan für 2030, 2020. https://ec.europa.eu/commission/presscorner/detail/de/qanda_20_1598 (accessed 18 February 2021).

[7] European Commission, State of the Union: Commission raises climate ambition and proposes 55% cut in emissions by 2030, 2020. https://ec.europa.eu/commission/presscorner/detail/en/ip_20_1599 (accessed 19 April 2022).

[8] Bundesministerium für Wirtschaft und Energie, Europäische Energiepolitik, 2020. https://www.bmwi.de/Redaktion/DE/Artikel/Energie/europaeische-energiepolitik.html (accessed 18 February 2021).

[9] Wissenschaftlicher Dienst Deutscher Bundestag, Aktuelle Klimaschutzziele auf internationaler, europäischer und nationaler Ebene: Nominale Ziele und Rechtsgrundlagen, 2018.

[10] Bundesministerium des Innern, für Bau und Heimat, Energetische Stadtsanierung: Das Quartier als Handlungsebene für die energetische Stadtsanierung fördern, 2020.

https://www.bmi.bund.de/DE/bauen-wohnen/bauen/energieeffizientes-bauen-sanieren/stadtsanierung/stadtsanierung-node.html (accessed 19 April 2022).

[11] Bundesministerium für Umwelt, Naturschutz, Bau und Reaktorsicherheit (BMUB), www.bmub.bund.de, Energetische Stadtsanierung - Zuschüsse für integrierte Quartierskonzepte und Sanierungsmanager, 2015. www.bmub.bund.de (accessed 22 February 2021).

[12] A. Lake, B. Rezaie, S. Beyerlein, Review of district heating and cooling systems for a sustainable future, Renewable and Sustainable Energy Reviews 67 (2017) 417–425. https://doi.org/10.1016/j.rser.2016.09.061.

[13] S. Werner, International review of district heating and cooling, Energy 137 (2017) 617–631. https://doi.org/10.1016/j.energy.2017.04.045.

[14] S. Baasch, Energy transition with biomass residues and waste: regional-scale potential and conflicts. A case study from North Hesse, Germany, Journal of Environmental Policy & Planning 23 (2021) 243–255. https://doi.org/10.1080/1523908X.2021.1888701.

[15] D. Thrän, M. Dotzauer, V. Lenz, J. Liebetrau, A. Ortwein, Flexible bioenergy supply for balancing fluctuating renewables in the heat and power sector—a review of technologies and concepts, Energ Sustain Soc 5 (2015). https://doi.org/10.1186/s13705-015-0062-8.

[16] A. Camia, J. Giuntoli, R. Jonsson, N. Robert, N.E. Cazzaniga, G. Jasinevičius, G. Grassi, J.I. Barredo, S. Mubareka, The use of woody biomass for energy production in the EU, Publications Office of the European Union, Luxembourg, 2021.

[17] M. Gaderer, Dezentrale Energiesysteme, 2017.

[18] J. Popp, Z. Lakner, M. Harangi-Rákos, M. Fári, The effect of bioenergy expansion: Food, energy, and environment, Renewable and Sustainable Energy Reviews 32 (2014) 559–578. https://doi.org/10.1016/j.rser.2014.01.056.

[19] Morten Tony Hansen, The future role of thermal biomass power in renewable energy systems. study of Garmany, 2019.

[20] S. Broberg Viklund, M. Karlsson, Industrial excess heat use: Systems analysis and CO2 emissions reduction, Applied Energy 152 (2015) 189–197. https://doi.org/10.1016/j.apenergy.2014.12.023.

[21] Matthias Gaderer, Wärmeversorgung mit fester Biomasse bei kleiner Leistung: Dissertation., 2007.

[22] P. Neuenschwander, J. Good, T. Nussbaumer, Grundlagen der Abgaskondensation bei Holzfeuerungen: Schlussbericht, 1998.

[23] S. Shang, X. Li, W. Chen, B. Wang, W. Shi, A total heat recovery system between the flue gas and oxidizing air of a gas-fired boiler using a non-contact total heat exchanger, Applied Energy 207 (2017) 613–623. https://doi.org/10.1016/j.apenergy.2017.05.169.

[24] M. Terhan, K. Comakli, Design and economic analysis of a flue gas condenser to recover latent heat from exhaust flue gas, Applied Thermal Engineering 100 (2016) 1007–1015. https://doi.org/10.1016/j.applthermaleng.2015.12.122.

[25] P. Ziembicki, J. Kozioł, J. Bernasiński, I. Nowogoński, Innovative System for Heat Recovery and Combustion Gas Cleaning, Energies 12 (2019) 4255. https://doi.org/10.3390/en12224255.

[26] Y. Xiong, H. Tan, Y. Wang, W. Xu, H. Mikulčić, N. Duić, Pilot-scale study on water and latent heat recovery from flue gas using fluorine plastic heat exchangers, Journal of Cleaner Production 161 (2017) 1416–1422. https://doi.org/10.1016/j.jclepro.2017.06.081.

[27] H. Pieper, T. Ommen, F. Buhler, B.L. Paaske, B. Elmegaard, W.B. Markussen, Allocation of investment costs for large-scale heat pumps supplying district heating, Energy Procedia 147 (2018) 358–367. https://doi.org/10.1016/j.egypro.2018.07.104.

[28] Arnemann, Application of industrial heat pump: IEA Industrial Energy-related Systems and Technologies Annex 13: IEA Heat Pump Programme Annex 35, Austria. https://iea-industry.org/ (accessed 25 February 2021).

[29] E. Jaunegg, Vergleich verschiedener Wärmepumpentechnologien für den Einsatz in Rauchgaskondensationsanlagen von Biomasseheizwerken: Masterthesis zur

Erlangung des akademischen Grades Diplom-Ingenieur für technisch wissenschaftliche Berufe, 2019.

[30] S. Xiao, D. Nefodov, T. Urbaneck, Overview of the use of heat pumps in Germany, KI Kälte · Luft · Klimatechnik 2020 (2020).

[31] C. Bernath, G. Deac, F. Sensfuß, Influence of heat pumps on renewable electricity integration: Germany in a European context, Energy Strategy Reviews 26 (2019) 100389. https://doi.org/10.1016/j.esr.2019.100389.

[32] A. Vannoni, A. Giugno, A. Sorce, Integration of a flue gas condensing heat pump within a combined cycle: Thermodynamic, environmental and market assessment, Applied Thermal Engineering 184 (2021) 116276. https://doi.org/10.1016/j.applthermaleng.2020.116276.

[33] H. Averfalk, P. Ingvarsson, U. Persson, M. Gong, S. Werner, Large heat pumps in Swedish district heating systems, Renewable and Sustainable Energy Reviews 79 (2017) 1275–1284. https://doi.org/10.1016/j.rser.2017.05.135.

[34] Stefano Frigo, Roberto Gabbriellib Monica Puccinib Maurizia Seggianib ,Sandra Vitolo, Chemical engineering transcations.

[35] M. Kaltschmitt, H. Hartmann, H. Hofbauer (Eds.), Energie aus Biomasse: Grundlagen, Techniken und Verfahren, 3rd ed., Springer Vieweg, Berlin, Heidelberg, 2016.

[36] P. Doering, H. Weimar, U. Mantau, Einsatz von Holz in Biomasse-Großfeuerungsanlagen 2016: Rohstoffmonitoring Holz: Teilbericht, Hamburg, 2018. http://www.infro.eu/downloads/studien/6_Holzeinsatz%20in%20Biomasse-Gro%C3%9Ffeuerungsanlagen%202016.pdf (accessed 9 September 2020).

[37] D. Peters, Anbau und Verwendung nachwachsender Rohstoffe in Deutschland, 2019. http://www.fnr-server.de/ftp/pdf/berichte/22004416.pdf (accessed 9 September 2019).

[38] Matthias Gaderer, Wärmeversorgung mit fester Biomasse bei kleiner Leistung: Dissertation., 2007.

[39] H. Hartmann, K. Reisinger, P. Turowski, P. Roßmann, Handbuch Bioenergie-Kleinanlagen: Leitfaden, third., vollst. überarb. Aufl., Fachagentur Nachwachsende Rohstoffe e.V, 2013.

[40] I. Obernberger, Nutzung fester Biomasse in Verbrennungsanlagen: Unter besonderer Berücksichtigung des Verhaltens aschebildender Elemente, third. korrigierte Auflage, dbv, TestOrt, 1998.

[41] H. Stockinger, I. Obernberger, Systemanalyse der Nahwärmeversorgung mit Biomasse, first ed., dbv-Verlag f. d. TU Graz, Graz, 1998.

[42] Obernberger, I., Hammerschmidt, A., Dezentrale Biomasse-Kraft-Wärme-Kopplungstechnologien, 1998.

[43] W. Winter, Optimierte Dimensionierung von Rohrleitungssystemen für dezentrale Biomassefernheizwerke: Projektphase II, Graz, 2001.

[44] T. Nussbaumer, Grundlagen der Holzvergasung, Heizung Klima 7 (1990) 52–60.

[45] T. Nussbaumer, An increasingly important renewable energy source: fundamentals of wood combustion; Ein erneuerbarer Energietraeger von zunehmender Bedeutung: Grundlagen der Holzverbrennung, Waermetechnik 44 (1999).

[46] Clyde Bergemann Power Group, Rußbläser - onload Kesselreinigungssysteme. https://www.cbpg.com/de/products-solutions/boiler-efficiency/russblaeser-onload-kesselreinigungssysteme (accessed 27 May 2020).

[47] B. Alt, Technische Anforderungen an die Überwachung von elektrostatischen Abscheidern in Biomasseheizwerken. Dissertation, München, 2021.

[48] Agency for Renewable Resources e. V., List bioenergy villages. https://bioenergiedorf.fnr.de/bioenergiedoerfer/liste/ (accessed 22 February 2021).

[49] Bene Müller, Bioenergy village Büsingen: Local heating network with heat from wood combined with solar thermal energy, 2017. bioenergiedorf.fnr.de (accessed 22 February 2021).

[50] Bioenergiedorf Jühnde eG, Bioenergy village Jühnde: Independent power generation and heat supply on the basis of Basis of biomass, Jühnde, Germany, 2005. www.bioenergiedorf.de (accessed 22 February 2021).

[51] M. Gaderer, WDesign: Auslegung von Wärmeerzeugern zur Nahwärme-Bedarfsdeckung und Stromerzeugung für dezentrale Biomasseheiz(kraft)werke, Berechnungsprogramm zur technischen und wirtschaftlichen Beurteilung von

Heiz(kraft)werken mit Nahwärmeverteilung, Bayerische Staatsministerium für Landwirtschaft und Forsten, Straubing, Bayern, 2005.

[52] Bundesministerium für Justiz, Erste Verordnung zur Durchführung des Bundes-Immissionsschutzgesetzes.

[53] Bundesministerium für Justiz, Vierte Verordnung zur Durchführung des Bundes-Immissionsschutzgesetzes (Verordnung über genehmigungsbedürftige Anlagen - 4. BImSchV).

[54] DIN 5499:2018-07, Brennwert und Heizwert_- Allgemeine Grundlagen, Beuth Verlag GmbH, Berlin.

[55] J. Saari, Heat exchanger thermal design guide (2010).

[56] Simon Jabornig, Abwasser aus Kondensation Kondensataufbereitung, 2019.

[57] G. Herberg, Der Luftüberschuß, in: G. Herberg (Ed.), Handbuch der Feuerungstechnik und des Dampfkesselbetriebes, Springer Berlin Heidelberg, Berlin, Heidelberg, 1913, pp. 69–73.

[58] G. Lachenmayr, H. Kreimes, Energietechnik für die Holzindustrie, Retru-Verlag, 2006.

[59] Johannes Beu, Emissionsminderungskonzepte für eine stationäre Wirbelschichtfeuerung kleiner Leistung. Dissertation, 2009.

[60] L. Eltrop, H. Hartmann, P. Heinrich, B. Jahraus, M. Kaltschmitt, K. Raab, S. Schneider, G. Schröder, Leitfaden Bioenergie: Planung, Betrieb und Wirtschaftlichkeit von Bioenergieanlagen, fourth., unveränderte Aufl., Fachagentur Nachwachsende Rohstoffe, Gülzow b Güstrow, 2007.

[61] O.Rentz, K. Gütling, U. Karl, Erarbeitung der Grundlagen für das BVT-Merkblatt: Großfeuerungsanlagen im Rahmen des Informationsaustausches nach Art. 16(2) IVU-Richtlinie, Hertzstr. 16, 76187 Karlsruhe, 2002.

[62] THE EUROPEAN PARLIAMENT AND THE COUNCIL OF THE EUROPEAN UNION, The Medium Combustion Plant (MCP) Directive, 2015. http://ec.europa.eu/environment/industry/stationary/mcp.htm, (accessed 2 December 2020).

[63] Referentenentwurf der neuen TA Luft 2017. https://www.vdi.de/technik/fachthemen/reinhaltung-der-luft/artikel/vdi-konferenz-2017-anpassung-der-ta-luft/ (accessed 2 December 2020).

[64] Bundesministrium der Justiz und für Verbraucherschutz, Erste Verordnung zur Durchführung des Bundes-Immissionsschutzgesetzes (Verordnung über kleine und mittlere Feuerungsanlagen - 1. BImSchV) § 15 Wiederkehrende Überwachung.

[65] Ökofen. https://oekofen-heizung.de/ (accessed 2 December 2020).

[66] Fröling. http://www.froeling.com/at/ (accessed 2 December 2020).

[67] M. Köfinger, D. Basciotti, R.R. Schmidt, E. Meissner, C. Doczekal, A. Giovannini, Low temperature district heating in Austria: Energetic, ecologic and economic comparison of four case studies, Energy 110 (2016) 95–104. https://doi.org/10.1016/j.energy.2015.12.103.

[68] Jens M. Kuckelkorn, W. Dallmayer, M. Reuß, M. Schmidt, W. Schölkopf, Systemsimulationen zum solaren Nahwärmesystem mit saisonalem Wärmespeicher und Heißwasser-Absorptionswärmepumpe: Solare Nahwärme Am Ackermannbogen (SNAB), München, D-85748 Garching.

[69] P. Standl, M. Gaderer, Efficiency Enhancement in Biomass Heating Plants by an Innovative Integration of Flue Gas Condensation and Heat Pumps, ETA-Florence Renewable Energies.

[70] DIN EN 255 Teil 1, Wärmepumpen-Anschlußfertige Wärmepumpen mit elektrisch angetriebenen Verdichtern zum Heizen oder zum Heizen und Kühlen: Benennungen, Definitionen und Bezeichnungen, Beuth Verlag GmbH, 1988.

[71] J. Dohmann, Thermodynamik der Kälteanlagen und Wärmepumpen, Springer Berlin Heidelberg, Berlin, Heidelberg, 2016.

[72] LÄNGAUER A., ADLER B., The Joule cycle realised in a rotation heat pump, International Institute of Refrigeration (IIR), 2020.

[73] W. Eder, F. Moser, Die Wärmepumpe in der Verfahrenstechnik, Springer, Wien, 1979.

[74] B. Bender, D. Göhlich, Dubbel Taschenbuch Für Den Maschinenbau 3, twenty-sixthth ed., Springer Berlin / Heidelberg, Berlin, Heidelberg, 2021.

[75] Renz, Kältemittel Report 21, 2020. https / /www. bitzer.de/ (accessed 27 December 2020).

[76] Bitzer Kühlmaschinenbau GmbH, Hermetische Scollverdichter, 2022. https://www.bitzer.de/shared_media/documentation/esp-100-6.pdf.

[77] Bitzer Kühlmaschinenbau GmbH, Halbhermetische Hubkolbenverdichter, 2022. https://www.bitzer.de/shared_media/documentation/kp-100-1-de.pdf.

[78] Bitzer Kühlmaschinenbau GmbH, NH3-Offene Schraubenverdichter, 2022. https://www.bitzer.de/shared_media/documentation/sp-520-2.pdf.

[79] G.U.N.T. Gerätebau GmbH, Basiswissen Verdichter in der Kältetechnik, 2022. https://www.gunt.de/images/download/compressors-in-refrigeration_german.pdf.

[80] M. Krause, Die Kältemaschinen und ihre thermodynamischen Grundlagen, de Gruyter, 1932.

[81] Bitzer Kühslmaschinenbau GmbH (Ed.), Competence in Capacity Control: Kompetenz in Leistungsregelung, 2016.

[82] W. Sandkötter, Kältemaschinen: Schraube oder Kolben?, 2015. https://www.ikz.de/detail/news/detail/kaeltemaschinen-schraube-oder-kolben/ (accessed 21 November 2020).

[83] K. Lüdtke, Turboverdichter, in: K.-H. Grote, J. Feldhusen (Eds.), Dubbel, Springer Berlin Heidelberg, 2005, R70-R82.

[84] Volume 7: Turbomachinery, Parts A, B, and C, ASMEDC, 2010.

[85] Westfalen AG, Leitfaden für die Kältemittelauswahl: Ein Ausblick auf die Kältemittel der Zukunft.

[86] C. Höges, V. Venzik, C. Vering, D. Müller, Bewertung alternativer Arbeitsmittel für Wärmepumpen im Gebäudesektor, Forsch Ingenieurwes 86 (2022) 213–224. https://doi.org/10.1007/s10010-022-00584-0.

[87] DIN EN 378-1:2021-06, Kälteanlagen und Wärmepumpen_- Sicherheitstechnische und umweltrelevante Anforderungen_- Teil_1: Grundlegende Anforderungen,

Begriffe, Klassifikationen und Auswahlkriterien; Deutsche Fassung EN_378-1:2016+A1:2020, Beuth Verlag GmbH, Berlin.

[88] ISO 817:2014, Refrigerants — Designation and safety classification, 3rd ed., Maintenance Agency or Registration Authority 71.100.45 Refrigerants and antifreezes, 2014. https://www.iso.org/obp/ui/#iso:std:iso:817:ed-3:v1:en (accessed 26 June 2022).

[89] DIN 8960:1998-11, Kältemittel_- Anforderungen und Kurzzeichen, Beuth Verlag GmbH, Berlin.

[90] Bitzer Kühlmaschinenbau GmbH, Kältemittel Report 21, 2020. https://www.bitzer.de/shared_media/documentation/a-500-21.pdf (accessed 27 December 2020).

[91] Sven Baumann, Cornelia Elsner, Daniel de Graaf, Gabriele Hoffmann, Kerstin Martens, Constance Noack, Wolfgang Plehn, Ludwig Ries, Diana Thalheim, 1987 - 2017: 30 Jahre Montreal Protokoll: Vom Ausstieg aus den FCKW zum Ausstieg aus teilfluorierten Kohlenwasserstoffen, Umweltbundesamt.

[92] L. Bernstein, Climate Change 2007: Synthesis Report: An Assessment of the Intergovernmental Panel on Climate Change, Intergovernmental Panel on Climate Change, [Place of publication not identified], 2007.

[93] Umwelt Bundesamt, EU-Verordnung über fluorierte Treibhausgase. https://www.umweltbundesamt.de/themen/klima-energie/fluorierte-treibhausgase-fckw/rechtliche-regelungen/eu-verordnung-ueber-fluorierte-treibhausgase#VO5172014 (accessed 12 May 2022).

[94] Vierundvierzigste Verordnung zur Durchführung des Bundes-Immissionsschutzgesetzes (Verordnung über mittelgroße Feuerungs- Gasturbinen- und Verbrennungsmotoranlagen - 44. BImSchV): § 10 Emissionsgrenzwerte für Feuerungsanlagen bei Einsatz von festen Brennstoffen, Bundesamt für Jusitz. http://www.gesetze-im-internet.de/bimschv_44/__10.html (accessed 25 January 2021).

[95] K. Langeheinecke, A. Kaufmann, K. Langeheinecke, G. Thieleke, Thermodynamik für Ingenieure, Springer Fachmedien Wiesbaden, Wiesbaden, 2017.

[96] K.J. Chua, S.K. Chou, W.M. Yang, Advances in heat pump systems: A review, Applied Energy 87 (2010) 3611–3624. https://doi.org/10.1016/j.apenergy.2010.06.014.

[97] M. Wang, C. Deng, Y. Wang, X. Feng, Exergoeconomic performance comparison, selection and integration of industrial heat pumps for low grade waste heat recovery, Energy Conversion and Management 207 (2020) 112532. https://doi.org/10.1016/j.enconman.2020.112532.

[98] A. Kahraman, A. Çelebi, Investigation of the Performance of a Heat Pump Using Waste Water as a Heat Source, Energies 2 (2009) 697–713. https://doi.org/10.3390/en20300697.

[99] F. Li, L. Duanmu, L. Fu, X.l. Zhao, Research and Application of Flue Gas Waste Heat Recovery in Co-generation Based on Absorption Heat-exchange, Procedia Engineering 146 (2016) 594–603. https://doi.org/10.1016/j.proeng.2016.06.407.

[100] X. Wang, J. Zhuo, J. Liu, S. Li, Synergetic process of condensing heat exchanger and absorption heat pump for waste heat and water recovery from flue gas, Applied Energy 261 (2020) 114401. https://doi.org/10.1016/j.apenergy.2019.114401.

[101] H. Zhang, Y. Dong, Y. Lai, X. Zhang, Waste heat recovery from coal-fired boiler flue gas: Performance optimization of a new open absorption heat pump, Applied Thermal Engineering 183 (2021) 116111. https://doi.org/10.1016/j.applthermaleng.2020.116111.

[102] M. Qu, O. Abdelaziz, H. Yin, New configurations of a heat recovery absorption heat pump integrated with a natural gas boiler for boiler efficiency improvement, Energy Conversion and Management 87 (2014) 175–184. https://doi.org/10.1016/j.enconman.2014.06.083.

[103] K. Zhu, J. Xia, X. Xie, Y. Jiang, Total heat recovery of gas boiler by absorption heat pump and direct-contact heat exchanger, Applied Thermal Engineering 71 (2014) 213–218. https://doi.org/10.1016/j.applthermaleng.2014.06.047.

[104] M. Wei, W. Yuan, Z. Song, L. Fu, S. Zhang, Simulation of a heat pump system for total heat recovery from flue gas, Applied Thermal Engineering 86 (2015) 326–332. https://doi.org/10.1016/j.applthermaleng.2015.04.061.

[105] D. Lu, G. Chen, M. Gong, Y. Bai, Q. Xu, Y. Zhao, X. Dong, J. Shen, Thermodynamic and economic analysis of a gas-fired absorption heat pump for district heating with cascade recovery of flue gas waste heat, Energy Conversion and Management 185 (2019) 87–100. https://doi.org/10.1016/j.enconman.2019.01.110.

[106] B. Yang, Y. Jiang, L. Fu, S. Zhang, Experimental and theoretical investigation of a novel full-open absorption heat pump applied to district heating by recovering waste heat of flue gas, Energy and Buildings 173 (2018) 45–57. https://doi.org/10.1016/j.enbuild.2018.05.021.

[107] B. Yang, W. Yuan, L. Fu, S. Zhang, M. Wei, D. Guo, Techno-economic study of full-open absorption heat pump applied to flue gas total heat recovery, Energy 190 (2020) 116429. https://doi.org/10.1016/j.energy.2019.116429.

[108] C. Keil, S. Plura, M. Radspieler, C. Schweigler, Application of customized absorption heat pumps for utilization of low-grade heat sources, Applied Thermal Engineering 28 (2008) 2070–2076. https://doi.org/10.1016/j.applthermaleng.2008.04.012.

[109] C. Marguerite, IEA Heat Pumping Technologies Annex 47: Heat Pumps in District Heating and Cooling Systems. https://heatpumpingtechnologies.org/annex47/ (accessed 23.02,2021).

[110] M.A. Sayegh, P. Jadwiszczak, B.P. Axcell, E. Niemierka, K. Bryś, H. Jouhara, Heat pump placement, connection and operational modes in European district heating, Energy and Buildings 166 (2018) 122–144. https://doi.org/10.1016/j.enbuild.2018.02.006.

[111] S.R. Jamil, L. Wang, D. Che, Techno‐economic analysis of a novel hybrid heat pump system to recover waste heat and condensate from the low‐temperature boiler exhaust gas, Int J Energy Res 44 (2020) 3821–3838. https://doi.org/10.1002/er.5172.

[112] S. Shamsi, A. Negash, G. Cho, Y. Kim, Waste Heat and Water Recovery System Optimization for Flue Gas in Thermal Power Plants, Sustainability 11 (2019) 1881. https://doi.org/10.3390/su11071881.

[113] A. Zajacs, R. Bogdanovics, A. Borodinecs, Analysis of low temperature lift heat pump application in a district heating system for flue gas condenser efficiency

improvement, Sustainable Cities and Society 57 (2020) 102130. https://doi.org/10.1016/j.scs.2020.102130.

[114] P. M. G. B. D. M. M. K. Hertle H, Wärmewende in Kommunen, Leitfaden für den klimafreundlichen Umbai der Wärmeversorgung, 2015.

[115] B. Hebenstreit, R. Schnetzinger, R. Ohnmacht, E. Höftberger, J. Lundgren, W. Haslinger, A. Toffolo, Techno-economic study of a heat pump enhanced flue gas heat recovery for biomass boilers, Biomass and Bioenergy 71 (2014) 12–22. https://doi.org/10.1016/j.biombioe.2014.01.048.

[116] R. Jakobs, Heat Pump Application in Commercial and Industrial Processes. Information centre on heat pumps and refrigeration, International Workshop on High-Temperature Heatpumps, Copenhagen Denmark, 2017.

[117] Stefan Wolf, Integration von Wärmepumpen in industrielle Produktionssysteme: Potenziale und Instrumente zur Potenzialerschließung. Dissertation, Stuttgart, 2016.

[118] B. Hebenstreit, R. Schnetzinger, E. Höftberger, Endbericht ActiveCond: Aktive Abgaskondensation mit Wärmepumpen zur Effizienzsteigerung bei seriennahen, automatisch beschickten Holzfeuerungen, 2012.

[119] Nussbaumer, T., Thalmann, S., Jenni, A. und Ködel, J., Planungshandbuch Fernwärme, Version first.first vom twenty-first. September twentiethseventeenth, EnergieSchweiz Bundesamt für Energie, Ittigen, Bern, 2017.

[120] M. Gaderer, G. Gallmetzer, H. Spliethoff, Biomass fired hot air gas turbine with fluidized bed combustion, Applied Thermal Engineering 30 (2010) 1594–1600. https://doi.org/10.1016/j.applthermaleng.2010.03.015.

[121] M. Gaderer, Wärmenutzung bei kleinen landwirtschaftlichen Biogasanlagen, Augsburg, 2007.

[122] Z.Y. Xu, J.T. Gao, B. Hu, R.Z. Wang, Multi-criterion comparison of compression and absorption heat pumps for ultra-low grade waste heat recovery, Energy 238 (2022) 121804. https://doi.org/10.1016/j.energy.2021.121804.

[123] Z. Tan, X. Feng, Y. Wang, Performance comparison of different heat pumps in low-temperature waste heat recovery, Renewable and Sustainable Energy Reviews 152 (2021) 111634. https://doi.org/10.1016/j.rser.2021.111634.

[124] F. Bühler, S. Petrović, K. Karlsson, B. Elmegaard, Industrial excess heat for district heating in Denmark, Applied Energy 205 (2017) 991–1001. https://doi.org/10.1016/j.apenergy.2017.08.032.

[125] T.K. Marek Miara, Heat Pump Efficiency: Analysis and Evaluation of Heat Pump Efficiency in Real-life Conditions, Freiburg. https://wp-monitoring.ise.fraunhofer.de/wp-effizienz/download/final_report_wp_effizienz_en.pdf (accessed 10 May 2021).

[126] W.C. Sebastian Pater, Real and theoretical energy efficiency of vapour compression heat pumps, Czasopismo Techniczne 5 (2017). https://doi.org/10.4467/2353737XCT.17.080.6437.

[127] Statista Research Department, Strompreise für Industriekunden in ausgewählten europäischen Ländern nach Verbrauchsmenge im Jahr 2021. https://de.statista.com/statistik/daten/studie/151260/umfrage/strompreise-fuer-industriekunden-in-europa/ (accessed 7 July 2022).

[128] DIN EN 13203-4:2021-03, Gasbeheizte Geräte für die sanitäre Warmwasserbereitung für den Hausgebrauch_- Teil_4: Bewertung des Energieverbrauchs von Gasgeräten mit Kraft-Wärme-Kopplung (Mikro-KWK) zur Warmwasserbereitung und Stromerzeugung; Deutsche und Englische Fassung prEN_13203-4:2021, Beuth Verlag GmbH, Berlin.

[129] I. Dincer, C. Zamfirescu, 1.5 Thermodynamic Aspects of Energy, in: Comprehensive Energy Systems, Elsevier, 2018, pp. 153–211.

[130] M.B. Raphael Lechner, Combined heat and power generation - Technology Overview. https://www.bayern-innovativ.de/en/networks-und-thinknet/overview-energy/energy-technology-cluster/page/combined-heat-and-power-a-technology-overview.

[131] O. Badr, S. Naik, P.W. O'Callaghan, S.D. Probert, Expansion machine for a low power-output steam Rankine-cycle engine, Applied Energy 39 (1991) 93–116. https://doi.org/10.1016/0306-2619(91)90024-R.

[132] Bidini G., Manuali A., Saetta S., Hubkolben-Dampfmaschinen-Kraftwerke, die mit Holzabfällen gespeist werden, Int. J. Energie Res, 1998.

[133] K. Alanne, K. Saari, M. Kuosa, J. Jokisalo, A.R. Martin, Thermo-economic analysis of a micro-cogeneration system based on a rotary steam engine (RSE), Applied Thermal Engineering 44 (2012) 11–20. https://doi.org/10.1016/j.applthermaleng.2012.03.026.

[134] M. Badami, M. Mura, Preliminary design and controlling strategies of a small-scale wood waste Rankine Cycle (RC) with a reciprocating steam engine (SE), Energy 34 (2009) 1315–1324. https://doi.org/10.1016/j.energy.2009.04.031.

[135] Organic Rankine Cycle (ORC) systems: Renewable and Sustainable Energy Reviews. Renewable and Sustainable Energy Reviews (2013).

[136] H. Yu, X. Feng, Y. Wang, Working Fluid Selection for Organic Rankine Cycle (ORC) Considering the Characteristics of Waste Heat Sources, Ind. Eng. Chem. Res. 55 (2016) 1309–1321. https://doi.org/10.1021/acs.iecr.5b02277.

[137] S. Quoilin, M. van den Broek, S. Declaye, P. Dewallef, V. Lemort, Techno-economic survey of Organic Rankine Cycle (ORC) systems, Renewable and Sustainable Energy Reviews 22 (2013) 168–186. https://doi.org/10.1016/j.rser.2013.01.028.

[138] U. Drescher, D. Brüggemann, Fluid selection for the Organic Rankine Cycle (ORC) in biomass power and heat plants, Applied Thermal Engineering 27 (2007) 223–228. https://doi.org/10.1016/j.applthermaleng.2006.04.024.

[139] Turboden S.p.A., ORC System. http://www.turboden.eu/en/references/references.php? (accessed 3 November 2020).

[140] F. Patuzzi, D. Prando, S. Vakalis, A.M. Rizzo, D. Chiaramonti, W. Tirler, T. Mimmo, A. Gasparella, M. Baratieri, Small-scale biomass gasification CHP systems: Comparative performance assessment and monitoring experiences in South Tyrol (Italy), Energy 112 (2016) 285–293. https://doi.org/10.1016/j.energy.2016.06.077.

[141] L. Tocci, T. Pal, I. Pesmazoglou, B. Franchetti, Small Scale Organic Rankine Cycle (ORC): A Techno-Economic Review, Energies 10 (2017) 413. https://doi.org/10.3390/en10040413.

[142] Ingwald Obernberger, Freidrich Biedermann, Peter Thonhofer, Neue Klein-ORC-Technologie (200 kWel) für dezentrale Biomasse-KWK-Anlagen, in: VDI-Bericht 2044 "Strom und Wärme aus biogenen Festbrennstoffen", pp. 133–150.

[143] Dietrich Vogel, Schmid AG energy solutions, Weiterentwicklung und Optimierung einer Heissluftturbine im kleineren Leistungsbereich (80-95 kWel), Bern, 2017.

[144] D.G. Thombare, S.K. Verma, Technological development in the Stirling cycle engines, Renewable and Sustainable Energy Reviews 12 (2008) 1–38. https://doi.org/10.1016/j.rser.2006.07.001.

[145] Petra Blank, skript-Stirlingmotor: Arbeitsunterlagen für den Hauptfach- und APMB-Versuch, Stuttgart, 2002.

[146] BIOS BIOENERGIESYSTEME GmbH, Beschreibung der Biomasse-Kraft-Wärme-Kopplungstechnologie auf Basis Stirlingmotor, 2005. https://www.bios-bioenergy.at/de/strom-aus-biomasse/stirlingmotor.html (accessed 6 December 2020).

[147] F. Biedermann, Henrik Carlsen, M. Schoech, I. Obernberger, Operating Experiences with a Small-scale CHP Pilot Plant based on a 35 kWel Hermetic Four Cylinder Stirling Engine for Biomass Fuels, in: Proceedings of the 11th International Stirling Engine Conference, Department of Mechanical and Aeronautical Engineering, 2003.

[148] Hien-Thanh Le, Huynh Hoang Nghia, Bui Minh Huy, Vu Thanh Phu, Vy Bui Hoang Quyen, STIRLING ENGINE: FROM DESIGN TO APPLICATION INTO PRACTICE AND EDUCATION (2022). https://doi.org/10.5281/zenodo.6499767.

[149] C. Dejtrakulwong, S. Patumsawad, Four Zones Modeling of the Downdraft Biomass Gasification Process: Effects of Moisture Content and Air to Fuel Ratio, Energy Procedia 52 (2014) 142–149. https://doi.org/10.1016/j.egypro.2014.07.064.

[150] J. François, L. Abdelouahed, G. Mauviel, M. Feidt, C. Rogaume, O. Mirgaux, F. Patisson, A. Dufour, Estimation of the energy efficiency of a wood gasification CHP plant using Aspen Plus, Chemical engineering transactions 29 (2012) 769–774.

[151] G. Jankes, M. Trninic, M. Stamenic, T. Simonovic, N. Tanasic, J. Labus, Biomass gasification with CHP production: A review of state of the art technology and near

future perspectives, Therm sci 16 (2012) 115–130. https://doi.org/10.2298/TSCI120216066J.

[152] Spanner Re² GmbH, Convert biomass into energy by gasification. https://www.holz-kraft.com/en/183-aktuelles/blogeintraege/344-18-09-13-nachhaltige-holz-wertschoepfung-vor-ort (accessed 2 March 2022).

[153] Burkhardt GmbH, Biomass power plants: cogeneration with wood: Heat and power from wood pellets. https://burkhardt-gruppe.de/en/power-engineering/heat-and-power-from-wood/ (accessed 2 March 2022).

[154] HARGASSNER Ges mbH, Hargassner - heating technology of the future: Modern and highly efficient heating systems. https://www.hargassner.at/en/ (accessed 2 March 2022).

[155] Fröling GmbH, Holzverstromungsanlage & Festbettvergaser CHP: Wärme UND Strom aus Holz mit dem Fröling CHP. https://www.froeling.com/at/produkte/waerme-und-strom/holzverstromungsanlage-chp-50.html (accessed 2 March 2022).

[156] SYNCRAFT® Engineering, Overview of wood power plants. https://en.syncraft.at/wood-power-plants/overview (accessed 2 March 2022).

[157] URBAS Energietechnik, Wood gas CHP - the innovation. https://www.urbas.at/wp-content/uploads/2020/09/p_URBAS_DE_KWK_7.8.web_WF.PDF-en.pdf (accessed 2 March 2022).

[158] Chaudhary Awais Salman, Hailong Li, Peng Li, Jinyue Yan, Improve the flexibility provided by combined heat and power plants (CHPs) - a review of potential technologies, e-Prime - Advances in Electrical Engineering, Electronics and Energy 1 (2021). https://doi.org/10.1016/j.prime.2021.100023.

[159] P.A. Ostergaard, A.N. Andersen, Booster heat pumps and central heat pumps in district heating, Applied Energy 184 (2016) 1374–1388. https://doi.org/10.1016/j.apenergy.2016.02.144.

[160] G. Vigants, G. Galindoms, E. Vigants, I. Veidenbergs, D. Blumberga, Heat Pump Application for Efficient DH Systems, Energy Procedia 61 (2014) 2168–2171. https://doi.org/10.1016/j.egypro.2014.12.101.

[161] Markus Köfinger, Roman Geyer, Daniele Basciotti, Methoden zur Auswahl, Auslegung und Integration von Wärmepumpen, 2017.

[162] Heizwerk St.Gilgen, Hydraulik Anlagenschemata aus VAS DOKU.

[163] J. Xu, C. Yu, Critical temperature criterion for selection of working fluids for subcritical pressure Organic Rankine cycles, Energy 74 (2014) 719–733. https://doi.org/10.1016/j.energy.2014.07.038.

[164] P.J. Mago, L.M. Chamra, C. Somayaji, Performance analysis of different working fluids for use in organic Rankine cycles, Proceedings of the Institution of Mechanical Engineers, Part A: Journal of Power and Energy 221 (2007) 255–263. https://doi.org/10.1243/09576509JPE372.

[165] I.H. Bell, J. Wronski, S. Quoilin, V. Lemort, Pure and Pseudo-pure Fluid Thermophysical Property Evaluation and the Open-Source Thermophysical Property Library CoolProp, Ind. Eng. Chem. Res. 53 (2014) 2498–2508. https://doi.org/10.1021/ie4033999.

[166] P. Byrne, R. Ghoubali, J. Miriel, Scroll compressor modelling for heat pumps using hydrocarbons as refrigerants, International Journal of Refrigeration 41 (2014) 1–13. https://doi.org/10.1016/j.ijrefrig.2013.06.003.

[167] H. Shen, C. Zhang, J. Zhang, B. Yang, B. Jia, Applicable and Comparative Research of Compressor Mass Flow Rate and Isentropic Efficiency Empirical Models to Marine Large-Scale Compressor, Energies 13 (2020) 47. https://doi.org/10.3390/en13010047.

[168] G. Wang, Z. Chen, C. Li, B. Jiang, Preliminary theoretical analyses of thermal performance and available energy consumption of two-stage cascade cycle heat pump water heater, International Journal of Refrigeration 82 (2017) 381–388. https://doi.org/10.1016/j.ijrefrig.2017.06.016.

[169] W.C. Whitman, W.M. Johnson, J.A. Tomczyk, Refrigeration & air conditioning technology, fifth. ed., Thomson Delmar Learning, Clifton Park, NY, 2005.

[170] S.-W. Hsu, H.-W. Chiang, C.-W. Yen, Experimental Investigation of the Performance of a Hermetic Screw-Expander Organic Rankine Cycle, Energies 7 (2014) 6172–6185. https://doi.org/10.3390/en7096172.

[171] A. Borsukiewicz-Gozdur, Pumping work in the organic Rankine cycle, Applied Thermal Engineering 51 (2013) 781–786. https://doi.org/10.1016/j.applthermaleng.2012.10.033.

[172] J. Ahrenfeldt, T.P. Thomsen, U. Henriksen, L.R. Clausen, Biomass gasification cogeneration – A review of state of the art technology and near future perspectives, Applied Thermal Engineering 50 (2013) 1407–1417. https://doi.org/10.1016/j.applthermaleng.2011.12.040.

[173] Magdalena Berberich, Entwicklung multifunktionaler Systeme zur solar unterstützten Kraft-Wärme-Kopplung – solare Fernwärme und saisonale Wärmespeicher für die Energiewende, Stuttgart, 2015.

[174] K. Koch, P. Höfner, M. Gaderer, Techno-economic system comparison of a wood gas and a natural gas CHP plant in flexible district heating with a dynamic simulation model, Energy 202 (2020) 117710. https://doi.org/10.1016/j.energy.2020.117710.

[175] M.A. Rosen, M.N. Le, I. Dincer, Efficiency analysis of a cogeneration and district energy system, Applied Thermal Engineering 25 (2005) 147–159. https://doi.org/10.1016/j.applthermaleng.2004.05.008.

[176] M. Wirtz, L. Kivilip, P. Remmen, D. Müller, 5th Generation District Heating: A novel design approach based on mathematical optimization, Applied Energy 260 (2020) 114158. https://doi.org/10.1016/j.apenergy.2019.114158.

[177] Bargel, Stefan, Entwicklung eines exergiebasierten Analysemodells zum umfassenden Technologievergleich von Wärmeversorgungssystemen unter Berücksichtigung des Einflusses einer veränderlichen Außentemperatur.

[178] VDI 2067 Sheet 1, Economic efficiency of technical building systems: Basics and cost calculation, 2012.

[179] The Chemical Engineering Plant Cost Index. https://www.chemengonline.com/pci-home (accessed 7 October 2022).

[180] Petra Icha, Development of the specific carbon dioxide emissions of the German electricity mix in the years 1990 - 2020, Dessau-Roßlau, 2021.

[181] A. Gonzalez-Garay, G. Guillen-Gosalbez, SUSCAPE: A framework for the optimal design of SUStainable ChemicAl ProcEsses incorporating data envelopment analysis,

Chemical Engineering Research and Design 137 (2018) 246–264. https://doi.org/10.1016/j.cherd.2018.07.009.

[182] L. Weimann, P. Gabrielli, A. Boldrini, G.J. Kramer, M. Gazzani, On the role of H2 storage and conversion for wind power production in the Netherlands, in: 29th European Symposium on Computer Aided Process Engineering, Elsevier, 2019, pp. 1627–1632.

[183] J. Kronqvist, D.E. Bernal, A. Lundell, I.E. Grossmann, A review and comparison of solvers for convex MINLP, Optim Eng 20 (2019) 397–455. https://doi.org/10.1007/s11081-018-9411-8.

[184] Bernhard Meindl, Matthias Templ (Eds.), Analysis of commercial and free and open source solvers for linear optimization problems, 2012.

[185] R.C. Pattison, C. Tsay, M. Baldea, Pseudo-transient models for multiscale, multiresolution simulation and optimization of intensified reaction/separation/recycle processes: Framework and a dimethyl ether production case study, Computers & Chemical Engineering 105 (2017) 161–172. https://doi.org/10.1016/j.compchemeng.2016.12.019.

[186] M. Skiborowski, M. Rautenberg, W. Marquardt, A Hybrid Evolutionary–Deterministic Optimization Approach for Conceptual Design, Ind. Eng. Chem. Res. 54 (2015) 10054–10072. https://doi.org/10.1021/acs.iecr.5b01995.

[187] D. Ibrahim, M. Jobson, G. Guillén-Gosálbez, Optimization-Based Design of Crude Oil Distillation Units Using Rigorous Simulation Models, Ind. Eng. Chem. Res. 56 (2017) 6728–6740. https://doi.org/10.1021/acs.iecr.7b01014.

[188] C.A. Coello Coello, G.B. Lamont, D.A. van Veldhuizen, Evolutionary algorithms for solving multi-objective problems, secondnd ed., Springer, New York, London, 2007.

[189] Z. Michalewicz, M. Schoenauer, Evolutionary Algorithms for Constrained Parameter Optimization Problems, Evolutionary Computation 4 (1996) 1–32. https://doi.org/10.1162/evco.1996.4.1.1.

[190] V. Jothiprakash, G. Shanthi, Single Reservoir Operating Policies Using Genetic Algorithm, Water Resour Manage 20 (2006) 917–929. https://doi.org/10.1007/s11269-005-9014-y.

[191] R.T. Marler, J.S. Arora, The weighted sum method for multi-objective optimization: new insights, Struct Multidisc Optim 41 (2010) 853–862. https://doi.org/10.1007/s00158-009-0460-7.

[192] M. Ehrgott, Multicriteria optimization, secondnd ed., Springer, Berlin, London, 2005.

[193] S.A. Hosseini, N. Amjady, M. Shafie-khah, J.P. Catalão, A new multi-objective solution approach to solve transmission congestion management problem of energy markets, Applied Energy 165 (2016) 462–471. https://doi.org/10.1016/j.apenergy.2015.12.101.

[194] V. Tulus, M.H. Abokersh, L.F. Cabeza, M. Vallès, L. Jiménez, D. Boer, Economic and environmental potential for solar assisted central heating plants in the EU residential sector: Contribution to the 2030 climate and energy EU agenda, Applied Energy 236 (2019) 318–339. https://doi.org/10.1016/j.apenergy.2018.11.094.

[195] Fei Guo, scikit-opt, Fei Guo.

[196] V. A. S. process engineering, plant systems mbH, Operating Instructions of V. A. S. Firing system: components, A-5084 GROSSGMAIN.

[197] W. Gappmaier, Technische Daten Heizwerk Tamsweg. Interview, Tamsweg, 2019.

[198] O. Askari, M. Janbozorgi, R. Greig, A. Moghaddas, H. Metghalchi, Developing alternative approaches to predicting the laminar burning speed of refrigerants using the minimum ignition energy, Science and Technology for the Built Environment 21 (2015) 220–227. https://doi.org/10.1080/10789669.2014.975059.

[199] Heizwerk St. Gilgen, Betrieb von Abgaskondensation, St.Gigen, 2019.

[200] Österreichisches Institut für Bautechnik, RICHTLINIEN DES ÖSTERREICHISCHEN INSTITUTS FÜR BAUTECHNIK: Energieeinsparung und Wärmeschutz. OIB-Leitfaden Energietechnisches Verhalten von Gebäuden, 2019.

[201] Forty-fourth Ordinance on the Implementation of the Federal Immission Control Act: § 10 Emission limit values for combustion plants using solid fuels, Federal Office of Justice. http://www.gesetze-im-internet.de/bimschv_44/__10.html (accessed 22 July 2022).

[202] Bitzer Kühlmaschinenbau GmbH, KÄLTEMITTEL REPORT 20, Eschenbrünnlestraße 15, 71065 Sindelfingen, 2018.

[203] A.G. Devecioğlu, V. Oruç, Characteristics of Some New Generation Refrigerants with Low GWP, Energy Procedia 75 (2015) 1452–1457. https://doi.org/10.1016/j.egypro.2015.07.258.

[204] Mark McLinden, Eric Lemmon, Marcia Huber (Eds.), The Refprop Database for the Thermophysical Properties of Refrigerants, Proceedings of the 20th International Congress of Refrigeration, 2003.

[205] J.M. Calm, The toxicity of refrigerants (1996).

[206] T. Erhart, J. Gölz, U. Eicker, M. van den Broek, Working Fluid Stability in Large-Scale Organic Rankine Cycle-Units Using Siloxanes—Long-Term Experiences and Fluid Recycling, Energies 9 (2016) 422. https://doi.org/10.3390/en9060422.

[207] G. Ratzberger, Untersuchung verschiedener Fluide im überkritischen ORC Prozess. Diplomarbeit, Graz, 2014.

[208] Marta Trninić, Goran Jankes, Mirjana Stamenić, Tomislav Simonović and Nikola Tanasić, Industrial Scale Demonstration Plant with Downdraft Gasifier coupled to Pebble Bed Regenerative Heater for CHP Production (2012).

[209] Chris Higman, Maarten van der Burgt (Eds.), Gasification, Gulf Professional Publishing, Burlington, 2003.

[210] M. Gaderer, WDesign: Auslegung von Wärmeerzeugern zur Nahwärme-Bedarfsdeckung und Stromerzeugung für dezentrale Biomasseheiz(kraft)werke, Berechnungsprogramm zur technischen und wirtschaftlichen Beurteilung von Heiz(kraft)werken mit Nahwärmeverteilung, Bayerische Staatsministerium für Landwirtschaft und Forsten, Straubing, Bayern, 2005.

[211] J. Piteľ, J. Mižáková, A. Hošovský, Biomass Combustion Control and Stabilization Using Low-Cost Sensors, Advances in Mechanical Engineering 5 (2013) 685157. https://doi.org/10.1155/2013/685157.

[212] A. Elorf, B. Sarh, Excess air ratio effects on flow and combustion caracteristics of pulverized biomass (olive cake), Case Studies in Thermal Engineering 13 (2019) 100367. https://doi.org/10.1016/j.csite.2018.100367.

[213] Y. Chen, P. Standl, S. Weiker, M. Gaderer, A general approach to integrating compression heat pumps into biomass heating networks for heat recovery, Applied Energy 310 (2022) 118559. https://doi.org/10.1016/j.apenergy.2022.118559.

[214] Yusheng Chen, Tong Guo, Matthias Gaderer, Thermodynamic Analysis of the Design of a Heat Pump for Heat Recovery in a Biomass Heating Network, EnerarXiv (2022).

[215] B. Sahin, K. Yakut, I. Kotcioglu, C. Celik, Optimum design parameters of a heat exchanger, Applied Energy 82 (2005) 90–106. https://doi.org/10.1016/j.apenergy.2004.10.002.

[216] D. Dović, I. Horvat, P. Filipović, Impact of velocities and geometry on flow components and heat transfer in plate heat exchangers, Applied Thermal Engineering 197 (2021) 117371. https://doi.org/10.1016/j.applthermaleng.2021.117371.

[217] W. Zhang, S. Wang, L. Mu, Condensation heat transfer characteristics of flue gas on anti-corrosive coated finned tubes, Applied Thermal Engineering 189 (2021) 116672. https://doi.org/10.1016/j.applthermaleng.2021.116672.

[218] S. Wang, Z. Wen, others, Heat transfer performance of condensing flue heat exchangers with anticorrosion films, Heating Ventilation Air Conditioning 35 (2005) 71–74.

[219] J. Malaťáková, M. Jankovský, J. Malaťák, J. Velebil, B. Tamelová, A. Gendek, M. Aniszewska, Evaluation of Small-Scale Gasification for CHP for Wood from Salvage Logging in the Czech Republic, Forests 12 (2021) 1448. https://doi.org/10.3390/f12111448.

[220] VDI 2067 Blatt 1, Wirtschaftlichkeit gebäudetechnischer Anlagen: Grundlagen und Kostenberechnung, 2012.

[221] C.A.R.M.E.N e.V., Marktpreise Hackschnitzel: Preisentwicklung bei Waldhackschnitzeln, 2020. https://www.carmen-ev.de/service/marktueberblick/marktpreise-energieholz/marktpreise-hackschnitzel/ (accessed 18 December 2020).

[222] German Pellet Institute, Fuel cost development of oil, gas and pellets: Price of pellets, 2022. https://www.depi.de/pelletpreis-wirtschaftlichkeit.

[223] German Federal Association of the Energy and Water Industries, BDEW electricity price analysis April 2022, 2022.

[224] Marek, Operation instructions: V.A.S. condensation systems.

[225] Dr. Martin Pehnt, Peter Mellwig, Sebastian Blömer, Hans Hertle, Michael Nast, Amany von Oehsen, Study on primary energy factors: Report in accordance with the framework contract for consulting services for Department II of the BMWi, Heidelberg. https://www.gih.de/wp-content/uploads/2019/05/Untersuchung-zu-Prim%C3%A4renergiefaktoren.pdf (accessed 22 April 2021).

List of Figures

List of Tables

List of Abbreviations

AP	Air preheater
BHN	Biomass Heating Network
BImSchV	German Federal Immission Control Ordinance
BMUB	German Federal Ministry for the Environment
BOI	Boiler
CAPEX	Annual Capital Expenditure
CFC	Chlorofluorocarbon
CHP	Combined Heat and Power
COND	Flue gas condenser
COP	Coefficient Of Performance
ECO	Economizer
EU	European Union
FUH	Annual Full Utilization Hours
GA	Genetic Algorithm
GCHP	biomass Gasifier Combined Heat and Power
GWP	Global Warming Potential
HEX	Heat Exchanger
HHV	Higher Heating Value
HP	Heat Pump
HT-RF	High Temperature Return Flow
LCOE	Levelized Cost of Energy
LHV	Lower Heating Value
LT-RF	Low Temperature Return Flow

MILP	Mixed Integer Linear Programming
MINLP	Mixed-Integer Non-Linear Problem
MIP	Mixed-Integer Programming
MOO	Multi-Objective Optimization
Net	Network
O&M	Operation & Maintenance
ODP	Ozone Depletion Potential
OPEX	Annual Operational Expenditure.
ORC	Organic Rankine Cycle
OWF	Organic Working Fluid
SRC	Steam Rankine Cycle
TAC	Annual Total Acquisition Cost
VDI	Verein Deutscher Ingenieure

List of Notations

Symbol	Description
η_{ulti}	Fuel utilization rate (-)
Q_{util}	Ultilized heat (KJ)
H_{fuel}	Chemical energy contained in fuel (MJ/kg)
U	heat transfer coefficient (W/m^2K)
$\dot{Q}_{hex}$	heat transfer rate of heat exchanger (W)
ΔT_m	Logarithmic mean temperature difference (K)
A	Area (m^2)
Nu	Nusselt number (-)
α	heat transfer coefficient (W/m^2K)
$L_{char.}$	characteristic length (m)
λ	thermal conductivity (W/mK)
Re	Reynolds number (-)
Ja	Jacob number (-)
u	Velocity (m/s)
ν	kinematic viscosity (m^2/s)
$x_{H20,fg,in}$	Water vapor content of the flue gas entering the condenser (kg_{H20}/m^3_{fg})
$x_{sat\ H20,fg,cond}$	Saturated water vapor content at the average temperature of the condensing surface (kg_{H20}/m^3_{fg})
$T_{fg,in}$	Inlet temperature of the flue gas in the condenser (°C)
$T_{fg,cond}$	Average temperature of the condensing surface (°C)
c_p	Specific heat capacity of water (*kJ/kgK*)
r	latent heat of condensation of water vapor (*KJ/kg*)
λ	Combustion air ratio (-)
n_{air}	Molar amount of supplied combustion air
$n_{air,min}$	Minimum amount of air required for complete combustion
$O_{2,dry}$	volume concentration of oxygen in dry flue gas
w	Fuel water content ($kg_{H20}/kg_{wet\ fuel}$)
u	Fuel moisture ($kg_{H20}/kg_{dry\ fuel}$)
π	Pressure ratio (-)

$\boldsymbol{p_c}$	Condensing pressure of heat pump (*bar*)
$\boldsymbol{p_e}$	Evaporating pressure of heat pump (*bar*)
$\boldsymbol{\dot{Q}_{sink}}$	heat flow for heat sink (kW)
$\boldsymbol{P_{comp}}$	power of the compressor (kW)
$\boldsymbol{T_c}$	Condensing temperature of heat pump (°C)
$\boldsymbol{T_e}$	Evaporating temperature of heat pump (°C)
$\boldsymbol{\eta_{relative}}$	relative coefficient of performance of heat pump (-)
$\boldsymbol{\dot{Q}_{des}}$	Desorption heat of absorption heat pump (kW)
$\boldsymbol{T_h}$	Heating temperature of absorption heat pump (kW)
$\boldsymbol{\dot{m}_s^{in}}$	Inlet mass flow of substance *s* (kg/s)
$\boldsymbol{\dot{m}_s^{out}}$	Outlet mass flow of substance *s* (kg/s)
$\boldsymbol{\dot{Q}_{boiler}}$	Boiler heat output (kW)
$\boldsymbol{\dot{Q}_{loss}}$	Boiler heat loss (kW)
$\boldsymbol{h_s^{in}}$	Inlet specific enthalpy of substance *s* (kJ/kg)
$\boldsymbol{h_s^{out}}$	Outlet specific enthalpy of substance *s* (kJ/kg)
$\boldsymbol{lhv_s}$	Lower heating value of substance *s* (kJ/kg)
$\boldsymbol{\dot{m}_f}$	Fuel mass flow (kg/s)
$\boldsymbol{\Delta\dot{m}_c}$	Mass flow of condensation water (kg/s)
$\boldsymbol{\dot{m}_{clt}^{in}}$	In-/outlet mass flow of cooling medium (kg/s)
$\boldsymbol{\dot{m}_{clt}^{out}}$	Outlet mass flow of cooling medium (kg/s)
$\boldsymbol{h_c}$	Specific enthalpy of condensing water (kJ/kg)
$\boldsymbol{t_{fg}^{out}}$	Outlet temperature of flue gas (°C)
$\boldsymbol{p_{H2O}^{in}}$	Inlet water vapor partial pressure (bar)
$\boldsymbol{p_{H2O}^{out}}$	Outlet water vapor partial pressure (bar)
$\boldsymbol{p_{H2O,sat}^{out}}$	Saturated outlet water vapor partial pressure (bar)
$\boldsymbol{p_{fg}^{in}}$	Inlet pressure of flue gas (bar)
$\boldsymbol{\dot{n}_{H2O}}$	molar amount of water vapor in wet flue gas (mol)
$\boldsymbol{\dot{n}_{fg,dry}^{tot}}$	molar amount of dry flue gas (mol)
$\boldsymbol{M_{H2O}}$	Molas mass of water (kg/kmol)
$\boldsymbol{\dot{Q}_{hex}}$	Heat output of heat exchanger (kW)
$\boldsymbol{\Delta T_e}$	Minimal temperature difference between source outlet and evaporating (K)

ΔT_c	Minimal temperature difference between sink outlet and condensing (K)
η_{is}	Isentropic efficiency (-)
η_m	Mechanical efficiency (-)
η_{el}	Electrical efficiency (-)
η_{th}	Thermal efficiency (-)
η_{iso}	Valve isolation efficiency (-)
η_{pump}	Pump efficiency (-)
η_{eg}	Generator efficiency (-)
η_{hex}	Energy efficiency of heat exchanger (-)
ΔT_{hex}	Minimal temperature difference inside heat exchanger (K)
ΔT_{sh}	Superheating temperature (K)
T_{crit}	Critical point of refrigerant (°C)
$ref.$	Refrigerant (-)
$\dot{m}_{ref}$	Mass flow of refrigerant (kg/s)
$\dot{m}_{wf}$	Mass flow of working fluid (kg/s)
k	Power drop factor (-)
z	Modulation of equipment (-)
σ	Power to heat ratio of the cogeneration (-)
$P_{el,gchp}$	Electrical output of GCHP (kW)
$\dot{Q}_{th,gchp}$	Thermal output of GCHP (kW)
η_{gchp}	Total efficiency of GCHP (-)
$\eta_{gasifier}$	Gasification efficiency of Gasifier (-)
$\dot{m}_{f,gchp}$	Fuel demand of GCHP (kg/s)
$\dot{m}_{main}^{net}$	Flow rate of main network (kg/s)
$\dot{Q}_{demand}$	Demand of heating network (kW)
T_{feed}^{net}	Feed forward temperature of main network (°C)
T_{return}^{net}	Return temperature of main network (°C)
x_i	Fuel element *i* composition (-)
H_f	Heating value of fuel (MJ/kg)
Q_n	Nominal heat output (kW)
$T_{combustion}$	Combustion temperature (°C)
T_{ash}	Ash temperature (°C)

$T_{surface}$	Surface temperature (°C)
$\dot{Q}_{furnace}$	Furnace total performance (kW)
$P_{gen.el}$	Generator power output (kW)
$\eta_{gen.el}$	Generator efficiency (-)
z_{min}	Minimal operating modulation (-)
z_{max}	Maximal operating modulation (-)
T_{in}^{hex}	Inlet temperature of heat exchanger (°C)
T_{out}^{hex}	Outlet temperature of heat exchanger (°C)
$\sum y_{fg,in}^{hex}$	Inlet flue gas composition of heat exchanger (-)
$\sum y_{fg,out}^{hex}$	Outlet flue gas composition of heat exchanger (-)
$\dot{Q}_{hp\ evap}$	Heat source for heat pump evaporator (kW)
$\dot{Q}_{cond}$	Heat output of flue gas condenser (kW)
$\dot{m}_{to\ hp\ evap}^{cooled\ net}$	Diverted network water flow to heat pump evaporator (kg/s)
$T_{to\ cond}^{cooled\ net}$	Temperature of cooled return flow (°C)
$\dot{Q}_{fg,latent}$	Latent heat performance of flue gas condensation (kW)
T_{dew}^{fg}	Dew point of flue gas (°C)
T_{hp}	Heat pump supply temperature (°C)
$\dot{Q}_{hp}$	Heat output of heat pump (kW)
$P_{hp,el}$	Electricity demand of heat pump (kW)
$\dot{Q}_{to\ chp}$	Required heat demand of CHP units (kW)
$\dot{Q}_{chp}$	Heat supply of CHP units to network (kW)
f_{size}	Sizing factor (-)
S_t	Set of time series over a year (-)
dt	Time interval of the demand time series (h)
$f_{lhv,sys}$	System overall energy efficiency (-)
$f_{ex,overall}$	System overall exergy efficiency (-)
$P_{surplus}$	Performance surplus electricity (kW)
$P_{el\ from\ grid}$	Auxiliary electricity for power grid (kW)
β_f	Merit of the fuel (-)
I_c	Initial investment of component c (€)

$a_{inv,c}$	Annualization factor of component c (1/a)
$f_{o\&m,c}$	Operating and maintenance factor (-)
$c_{f,i}$	Price of fuel I (€/kWh)
c_{el}	Price of electricity (€/kWh)
$c_{ash\ \&\ cleaning}$	Price of ash disposal and cleaning (€/kWh)
$e_{CO2,sys}$	System specific equivalent CO_2 emissions (kg_{CO2}/kWh)
f_{CO2}	CO_2 emission factor (kg_{CO2}/kWh)
$e_{PE,sys}$	System specific equivalent primary energy demand (kWh_{PE}/kWh)
f_{PE}	Primary energy factor (kWh_{PE}/kWh)
v	Connection variant of the heat pump (-)
b	Type of CHP unit (-)
lb	Lower boundary (-)
ub	Upper boundary (-)
α_i	Non-negative scalar weight (-)
$\vec{x}$	Vector of the decision variables (-)
$f_i(\vec{x})$	Objective function *i* (-)
f_i^{ut}	Utopia points of the i corresponded $f_i(\vec{x})$ (-)
f_i^{na}	Pseudo nadir points of the i corresponded $f_i(\vec{x})$ (-)
$\hat{f}_i(\vec{x})$	Normalization function *i* (-)

Publications

Previous publications resulting within the frame of this dissertation:

- Y. Chen, P. Standl, S. Weiker; M. Gaderer (2021): Data and Model Based Analysis of Heat Pump Integrated Biomass Heating Plants. Proceedings of the 29th European Biomass Conference and Exhibition 26-29 April 2021, 2021, pp. 1297-1299. doi:10.5071/29THEUBCE2021-5CO.5.3.
- Y. Chen, T. Guo, M. Gaderer, Volume 19: Sustainable Energy Solutions for a Post-COVID Recovery towards a Better Future: Part II, 2021. doi:https://doi.org/10.46855/energy-proceedings-9239.
- Y. Chen, P. Standl, S. Weiker, M. Gaderer, A general approach to integrating compression heat pumps into biomass heating networks for heat recovery, Applied Energy 310 (2022) 118559. https://doi.org/10.1016/j.apenergy.2022.118559.
- Y. Chen, T. Guo, J. Kainz, M. Krigel, M. Gaderer, Design of a biomass-heating network with an integrated heat pump: A simulation-based multi-objective optimization framework, Applied Energy 326 (2022) 119922. https://doi.org/10.1016/j.apenergy.2022.119922.
- M. Gaderer, Y. Chen, Professur für Regenerative Energiesysteme, Schlussbericht BioKond: Biomasseheizwerke mit hocheffizienter Wärmeauskopplung durch die innovative Integration einer Abgaskondensationswärmepumpe, 2022, https://www.fnr.de/ftp/pdf/berichte/22409517.pdf